



Multistability, synchronization, and self-organization in  
networks of nonlinear systems with changing graph  
topologies

Nicholas J. Jarman<sup>1,2</sup>

<sup>1</sup>Department of Mathematics, University of Leicester, United Kingdom.

<sup>2</sup>Laboratory for Perceptual Dynamics, PPW, KU Leuven, Belgium.

A dissertation submitted to  
the Department of Mathematics  
of The University of Leicester  
in partial fulfilment of the requirements  
for the degree of Doctor of Philosophy

Supervisors:

Prof. Alexander N. Gorban<sup>1</sup>, Dr. Erik Steur<sup>5,6</sup>, Dr. Chris Trengove<sup>1</sup>

Dr. Ivan Y. Tyukin<sup>1,3</sup>, Prof. Cees van Leeuwen<sup>2,4</sup>

<sup>3</sup>Saint-Petersburg State Electrotechnical University, Saint-Petersburg, Russian Federation.

<sup>4</sup>Center for Cognitive Science, Kaiserslautern University of Technology, Germany.

<sup>5</sup>Institute for Complex Molecular Systems,  
Eindhoven University of Technology, The Netherlands.

<sup>6</sup>Department of Mechanical Engineering,  
Eindhoven University of Technology, The Netherlands.

To whom correspondence should be addressed; E-mail: [nickjarman89@gmail.com](mailto:nickjarman89@gmail.com)

November 27, 2017

# Abstract

Nicholas Jarman

## **Multistability, synchronization, and self-organization in networks of nonlinear systems with changing graph topologies**

Complex network structures appear in myriad contexts. From social networks to computer networks, protein and transport networks, and neuronal networks of the mammalian brain. Furthermore, many of these networks share common structural properties. Are there general underlying mechanisms for the emergence of certain complex network structures? One such shared principle is the mutual relationship between structure and function in self-organising networks. Understanding their emergence can be decomposed into two simpler problems: (1) How does structure effect dynamics? (2) How do dynamics shape the structure? Concepts of nonlinear systems theory provide a tool-set for stability analysis of dynamics on a network. Here, stability analysis is applied to the problem of how a small change in network structure effects the dynamics. Two connectivity configurations are considered; the directed chain and the directed cycle, distinguished by a single edge. Their linear stability is first analysed, followed by the stability of interconnected nonlinear oscillators. Stability analysis reveals radical changes in the patterns of dynamics; while the directed chain possess only one stable solution (synchronization), the directed cycle possesses multistability (synchronization and rotating waves). This capacity for multistability is realised by the extremal properties of the directed cycle; the slow decay of oscillations in the coupling dynamics resonates with the dynamics of the individual oscillators. This result is generalised to networks that contain modular structures and heterogeneous dynamics. For applications of evolving network structures, systems theory is limited. Computational modelling, on the other hand, provides an efficacious alternative. A well-established driving mechanism for network structure evolution is adaptive rewiring; adaptation of structure to function. Computational modelling reveals a synergy between spatial organisation and adaptive rewiring. Emergence of modular small-world network structures are more pronounced, and evolution more robust, than

in models without spatial organisation. However, studies employing adaptive rewiring have been frustrated by the need to explicitly specify dynamics. To address this, explicit dynamics are replaced by an abstract representation of network diffusion (information transfer or traffic flow): shortcuts are created where traffic flow is intense, while annihilating underused connections - like pedestrians define walkways in parks. The resulting networks are a family of small-world structures; networks may be modular or centralised. Moreover, at the critical point of phase transition of network structure, hierarchical structures emerge - like those found in the brain. This thesis therefore serves to help bridge the gap between dynamical systems theory and computational modelling in the field of complex network theory; the importance of connectivity on dynamics, as detailed in systems theory, is captured using graph diffusion, and applied in the context of computational modelling. This successfully reduces the highly complex problem of complex network emergence to a much simpler one, namely, patterns of connectivity. In doing so, the generality of this machinery provides a more lucid understanding for the self-organisation of complex network structures across a broad range of contexts.

# Acknowledgements

Firstly, I would like to express my sincere gratitude to my supervisors Dr. Ivan Y. Tyukin, Prof. Cees van Leeuwen, Dr. Erik Steur, Dr. Chris Trengove, and Prof. Alexander Gorban for the continuous support of my Ph.D study and related research, for their patience, motivation, and immense knowledge. I could not have imagined having better supervisors, and mentors, for my Ph.D study.

Besides my supervisors, I would like to thank my University of Leicester thesis committee Prof. Jeremy Levesley and Dr. Valeri A. Makarov for their insightful comments and engaging discussion on my thesis. Also, Dr. Sergei Petrovskii and Prof. Alexander Gorban, my second year assessors, for their insightful comments which incented me to consider my research from various perspectives.

I thank also my fellow labmates, of which I have seen many come and go. It has been a rare life experience to be a part of such a globally far reaching, yet small, community of internationals.

I thank my closest friends, for however much time elapsed living in Belgium, the friendship was never any less.

Last but not the least, I would like to thank my family. Sadly, my father, Philip John Jarman, passed away in the year before the completion of my thesis. Without the support of both my father and mother, Susan Jarman, and my sister and brother, Samantha and Peter, I do not believe I would have succeeded.

# Contents

<b>1</b>	<b>Introduction</b>	<b>12</b>
<b>2</b>	<b>Dynamical Systems Theory</b>	<b>20</b>
2.1	Preliminaries: Nonlinear systems theory . . . . .	20
2.2	Methods for stability analysis on networks . . . . .	34
2.2.1	Stability of synchronization . . . . .	35
2.2.2	Stability of periodic solutions: Basic Floquet theory . . . . .	51
<b>3</b>	<b>Small Changes In Topology May Have Big Consequences On Activity</b>	<b>57</b>
3.1	Introduction . . . . .	57
3.2	Preliminaries: Circulant matrices . . . . .	58
3.3	Leaders do not look back, or do they? . . . . .	61
3.3.1	Minimal properties of the directed chain . . . . .	61
3.3.2	Extremal properties of the directed cycle . . . . .	63
3.3.3	Synchronization in the simple chain . . . . .	71
3.3.4	Synchronization in the simple cycle . . . . .	74
3.3.5	Numerical analysis: Synchronization and rotating waves . . . . .	79
3.4	Multi-Stability of coherent dynamics in directed networks with modular topology . . . . .	92
3.4.1	Network definition . . . . .	93
3.4.2	Extremal properties of the modular cycle . . . . .	95
3.5	Conclusion . . . . .	101
<b>4</b>	<b>Emergence of Complex Network Structures</b>	<b>104</b>
4.1	Introduction . . . . .	104
4.2	Preliminaries: Characterising graph structure . . . . .	106
4.3	Spatially constrained adaptive rewiring in cortical networks creates spatially modular small-world structures . . . . .	111

4.3.1	Dynamics: Coupled maps . . . . .	112
4.3.2	Stability of synchronization . . . . .	113
4.3.3	Adaptive rewiring: Spatial bias . . . . .	115
4.3.4	Results . . . . .	117
4.4	“Go with the flow”; Self-organisation of small-world network . . . . .	133
4.4.1	Preliminaries: Network diffusion . . . . .	136
4.4.2	Adaptive rewiring: In response to network diffusion . . . . .	142
4.4.3	Results . . . . .	143
4.5	Conclusion . . . . .	153
<b>5</b>	<b>Conclusion</b>	<b>159</b>
5.1	Future work . . . . .	163
	<b>Bibliography</b>	<b>166</b>

# List of Figures

3.1	The imaginary axis (Im) in the vertical, and the real axis (Re) in the horizontal. (a) Example of Gershgorin discs where the maximum eigenvalue is zero. (b) Zoom of (a). . . . .	65
3.2	The polygon $\mathcal{A}$ is presented as a sequence of vectors $\mathbf{x}_i$ . The angle $\beta_i$ between vectors $\mathbf{x}_i$ and $\mathbf{x}_{i+1}$ and the angles $\alpha_i$ and $\gamma_i$ of the triangle with sides $\mathbf{x}_i$ and $\mathbf{x}_{i+1}$ are shown. In the Figure, rotation goes anticlockwise, i.e. $\Im\lambda < 0$ . In this case, the polygon $\mathcal{A}$ is invariant with respect to the semigroup $\exp(t\mathcal{K})$ ( $t \geq 0$ ) if and only if $\delta \leq \alpha_i$ for all $i = 1, \dots, m$ , where $\delta$ is the angle between the vector field $\mathcal{K}\mathbf{x}$ and the radius-vector $\mathbf{x}$ . . . . .	67
3.3	In blue are the vectors of the phase portrait; the trajectories of the system $(\dot{z}, \dot{y})$ for initial conditions taken over a discrete grid. In red the $z$ nullclines: $z = \frac{1}{\beta}y$ . In green the $y$ nullcline: $z = y - \gamma y^3$ . In black the box $B_{z,y} = \{y, z \in \mathbb{R} \mid  z  \leq \frac{15}{8}\sqrt{3},  y  \leq \frac{3}{2}\sqrt{3}\}$ for which the system $(\dot{z}, \dot{y})$ is forward invariant. . . . .	72
3.4	Synchronization of two FHN oscillators for $\sigma = 1.5$ . a. Outputs of FHN oscillator 1 (leader, black) and FHN oscillator 2 (follower, red). b. Synchronization output error $\tilde{y} := y_1 - y_2$ . . . . .	75
3.5	Synchronization output errors $\tilde{y}_j := y_j - y_{j-2}$ , $j = 2, \dots, n$ , for $\sigma = 1.5$ and different lengths of the chain. . . . .	75
3.6	Bifurcation diagram for directed rings of FHN oscillators. The <i>guaranteed synchronization (analytical)</i> region in the parameter space corresponds to global asymptotic synchronization that is guaranteed by the semi-passivity argument, the <i>synchronization (numerical)</i> is the domain where numerical simulations found synchronization to be registered for every set of random initial conditions. The <i>co-existence</i> region shows the domain of parameter values in which both fully synchronous and rotating wave solutions have been found. . . . .	80

3.7	Proportion of samples that yield a rotating wave solution. Red curve shows the boundary the rotating wave is stable determined by Floquet multipliers. .	81
3.8	Proportion of samples that yield a rotating wave solution for all mode types.	82
3.9	(a) The $y$ dynamics over one oscillation. (b) The periodic $y$ dynamics in the time interval $[0, T]$ . The $z$ dynamics show the same type of time shifted and periodic behavior as the $y$ dynamics. . . . .	83
3.10	Solutions of the auxiliary system characterized in the parameter domain of period time, delay, and coupling strength $(T, \tau, \sigma)$ presented as a surface for $T$ a function of pairs $(\tau, \sigma)$ . . . . .	86
3.11	Solutions of the auxiliary system characterized in the parameter domain of period time and delay $(T, \tau)$ for given coupling strengths: (a) $\sigma = 0.95$ . (b) $\sigma = 6.75$ . Dashed lines indicate solutions that satisfy relation . . . . .	87
3.12	Two coupled cycles and their $y$ -dynamics; in red the $y$ -dynamics of the first cycle, and in green the $y$ -dynamics of the second cycle. . . . .	92
3.13	Modular network architecture specified by (3.61) . . . . .	94
3.14	Proportion of samples yielding rotating wave solutions in the $(N, \sigma)$ plane (identical oscillators). The horizontal axis shows the values of $\sigma$ ; the vertical axis shows the values of $N$ . . . . .	100
3.15	Proportion of samples that yield solutions resembling rotating waves in the $(N, \sigma)$ plane (heterogeneous oscillators). The horizontal axis corresponds to the values of $\sigma$ , vertical axis stands for the values of $N$ . . . . .	101
3.16	Proportion of samples that yield a nearly fully synchronous solution in the $(N, \sigma)$ plane (heterogeneous oscillators). The horizontal axis corresponds to the values of $\sigma$ ; the vertical axis stands for the values of $N$ . . . . .	102
3.17	Proportion of samples that we were unable to relate to either of the classes (rotating wave or fully synchronous state). The horizontal axis corresponds to the values of $\sigma$ ; the vertical axis stands for the values of $N$ . . . . .	102
4.1	Cost functions of spatial distance: linear in blue, exponential in green, logarithmic in red. . . . .	116
4.2	Evolution of A, the clustering coefficient values $C$ averaged over five runs; and B, the average shortest path length values $L$ averaged over five runs; for the non-spatial and spatial rewiring processes, regular lattice on the sphere, and random network. . . . .	119

4.3	(a) Evolution of the clustering coefficient; and (b), the average shortest path length; for the non-spatial and spatial rewiring processes, regular lattice on the sphere, and random network. Individual runs in blue and their average value in red. . . . .	120
4.4	(a) Evolution of the spatially-weighted clustering coefficient values $C^w$ averaged over five runs; and (b), the network wiring cost values $M$ averaged over five runs; for the non-spatial and spatial rewiring processes, regular lattice on the sphere, and random network. . . . .	122
4.5	(a) Evolution of the spatially-weighted clustering coefficient values $C^w$ ; and (b), the network wiring cost values $M$ ; for the non-spatial and spatial rewiring processes, regular lattice on the sphere, and random network. Individual trials in blue and averaged value of five runs in red. . . . .	123
4.6	Linear correlation coefficient $\rho$ between edge betweenness and spatial distance averaged over five runs versus rewiring iterations. (a) The full course of rewiring; and (b), early course of rewiring. . . . .	126
4.7	Scatter plots of edge betweenness versus spatial distance. Betweenness values presented here were obtained by uniformly randomly selecting 4% of nodes from the combined five runs and plotting the betweenness values of all their connections. Rows top to bottom for rewiring steps, 1, $0.75 \times 10^3$ , $1.5 \times 10^4$ , $5 \times 10^4$ , $3 \times 10^5$ , columns are for different rewiring processes. . . . .	127
4.8	Evolution of the value of the modularity $Q$ . (a) The average of five runs; and (b), the individual runs; for the non-spatial and spatial rewiring processes, regular lattice on the sphere, and random network. Individual runs in blue and their average values in red. . . . .	128
4.9	Permuted adjacency matrices that correspond to the module structure of the non-spatial, linear, exponential, and logarithmic rewiring processes. A point with coordinates $(i', j')$ is white if $i', j'$ are the permuted indices of nodes $i, j$ that are connected; otherwise it is black. . . . .	129
4.10	Final community structure of one run of the linear rewiring process. (a) and (b) show opposite hemispheres. Nodes are coloured according to the module to which they belong. . . . .	131
4.11	Final community of the logarithmic rewiring process. (a) and (b) show opposite hemispheres. Nodes are coloured according to the module to which they belong. . . . .	132

4.12	Clustering coefficient, $C$ , and average shortest path length $L$ , for (a), (b), non-spatial; (c), (d), linear; and (e), (f), exponential cost functions as function of edge density. Maximum, average, and minimum values from the five independent runs are shown, along with values for the corresponding random and regular graphs. . . . .	134
4.13	Small-worldness measure $\Sigma$ averaged over five runs for non-spatial, linear, and exponential rewiring processes as a function of edge density. . . . .	135
4.14	The small-world index $S$ as a function of decreasing random rewiring probability $p$ : Coloured lines indicate values of heat kernel parameter $\tau$ , black line indicates the Watts-Strogatz algorithm. . . . .	144
4.15	As functions of decreasing $p$ along the horizontal axis: A clustering coefficient $C$ ; B global efficiency $E$ , with upper right region magnified in subplot. . . . .	146
4.16	Along the vertical axis is the global efficiency $E$ as a function of random rewiring probability $p$ along the horizontal axis: Coloured lines indicate values of heat kernel parameter $\tau$ . . . . .	147
4.17	The average modularity $Q$ as a function of decreasing random rewiring probability $p$ : Coloured lines indicate values of heat kernel parameter $\tau$ . . . . .	148
4.18	Single trial. Example modular SWN. Adjacency matrices mapped to an $n$ -by- $n$ grid where rows (and columns) represent vertices and white indicates the existence of an edge. Rows and columns of adjacency matrices have been permuted to visualise the modules, in accordance with [127]. <b>a</b> : $(\tau, p) = (\epsilon, 0.1)$ ; <b>b</b> : $(\tau, p) = (1, 0.3)$ . . . . .	149
4.19	The average $\pi$ - maximum component of PageRank vector normalised by its mean - as a function of decreasing random rewiring probability $p$ : Coloured lines indicate values of heat kernel parameter $\tau$ . . . . .	150
4.20	A bar-plot graph where the height of individual bars are the average number of vertices having degree $d_v$ . Coloured bars indicate values of heat kernel parameter $\tau$ . . . . .	151
4.21	Single trial. Example centralised SWN. Adjacency matrices mapped to an $n$ -by- $n$ grid where rows (and columns) represent vertices and white indicates the existence of an edge. Rows and columns of adjacency matrices have been permuted to visualise the modules, in accordance with [127]. <b>a</b> : depicts $(\tau, p) = (8, 0.5667)$ ; <b>b</b> : depicts $(\tau, p) = (\delta, 0.5667)$ . . . . .	152
4.22	In the plane $\tau$ along the horizontal axis and random rewiring probability $p$ along the vertical axis: <b>a</b> : depicts the modularity index $Q$ ; <b>b</b> : depicts $\pi$ , the maximum component of PageRank vector normalised by its mean value. . . . .	154

- 4.23 **a:** For  $\tau = 0.5$ . Along the horizontal axis random rewiring probability  $p$ . Along the vertical axis are  $Q$  the modularity index (left), and  $\pi$  is the maximum component of PageRank vector normalised by its mean value (right).
- b:** Single trial. Example centralised SWN. Adjacency matrix mapped to an  $n$ -by- $n$  grid where rows (and columns) represent vertices and white indicates the existence of an edge. Rows and columns of adjacency matrices have been permuted to visualise the modules, in accordance with [127]. Pair  $(p, \tau) = (5, 0.522)$ . . . . . 155
- 4.24 For four single trials, (a)–(d), where in each the pair  $(p, \tau) = (5, 0.522)$ , the adjacency matrix permuted to visualise the modules, in accordance with [127]. 156

# List of Tables

4.1 Column wise  $\tau$ . Row wise:  $a$  assortativity coefficient;  $c$  maximised core-periphery statistic. Values presented are averages over trials. . . . . 150

The following table describes the significance of various abbreviations and acronyms used throughout the thesis. The page on which each one is defined or first used is also given. Acronyms that are used in some places to abbreviate the names of certain white matter structures are not in this list.

<b>Abbreviation</b>	<b>Meaning</b>	<b>Page</b>
CGS	Connection Graph Stability	27
MSF	Master Stability Function	27
KYP	Kalman-Yacubovich-Popov	36
FHN	FitzHugh-Nagumo	59
SWN	Small-world network	95
WS	Watts-Strogatz	95
ER	Erdős-Rényi	123

# Chapter 1

## Introduction

Synchronization is the phenomenon of spontaneous order, events occurring in complete unison. For instance, the flocking of birds or the schooling of fish are examples of how a large number of individuals may act in unison [125]. In these cases, an advantage of synchronizing their movement serves as a defence from predators. In other contexts, such as neuronal networks, synchronization of neurons is a well-established mechanism for communication and information processing [1; 107; 136]. At a larger scale, populations of neurons are responsible for functions such as circadian rhythm [124] - our (almost) 24 hour day-night cycle -, and synchronized pacemaker neurons are responsible for regulating heartbeats [157].

However, synchronization is not always advantageous, for example, epilepsy is the synchronized discharge of a large number of neuronal cells in the brain [148; 106]. In ecology, synchronization of species' reproduction cycles may be undesirable for prey [86; 68].

Synchronization is not restricted to biological organisms, indeed, inanimate objects may also exhibit synchronizing behaviour. Christiaan Huygens first reported the synchronization of inanimate objects in 1665 where he found that two pendulum clocks coupled by a wooden structure would always synchronize [123]. This later proved revolutionary in naval navigation. More remarkably, highly complex inanimate objects also synchronize, such as that of chaotic signals, for the secure transmission and receiving of radio signals [35]. More recently, this has evolved into more sophisticated means of secure communication: image processing, pattern recognition, etc. And in other domains, the synchronization observed in fish schools and bird flocks can be applied to swarm technologies; large numbers of robots working collectively.

However, many real world systems are typically not restricted to just one emergent behaviour. When a system exhibits multiple stable states, we call it *multistable*. Moreover, complex systems may *switch* from one behaviour to another, such as switching from

synchronised motion to periodic. The simplest form of multistability is bistability in a one-dimensional space, i.e., two stable equilibrium points and one state variable. For example, in the pluripotency gene regulatory network, a stable state of self-renewal is destabilised by random fluctuations resulting in cellular differentiation [98].

Similarly to synchronization, multistability plays an important role in brain dynamics [80]. The human brain, for instance, is well-documented to exhibit many different stable states, from the low frequency oscillations of rest state [19; 151], the brain can switch to uncorrelated activity [49; 48], or phase-synchronised activity [152], such as in the case of travelling waves.

Dynamic stability, and instability, can provide flexibility in brain networks, allowing for multiple patterns, and to switch between them. However, in the case of ambiguity, i.e., competition of multiple stable states, we may experience multistable perception; spontaneous alternation between two or more perceptual states that occurs when sensory information is ambiguous [81]. For example, the work of M. C. Escher was strongly influenced by multistable perception, in which we see a dissociation of dynamic perception from constant sensory stimulation.

The concept of self-organisation follows naturally from synchronization and multistability, since, in its most basic form, it is a non-equilibrium phase-transition. In other words, at a critical threshold of instability, a systems state may move from one basin of attraction to another. When the individuals of a complex system approach a critical threshold of instability, a kind of “tipping point”, they reorganise themselves to accommodate those conditions. Self-organization, or spontaneous order, can therefore be considered as the emergence of global patterns arising from the coordination of local interactions in a dynamical system. From an initially less ordered state, without external stimuli, random fluctuations (or perturbations) can trigger amplifying feedback processes that over time increase the degree of order to a convergent state.

Self-organization occurs in many contexts, from computer science [100] and economics [156; 89] to neuroscience [82; 27]. In neuronal systems, local cues and local interaction are particularly important for development. In the initial stages of development of the neural plate or tube (neuroectoderm), self-organisation is in response to the local mechanics of diffusible proteins [102]. In later stages, for instance axonal growth, axonal growth cones that guide their migration are directed, in part, by local chemical cues [7]. Following the exuberant growth of axons [69], to ensure the proper formation of functional circuitry, neuronal branches and connections are selectively pruned [99].

The result of self-organisation is a highly ordered complex global structure. The degree of complexity in the structure, and the continued evolution and adaptation cannot be ex-

plained by genetic “blueprints” alone [34], ongoing biophysical processes must clearly play an important role.

The resulting patterns of activity display coordinated collective behaviour; neurons or populations of neurons can generate through their combined activity complex patterns and behaviour that far exceed the capacity or capability of any individual neuron. For example, the notion of self-organising polychronous neuronal groups (PNG) [73]; reproducible time-locked but asynchronous firing patterns for which the number of coexisting patterns vastly exceeds the number of individual neurons. Such patterns are hypothesised to underpin memory and learning, functions that have seemingly little or no limit.

The study of self-organization in the brain may therefore provide valuable insight into the processes of brain growth, development, maintenance, and learning. Moreover, how disruptions to these processes can lead to brain diseases [90], such as schizophrenia [126], Parkinsons [47], Alzheimers [160], autism [11; 129], epilepsy [15], dyslexia [158], among others.

Processes in the brain - structural and functional - take place over multiple time-scales [115]. Typically, on what we may consider a fast time-scale, in the range of milliseconds, we observe the functional activity [21], whereas on slower time-scales, ranging anywhere from millisecond time-scale to years, we can observe evolving structural connectivity [137; 25].

At the level of neuronal cells, electrical polarization maintained by a voltage gradient across the cells membrane rapidly depolarises, causing a ‘spike. This is the most basic unit of activity in nervous systems, called a neuronal action potential, and occurs in time-scales ranging from sub-millisecond, for sodium-based action potentials, up to approximately 100 milliseconds, for calcium-based ones [10; 84]. Communication between neuronal cells also spans multiple time-scales: electrical coupling (conductance) between neighbouring neuronal cells via gap junctions allows for sub-millisecond communication; whereas chemical coupling via axonal propagation of action potentials ranges from sub-millisecond to 100s of milliseconds [3].

The time-scale of activity is also affected by the spatial-scale that it spans. At the scale of individual neurons, the time-scale for propagation of an action potential depends upon several spatial factors. For example, the extent to which an axon is myelinated (a layer of insulating lipids); the greater the thickness of myelination, the greater the conduction velocity [155; 122]. At greater spatial scales, interactions between large populations of neurons may be characterized by frequency specific brain functional networks ranging over classical frequency bands  $\delta$ ,  $\theta$ ,  $\alpha$ ,  $\beta$ , and  $\gamma$  [76; 29]. For example, task-related activity shows that over long-ranges, functional correlations exist predominantly between high-frequency activity, compared to resting state in which short-range local functional correlations are pre-

dominantly high-frequency and low-frequency functional correlations dominate long-ranges [9].

Over all time- and spatial-scales, patterns of activity are shown to reflect the underlying structural (anatomical) connectivity on slow time-scales, however, significantly less so on faster time-scales [66]. Studies that have explored the relationship between function and structure have found that, across all time- and spatial-scales, the relationship between activity and structure typically obeys the (Hebbs) postulate, that “what fires together wires together” [64]. This simple notion prescribes how structural connectivity changes in adaptation to the activity patterns, and that typically, pairwise correlations in activity promotes structural connections.

This influence of activity on structure is observed over multiple time-scales [161]; on a relatively fast time-scale, synaptic plasticity takes place, where the strengths of connections change depending on growth and retraction of synaptic boutons. On a slower time-scale, there is rewiring of brain connectivity through growth of axonal spines and somatic dendrites [31; 77]. On the slowest time-scale, there is axonal rewiring; operating over the lifespan, and varying over different phases, e.g., exuberance of connections in early development [69], and pruning in the maturing brain [30].

It is clear that, on the one hand, structural connectivity is key to understanding activity in neural systems, but on the other, understanding activity patterns is key to answering the question of how complex patterns of connectivity emerge. How these two distant processes, yet operating in seeming harmony, give rise to self-organization remains relatively unknown.

This problem of self-organisation of complex network structures is not limited to the mammalian brain, in fact, complex network structures are found across myriad contexts. From social networks to computer networks, protein and transport networks [56; 112; 17]. Moreover, despite having no connection to one another, many of these different networks share the same structural properties. This raises the question: Are there general underlying mechanisms for the emergence of certain complex network structures?

To answer such a complex problem, it often helps to decompose the problem into smaller, simpler ones. Here, the complex problem of self-organisation is first rephrased as the mutual interplay between the dynamics of structure and function [128]. Then this problem is decomposed into two simpler ones: the effects network structure has on dynamics; and the effects dynamics have on evolving network structures. These two problems typically require very different tools. Determining dynamics from the underlying connectivity is a common problem in the field of mathematics and control theory, whereas more complex problems such as network evolution cannot yet be solved with as much rigour, instead, computational models may serve to help shed greater insight.

Mathematical formalizations in the context of brain dynamics are particularly useful as they allow verifiable connections to be made between different scales and different levels of description of configurations of neural models [38], and ultimately unifying over such scales concepts and principles.

For instance, the dynamics of individual neurons can be described by sets of coupled ordinary differential equations (ODE). One such example is the Hodgkin-Huxley model of the squid giant axon, where state variables represent cell membrane potential, firing rate, and ion channel conductances [65]. This model is considered a “bottom-up” model of neural dynamics since the coupled ODE’s describe observed physical processes. On the other hand, an example of a “top-down” model of neural dynamics is the Izhikevich neuron model [71; 70], which derives its differential equations from mathematical objects, such as attractors. Attractors can capture characteristics of neuronal activity, such as steady state, periodic, or chaotic behaviour, for example, a regular firing neuron can be described by a limit cycle attractor. In the Izhikevich model, a saddle-node bifurcation on a limit cycle represents the rest potential and bifurcating generation of an action potential.

An important tool for assessing systems on larger spatial-scales, graph theory enables us to model certain properties of structural and functional networks present in the brain by reducing regions, populations of, or individual neurons to vertices of a network, and structural or functional connections to weighted and directed edges connecting them [9]. Neural systems may therefore be characterised by interconnecting such ODEs describing the individual dynamics of neurons, or populations of. Commonly, in networks with dynamic units, it is of interest to understand how synchronization can be determined from the connectivity structure and coupling strength. Many methods exist that aim to determine the minimum sufficient coupling strength for global synchronization [117; 159; 14; 121], and this has been extended to cases of partial synchronization in networks [140; 120], and to networks with coupling delays [140; 143], and recently, to networks with heterogeneous dynamics [114].

By applying concepts learnt from graph-theoretic models to the brain, new light may be shed on the basic principles underlying adaptive cognitive processes: schizophrenia has been understood as a cognitive disorder based on the breakdown of large-scale cortico-cerebellar-thalamo-cortical circuits [126], or more generally, the inability to integrate neuronal processes in different brain regions, a syndrome termed dysconnectivity [150]. Epilepsy is understood to arise from higher than the normal mean node degrees [118], and autism is thought to arise from accentuated segregation and attenuated integration of connectivity [129].

In this thesis, stability analysis is applied to the problem of how a small change in network structure effects the dynamics. In particular, two basic and extreme topologies,

which any network will contain as a subgraph, and that differ by only a single edge. For a system with  $n$  states  $A_i$ ,  $i = 1, \dots, n$ : the directed chain such that  $A_1 \rightarrow A_2 \rightarrow \dots \rightarrow A_n$ ; and the directed cycle (simple cycle), such that  $A_1 \rightarrow A_2 \rightarrow \dots \rightarrow A_n \rightarrow A_1$ .

In contrast to the simple stability properties of the directed chain, the eigenspectrum of the simple cycle reveals that it possesses extremal properties. Namely, the simple cycle with the equal rate constants has the slowest decay of the oscillations among all first order kinetic systems with the same number of states.

Considering the unique extremal properties of the simple cycle in a linear system, this sensitivity to perturbations is investigated for nonlinear systems connected in a simple cycle configuration. FitzHugh-Nagumo (FHN) nonlinear oscillators are interconnected with equal coupling strengths to form a simple cycle. In addition to the fully synchronous state, the simple cycle of FHN oscillators exhibits a second stable solution. The small perturbations of the simple cycle do not always decay; the slow oscillatory relaxation of the simple cycle resonates with the nonlinearity of the individual dynamics and generates a regime in which the perturbations persist. In particular, the individual oscillators are phase-locked producing a rotating wave solution. The simple cycle of nonlinear oscillators therefore possesses multistability. In contrast, nonlinear oscillators coupled in the directed chain configuration exhibit only one stable solution, namely, synchronization. This profound difference in the stability diagram of the two systems arises as the result of a small change in the underlying connectivity - the addition/removal of a single edge for any arbitrarily large (finite) number of coupled oscillators.

This result is then generalised to the case of more complex network structures - modular networks. In particular, densely interconnected modules of FHN oscillators are connected via feedforward connections forming a directed cycle of modules. The multistability found in the simple cycle is preserved, furthermore, phase-locked rotating waves solutions are more prominent, i.e., they are stable for a larger domain of coupling strength parameter as compared to the case of the simple cycle. This result is further generalised to heterogeneous dynamics, i.e. individual FHN oscillators are non-identical in their parameters. The modular structure serves to minimise the destabilising effects of heterogeneity in the dynamics allowing for an overall global stability. The message is clear - connectivity is key to determining patterns of dynamics.

For applications of evolving network structures, systems theory is limited. Computational modelling, on the other hand, provides an efficacious alternative. By taking arrays of differential equations describing neural activity as vertices, and coupling functions as connections, or graph edges, computational modelling allows one to observe emerging complex patterns of dynamics far beyond such tractable solutions as synchronization, or periodic

solutions. The resulting data obtained from such simulations can then be analysed using a large array of tools, for example, statistical or signal analyses. In addition, computational modelling gives one the ability to manipulate certain components not feasible in *in vivo* and *in vitro* experiment. And furthermore, provide insight into processes that operate on large time-scales that are not possible to examine directly, and even allow predictions of patterns of functional activity to be made [25].

To address the problem of how dynamics shape structure, a rule for structural changes dependent on function must be established. Such a rule, for which network structure adapts to patterns of synchronization, known as *adaptive rewiring*, was first proposed over a decade ago by [59]. Since then, there have been several studies that have aimed to deepen the understanding of network evolution in response to patterns of dynamics [58; 59; 91; 150; 127]. However, missing from these studies was any notion of spatial organisation, a potentially significant factor as many real-world networks are spatially organised.

Here, spatial bias is introduced in the mechanism of adaptive rewiring. It is found that a clear synergy between spatial organisation and adaptive rewiring exist. In particular, spatially biased adaptive rewiring gives rise to more pronounced modular small-world structures as compared to network evolution without spatial organisation. Moreover, self-organisation in a spatially organised system is more robust to parameter changes that would otherwise (in the case of no spatial organisation) destabilise the emergence of complex network structures. In particular, previous reports of network vulnerability to low connectivity densities show how below a certain threshold networks fail to self-organise [150].

However, studies of adaptive rewiring have been frustrated by the need to explicitly specify dynamics [58; 59; 91; 150; 127; 75]. As we will show, the stability of solutions can be determined from the underlying connectivity. Therefore, taking connectivity as the driving force behind complex network emergence, we may remove the need to define explicit dynamics. To an extent, this renders the influence of dynamics on structural evolution as essentially impotent.

The graph heat kernel describes diffusion on graphs [92] (information transfer or traffic flow), and we propose it as a generic model of dynamics. Adaptive rewiring in response to graph diffusion is effectuated by creating shortcuts where traffic flow is intense, while annihilating underused connections - like pedestrians define walkways in parks. One advantage of utilising graph diffusion is that it is well-formulated, it can therefore bridge the gap between mathematical formalisation and computational analysis. Moreover, is a highly simplified, and tractable description of ongoing processes on the graph. Furthermore, it is easily parametrised; the diffusion rate biases between local and global connectivity structures, where the later approaches a process of preferential attachment.

We therefore propose a highly abstract model of network evolution that is a blend of mathematical formalisation and computational modelling. We are able to show that a very simple process, graph diffusion, can explain the ubiquitous and robust emergence of a wide class of small-world networks, including modular, centralised, and hierarchical.

In Chapter 2 we introduce some basic concepts of nonlinear systems theory and review methods for stability analysis. In particular, we briefly introduce the Connection Graph Stability method [14], the Wu-Chua conjecture [159], the master stability function [117], the semi-passivity argument [121], and for periodic solutions the Floquet multipliers [88; 83].

In Chapter 3 we apply some of these methods, complimented by numerical simulations. Stability methods are applied to two different network coupling configurations, along with numerical simulations, to study the effects on dynamics by a small change in connectivity. In particular, we consider how a small change - the addition of a single edge - in network structure has dramatic effects on patterns of dynamics. Following this, the result is extended to a more general case of network structure, and numerical simulations support the result for the case of non-identical oscillators.

In Chapter 4 the problem of network evolution in response to dynamics is investigated using computational modelling. A simple model of adaptive rewiring in a spatially organised system reveals that the importance of connectivity structure extends to the spatial domain. Following this, a more general model of network self-organisation is proposed, one in which explicit dynamics are replaced by graph diffusion.

In Chapter 5 the thesis is concluded, including also future directions of research.

## Chapter 2

# Dynamical Systems Theory

### 2.1 Preliminaries: Nonlinear systems theory

The main objective of this chapter is to introduce the reader to the methods of stability analysis of nonlinear dynamical systems. However, first the reader must be familiar with some basic concepts in nonlinear systems theory. Hitherto, the first part of this chapter is dedicated to reviewing those concepts central to stability analysis. Much of what is presented can be found in [28; 83; 50; 40], and the reader is directed to these texts for a more in depth introduction to the topic.

The concepts introduced are primarily restricted to the class of time-invariant nonlinear systems. In particular, those that are linear with respect to input, also known as control-affine systems. Control-affine systems are typically linear in the actions but nonlinear with respect to the state and form an important family of nonlinear systems. Such a system may be expressed in the compact vector form

$$\Sigma = \begin{cases} \frac{dx}{dt} = f(x) + g(x)u \\ y = h(x) \end{cases} \quad (2.1)$$

where  $x \in X \subset \mathbb{R}^n$  are the state variables,  $u \in U \subset \mathbb{R}^m$  is the set of all admissible inputs, and  $y \in Y \subset \mathbb{R}^m$  is the output controlled by the function  $h$ . Functions  $f : \mathbb{R}^n \rightarrow \mathbb{R}^n$  and  $g : \mathbb{R}^n \rightarrow \mathbb{R}^{n \times m}$  are assumed to be continuously differentiable, denoted by  $C^\infty$ , vector fields, and  $h$  assumed to be a  $C^\infty$  mapping.

Naturally arising as a solution set to such a system are *manifolds*. A manifold is a topological space with the property that it is locally Euclidean. Denote a manifold  $M \subset \mathbb{R}^n$ , then for any point  $p \in M$ , a neighbourhood  $U$  of  $p$  is homeomorphic to a Euclidean space. Two topological spaces are diffeomorphic if there exists a continuous function mapping

from one to the other, and it admits an inverse that is also continuous. Denote a continuous mapping as  $\psi$  and its inverse  $\psi^{-1}$ , then one can define a *coordinate chart* in a neighbourhood  $U$  of  $p$  as the ordered pair  $(U, \psi)$ . This allows for a manifold  $M$  to be expressed in terms of Euclidean coordinates. On a smooth manifold the mapping  $\psi$  must be a diffeomorphism.

Considering the system  $\Sigma$  (2.1) having multiple state variables, a *vector map* associates a particular point  $x = (x_1, \dots, x_n)$  on a manifold  $M \subset \mathbb{R}^n$  with the vector in  $\mathbb{R}^m$ .

$$f(x_1, \dots, x_n) = \begin{pmatrix} f_1(x_1, \dots, x_n) \\ f_2(x_1, \dots, x_n) \\ \vdots \\ f_m(x_1, \dots, x_n) \end{pmatrix}. \quad (2.2)$$

A *vector field* is an assignment of a vector to each point in a subset of space, i.e. a vector field  $f(x)$  on  $\mathbb{R}^n$  is the mapping which assigns to every point  $p \in M$  a tangent vector  $f(p)$  in the tangent space to  $M$ . A vector mapping,  $f$ , is a *global diffeomorphism* if for all  $x$  there exists an inverse  $f^{-1}$  and both  $f$  and  $f^{-1}$  are  $C^\infty$  functions.

An important object, the *Jacobian matrix* generalises the gradient of a scalar valued function. For a multivariate function  $f$ , it is the matrix of partial derivatives, defined as follows.

**Definition 2.1.1.** (Jacobian matrix) Let  $f : \mathbb{R}^n \rightarrow \mathbb{R}^m$  with input vector  $x \in \mathbb{R}^n$  and output vector  $f(x) \in \mathbb{R}^m$ . The Jacobian matrix  $J$  of  $f$  is the  $m \times n$  matrix of partial derivatives:

$$J = \begin{bmatrix} \frac{\partial f}{\partial x_1} & \dots & \frac{\partial f}{\partial x_n} \end{bmatrix} = \begin{bmatrix} \frac{\partial f_1}{\partial x_1} & \dots & \frac{\partial f_1}{\partial x_n} \\ \vdots & \ddots & \vdots \\ \frac{\partial f_m}{\partial x_1} & \dots & \frac{\partial f_m}{\partial x_n} \end{bmatrix}. \quad (2.3)$$

If  $n = m$  then the Jacobian is a square matrix, and thus one can take the determinant. The determinant of the Jacobian gives information about the local behaviour of the function  $f$  evaluated at the point  $x_0$ . The determinant of the Jacobian plays an important role in the remainder of this section, as it provides an important condition on the existence of a continuous inverse, otherwise known as the Inverse Function theorem.

The *Implicit Function theorem* and *Inverse Function theorem* allow one to find partial derivatives of an implicitly defined multivariable function. The Implicit Function theorem provides conditions under which a relationship of the form  $f(x, y) = 0$  can be rewritten as a function  $y = g(x)$  locally, where  $g(x)$  is an unknown, and hence implicit function. The purpose of the Implicit Function theorem is, therefore, that while we may not know the form of the function  $y = g(x)$ , the theorem asserts its existence, providing that for every  $x$  we have a unique  $y$  such that  $f(x, y) = 0$  is satisfied. In particular, the Implicit Function

theorem is central to the existence of a function we will refer to later as the *zero dynamics*. The purpose of the Inverse Function Theorem is that it is central to the result of *coordinate transformations*, discussed later in this section. Moreover, it can be used to imply the Implicit Function theorem.

**Theorem 2.1.1** (Implicit Function Theorem). *Let  $A$  be an open set of  $\mathbb{R}^{n+m}$  and let  $f : A \rightarrow \mathbb{R}^n$ . Let  $(x_0, y_0)$  be a point in  $A$  such that  $f(x_0, y_0) = (0, 0)$ . Then, if the Jacobian of  $f$  evaluated at  $(x_0, y_0)$  is nonsingular, i.e. the matrix*

$$\frac{\partial F}{\partial y} = \begin{pmatrix} \frac{\partial f_1}{\partial y_1} & \cdots & \frac{\partial f_1}{\partial y_n} \\ \vdots & \ddots & \vdots \\ \frac{\partial f_n}{\partial y_1} & \cdots & \frac{\partial f_n}{\partial y_n} \end{pmatrix} \quad (2.4)$$

*has nonzero determinant, then there exists an open neighbourhood  $A_0 \subset A$  and a unique mapping  $g : \mathbb{R}^n \rightarrow \mathbb{R}^m$  such that*

$$f(x, g(x)) = 0 \quad (2.5)$$

*for all  $x \in A_0$ .*

The Inverse Function theorem is deduced from the Implicit Function theorem and provides sufficient conditions which guarantee the existence of a locally-defined function  $f^{-1}$  for the function  $f$ .

**Theorem 2.1.2** (Inverse Function Theorem). *Let  $f : \mathbb{R}^n \rightarrow \mathbb{R}^n$  be a continuously differentiable map on the open set  $A \in \mathbb{R}^n$  and let  $x_0 \in A$  be a point in  $A$ . Suppose the Jacobian of  $f$  evaluated at  $x_0$  is nonsingular. Then there exists an open set  $B \in \mathbb{R}^n$  that contains the point  $f(x_0)$ , i.e.  $f$  is a continuous mapping from  $A$  to  $B$ , and there exists a continuous inverse  $f^{-1}$  from  $B$  to  $A$ ,  $f : A \rightarrow B$ , and  $f^{-1} : B \rightarrow A$ .*

One immediate consequence of Inverse and Implicit function theorems is the local analysis of stability. For instance, the Hartman-Grobman theorem asserts that the behaviour of a dynamical system near a hyperbolic equilibrium point - a fixed point without any center manifold - is qualitatively the same as the behaviour of its linearisation near this equilibrium point, provided that no eigenvalue of the linearisation has its real part equal to zero. Essentially, the theorem deals with the local behaviour of dynamical systems in the neighbourhood of a hyperbolic equilibrium point and shows the effectiveness of linearisation.

**Theorem 2.1.3** (Hartman-Grobman Theorem). *Let  $f : \mathbb{R}^n \rightarrow \mathbb{R}^n$  be a smooth map of the dynamical system*

$$\dot{x} = f(x). \quad (2.6)$$

Suppose the map has a hyperbolic equilibrium point  $x_0$ . That is,  $f(x_0) = 0$  and the Jacobian matrix of  $f$  at  $x_0$  has no eigenvalue with real part equal to zero. Then there exists a neighbourhood  $U$  of the equilibrium point  $x_0$  and a homeomorphism  $h : U \rightarrow \mathbb{R}^n$  such that  $h(x_0) = 0$  and such that in the neighbourhood  $U$  the flow of  $\dot{x} = f(x)$  is topologically conjugate by a smooth map  $X = h(x)$  to the flow of its linearisation  $\dot{X} = AX$ .

## The Lie Derivative

Possibly the most significant result we describe in this chapter is the *Lie derivative*. The space of vector fields with respect to a Lie derivative is called a *Lie algebra* and appears in myriad contexts, playing important roles in harmonic analysis, algebraic topology and geometry, combinatorics, number theory, finite group theory, and of course, differential geometry. For a full introduction to Lie derivatives, in addition to [40] one should also consider [50; 41]. In particular, here we review the notes by [62].

The role of the Lie derivative is to determine relationships between the motion of points along a vector field with respect to another vector field. Every vector field on a manifold defines infinitesimal motion. If the vector field is differentiable, then it is an infinitesimal diffeomorphism. A key property of the Lie derivative is that it is coordinate invariant, and so it is defined on any abstract differentiable manifold.

Consider a smooth vector field  $v$  on the manifold  $M$ , and let  $f : M \rightarrow \mathbb{R}$  define a smooth real-valued function on  $M$ . For a point  $p \in M$  the vector field  $v$  for a given function  $f$  takes the value  $v[f](p)$  and the collection of such maps for points  $p \in M$  defines the tangent space  $TM_p$ .

In a local neighbourhood of the point  $p$ , the coordinates are denoted  $x^\mu(p)$  for  $\mu = 1, \dots, n$ , and the local neighbourhood of the vector space denoted  $v^\mu$ . The components of  $v^\mu$  in the coordinate system  $x^\mu$  are given by

$$v[f] = v^\mu \frac{\partial}{\partial x^\mu} \in TM \tag{2.7}$$

for the vector field  $v$  without reference to a function in the tangent space  $TM$ .

Given two vector fields  $v$  and  $w$  it is possible to define a new vector field using the Lie bracket. The Lie bracket is the binary operation (product) on  $v$ :  $[v, v] \equiv v \times v \rightarrow v$  that satisfies the following properties for smooth vector fields  $v_1, v_2, v_3$ :

1. The operator is skew commutative:  $[v_1, v_2] = -[v_2, v_1]$ .
2. The operator is bilinear over  $\mathbb{R}$ :  $[\alpha v_1 + \beta v_2, v_3] = \alpha[v_1, v_3] + \beta[v_2, v_3]$ , where  $\alpha, \beta \in \mathbb{R}$ .
3. The operator satisfies the Jacobi Identity:  $[v_1, [v_2, v_3]] + [v_2, [v_3, v_1]] + [v_3, [v_1, v_2]] = 0$ .

In terms of the components, for local coordinates  $x^\mu$  we have

$$[v_1, v_2]^\mu = v_1^\nu \frac{\partial v_2^\mu}{\partial x^\nu} - v_2^\nu \frac{\partial v_1^\mu}{\partial x^\nu}. \quad (2.8)$$

Thus, using the Lie bracket, one yields that

$$\left[ \frac{\partial}{\partial x^m u}, \frac{\partial}{\partial x^n u} \right] = 0. \quad (2.9)$$

The vector fields  $\partial/\partial x^\mu$  associated to the coordinates  $x^\mu$  all commute with each other.

For any smooth vector field  $v$  on  $M$  there exists a smooth map  $\sigma : \mathbb{R} \rightarrow M$  called an integral curve. The integral curve of a vector field  $v$  is simply the path taken if one were place a particle in the vector field; the derivative of the curve with respect to time is precisely the value of the vector field at that point. A particular integral curve is selected once an initial point  $p \in M$  is chosen, and maps to a point  $\sigma_t(p) = m$  for some time  $t \in \mathbb{R}$ .

A *flow*, on the other hand, is the smooth map  $\sigma_t : \mathbb{R} \times M \rightarrow M$ . The flow gives no additional information than what an integral curve tells us, but provides a different way of looking at the same thing. For a given time  $t \in \mathbb{R}$  the flow is the set of all points  $\sigma_t(p)$  for all  $p \in M$ , i.e., for a particular time  $t$ , the flow maps each  $p$  to  $\sigma_t(p)$ . Denote for time  $t \in \mathbb{R}$  and point  $p \in M$ , then the flow  $\sigma_t(p)$  on the vector field  $v$  is defined as

$$\dot{\sigma}_t = v(\sigma_t(p)). \quad (2.10)$$

Since  $\sigma_t$  is a map  $M \rightarrow M$  then the components of  $\sigma_t^\mu$  with respect to the local coordinates  $x^\mu$  are such that the Taylor expansion for  $t$  small

$$\sigma_t^\mu(p) = x^\mu(p) + tv^\mu(p) + O(t^2). \quad (2.11)$$

The Lie derivative of function  $f$  on a vector field  $v$  is the amount of change of  $f$  with respect to  $v$ . Considering the change of  $f$  along the flow  $\sigma_t$ , one can consider the difference  $f(\sigma_t(p)) - f(p)$ , i.e., the difference between  $f$  at the point  $p$  and  $f$  at the translated point  $\sigma_t(p)$ . This difference gives a measure of the change of  $f$  in the direction of the flow of  $v$ .

The Lie derivative of the function  $f : M \rightarrow \mathbb{R}$  is denoted  $L_v f$  and can be seen as the infinitesimal

$$L_v f(p) = \lim_{t \rightarrow 0} \frac{1}{t} [f(\sigma_t(p)) - f(p)] \quad (2.12)$$

for any point  $p \in M$  and map  $\sigma_t$  the flow of  $v$ .

Using the Taylor expansion of  $\sigma_t$  at the point  $p$  one can see then that the function  $f$  at the point point  $\sigma_t(p)$  may be expressed similarly

$$f(\sigma_t(p)) = f(p) + tv^\mu \frac{\partial f}{\partial x^\mu}(p) + O(t^2). \quad (2.13)$$

Therefore, in the local coordinate system  $x^\mu$  we have

$$L_v f = v^\mu \frac{\partial f}{\partial x^\mu}. \quad (2.14)$$

Determining the Lie derivative of a vector field is less simple than over the flow. Consider the vector field  $w$ . To calculate the Lie derivative of  $w$  with respect to a vector field  $v$  one cannot simply repeat the above in taking the difference. This is because for the flow  $\sigma_t$  on  $v$ , the vectors  $w(\sigma_t(p))$  and  $w(p)$  are in different tangent spaces:  $w(\sigma_t(p)) \in TM_{\sigma_t(p)}$  and  $w(p) \in TM_p$ . Hence, it is not possible to simply subtract one from the other. Instead, one must map  $w(\sigma_t(p)) \in TM_{\sigma_t(p)}$  into a vector in the tangent space  $TM_p$ . This can be achieved using an *induced map*.

Let  $\Phi : M \rightarrow M$  be a map from  $M$  onto itself. For a given point  $p \in M$  the induced map may be written

$$D_p \Phi : TM_p \rightarrow TM_{\Phi(p)}. \quad (2.15)$$

Now, in order to map  $w(\sigma_t(p)) \in TM_{\sigma_t(p)}$  into a vector in the tangent space  $TM_p$ , define the induced map

$$D_{\sigma_t(p)} \sigma_{-t} : TM_{\sigma_t(p)} \rightarrow TM_p \quad (2.16)$$

that is, going in the reverse along the flow  $\sigma_t$  from initial point  $\sigma_t(p)$ . The Lie derivative may therefore be defined for vector field  $w$  on vector field  $v$  as

$$L_v w(p) = \lim_{t \rightarrow 0} \frac{1}{t} [D_{\sigma_t(p)} \sigma_{-t}(w) - w(p)] \quad (2.17)$$

for any point  $p \in M$  and flow  $\sigma_t$  of vector field  $v$ .

In the coordinates of the vector field

$$D_{\sigma_t(p)} \sigma_{-t}(w)[f] = w^\nu(\sigma_t(p)) \frac{\partial \sigma_{-t}^\mu}{\partial x^\nu}(\sigma_t(p)) \frac{\partial f}{\partial x^\mu}(p). \quad (2.18)$$

Taking the Taylor expansion of  $w^\nu(\sigma_t(p))$  and  $\frac{\partial \sigma_{-t}^\mu}{\partial x^\nu}$ , and recalling that the coordinate components commute ( $[\frac{\partial}{\partial x^\mu}, \frac{\partial}{\partial x^\nu}]$ ), then

$$\begin{aligned} w^\nu(\sigma_t(p)) &= w^\nu(p) + t v^\rho \frac{\partial w^\nu}{\partial x^\rho}(p) + O(t^2) \\ \frac{\partial \sigma_{-t}^\mu}{\partial x^\nu} &= \delta_\nu^\mu - t \frac{\partial v^\mu}{\partial x^\nu}(p) + O(t^2). \end{aligned}$$

Therefore, the components of the Lie derivative  $L_v w$  are given by

$$(L_v w)^\mu = v^\nu \frac{\partial w^\mu}{\partial x^\nu} - w^\nu \frac{\partial v^\mu}{\partial x^\nu} \quad (2.19)$$

which are simply the local coordinate components of the commutator  $[v, w]$ , the Lie bracket of  $v$  and  $w$ .

The expansion of (2.19) for components  $x = (x^1, \dots, x^n)$  for  $1 \leq \mu, \nu \leq n$ ,

$$L_v w(p) = [v, w](p) = \begin{pmatrix} \frac{\partial w^1}{\partial x_1} & \dots & \frac{\partial w^1}{\partial x_n} \\ \vdots & \ddots & \vdots \\ \frac{\partial w^n}{\partial x_1} & \dots & \frac{\partial w^n}{\partial x_n} \end{pmatrix} \begin{pmatrix} v^1 \\ \vdots \\ v^n \end{pmatrix} - \begin{pmatrix} \frac{\partial v^1}{\partial x_1} & \dots & \frac{\partial v^1}{\partial x_n} \\ \vdots & \ddots & \vdots \\ \frac{\partial v^n}{\partial x_1} & \dots & \frac{\partial v^n}{\partial x_n} \end{pmatrix} \begin{pmatrix} w^1 \\ \vdots \\ w^n \end{pmatrix}. \quad (2.20)$$

Thus,

$$L_v w = [v, w]. \quad (2.21)$$

For repeated Lie Derivatives, we may use the following notation:  $L_v(L_v w(x)) = L_v^2 w(x)$ .

As the purpose of Lie derivatives is to be defined on abstract manifolds, it may be helpful for the reader to understand them in a physical context. A very intuitive description of the Lie derivative is provided by [50] in the context of fluid flow, for which Lie derivatives arise naturally, and recall that description here:

Consider a stationary fluid flow  $\sigma_t(p)$  in some volume. A function  $f$  is said to be *dragged along* by the fluid flow, or *Lie derived* by the vector field  $v$  that generates the flow, if the value of  $f$  is constant on a fluid element, that is, constant along a fluid trajectory  $p(t)$  for a point  $p \in M$  at time  $t$ :

$$\frac{d}{dt} f[p(t)] = v \cdot \nabla f = 0. \quad (2.22)$$

The Lie derivative of a function  $f$  is therefore the directional derivative of  $f$  along  $v$ , defined by

$$L_v f = v \cdot \nabla f. \quad (2.23)$$

In other words, it is the rate of change of  $f$  measured by a comoving observer. Consider next a vector that joins two nearby fluid elements, two points  $p_1(t)$  and  $p_2(t)$  that move with the fluid: Call the connecting vector  $\lambda w = p_2(t) - p_1(t)$ . Then  $\lambda w$  is said to be *dragged along* by the fluid flow. A vector field  $w$  is *Lie derived* by  $v$  if, for small  $\lambda$ ,  $\lambda w$  is dragged along by the fluid flow. This requires that the equation

$$p_1(t) + \lambda w(p_1(t)) = p_2(t) \quad (2.24)$$

be satisfied to the order  $O(\lambda)$ . Taking the derivative of both sides of the equation with respect to  $t$  at  $t = 0$ , we have

$$\begin{aligned} \sigma_t(p_1) + \lambda v \cdot \nabla w(p_1) &= \sigma_t(p_2) = v[p_1 + \lambda w(p_1)] \\ &= \sigma_t(p_1) + \lambda w \cdot \nabla \sigma_t(p_1) + O(\lambda^2) \end{aligned}$$

which holds if and only if

$$[v, w] \equiv v \cdot \nabla w - w \cdot \nabla v = 0. \quad (2.25)$$

The commutator  $[v, w]$  is the *Lie derivative* of  $w$  with respect to  $v$ , written

$$L_v w = [v, w]. \quad (2.26)$$

Then  $w$  is Lie-derived by  $v$  when  $L_v w = 0$ . The Lie derivative  $L_v w$  compares the change in the vector field  $w$  in the direction of  $v$  to the change that would occur if  $w$  were dragged along by the flow generated by  $v$ .

**Definition 2.1.2.** (Relative degree) A control affine nonlinear system  $\Sigma$  (2.1) is said to have relative degree  $r$  at the point  $x_0$  if for smooth vector fields  $f, g$  and smooth map  $h$  the following are satisfied:

1.  $L_g L_f^k h(x) = 0$  for all  $x$  in a neighbourhood of  $x_0$  and all  $k < r - 1$ .
2.  $L_g L_f^{r-1} h(x_0) \neq 0$

where  $L_f^k h(x)$  is the  $k$ -th order Lie derivative of  $h$  along  $f$ .

In other words, where  $y = h(x)$  is the output, the relative degree can be seen to be

$$\begin{aligned} \dot{y} &= \frac{dh}{dt} = \frac{\partial h}{\partial x} \frac{\partial x}{\partial t} = L_f h(x) \\ \ddot{y} &= L_f^2 h(x) \\ &\vdots \\ \frac{d^{r-1}y}{dt^{r-1}} &= L_f^{r-1} h(x) \\ \frac{d^r y}{dt^r} &= L_f^r h(x) + L_g L_f^{r-1} h(x)u. \end{aligned}$$

As with linear systems, the relative degree can be understood to be the lowest order derivative of  $y$  that is explicitly dependent on  $u$ , i.e. the number of times the output function must be differentiated so that the input appears explicitly.

**Definition 2.1.3.** (Zero-output dynamics) Consider the system  $\Sigma$  (2.1) with the restriction that  $y = 0$ , then

$$\begin{aligned} \dot{x} &= f(x) + g(x)u \\ 0 &= h(x) \end{aligned}$$

are called the *zero-output dynamics*.

## Distributions and Frobenius Theorem

Using the Lie derivative, we may now review a central theorem for nonlinear systems theory, the *Frobenius theorem*, which relates integrability to foliation. Using the concept of foliation,

a geometric tool for understanding manifolds, the Frobenius theorem asserts conditions for integrability of a manifold. To state the theorem, both concepts of integrability and foliations must be clearly understood. For a more comprehensive description, one should consider [43], as much of the following can be found there.

Every smooth manifold  $M$  has a tangent bundle  $TM$ , which consists of the tangent space  $TM_p$  at all points  $p \in M$ . The tangent bundle is the collection of all tangent vectors  $TM = \{(p, v) : p \in M, v \in TM_p\}$ . A *distribution* is a subset of the tangent bundle of a manifold satisfying certain properties. Distributions are used to build up notions of integrability, and specifically of a *foliation* of a manifold.

If the vector field  $v$  is non-vanishing, i.e., zero nowhere, then the set of all integral curves are connected, immersed 1-dimensional submanifold of  $M$ . For those unfamiliar, the two following definitions should make clear.

**Definition 2.1.4.** A topological space  $X$  is *pathwise-connected* if and only if for every two points  $x, y \in X$ , there is a continuous function  $f$  from  $[0, 1]$  in  $X$  such that  $f(0) = x$  and  $f(1) = y$ .

Roughly speaking, a space  $X$  is pathwise-connected if, for every two points in  $X$ , there is a path connecting them.

**Definition 2.1.5.** An *immersion* is a differentiable function between differentiable manifolds whose derivative is everywhere injective. Explicitly,  $f : M \rightarrow N$  is an immersion if

$$Df_p : TM_p \mapsto TN_{f(p)}. \quad (2.27)$$

The introduction of *distributions* and *foliations* are a generalisation to connected, immersed  $m$ -dimensional submanifolds, i.e., they allow for integration on  $m$ -dimensional abstract manifold.

Let  $v_1, \dots, v_m$  be a set of vector fields on the manifold  $M$ , and let  $\Delta_p = \text{span}\{v_1(p), \dots, v_m(p)\}$  be the subspace  $TM_p$ , the tangent space of a point  $p \in M$ .

**Definition 2.1.6.** (Distribution) A  $m$ -dimensional distribution on  $M$  is the assignment of an  $m$ -dimensional subspace  $\Delta_p \subset TM_p$  at each point  $p \in M$ : it is the span set of  $m$  linearly independent (smooth) vector fields such that  $\Delta_p = \text{span}\{v_1(p), \dots, v_m(p)\}$ . The  $m$ -dimensional distribution  $\Delta$  is the collection of all  $\Delta_p$  for all  $p \in M$ . The set of smooth vector fields  $\{v_1, \dots, v_r\}$  is called a *local basis* of  $\Delta$ .

In other words, a distribution  $\Delta$  on  $M$  is a map which assigns to each point  $p \in M$ , a subspace of the tangent space to  $M$  at  $p$ .

**Definition 2.1.7.** An *immersed submanifold*  $S$  is an integral manifold of the distribution  $\Delta$  if  $TS_p = \Delta_p$  for all  $p \in S$ .

Immersed submanifolds are important in that the distribution can be said to be integrable if each point of  $M$  is an integral manifold of  $\Delta$ . However, there are distributions for which no integrable manifold exists. To ensure that a manifold is integrable, one must consider the previously discussed Lie bracket, in particular, the Lie bracket of the two vector fields  $v, w$  is  $[v, w] = vw - wv$ . Then, for a given distribution  $\Delta$ , if any two vector fields  $v, w$  with  $v_p, w_p \in \Delta_p$  for all  $p$  in some neighbourhood  $U$ , then if  $[v_p, w_p] \in \Delta_p$  is satisfied, then the manifold is integrable. In other words, the distribution  $\Delta$  is *involutive*; the distribution  $\Delta$  is its own inverse.

**Definition 2.1.8.** (Involutive Distribution) A distribution  $\Delta$  on  $M$  is *involutive* if for every point  $p \in M$  there exists a local basis  $\{v_1, \dots, v_m\}$  of the distribution in a neighbourhood of  $p$  such that for all  $1 \leq i, j \leq m$ ,  $[v_i, v_j]$  (the Lie bracket of the two vector fields) is in the span of  $\{v_1, \dots, v_m\}$ . That is, if  $[v_i, v_j]$  is a linear combination of  $\{v_1, \dots, v_m\}$ . Normally, this is written as  $[\Delta, \Delta] \in \Delta$ .

**Theorem 2.1.1.** (*Frobenius Theorem*) A nonsingular distribution is completely integrable if and only if it is involutive.

The Frobenius Theorem gives necessary and sufficient conditions for the existence of a foliation by maximal integral manifolds each of whose tangent bundles are spanned by a given family of vector fields (satisfying the integrability condition) in much the same way as an integral curve may be assigned to a single vector field.

## Coordinate transformation: Normal form

Now, using the definition of relative degree and the Frobenius theorem, in particular, a system  $\Sigma$  is said to have relative degree  $\{1, \dots, 1\}$  at  $x = 0$  if its Lie derivative  $L_g h(0)$  is nonsingular, and that a nonsingular distribution is completely integrable if and only if it is involutive. Then, if the distribution spanned by the vector fields  $g_1(x), \dots, g_m(x)$  is involutive, then it is possible to find  $n - m$  real valued functions  $z_1(x), \dots, z_{n-m}(x)$ , defined locally near, and vanishing at,  $x = 0$ . This result, along with the  $m$  components of the output function  $y = h(x)$  provide a new set of coordinates commonly known as the *normal form* [28] (or Isidori's normal form).

$$\begin{pmatrix} y \\ z \end{pmatrix} = \Phi(x) = \begin{pmatrix} h(x) \\ L_f h(x) \\ \vdots \\ L_f^{r-1} h(x) \\ \varphi_1(x) \\ \vdots \\ \varphi_{n-r}(x) \end{pmatrix}. \quad (2.28)$$

The  $\varphi_i(x)$  functions are obtained as the solution to the partial differential equation:

$$L_g \varphi(x) = 0. \quad (2.29)$$

As long as the relative degree is well defined, i.e. no singular points, then the existence of  $\varphi_i(x)$  satisfying this equation is guaranteed. This coordinate transformation produces the Byrnes-Isidori normal form:

$$\begin{aligned} y_1 &= h(x) \\ \dot{y}_1 &= y_2 \\ \dot{y}_2 &= y_3 \\ &\vdots \\ \dot{y}_{r-1} &= y_r \\ \dot{y}_r &= a(z, y) + b(z, y)u \\ \dot{z}_1 &= q_1(z, y) \\ &\vdots \\ \dot{z}_{n-r} &= q_{n-r}(z, y) \end{aligned}$$

where  $a = \left[ L_f^r h(x) \right]_{x=\Phi^{-1}(z,y)}$ ,  $b = \left[ L_g L_f^{r-1} h(x) \right]_x = \Phi^{-1}(z, y)$ , and  $q_i = \left[ L_f \Phi_i(x) \right]_{x=\Phi^{-1}(z,y)}$ .

In compact vector form, these new coordinates  $(z, y)$

$$\begin{aligned} \dot{z} &= q(z, y) \\ \dot{y} &= a(z, y) + b(z, y)u \end{aligned}$$

where the matrix  $a(z, y)$  is nonsingular for all  $(z, y)$  near  $(0, 0)$ .

Restricting the output function  $y = 0$  yields the *zero dynamics* of the system. The existence of the zero dynamics are guaranteed locally if the system has relative degree  $\{1, \dots, 1\}$  at  $x = 0$ . In the normal form, these zero dynamics are characterised by the equation

$$\dot{z} = q(z, 0). \quad (2.30)$$

For the case of when the inverse system is used as a controller to constrain the system to a constant value, then the stability is completely determined by the internal dynamics of the system.

**Definition 2.1.9.** Consider the system  $\Sigma$  (2.1). Suppose  $L_g h(0)$  is nonsingular. Then the system is said to be:

1. *minimum phase* if its zero dynamics are asymptotically stable in a neighbourhood of  $z = 0$ ;
2. *weakly minimum phase* if there exists a  $C^1$  positive definite function  $W(z)$  with  $W(0) = 0$ , such that

$$\frac{\partial W(z)}{\partial z} q(z, 0) \leq 0 \quad (2.31)$$

in a neighbourhood of  $z = 0$ .

In addition, minimum phase can be defined globally if the normal form is global, and moreover weakly minimum phase can be defined globally if the minimum phase is defined globally.

## Periodic Orbit Theory

A linear system  $\dot{x} = Ax$  can have a closed orbit but they won't be isolated. Consider periodic solution  $x(t)$ , then so is  $cx(t)$  periodic for any constant  $c \neq 0$ . Hence,  $x(t)$  is surrounded by a one-parameter family of closed orbits. For the case of nonlinear systems, the problem is much less trivial.

Let us begin by first understanding under which conditions a periodic solution cannot exist entirely within a given region. One way to prove a particular system has no periodic solution is to employ a Lyapunov function; if a Lyapunov function exists then closed orbits are forbidden.

Consider a system  $\dot{x} = f(x)$  with a fixed point  $x_0$ . Suppose that we find a continuously differentiable, real-valued and positive semi-definite function  $V(x)$  where  $V(x_0) = 0$  at  $x_0 = 0$ , and its derivative  $\dot{V} < 0$ . Then  $x_0$  is globally asymptotically stable for all initial conditions,  $x(t) \rightarrow x_0$  as  $t \rightarrow \infty$ . Such a function is known as a Lyapunov function, which is described in greater detail in subsection 2.2.1.

If the solution is periodic, then the trajectory of  $V$  does not approach the fixed point  $x_0$ , which contradicts the condition  $\dot{V} < 0$  since such a condition ensures monotonic trajectory down the graph of  $V(x)$  toward  $x_0$ . Thus, if a Lyapunov function exists, then no periodic solution can exist.

An alternative method for ruling out the existence of periodic orbits is *Dulac's criterion*. In particular, it provides sufficient conditions for the non-existence of periodic orbits in simply connected regions of the plane.

Let  $\dot{x} = f(x)$  be a continuously differentiable vector field defined on a simply connected subset  $R$  of the plane. A region  $R$  of the plane is said to be simply connected if every closed loop within  $R$  can be shrunk to a point without leaving  $R$ , i.e.  $R$  has no holes.

**Theorem 2.1.2.** (*Dulac's criterion*) *Let  $R$  be a simply connected region in  $\mathbb{R}^2$  and consider a planar dynamical system in  $R$  given by*

$$\dot{x} = f(x, y) \tag{2.32}$$

where  $f$  is a continuously differentiable, real-valued function in  $R$ . Suppose that there exists a  $C^1$  function  $\varphi(x)$  in  $R$ , called the *Dulac function*, such that

$$\nabla \cdot \varphi(\dot{x} + \dot{y}) \tag{2.33}$$

has a definite sign in  $R$ . Then, the dynamical system (2.32) cannot have any periodic orbits in  $R$ .

In other words, if  $\nabla \varphi \dot{x}$  has one sign throughout  $R$ , then there are no closed orbits lying entirely in  $R$ .

*Proof.* Suppose there is a closed orbit  $C$  lying entirely in the region  $R$ . Let  $A$  denote the region inside  $C$ . Then, Green's theorem yields

$$\int \int_A \nabla \cdot (\varphi \dot{x}) dA = \oint_C \varphi \dot{x} \cdot \underline{n} dl \tag{2.34}$$

where  $\underline{n}$  is the outward normal and  $dl$  is the element of the arc length along  $C$

Consider first the left hand side double integral. It must be nonzero, since  $\nabla \cdot (\varphi(\dot{x} + \dot{y}))$  has one sign in  $R$ . On the other hand, the right hand side line integral must equal zero, since  $(\dot{x} + \dot{y}) \cdot \underline{n} = 0$  everywhere, by the assumption that  $C$  is a trajectory (the tangent vector  $\dot{x} + \dot{y}$  is orthogonal to  $\underline{n}$ ). This is a contradiction since no such  $C$  can exist.  $\square$

Consider now the problem of showing the existence of a periodic orbit. The *Poincaré-Bendixon theorem* provides sufficient conditions for the existence of a periodic solution entirely within a given region.

Let  $\dot{x} = f(x)$  be a dynamical system and consider a trajectory  $\gamma : t \mapsto x(t)$ . A *positive limit point* is a point  $x$  for which there exists a sequence  $t_1, t_2, \dots, \rightarrow \infty$  such that

$$\lim_{n \rightarrow \infty} x(t_n) = x. \tag{2.35}$$

The concept of the *negative limit point* is defined similarly. The  $\omega$ -*limit set* of a trajectory  $\gamma$ , denoted  $\omega(\gamma)$ , is defined as the set of all positive limit points of that orbit. Similarly, the  $\alpha$ -*limit set* is the set of all negative limit points.

The importance of the  $\omega$ -limit set lies in the fact that trajectories in a bounded region of the plane will spiral inward to the  $\omega$ -limit set. The Poincaré-Bendixon theorem tells us that  $\omega(\gamma)$  will either contain a fixed point or it will be a closed orbit of the flow.

**Definition 2.1.10.** A *limit cycle*  $\gamma$  of a dynamical system in the plane is a periodic orbit which is the  $\alpha$ - or  $\omega$ -limit set of a trajectory  $\gamma'$  other than  $\gamma$ . If a limit cycle  $\gamma$  is the  $\omega$ -limit set of every other trajectory in a neighbourhood of  $\gamma$ , then  $\gamma$  is said to be an  $\omega$ -*limit cycle of stable limit cycle*. Likewise, if  $\gamma$  is the  $\alpha$ -limit set of neighbouring trajectories,  $\gamma$  is said to be an  $\alpha$ -*limit cycle or unstable limit cycle*.

Strogatz [144] defines limit cycles informally as closed orbits such that nearby trajectories are either attracted to or repelled by the limit cycle.

The first main result of this section is the Liénard theorem which asserts the existence and uniqueness of a periodic orbit. Any second-order differential equation of the form

$$\ddot{x} + f(x)\dot{x} + g(x) = 0 \tag{2.36}$$

is referred to as a Liénard equation. For there to exist a unique and stable limit cycle,  $f$  and  $g$  must satisfy a number of conditions.

**Theorem 2.1.3.** (*Liénard's Theorem*) Suppose that  $f(x)$  and  $g(x)$  satisfy the conditions:

1.  $f(x)$  and  $g(x)$  are continuously differentiable for all  $x$ ;
2.  $g(-x) = -g(x)$  for all  $x$  (i.e.,  $g(x)$  is an odd function);
3.  $f(-x) = f(x)$  for all  $x$  (i.e.,  $f(x)$  is an even function);
4.  $g(x) > 0$  for all  $x > 0$ ;
5. The odd function  $F(x) = \int_0^x f(u)du$  has exactly one positive zero at  $x = a$ , is negative for  $0 < x < a$ , is positive and nondecreasing for  $x > a$ , and  $F(x) \rightarrow \infty$  as  $x \rightarrow \infty$ .

Then the system (2.36) has a unique, stable limit cycle surrounding the origin in the phase plane.

Having established the existence of a unique and stable limit cycle, it follows to strengthen the property of stability to asymptotic stability. This is achieved by showing that the limit cycle is closed. If the limit cycle is closed, then by definition at least one trajectory converges to the limit cycle as time goes to infinity. The Poincaré-Bendixon theorem asserts that in

a given trapping region - a closed and bounded set containing  $x(t)$  for all time  $t$  - there exists just one stable limit cycle that is closed. In doing so, all trajectories beginning inside the trapping region must asymptotically converge to the closed limit cycle as time goes to infinity.

**Theorem 2.1.4.** (*Poincaré-Bendixon Theorem*) *Suppose that:*

1.  $R$  is a closed, bounded subset of the plane;
2.  $\dot{x} = f(x)$  is a continuously differentiable vector field on an open set containing  $R$ ;
3.  $R$  does not contain any fixed points; and
4. There exists a trajectory  $C$  that is “confined” in  $R$ , in the sense that it starts in  $R$  and stays in  $R$  for all future time.

*Then either  $C$  is a closed orbit, or it spirals toward a closed orbit as  $t \rightarrow \infty$ . In either case,  $R$  contains a closed orbit.*

When applying the Poincaré-Bendixon theorem it is relatively easy to satisfy conditions (1)-(3), however, it is not so easy to satisfy the last; to show the existence of the confined trajectory  $C$ . The standard method is to construct a *trapping region*  $R$ , i.e. a closed connected set such that the vector field points inward everywhere on the boundary of  $R$ . Then, all trajectories in  $R$  remain in  $R$  for all future time.

## 2.2 Methods for stability analysis on networks

The next step to consider are the various methods used for determining the stability of solutions. Most commonly is the solution for synchronization, however, we also consider stability of periodic solutions. Here we review some of the more common methods, these include the Connection Graph Stability (CGS) method [14], the Wu-Chua conjecture [159], the Master Stability Function (MSF) [117], and semi-passivity [121]. For periodic solutions we consider the field of Floquet theory; an eigenvalue based approach known as the Floquet multipliers.

In Chapter 3 we encounter problems of stability analysis of both synchronization and periodic solutions and therefore make use of the methods presented here, in particular, arguments of semi-passivity, and numerical analysis of Floquet multipliers. Throughout this section we assume that: (i) dynamical systems on a graph are identical; (ii) systems are coupled via the same component. In addition, we assume that solution manifolds are invariant. A less important condition is that the graph is a connected component, i.e. has one zero eigenvalue.

The main question to address in this section regards the coupling gain, otherwise known as the coupling strength or coupling coefficient, for which a solution is stable.

### 2.2.1 Stability of synchronization

A central and classical tool in the stability analysis on nonlinear systems is the *Lyapunov stability criterion*. The strength of Lyapunov stability, is that it can determine the stability of an equilibrium point without the need to solve the state equation. Consider the system

$$\dot{x} = f(x, u) \tag{2.37}$$

for state  $x \in X \subset \mathbb{R}^n$  and input  $u \in U \subset \mathbb{R}^m$ , and the function  $f$  is assumed to be Lipschitz continuous. The stability of this system is concerned with its zero dynamics  $\dot{x} = f(x, 0)$ . For initial condition  $x(0) = x_0$  the condition of Lipschitz continuity ensures the existence of a unique solution  $f^*$

$$f^*(x) = f(x). \tag{2.38}$$

An equilibrium point is therefore a point  $x^* \in X$  for which  $f^*(x^*) = 0$ . A sufficient condition for the stability of this point is given by the Lyapunov stability criterion.

**Definition 2.2.1** (Lyapunov function). A system (2.37) has a real-valued, non-negative, and  $C^0$  function  $V : X \rightarrow \mathbb{R}$  defined for all  $u \in U$ ,  $x \in X$ ,  $t \geq 0$  called a Lyapunov function if it is non-increasing along all trajectories such that,

$$V(x(t)) - V(x(0)) \leq 0. \tag{2.39}$$

**Theorem 2.2.1** (Lyapunov stability criterion). A system (2.37) has a stable equilibrium point  $x^*$  if there exists a Lyapunov function  $V$  such that  $V(x) > 0$  except for  $V(x^*) = 0$  and

$$\frac{dV}{dt} \leq 0. \tag{2.40}$$

Moreover, the equilibrium point is asymptotically stable if

$$\frac{dV}{dt} < 0. \tag{2.41}$$

Here, Lyapunov stability of an equilibrium point means that solutions starting close to the equilibrium remain close, while asymptotic stability means that solutions converge to the equilibrium.

**Corollary 2.2.1.** A system (2.37) has an unstable equilibrium point  $x^*$  if there exists a real-valued, non-negative, and  $C^1$  function  $V : X \rightarrow \mathbb{R}$  defined for all  $u \in U$ ,  $x \in X$ ,  $t \geq 0$  such that  $V(x) > 0$  except for  $V(x^*) = 0$  and

$$\frac{dV}{dt} > 0. \tag{2.42}$$

## Connection Graph Stability

The Connection Graph Stability (CGS) method provides a lower bound, or threshold, on the coupling strength for a given configuration of coupled oscillators to synchronize [12]. The CGS method relates synchronization to the coupling configuration by considering the coupling threshold for two oscillators and relating this to properties of graph structure. In this case, the graph property of concern is the maximum (shortest) path length.

The main step in the CGS method is to choose a path  $l_{ij}$  from the coupling configuration between all pairwise vertices  $i, j$  in the graph. Then, for each edge  $e_k$ , the summed length of all paths including  $e_k$  are calculated. The coupling constant that guarantees complete synchronization is proportional to this sum.

Consider a network of linearly coupled (identical) oscillators

$$\dot{x}_i = f(x_i) + \sum_{j=1}^n \epsilon_{ij}(t) H x_j, \quad i = 1, \dots, n \quad (2.43)$$

where  $x_i$  is the  $m$ -dimensional vector of state variables for the  $n$  oscillators  $i = 1, \dots, n$ ,  $G = \{\epsilon_{ij}\}$  is the symmetric  $n \times n$  matrix Laplacian (zero sum rows) that describes the coupling configuration and the coupling strengths between all pairwise oscillators, and  $H$  is the  $n \times m$  matrix output function describing which variables couple the oscillators.

**Theorem 2.2.2.** *The synchronization manifold of the system 2.43 is globally asymptotically stable if*

$$\epsilon_k(t) > \frac{a}{n} b_k(n, m) \quad (2.44)$$

for all  $k = 1, \dots, m$  and for all  $t$ . Here,  $a = 2\epsilon_2^*$  is double the coupling strength sufficient for global synchronization of two coupled oscillators ( $\epsilon_2^*$  is the minimum coupling strength between two oscillators s.t.  $\|Hx_2 - Hx_1\|^2$  is a global Lyapunov function). The quantity  $b_k(n, m) = \sum_{j>i; k \in l_{ij}}^n |l_{ij}|$  is the sum of all chosen paths  $l_{ij}$  which pass through an edge  $k$  belonging to the coupling configuration.

The first step of the method is to determine the value of the parameter  $a$  and to prove that two coupled oscillators completely synchronize when their coupling strength exceeds  $a$ . The value of  $a$  will vary for different oscillators, and for certain oscillators there will exist an upper bound,  $\bar{a}$ , on the parameter  $a$ , such that exceeding  $\bar{a}$  results in destabilizing behaviour. Usually one takes for  $l_{ij}$  the shortest path from vertex  $i$  to vertex  $j$ . However, sometimes a different choice of path can lead to lower bounds on coupling strength needed for synchronization. This is achieved by redistributing the chosen paths that pass through the most loaded edge. What always matters for synchronization is the “weakest link”, i.e. the link having the maximum traffic load. This edge is a bottle neck for synchronization as

the whole network requires the coupling strength  $\epsilon^* = \max_k \epsilon_k$  to synchronize all oscillators of the network.

An advantage of the CGS method is that it does not require calculation of eigenvalues. Methods that require calculation of eigenvalues of the coupling matrices, together with the dynamics of the oscillators, can be computationally expensive. The CGS method therefore can have applications to larger graphs, or to networks whose configuration is not static, but changing over time, requiring repeated recalculation.

### Wu-Chua Conjecture

Similarly to the CGS method, the Wu-Chua [159] conjecture relates synchronization to the coupling configuration by considering the coupling threshold for two oscillators to synchronize. In particular, the coupling strength needed to synchronize an array of coupled oscillators is inversely proportional to the smallest absolute value non-zero eigenvalue of the Laplacian matrix. Assuming the graph is strongly connected, and eigenvalues are ordered as  $0 = \lambda_1 < \lambda_2 \leq \lambda_3 \leq \dots \leq \lambda_n$ , then coupling strength is proportional to  $1/\lambda_1$ .

**Conjecture 2.2.1** (Wu-Chua). Consider two arrays of coupled systems of  $n_1$  cells and  $n_2$  cells, respectively.

$$\dot{x} = \begin{pmatrix} f(x_1, t) \\ \vdots \\ f(x_{n_1}, t) \end{pmatrix} + \alpha_1(G_1 \otimes D)x \quad (2.45)$$

$$\dot{\tilde{x}} = \begin{pmatrix} f(\tilde{x}_1, t) \\ \vdots \\ f(\tilde{x}_{n_2}, t) \end{pmatrix} + \alpha_2(G_2 \otimes D)\tilde{x} \quad (2.46)$$

where  $G_1$  and  $G_2$  are  $n_1$ -by- $n_1$  and  $n_2$ -by- $n_2$  matrices, respectively, ( $n_1, n_2 \geq 2$ ) and  $\alpha_1, \alpha_2$  are real numbers. Assume that  $G_1$  and  $G_2$  are real symmetric matrices having zero row sums such that all eigenvalues are nonpositive and 0 is an eigenvalue of multiplicity 1, i.e., undirected, connected graph.. Let  $\mu_1$  and  $\mu_2$  be the least negative nonzero eigenvalues, called the *algebraic connectivity*, of matrices  $G_1$  and  $G_2$ , respectively. Suppose  $\mu_1$  and  $\mu_2$  are related as follows:

$$\mu_1 \times \alpha_1 = \mu_2 \times \alpha_2. \quad (2.47)$$

Then, Array (2.45) globally synchronizes if and only if Array (2.46) synchronizes.

In other words, this can be seen that if for some  $\alpha_1$  the Array 2.45 globally synchronizes, then for  $\alpha_2 = \frac{\mu_1 \alpha_1}{\mu_2}$  the Array 2.46 also globally synchronizes. A weakness of this method,

however, is that it does not accommodate desynchronizing bifurcations, such as the short wavelength bifurcation, and is limited in the number of coupled systems [117].

### Master Stability Function

A more robust method for stability analysis is the Master Stability Function (MSF) [117]. Whereas the CGS method and Wu-Chua conjecture are vulnerable to desynchronizing bifurcations, the MSF predicts regions of spatial-mode instabilities, for instance changes in the size of the network such as the case of a particular coupling scheme having an upper limit on the number of oscillators for stable synchrony. The MSF achieves this by assessing the *maximum Lyapunov exponent* (MLE),  $\lambda_{\max}$ , of the variational equations of a given system as a function of the eigenvalues of the coupling configuration.

The spectrum of Lyapunov exponents for a deterministic dynamical system characterises the rate of separation, or contraction, of trajectories in a multi-dimensional phase space. The size of this spectrum is equal to the dimensionality of the phase space where each exponent corresponds to a vector in the tangent space of the phase space. Let  $\tilde{x}$  denote the separation of two trajectories  $x_1, x_2$  in phase space. The two trajectories converge or diverge in time  $t$  with the rate

$$|\tilde{x}(t)| \approx \exp^{\lambda t} |\tilde{x}(t_0)| \quad (2.48)$$

for  $t \geq t_0$  and where  $\lambda$  is a Lyapunov exponent describing the exponential separation or contraction in the direction of the initial separation  $\tilde{x}(0)$  in the phase space.

The MLE is the absolute greatest Lyapunov exponent in the spectrum. It describes the average exponential rate of separation of two initially close trajectories. Equation (2.48) is solved for  $\lambda$  as follows

$$\lambda \approx \frac{1}{t} \log \frac{|\tilde{x}(t)|}{|\tilde{x}(0)|}. \quad (2.49)$$

For infinitesimal separation  $\tilde{x}$ , the Jacobian matrix provides the following formula for  $\lambda$  in the infinite limit of time,

$$\lambda(\tilde{x}_0) = \lim_{t \rightarrow \infty} \frac{1}{t} \log \frac{\|J_t \tilde{x}(0)\|}{\|\tilde{x}(0)\|} \quad (2.50)$$

$$= \lim_{t \rightarrow \infty} \frac{1}{2t} \log(\hat{n} J_t^\top J_t \hat{n}) \quad (2.51)$$

where  $J_t = J(f(\tilde{x}(t)))$  is the Jacobian matrix of the variational dynamics,  $\hat{n}$  is the normal vector in the direction of the initial separation such that  $\hat{n} = \tilde{x}(0)/\|\tilde{x}(0)\|$ , and  $J_t^\top J_t$  is the Cauchy-Green strain tensor matrix which describes how linearised neighbourhoods deform over a flow.

To calculate the MLE is not a trivial exercise as this requires assessing the eigenvalues of the corresponding Jacobian matrix of the systems dynamics. In fact, there is no such ana-

lytical method for calculating them, since the Jacobian matrix is typically neither diagonal nor diagonalisable. To determine the MLE requires numerical methods, such as Oseledec's multiplicative ergodic theorem, or Householder's transformation. This is beyond the scope of this thesis; the reader may wish to consult [36] for a more comprehensive description.

By the Perron-Frobenius theorem, the behaviour of the matrix  $J_t$  in the infinite limit of time can be described by its leading eigenvalue and eigenvector. Let  $\lambda_1$  denote the leading eigenvalue of matrix  $J_t$ , then,

$$\lambda_{\max} = \lim_{t \rightarrow \infty} \frac{1}{t} \log(\lambda_1(\tilde{x}(0), t)) \quad (2.52)$$

Therefore, contraction or expansion of two trajectories can be generalised to neighbourhoods of a trajectory using the eigenvalues of the Jacobian matrix evaluated at a point in the flow with infinitesimal motion. Stability, then, of a trajectory can be considered as the deformation of its neighbourhood as it moves along the flow of the vector field.

A positive maximum Lyapunov exponent indicates chaotic motion; initially infinitesimally close trajectories diverge at an exponential rate. On the other hand, a negative MLE indicates stability of fixed points. However, this criteria does not guarantee that there does not exist some unstable invariant manifold or local instability of an attractor.

Consider a network of  $n$  oscillators. Let  $x_i \in \mathbb{R}^m$  be the vector of dynamical variables of the  $i$ -th oscillator. Functions  $f : \mathbb{R}^m \rightarrow \mathbb{R}^m$  and  $h : \mathbb{R}^m \rightarrow \mathbb{R}^m$  are smooth functions that describe individual oscillator dynamics and the output function, respectively. Let  $L$  be the Laplacian matrix for coupling configuration  $G$ , and  $\sigma$  the coupling strength. Let  $x = (x_1, \dots, x_n)$ ,  $F(x) = (f(x_1), \dots, f(x_n))$ ,  $H(x) = (h(x_1), \dots, h(x_n))$ , then system  $\Sigma$  (2.1) may be expressed in the following matrix form

$$\dot{x} = F(x) + \sigma L \otimes H(x) \quad (2.53)$$

where  $\otimes$  is the Kronecker product; the matrix operator which given two arbitrarily sized matrices yields a block matrix, as follows,

$$A \otimes B = \begin{bmatrix} a_{11}B & \cdots & a_{1m}B \\ \vdots & \ddots & \vdots \\ a_{n1}B & \cdots & a_{nm}B \end{bmatrix} \quad (2.54)$$

for  $n \times m$  matrix  $A$  and arbitrary size matrix  $B$ . If matrix  $B$  has dimensions  $p \times q$  then  $A \otimes B$  has dimension  $np \times mq$ .

Linearisation of (2.53) around the synchronous state is obtained by taking the Jacobian functions  $Df$  and  $Dh$ , the Jacobian of  $F$  and  $H$ , respectively. Let  $\varsigma = (\varsigma_1, \dots, \varsigma_n)$  be the

collection of variations. Then

$$\dot{\zeta} = [I_n \otimes Df(x) + \sigma L \otimes Dh(x)]\zeta \quad (2.55)$$

where  $I_n$  is the  $n \times n$  identity matrix. Assuming the coupling matrix  $L$  is nonsingular, then there exists an orthonormal set of eigenvectors such that  $L = Q^{-1}\Gamma Q$  for diagonal matrix of eigenvalues  $\Gamma_{ii} = \gamma_i$ . Assuming  $L$  is connected, order the eigenvalues such that  $0 = \gamma_1 < \gamma_2 \leq \gamma_3 \leq \dots \leq \gamma_n$ . Multiplication of (2.55) on both left hand sides by  $Q \otimes I_m$  yields the block diagonal matrix  $\Theta$  satisfying

$$\dot{\Theta} = [I_n \otimes Df(x) + \sigma \Gamma \otimes Dh(x)]\Theta \quad (2.56)$$

where each block  $m \times m$  block  $\theta_i$ ,  $\Theta = \text{diag}(\theta_1, \dots, \theta_n)$ , can be expressed using the eigenvalues  $\lambda_i$  in the following

$$\dot{\theta}_i = [Df(x) + \sigma \gamma_i Dh(x)]\theta_i \quad (2.57)$$

and  $\theta_i$  corresponds to the mode of  $\zeta_i$  corresponding to the  $i$ -th eigenvector. This is possible since the diagonalisation of  $\sigma L$  in the second term of Equation (2.55) has no affect on the identity matrix  $I_n$ , in the first term.

The block associated to the eigenvalue  $\gamma_1$  corresponds to the dynamics on the synchronous manifold, whereas the other ones correspond to orthogonal modes, i.e. transversal to the synchronization manifold.

Calculate the maximum Lyapunov exponent  $\lambda_{\max}$  for the generic variational equation, called the *Master Stability Equation*

$$\dot{\theta}_i = [Df(x) + (\alpha + i\beta)Dh(x)]\theta_i \quad (2.58)$$

as a function of  $\alpha$  and  $\beta$ .

The Lyapunov (or Floquet) exponent  $\lambda_{\max}$  is the associated MSF, and as a function of  $\alpha$  and  $\beta$ ,  $\lambda_{\max}$  yields a surface over the complex plane for which regions of stability and instability are found. For a given coupling strength  $\sigma$ , the sign of  $\lambda_{\max}$  at the point in the complex plane  $\sigma \mu_k$  describes the stability of that eigenmode. If all the eigenmodes are stable, then the synchronous state is stable at that coupling strength.

The main advantage of the MSF is that it predicts regions of stability, and hence also regions of instability. Changes in coupling strength and network size may cause a desynchronizing bifurcation. The MSF is capable of predicting such bifurcations where the CGS and Wu-Chua methods do not. Another advantage of the MSF is that is is less dependent on the dynamics  $f$  and  $h$  than the CGS and Wu-Chua method, since the size of regions

of stability depend also on the spread of the eigenvalues. If the eigenvalues of the graph Laplacian are more spread out, then it is more likely that the synchronous state will be unstable. Moreover, if the graph is undirected and connected, then all eigenvalues are real, and the spread is simply the ratio of the largest and smallest nonzero eigenvalues  $\gamma_n/\gamma_2$ .

### Dissipative and Passive Systems

Here we briefly review the concepts of dissipative and passive systems, and the reader is directed to the texts [8; 28] for a more comprehensive description. Applied to state-space representations of nonlinear systems, passivity allows for interpretation of notions such as available, stored, and dissipated energy in terms of Lyapunov functions [28]. Intuitively, if the rate of change of the stored energy of some system (of the form (2.1)) is less than the total energy supplied externally, known as the supply rate, then the total energy of the system is said to dissipate. Notions of storage function and supply rate allow the dissipation of energy to be represented as a function of the input and output of the system. Moreover, the storage function shares with the Lyapunov function the property of positive definiteness of the state variable and, under an additional condition, can be treated as a Lyapunov function. Treating the storage function as a Lyapunov function then allows for properties of stability of equilibria to be determined.

Let  $w$  be a real-valued function defined on  $U \times Y$ , called the *supply rate*. Assume that for any  $u \in U$  and any  $x_0 \in X$  the output  $y(t) = h(\Phi(t, x_0, u))$  of system (2.1) is such that  $w(s) = w(u(s), y(s))$  satisfies

$$\int_0^t |w(s)| ds < \infty, \quad \forall t \geq 0. \quad (2.59)$$

**Definition 2.2.2** (Dissipativity and Storage Function). A system  $\Sigma$  (2.1) with supply rate  $w$  is said to be *dissipative* if there exists a continuous non-negative function  $V : X \rightarrow \mathbb{R}$  called the *storage function*, such that for all  $u \in U$ ,  $x(0) = x_0 \in X$ ,  $t \geq 0$

$$V(x(t)) - V(x(0)) \leq \int_0^t w(u(s), y(s)) ds \quad (2.60)$$

where  $x = \Phi(t, x_0, u)$ .

The stored energy  $V(x(t))$  of  $\Sigma$  (2.1) at any time  $t \geq t_0$  is less than or equal to the sum of the stored energy  $V(x(0))$  at time  $t = 0$  and the total energy  $\int_t^t w(u(s), y(s)) ds$  supplied externally. This inequality is called the *dissipation inequality*, and it expresses the concept that if rate of change of the stored energy is less than the supply rate, then energy is dissipated, i.e. there is no internal creation of energy, and so the system absorbs more energy than it supplies. In determining whether a given system is dissipative or not, one

must consider its *available storage*; the largest amount of energy that can be extracted given initial conditions  $x_0$ .

**Definition 2.2.3** (Available storage). The *available storage*, denoted  $V_a$ , of a system  $\Sigma$  (2.1) with supply rate  $w$  is given by the function  $V_a : X \rightarrow \mathbb{R}$ ,

$$V_a(x) = \sup_{\substack{u \in U \\ t \geq 0}} \left\{ - \int_0^t w(s) ds \right\}. \quad (2.61)$$

If  $V_a(x)$  is continuous, then it is itself a storage function.

The available storage  $V_a(x)$  is the *supremum* over a set of numbers containing zero and hence is necessarily non-negative.. If a system  $\Sigma$  (2.1) is dissipative with respect to the supply rate  $w = (u(s), y(s))$ , then the available storage is finite for each  $x \in X$ . Moreover, for all possible storage functions  $V(x)$ , the following inequality holds

$$0 \leq V_a(x) \leq V(x) \quad (2.62)$$

for each  $x \in X$ .

This is formulated in the following theorem.

**Theorem 2.2.3.** *Consider the system  $\Sigma$  (2.1) with supply rate  $w$  and available storage function  $V_a(x)$ . Then  $\Sigma$  is dissipative with respect to the supply rate  $w$  if and only if the available storage  $V_a(x)$  is uniformly bounded, i.e.  $V_a(x) < \infty$  for all  $x \in \mathbb{R}^n$ . Furthermore, if  $V_a(x)$  is uniformly bounded, then any possible storage function satisfies*

$$0 \leq V_a(x) \leq V(x) \quad (2.63)$$

for each  $x \in X$ .

*Proof.* [8] Suppose  $V_a(x) < \infty$  for all  $x \in \mathbb{R}^n$ . Since  $V_a(x)$  is the supremum over all  $w$ , then it follows that

$$V_a(x(t_0)) \geq V_a(x(t_1)) - \int_{t_0}^{t_1} w(u(s), y(s)) ds \quad (2.64)$$

and thus  $V_a(x)$  is finite and hence a storage function. This then proves that the system  $\Sigma$  is dissipative for supply rate  $w$ .

Conversely, suppose that  $\Sigma$  is dissipative. Then there exists  $V \geq 0$  such that for all  $w$ ,

$$V(x(0)) + \int_0^T w(u(s), y(s)) ds \geq V(x(T)) \geq 0 \quad (2.65)$$

and it follows that

$$V(x(0)) \geq \sup_{\substack{u \in U \\ T \geq 0}} \left\{ - \int_0^T w(u(s), y(s)) ds \right\} = V_a(x(0)) \quad (2.66)$$

proving finiteness of  $V_a$ , as well as  $V_a(x) \leq V(x)$ .  $\square$

The theorem therefore states that  $\Sigma$  (2.1) is dissipative if and only if the available storage (maximally extractive energy) is finite for all initial conditions. This result is not necessary to show for all initial conditions provided the system  $\Sigma$  (2.1) has the property of *reachability*.

**Definition 2.2.4** (Reachability). Consider system  $\Sigma$  (2.1). For smooth functions  $f, g, h$ , piecewise continuous input  $u \in U$ , and initial state  $x(0) = x_0 \in X$  denote the set of initial states  $\mathcal{R}(0) \subset \mathbb{R}^n$ . Then, the set of possible reachable states is

$$\mathcal{R}([0, r]) := \{X(t, x_0, u) | x_0 \in \mathcal{R}(0), t \in [0, r], u \in U\} \quad (2.67)$$

Therefore, for all  $x \in \mathcal{R} \subset X$  for initial condition  $x_0 \in \mathcal{R}(0)$  one needs only to check for the initial state  $x_0$  that the available storage  $V_a(x_0)$  is finite. Conversely, if the system  $\Sigma$  (2.1) is dissipative, then its available storage is finite for each  $x \in X$ . Note that by linking dissipativity with the existence of the function  $V_a$ , attention to the dissipation inequality has changed to finding a solution of an optimization problem.

**Lemma 2.2.1.** *Assume system  $\Sigma$  (2.1) is reachable from  $x_0 \in X$ . Then  $\Sigma$  is dissipative if and only if  $V_a(x_0) < \infty$ .*

The supply rate for dissipative systems can be any function defined on the input and output space that satisfies (2.59). For the case where the supply rate  $w$  is defined as the bilinear inner product of the input  $u$  and output  $y$ ,

$$w = \langle u, y \rangle = y^\top u, \quad (2.68)$$

the dissipative system is known then as a *passive system*.

**Definition 2.2.5** (Passivity). A system  $\Sigma$  (2.1) is said to be *passive* if it is dissipative with supply rate  $w$  (2.68), and the storage function  $V$  satisfies  $V(0) = 0$ . In other words,

$$V(x(t)) - V(x(0)) \leq \int_0^t y^\top(s)u(s)ds \quad (2.69)$$

The two limiting cases of passive systems are *lossless* and *strictly* passive systems. The former may be interpreted as the case in which no energy is lost from the system, while the latter that the maximal amount of energy is extracted.

**Definition 2.2.6** (Lossless system). A passive system  $\Sigma$  with positive definite storage function  $V$  is said to be *lossless* if for all  $u \in U$ ,  $x_0 \in X$ ,  $t \geq 0$ ,

$$V(x(t)) - V(x(0)) = \int_0^t y^\top(s)u(s)ds. \quad (2.70)$$

**Definition 2.2.7** (Strictly passive). A passive system  $\Sigma$  with positive definite storage function  $V$  is said to be *strictly passive* if there exists a positive definite function  $S : X \rightarrow \mathbb{R}$  such that for all  $u \in U$ ,  $x_0 \in X$ , and  $t \geq 0$

$$V(x(t)) - V(x(0)) = \int_0^t y^\top(s)u(s)ds - \int_0^t S(s)ds. \quad (2.71)$$

With the supply rate defined as in (2.68), one can relate the passivity of a system to Lyapunov stability. Setting the input  $u = 0$ , then the supply rate becomes non-positive, and hence the change in the storage function over time is less than 0. It can therefore be seen that the system Lyapunov stable.

**Lemma 2.2.2.** *Let  $V \in C^\infty$  be a storage function of system  $\Sigma$  (2.1) and assume that the supply rate  $w$  satisfies*

$$w(0, y) \leq 0, \forall y \in \mathbb{R}^m. \quad (2.72)$$

*Let  $x = 0$  be a minimum of  $V(x)$ . Then  $x = 0$  is locally asymptotically stable for the unforced system ( $u = 0$ ) and  $\mathcal{V}(x) = V(x) - V(0)$  is a local Lyapunov function.*

To establish a more general relation between passivity and Lyapunov stability, conditions on zero-state detectability and observability are needed. This is needed because stability is not always ensured by passivity; stability is not guaranteed for a passive system of multiple states.

**Definition 2.2.1.** (Zero-state detectability and observability) A system (2.1) is zero-state observable if for any  $x \in X$ ,

$$y(t) = h(\phi(t, t_0, x, 0)) = 0, \quad \forall t \geq t_0 \geq 0 \Rightarrow x = 0. \quad (2.73)$$

The system is locally zero-state observable if there exists a neighbourhood  $X_n$  of 0, such that for all  $x \in X_n$ , (2.73) holds. The system is zero-state detectable if for any  $x \in X$ ,

$$y(t) = h(\phi(t, t_0, x, 0)) = 0, \quad \forall t \geq t_0 \geq 0 \Rightarrow \lim_{t \rightarrow \infty} \phi(t, t_0, x, 0) = 0, \quad (2.74)$$

and the system is locally zero-state detectable if there exists a neighbourhood  $X_n$  of 0, such that for all  $x \in X_n$ , (2.74) holds.

**Theorem 2.2.1.** (*Passivity and stability*) *Let a system  $\Sigma$  be passive with a  $C^1$  storage function  $V(x)$ . Then the following properties hold:*

1. *If  $V(x)$  is positive definite, then the equilibrium  $x = 0$  of  $\Sigma$  with  $u = 0$  is Lyapunov stable.*
2. *If  $\Sigma$  is zero-state detectable, then the equilibrium  $x = 0$  of  $\Sigma$  with  $u = 0$  is Lyapunov stable.*
3. *If in addition to either 1 or 2,  $V(x)$  is radially unbounded, then the equilibrium  $x = 0$  is globally stable.*

If the system  $\Sigma$  is strictly passive with positive definite storage function, then the equilibrium  $x = 0$  with  $u = 0$  is asymptotically stable.

One of the most important properties of passive systems relates to the Kalman-Yacubovich-Popov (KYP) property. In particular, if a given system possesses the KYP property, then it is passive. The KYP property is defined as follows:

**Definition 2.2.2.** (Kalman-Yacubovich-Popov (KYP) property) Recall the control affine system  $\Sigma$  (2.1). System  $\Sigma$  is said to have the KYP property if there exists a  $C^1$  nonnegative function  $S(x) : \mathbb{R}^n \rightarrow \mathbb{R}^+$ , with  $S(0) = 0$  such that

$$\begin{aligned} L_f S(x) &= \frac{\partial S(x)}{\partial x} f(x) \leq 0, \\ L_g S(x) &= \frac{\partial S(x)}{\partial x} g(x) = h^\top(x), \end{aligned}$$

for each  $x \in \mathbb{R}^n$ .

**Proposition 2.2.4.** *A system  $\Sigma$  with the KYP property is passive with storage function  $S(x)$ . Conversely, a passive system with  $C^1$  storage function has the KYP property.*

A basic property of passive systems, which makes passive systems very attractive from a stabilization point of view, is that they are stabilisable by the following simple output-input feedback control law.

**Theorem 2.2.5** ([28]). *Suppose  $\Sigma$  is passive with positive definite storage function  $V$ , and suppose that  $\Sigma$  is locally zero-state detectable. Let  $\phi : Y \rightarrow U$  be any smooth function such that  $\phi(0) = 0$  and  $y^\top \phi(y) > 0$  for each nonzero  $y$ . The control law*

$$u = -\phi(y) \tag{2.75}$$

*asymptotically stabilizes the equilibrium  $x = 0$ . Moreover, if  $V$  is proper - if the preimage of every compact set is compact-, then the control law (2.75) globally asymptotically stabilizes the equilibrium  $x = 0$ .*

It follows that for all passive systems the output feedback  $u = -y$  will stabilise the system.

We are interested in the stability properties of linearly interconnected systems. Another fundamentally important property of passive systems is that any linear interconnection of passive systems is also passive. Let us demonstrate this principle with two systems  $\Sigma_1$  and  $\Sigma_2$  as defined in (2.1).

**Theorem 2.2.2.** *Consider two systems  $\Sigma_1$  and  $\Sigma_2$ ,*

$$\Sigma_1 = \begin{cases} \dot{x} = f_1(x_1) + g_1(x_1)u_1 \\ y_1 = h_1(x_1). \end{cases} \tag{2.76}$$

$$\Sigma_2 = \begin{cases} \dot{x} = f_2(x_2) + g_2(x_2)u_2 \\ y_2 = h_2(x_2). \end{cases} \quad (2.77)$$

defined similarly as (2.1). Assume that they are each passive, and that they are interconnected by linear and symmetric input functions

$$u_1 = -\gamma(y_1 - y_2), \quad u_2 = -\gamma(y_2 - y_1) \quad (2.78)$$

for some  $\gamma \geq 0$ . Then both systems are passive. Moreover, assume that both systems are zero-state detectable, and their storage functions  $V_1(x_1)$  and  $V_2(x_2)$  are  $C^1$ . Then the equilibrium  $(x_1, x_2) = (0, 0)$  of both interconnections is stable.

*Proof.* If systems  $\Sigma_1$  and  $\Sigma_2$  are each passive, then there exists storage functions  $V_1(x_1)$  and  $V_2(x_2)$  such that

$$V_i(x_i(t)) - V_i(x_i(0)) \leq \int_0^t y_i^\top(s)u_i(s)ds, \quad i = 1, 2 \quad (2.79)$$

where  $x_1, x_2$  are the state variables of  $V_1$  and  $V_2$ , respectively. Denote  $x = [x_1^\top, x_2^\top]^\top$ , and define  $V = V_1(x_1) + V_2(x_2)$  and note that  $V$  is positive definite and  $V(0) = 0$  and satisfies the dissipation inequality

$$V(x(t)) - V(x(0)) \leq \int_0^t (y_1^\top(s)u_1(s) + y_2^\top(s)u_2(s))ds. \quad (2.80)$$

Notice also the result of symmetric coupling  $u_1$  and  $u_2$

$$y_1^\top u_1 + y_2^\top u_2 = -y_1^\top y_1 + 2y_1^\top y_2 - y_2^\top y_1 \leq 0. \quad (2.81)$$

Clearly, the function  $V$  is compact and radially unbounded and one obtains that

$$V_i(x_i(t)) - V_i(x_i(0)) \leq 0. \quad (2.82)$$

Thus the function  $V$  is bounded for all  $t \geq 0$  and the system is passive.

If systems  $\Sigma_1$  and  $\Sigma_2$  are zero-state detectable, then by Theorem 2.2.1 the equilibrium  $(x_1, x_2) = (0, 0)$  is Lyapunov stable.  $\square$

By induction, this result may be generalised to any finite number of systems  $\Sigma_k$ , each having positive definite storage function  $V_k$ .

## Semi-passive systems

We now consider a weakened version of passive systems called *semi-passive* systems. Semi-passivity briefly describes the notion that the state trajectories of some system of the form  $\Sigma$  (2.1) remain oscillatory but bounded provided that the supply rate is also bounded. A consequence, provided systems are diffusively coupled, is that any coupling configuration can

be shown to possess ultimately bounded solutions. Moreover, when the coupling strength is sufficiently strong, then it can be shown analytically that all systems asymptotically synchronize. In this section we introduce the concept of semi-passive systems and the machinery for determining the critical coupling strength for which in an array of diffusively coupled semi-passive systems asymptotically synchronize. The reader is directed to the texts [121; 142] for a more comprehensive description of the topic, and from which we review these notions. In Chapter 3 we apply the argument of semi-passivity to an array of diffusively coupled FitzHugh-Nagumo oscillators [46].

**Definition 2.2.3.** The system  $\Sigma$  (2.1) is called  $\mathcal{C}^r$ -semi-passive if there exists a  $\mathcal{C}^r$ -smooth,  $r \geq 0$  nonnegative function  $V : \mathbb{R}^n \rightarrow \mathbb{R}^+$  and a function  $H : \mathbb{R}^n \rightarrow \mathbb{R}^1$  such that for any initial conditions  $x(0)$  and any admissible input  $u \in \mathcal{C}^0 \cup \mathcal{L}_\infty$  the following dissipation inequality holds

$$V(x(t)) - V(x(0)) \leq \int_0^t (y^\top(s)u(s) - H(x(s)))ds \quad (2.83)$$

for all  $0 \leq t < T_{u,x_0}$ , where for the set

$$\mathcal{B} := \{\exists \rho > 0 \mid |x| \geq \rho\} \quad (2.84)$$

the function  $H$  is non-negative for  $x \notin \mathcal{B}$ , i.e.,  $H(x \geq \rho) \geq 0$ .

By the introduction of the function  $H$ , it is clear that semi-passive systems are a weakened version of passive systems, however, there are two important properties to note. The first is that for large enough  $|x|$ , semi-passive systems behave in the same way as passive ones. Hence, a semi-passive system that is interconnected by a feedback of the form  $u = \phi(y)$  satisfying  $y^\top \phi(y) \leq 0$  has ultimately bounded solutions, i.e. for all initial conditions state trajectories converge in finite time to a compact set and remains there for all future time. The second is that like passive systems, linearly interconnected semi-passive systems are also themselves semi-passive.

A stronger definition is that of *strict semi-passivity*. Strictly semi-passive systems possess the property that solutions are *ultimately bounded*, i.e., solutions do not depend upon initial conditions.

**Definition 2.2.4.** The system  $\Sigma$  (2.1) is called  $\mathcal{C}^r$ -strictly semi-passive if it is passive and there exists function  $H : \mathbb{R}^n \rightarrow \mathbb{R}^1$  such that for any initial conditions  $x(0)$  and any admissible input  $u \in \mathcal{C}^0 \cup \mathcal{L}_\infty$  the following equality holds

$$V(x(t)) - V(x(0)) = \int_0^t (y^\top(s)u(s) - H(x(s)))ds \quad (2.85)$$

for all  $0 \leq t < T_{u,x_0}$  and where the function  $H$  is strictly positive outside the ball  $\mathcal{B}$  (2.84), i.e.,  $H(x \geq \rho) > 0$ .

It is beyond the scope of this thesis to assess the stability of non-linear feedback functions  $g(x), h(x)$ , so consider the system  $\Sigma$  (2.1) for which the functions  $g(x)$  and  $h(x)$  are linear functions given by the vectors  $B, C \in \mathbb{R}^m$ , then it may be written

$$\begin{aligned}\dot{x}_j &= f(x_j) + Bu_j \\ y_j &= Cx_j\end{aligned}\tag{2.86}$$

for which  $1 \leq j \leq k$  denotes each system, and as before  $x_j \in X \subset \mathbb{R}^n$  denotes the state variable,  $u_j \in U \subset \mathbb{R}$  the input, and  $y_j \in Y \subset \mathbb{R}$  the output.

Assume  $k$  many systems are diffusively coupled where the coupling of systems is given by the matrix

$$\Gamma = \begin{bmatrix} \sum_{j=2}^k \gamma_{1j} & -\gamma_{12} & \cdots & -\gamma_{1k} \\ -\gamma_{21} & \sum_{j=1, j \neq 2}^k \gamma_{2j} & \cdots & -\gamma_{2k} \\ \vdots & \vdots & \ddots & \vdots \\ -\gamma_{k1} & -\gamma_{k2} & \cdots & \sum_{j=1}^{k-1} \gamma_{kj} \end{bmatrix}\tag{2.87}$$

for coupling strength  $\gamma_{ij}$  between systems  $i$  and  $j$ . The feedback is written in the compact matrix form

$$u = -\Gamma y.\tag{2.88}$$

It is well-established that the matrix  $\Gamma$  is positive semi-definite. This can be seen from the fact that  $\Gamma$  is constructed as the Laplacian matrix which takes the quadratic form

$$x^\top \Gamma x = \sum_{(i,j) \in E} x^\top \Gamma(i,j) x = \sum_{(i,j) \in E} \gamma_{ij} (x_i - x_j)^2\tag{2.89}$$

where  $E$  is the set of edges such that  $\gamma_{ij} > 0$  corresponds to the existence of the edge  $(i, j) \in E$ , the edge set  $E$  of the network. Hence the matrix  $\Gamma$  is positive semi-definite.

**Proposition 2.2.6.** *Consider  $k$  diffusively coupled systems of the form  $\Sigma$  (2.86) closed by the feedback (2.88). Assume also that each system is semi-passive. Then, the solutions of all connected systems are ultimately bounded.*

*Proof.* [142] Let the  $j$ -th system be semi-passive with storage function  $V(x_j)$ , where  $x_j$  is the state of the  $j$ -th system. Denote  $W(x) = \sum_{j=1}^k V(x_j)$  where  $x = \text{col}(x_1, \dots, x_k)$ . Then,

$$\dot{W}(x) = \sum_{j=1}^k \dot{V}(x_j) \leq \sum_{j=1}^k y_j^\top u_j - H(x_j) = -y^\top \Gamma y - \sum_{j=1}^k H(x_j) \leq 0,\tag{2.90}$$

outside some ball in  $\mathcal{R}^{nk}$ . Note that the quadratic term  $y^\top \Gamma y$  is nonnegative since  $\Gamma$  is semi-positive definite. This directly implies that the solutions of the interconnected systems are bounded and exist for all  $t \geq t_0$ .  $\square$

The property that any interconnection of semi-passive is also semi-passive, as shared with passive systems, naturally extends to the case of heterogeneous passive systems, i.e. non-identical dynamics. For the case of non-identical semi-passive systems interconnected, then their state trajectories remain bounded since the sum of their storage functions is simply a superposition.

Once boundedness of solutions is established, one may then consider the problem of establishing conditions guaranteeing synchronization. Recall the normal form transformation. Then, assuming each system has relative degree  $(1, \dots, 1)$ , then the matrices  $(\nabla h(x))^\top g_1(x)$  and  $(\nabla h(x))^\top g_2(x)$  are nonsingular in the neighbourhood of the origin, in this case it is the condition that the matrix  $CB$  is non-singular. Recall also the Frobenius theorem, such that if the distribution spanned by the matrix  $g(x)$  is involutive, then one can find  $n - m$  change of coordinates into the (Isidori) normal form [28].

Consider  $k$  semi-passive systems described by system  $\Sigma$  (2.86) transformed into normal form

$$\dot{z}_j = q(z_j, y_j) \quad (2.91)$$

$$\dot{y}_j = a(z_j, y_j) + b_j(z_j, y_j)u_j \quad (2.92)$$

for  $j = 1, \dots, k$ , and where functions  $q, a, b_i$  are smooth

**Theorem 2.2.7** ([142]). *Consider the  $k$  systems (2.91) and assume that:*

1. *The functions  $q, a, b_i$  ( $1 \leq i \leq m$ ) are continuous and locally Lipschitz.*
2. *Each system*

$$\begin{aligned} \dot{z}_j &= q(z_j, y_j) \\ \dot{y}_j &= a(z_j, y_j) + b_j(z_j, y_j)u_j \end{aligned}$$

*is strictly semi-passive.*

3. *There exists a  $C^2$ -smooth positive definite function  $V_0 : \mathbb{R}^m \rightarrow \mathbb{R}_+$  and a positive number  $\alpha \in \mathbb{R}$  such that the following inequality is satisfied*

$$(\nabla V_0(z_i - z_j))^\top (q(z_i, y_i) - q(z_j, y_j)) \leq -\alpha \|z_i - z_j\|^2 \quad (2.93)$$

*for any  $1 \leq i, j \leq k$  and for all  $z_i \in \mathbb{R}^m$  and  $y_i \in \mathbb{R}$ .*

4. *The matrix  $b_1(z_1, y_1) + \dots + b_m(z_m, y_m)$  is positive definite:*

$$b_1(z_1, y_1) + \dots + b_m(z_m, y_m) > 2\beta I_m, \quad \beta > 0. \quad (2.94)$$

Then for all positive semi-definite matrices  $\Gamma$  all solutions of the closed-loop system (2.91) with coupling (2.88) are ultimately bounded. Order the eigenvalues  $\lambda_i$  of  $\Gamma$  such that  $0 = \lambda_1 \leq \lambda_2 \leq \dots \leq \lambda_k$ . Then there exists a positive number  $\bar{\lambda}$  such that if  $\lambda_2 \geq \bar{\lambda}$  then there exists a globally asymptotically stable subset of the diagonal set

$$\mathcal{A} = \{y_j \in \mathbb{R}, z_j \in \mathbb{R}^m | y_i = y_j, z_i = z_j, i, j = 1, \dots, k\}. \quad (2.95)$$

Therefore, one can see that in Theorem 2.2.7 that synchronization is determined in a similar way as for the previous method, the Wu-Chua conjecture [159]. That is, the problem of determining stability of synchronization relates to two properties of the system: (i) assumptions of the individual oscillators; and (ii) the eigenvalues of the coupling configuration. One advantage of the semi-passivity argument over such other method of stability, is that it is robust to desynchronizing bifurcations. It follows that for any given network topology, for a coupling strength sufficiently strong such that  $\lambda_2$  exceeds the threshold  $\bar{\lambda}$ , then synchronization of all oscillators is guaranteed.

For the case where the input and output functions  $B$  and  $C$  are given by the functions  $g$  and  $h$ , respectively, additional conditions are required

To check whether the inequality (2.93) of Theorem (2.2.7) is satisfied, one may consider the *convergence* property of the system.

**Definition 2.2.8** (Demidovich convergence). [142; 116] Consider the system

$$\dot{z} = q(z, w(t)) \quad (2.96)$$

where the external signal  $w(t)$  is taking values from a compact set  $\mathcal{W} \subset \mathbb{R}$ . The system is said to be *convergent* if:

1. All solutions  $z(t)$  are well-defined for all  $t \in (-\infty, +\infty)$  and for all initial conditions  $z(0)$ .
2. There exists a unique globally asymptotically stable solution  $z_w(t)$  on the interval  $t \in (-\infty, +\infty)$  from which it follows that

$$\lim_{t \rightarrow \infty} \|z(t) - z_w(t)\| = 0 \quad (2.97)$$

for all initial conditions.

According to Demidovich [116] there exists a simple sufficient condition that guarantees convergence.

**Theorem 2.2.8** ([142]). *If there exists a square symmetric and positive definite matrix  $P$  such that all eigenvalues  $\lambda_i(Q)$  of the matrix symmetric  $Q$ ,*

$$Q(z, w) = \frac{1}{2} \left[ P \left( \frac{\partial q}{\partial z}(z, w) \right) + \left( \frac{\partial q}{\partial z}(z, w) \right) P \right] \quad (2.98)$$

are negative and separated from zero, i.e.  $\exists \delta > 0$  such that

$$\lambda_i(Q) \leq -\delta < 0, \quad (2.99)$$

for  $i = 1, \dots, m$  and for all  $z \in \mathbb{R}^m$ ,  $w \in \mathcal{W}$ , then the system (2.96) is convergent.

This completes the introduction of stability by semi-passivity to the extent needed for our application in Chapter 3.

## 2.2.2 Stability of periodic solutions: Basic Floquet theory

Previously we have introduced coordinate transformation of the state-space representation. Now, we consider another type of coordinate transformation, one that transforms a time-variant system into a time-invariant one. This is particularly helpful for the stability analysis of periodic solutions. The main result in this section is the introduction of the concept of *Floquet stability*, an efficient method for studying the stability of periodic solutions. For a more comprehensive description of stability analysis of periodic systems the reader is directed to the texts [36; 153; 113], from which the following section reviews.

**Definition 2.2.5.** (Poincaré Map) Consider  $\dot{x} = f(x)$  with periodic solution  $\bar{x}(t)$ . Construct an  $(n - 1)$ -dimensional transversal  $\Gamma$  to a corresponding closed orbit  $\Theta$ . Let  $a$  be the point where  $\Theta$  intersects  $\Gamma$ . For an orbit  $\phi(x_0)$  starting at  $x_0 \in \Gamma$  close to  $a$ , the phase flow with return to  $\Gamma$ . The *first return* or *Poincaré map*  $P : U \subset \Gamma \rightarrow \Gamma$  is defined by

$$P(x_0) = \phi(\tau; x_0). \quad (2.100)$$

Notice that  $a$  is a fixed point of the map  $P$ .  $P$  reduces the study of the stability of a periodic orbit  $\bar{x}(t)$  to the study of the stability of a fixed point  $a$ .

**Definition 2.2.6.** (Stability of Periodic Orbits) The periodic solution  $\bar{x}(t)$  (the closed orbit  $\Theta$ ) is *stable* if for each  $\epsilon > 0$ , there exists  $\delta$  such that

$$\|x_0 - a\| < \delta \Rightarrow \|P^n(x_0) - a\| < \epsilon. \quad (2.101)$$

**Definition 2.2.7.** The periodic solution  $\bar{x}(t)$  is *asymptotically stable* if it is stable and if there exists a  $\delta > 0$  such that

$$\|x_0 - a\| < \delta \Rightarrow \lim_{n \rightarrow \infty} P^n(x_0) = a. \quad (2.102)$$

The stability of the fixed point  $a$  may now be assessed by considering the linearisation of  $P$ . The linearisation of the discrete map  $P$  at the fixed point  $a$  is given by the matrix  $\frac{\partial P}{\partial x_0}(a)$ . If the moduli of all eigenvalues of this matrix are less than one, then the fixed point  $a$  is stable.

To construct a Poincaré map analytically is not in general an easy task. This becomes particularly difficult for high-dimensional systems, hence, for practical problems numerical methods are generally needed. Closely related to stability by the Poincaré section is *Floquet theory*, the main result of this section. Floquet theory differs from the Poincaré section in that solutions are analytical, i.e., no such transversal to the orbit need be constructed. Floquet theory is therefore not limited by the high dimension of a given system.

When one wishes to transform a periodic system into a time-invariant one, we call this the Floquet problem. For a given  $T$ -periodic system, the Floquet problem is the finding of an invertible state-space coordinate transformation such that in the new coordinates the system is time-invariant and  $T$ -periodic. In the new basis, the state after one period is described by a constant matrix. In this new basis

$$\dot{x}(t) = A(t)x(t) \quad (2.103)$$

with periodic solution  $\bar{x}(t) = \bar{x}(t+T)$ . The Floquet problem becomes finding a time-invariant  $T$ -periodic invertible state-space transformation of the form:

Consider the linear continuous and  $T$ -periodic system

$$\begin{aligned} \dot{x}(t) &= A(t)x(t) \\ x(0) &= x_0 \end{aligned} \quad (2.104)$$

where  $A(t) = A(t+T)$  is continuous over  $[0, T]$ . Under assumptions of Lipschitz continuity, the Picard-Lindelöf theorem states that a solution  $x(t)$  exists and is unique if and only if it satisfies

$$x(t) = x(0) + \int_0^t A(\tau)x(\tau)d\tau. \quad (2.105)$$

This result is achieved by a series of “Picard iterates”, which we denote as  $x_k$ , that are convergent such that the solution is the limit of the sequence. In particular, the  $k$ -th Picard iterate may be written

$$x_k(t) = x_0 + \int_{t_0}^t A(\tau)x_{k-1}(\tau)d\tau. \quad (2.106)$$

Consider the Peano-Baker series that takes the derivative of each Picard iterate in the convergent series. In doing so, the solution  $x(t)$  can be written in terms of the *state-transition matrix*

$$x(t) = \left[ I + \int_{t_0}^t A(\tau_1)d\tau_1 + \int_{t_0}^t A(\tau_1) \int_{t_0}^{\tau_1} A(\tau_2)d\tau_2d\tau_1 + \dots \right] x_0 \quad (2.107)$$

where

$$\Phi(t, t_0) := I + \int_{t_0}^t A(\tau_1)d\tau_1 + \int_{t_0}^t A(\tau_1) \int_{t_0}^{\tau_1} A(\tau_2)d\tau_2d\tau_1 + \dots \quad (2.108)$$

is the state-transition matrix. This matrix is unique, and now the solution  $x(t)$  can be written in the more compact form

$$x(t) = \Phi(t, t_0)x_0. \quad (2.109)$$

Alternatively, starting from a generic initial condition  $x(\tau)$  at time  $\tau$ , the solution is obtained as:

$$\begin{aligned} x(t) &= \Phi(t, \tau)x(\tau) \\ \Phi(\tau, \tau) &= I. \end{aligned}$$

Therefore, for any given  $\tau$ , the matrix  $\Phi(\tau, \tau)$  is the *principal fundamental matrix* which is the unique solution of the matrix initial value problem

$$\begin{aligned} \dot{x}(t) &= A(t)x(t) \\ x(\tau) &= x_0. \end{aligned}$$

It can be seen that periodicity of the system involves the double periodicity of the matrix  $\Phi(t, \tau)$  such that

$$\Phi(t + T, \tau + T) = \Phi(t, \tau). \quad (2.110)$$

Properties of the transition matrix:

1.  $\frac{\partial}{\partial \tau} \Phi(t, \tau) = -\Phi(t, \tau)A(\tau)$ .
2.  $\Phi(t, \tau) = \Phi(t, \sigma)\Phi(\sigma, \tau)$ ,  $\forall t, \tau, \sigma$ .
3.  $\Phi(t, \tau)$  is non-singular for all  $t$ , and:

$$\Phi^{-1}(t, \tau) = \Phi(\tau, t). \quad (2.111)$$

Without loss of generality, we can assume  $\tau = 0$ , and denote  $\Phi(t, t_0) = \Phi(t)$  such that

$$\dot{\Phi}(t) = A(t)\Phi(t). \quad (2.112)$$

**Lemma 2.2.3.** *If  $\Phi(t)$  is a fundamental matrix solution, then for some constant and non-singular square matrix  $B$ , the matrix  $\Upsilon(t) = \Phi(t)B$  is also a fundamental matrix solution.*

*Proof.*

$$\dot{\Upsilon}(t) = \dot{\Phi}B = A\Phi B = A\Upsilon. \quad (2.113)$$

Moreover, since the matrices  $\Phi$  and  $B$  are non-singular, then it follows that

$$(\Phi B)^{-1} = B^{-1}\Phi^{-1} = \Upsilon^{-1} \quad (2.114)$$

and so the matrix  $\Upsilon$  is also non-singular.  $\square$

**Theorem 2.2.9.** Let  $A(t)$  be a  $T$ -periodic matrix. If  $\Phi(t)$  is a fundamental matrix then so is  $\Phi(t+T)$  and there exists a non-singular matrix  $B$  such that

1.  $\Phi(t+T) = \Phi(t)B$  for all  $t$ ,
2.  $\det(B) = \exp\left(\int_0^T \text{tr}(A(s))ds\right)$ .

Since matrix  $B$  is constant then setting  $t = 0$  such that  $B = \Phi^{-1}(0)\Phi(T)$ , and taking initial conditions  $\Phi(0) = I$ , then

$$B = \Phi(T). \quad (2.115)$$

The transition matrix over one period defines an important matrix, called the *monodromy matrix*

$$\Psi(t) = \Phi(t+T, t). \quad (2.116)$$

The monodromy matrix  $\Psi(t)$  relates the value of the state at time  $t$  to the value after one period  $T$ ,

$$x(t+T) = \Psi(t)x(t). \quad (2.117)$$

The eigenvalues of the monodromy matrix are called *characteristic multipliers* and is hence a central tool in the stability analysis of periodic systems since its eigenvalues determine how perturbations of the periodic orbit grow or decay.

**Definition 2.2.9** (Characteristic multipliers and exponents). The eigenvalues  $\rho_1, \dots, \rho_n$  of  $B$  are called the *characteristic multipliers* for  $\dot{\Phi}(t) = A(t)\Phi(t)$ . The *characteristic exponents* or *Floquet multipliers* are the  $\mu_1, \dots, \mu_n$  satisfying

$$\rho_1 = \exp^{\mu_1 T}, \rho_2 = \exp^{\mu_2 T}, \dots, \rho_n = \exp^{\mu_n T}. \quad (2.118)$$

Note that  $\mu_j$  for  $j \in \mathbb{N}$  may be complex.

These characteristic multipliers satisfy the following properties:

1. For  $B = \Phi(T)$  and  $\Phi(0) = I$ ,

$$\det(B) = \rho_1 \rho_2 \cdots \rho_n = \exp\left(\int_0^T \text{tr}(A(s))ds\right). \quad (2.119)$$

2. Since the trace is the sum of the eigenvalues

$$\text{tr}(B) = \rho_1 + \rho_2 + \cdots + \rho_n. \quad (2.120)$$

3. The characteristic exponents are not unique since if  $\rho_j = \exp^{\mu_j T}$ , then  $\rho_j = \exp^{(\mu_j + 2\pi i/T)T}$ .

4. The characteristic multipliers  $\rho_j$  are an intrinsic property of the equation  $\dot{\Phi}(t) = A(t)\Phi(t)$  and do not depend on the choice of the fundamental matrix.

Consider a nonsingular matrix  $Q$ . Then there exists a complex matrix  $A_0$  such that  $Q = \exp^{A_0}$ . Moreover, the matrix  $A_0$  is not unique: for any integer  $k$ ,

$$\exp^{A_0+2\pi ikI} = \exp^{A_0} \exp^{2\pi ik} I = e^{A_0}. \quad (2.121)$$

Now, we may state the main result, the Floquet theorem. The main result here is to find a constant matrix, i.e. time invariant matrix, representation for the system dynamics.

**Theorem 2.2.10.** *If the  $T$ -periodic system  $\dot{x}(t) = A(t)x(t)$  has fundamental matrix solution  $\Phi(t, \tau)$ , then it also has as solution  $\Phi(t+T, \tau)$ . Moreover, if  $A_0$  is such that  $\Psi(\tau) = \exp^{A_0}$ , then there exists a non-singular  $T$ -periodic matrix  $P(t)$  such that*

$$\Phi(t, 0) = P(t) \exp^{A_0 t}. \quad (2.122)$$

*Proof.* Let  $\Psi(t) = \Phi(t+T)$  be the monodromy matrix. Then  $\Psi$  is also a fundamental matrix solution. It follows that there exists a non-singular and constant matrix  $B$  called the Floquet multiplier matrix such that  $\Phi(t+T) = \Phi(t)B$ . Since matrix  $B$  is non-singular, then one can find a matrix  $Q$  such that  $\exp^{TQ} = B$  for period  $T$ . Consider now the matrix  $P(t)$  defined for all  $t$  such that  $P(t) = \Phi(t) \exp^{-Qt}$ . It remains to be shown that the matrix  $P(t)$  is periodic with period  $T$ .

$$\begin{aligned} P(t+T) &= \Phi(t+T) \exp^{-Q(t+T)} = \Phi(t) \exp^{-QT} \exp^{-Qt} \\ &= \Phi(t) \exp^{-Qt} = P(t). \end{aligned}$$

□

This completes the introduction of stability analysis of periodic solutions by Floquet multipliers. In Chapter 3 we employ the use of the software *DDE-Biftool* [44], that provides numerical analysis of stability of periodic behaviour by Floquet multipliers, to the study of diffusively coupled FitzHugh-Nagumo oscillators [46] exhibiting periodic motion.

## Conclusion

In the first section we introduced core concepts on nonlinear system needed in order to study stability properties. In the second section, we reviewed some popular methods for studying the stability properties of a system of identical oscillators.

For stability of the synchronous state we described the Connection Graph Stability [12], the Wu-Chua conjecture [159], Master stability function [117], semi-passivity argument [121].

The semi-passivity argument is an extension of the classical dissipativity and passivity methods for analysing stability of synchronization [28] and generalises well to systems of non-identical oscillators. These methods, however, are limited by more complex equilibria. For stability of periodic solutions we briefly introduce Floquet theory, the attraction of solutions to a limit cycle. In the next chapter, we apply stability methods of semi-passivity and Floquet multipliers to determine regions of stability for synchronization and periodic solutions, in particular *rotating waves*.

## Chapter 3

# Small Changes In Topology May Have Big Consequences On Activity

### 3.1 Introduction

Understanding the dynamics of interconnected systems of nonlinear ordinary differential equations is arguably amongst the oldest and inspiring problems. Objects of this type occur in a broad range of fields of engineering and science [145]. Significant progress has been made in this area with regards to general laws governing the emergence of various synchronous states, see e.g. [119] and references therein; and the presence of intricate dependencies between network topologies, properties of individual nodes and dynamics in networks have now been elucidated by many authors [57; 121; 132; 120; 13; 14]. Despite this progress, however, a few fundamental questions remain, including the question, how a specific configuration of network topology and weights may affect the overall behaviour of the network. This problem is closely related to the fundamental question of how a change in network topology may influence the behaviour of systems.

This issue is critical for understanding patterns of activity [52]. It is well known that a sufficiently strong diffusive coupling will lead to synchronization in a large assemble of nonlinear systems [121]. However, it has been shown that small changes in topology can have a dramatic affect on this relation between coupling strength and synchronization: [14] showed that shortcuts in otherwise regular lattices significantly reduce the critical coupling strength needed for achieving globally asymptotically stable synchronization. Hence, networks with

shortcuts can be considered more efficient than regular ones in terms of resources spent such as the total number of connections and their strength needed to reach and maintain synchronization. Understanding the problem of how the network topology affects its dynamics is a huge theoretical and practical challenge if considered in its full generality.

In this chapter, we consider two basic and extreme network topologies which any network will contain as a subgraph: the directed chain and the directed cycle. These two configurations are closely related, differing only by one edge.

These two network motifs may constitute basic building blocks for arbitrary network topologies. On large scales, directed chains and directed cycles may take complex forms, such as large scale feedforward and feedback loops in the V1 visual processing region of the brain [93]. Feedforward connections may transfer information from one region to another, for example the transfer of visual information into behavioural responses. On the other hand, feedback loops may give rise to attentional mechanisms that go beyond the capacity of feedforward topologies, such as visual awareness.

Feedback loops are of great importance in the mammalian nervous system. Recent computational studies revealed that cycles could be important on their own for sustaining coherent oscillatory network activity [54]. Moreover, on a much smaller spatial scale, positive feedback loops are responsible for action potential generation of individual neurons. If a neuron is depolarized sufficiently to raise the membrane potential above a threshold level, a positive feedback process is initiated, and the neuron generates an action potential. Associative memory networks have been suggested as models of various parts of the mammalian brain in which there is substantial recurrent feedback, including area CA3 of the hippocampus and parts of the prefrontal cortex [85]. In reinforcement learning, the network output is not constrained by a teacher, but evaluative feedback in network performance is provided in the form of reward or punishment [146].

To better understand the role that these two simple network topologies play, we begin by first considering them in their most basic form; a system of linear equations. Then, we extend to the highly non-trivial case of coupled nonlinear systems. Finally, we finish this chapter by considering a more generalised network structure, and hence better model for natural systems, that of a directed cycle with modular subgraphs.

## 3.2 Preliminaries: Circulant matrices

First, let us introduce some basic concepts of circulant matrices that will be of use later in this chapter. Circulant matrices are on their own a special class of matrix, and carry with them a special set of properties. In particular, the main result we present is the diagonalisation

of circulant matrices. This result will aid later analysis of such graph configurations. This section is a review of [133], for which the reader is directed for a more comprehensive discussion on circulant matrices.

Consider the complex  $n$ -row vector

$$v = (v_0, \dots, v_{n-1}) \in \mathbb{C}^n$$

and define a *shift operator*  $T : \mathbb{C}^n \rightarrow \mathbb{C}^n$  by

$$T(v_0, \dots, v_{n-2}, v_{n-1}) = (v_{n-1}, v_0, \dots, v_{n-2}).$$

Then, a circulant matrix may be defined as follows.

**Definition 3.2.1.** The *circulant matrix*  $V = \text{circ}\{v\}$  associated to the vector  $v \in \mathbb{C}^n$  is the  $n \times n$  matrix whose rows are given by iterations of the shift operator acting on  $v$ ; its  $k$ -th row is  $T^{k-1}v$ ,  $k = 1, \dots, n$ :

$$V = \begin{bmatrix} v_0 & v_1 & \cdots & v_{n-2} & v_{n-1} \\ v_{n-1} & v_0 & \cdots & v_{n-3} & v_{n-2} \\ \vdots & \vdots & \ddots & \vdots & \vdots \\ v_2 & v_3 & \cdots & v_0 & v_1 \\ v_1 & v_2 & \cdots & v_{n-1} & v_0 \end{bmatrix}. \quad (3.1)$$

We denote by  $\text{Circ}(n)$  the set of all  $n \times n$  complex circulant matrices.

The ordered  $n$ -tuples of complex numbers can be viewed as the elements of the inner product space  $\mathbb{C}^n$  with the following basis. Define for  $l = 0, \dots, n-1$ ,

$$x_l = \frac{1}{\sqrt{n}}(1, \epsilon^l, \epsilon^{2l}, \dots, \epsilon^{(n-1)l}) \in \mathbb{C}^n \quad (3.2)$$

where  $\epsilon = e^{\frac{2\pi i}{n}}$  is the primitive  $n$ -th root of unity. Introduce a special case of the *Vandermonde matrix*

$$E = \frac{1}{\sqrt{n}} \begin{bmatrix} 1 & 1 & \cdots & 1 & 1 \\ 1 & \epsilon & \cdots & \epsilon^{n-2} & \epsilon^{n-1} \\ \vdots & \vdots & \ddots & \vdots & \vdots \\ 1 & \epsilon^{n-2} & \cdots & \epsilon^{(n-2)^2} & \epsilon^{(n-2)(n-1)} \\ 1 & \epsilon^{n-1} & \cdots & \epsilon^{(n-1)(n-2)} & \epsilon^{(n-1)^2} \end{bmatrix}.$$

The  $n$ -th root of unity, where  $n$  is a positive integer, satisfies  $\epsilon^n = 1$ . An  $n$ -th root of unity is *primitive* if it is not a  $k$ -th root of unity for  $k$  smaller:  $\epsilon^k \neq 1$ ,  $k = 1, 2, \dots, n-1$ . Note that the matrix  $E$  is unitary, i.e.,  $E^{-1} = \bar{E}^\top$  or  $E^*E = EE^* = I$ , where  $I$  is the identity matrix. Non-singularity of matrix  $E$  can be seen by the calculation that

$$\det E = n^{-\frac{n}{2}} \prod_{0 \leq i < j \leq n-1} (\epsilon^j - \epsilon^i) \neq 0.$$

This result is realised using the Leibniz formula for square Vandermonde matrices.

Since  $E$  is non-singular, then the  $\{x_l\}$  form an orthonormal basis for  $\mathbb{C}^n$ , to be denoted by  $\mathbf{x}$ .

**Definition 3.2.2.** The (polynomial in the indeterminate  $X$ ) *representer*  $P_V$  of the circulant matrix  $V$  is

$$P_V(X) = \sum_{i=0}^{n-1} v_i X^i.$$

**Theorem 3.2.1.** If  $v = (v_0, \dots, v_{n-1}) \in \mathbb{C}^n$  and  $V = \text{circ}\{v\}$ , then

$$\det V = \prod_{t=0}^{n-1} \left( \sum_{j=0}^{n-1} \epsilon^{jt} v_j \right) = \prod_{l=0}^{n-1} P_V(\epsilon^l).$$

*Proof.* We view the matrix  $V$  as a self-map  $V_{\mathbf{e}, \mathbf{e}}$  of  $\mathbb{C}^n$ . For each integer  $l$ ,  $0 \leq l \leq n-1$ , let

$$\lambda_l = v_0 + \epsilon^l v_1 + \dots + \epsilon^{(n-1)l} v_{n-1} = P_V(\epsilon^l).$$

A calculation shows that  $Vx_l = \lambda_l x_l$ . Thus  $\lambda_l$  is an eigenvalue of  $V$  with normalised eigenvector  $x_l$ . Since, by ref eq,  $\{x_0, x_1, \dots, x_{n-1}\}$  is a linearly independent set of vectors in  $\mathbb{C}^n$ , the diagonal matrix with the corresponding eigenvalues is conjugate to  $V$  and we conclude that  $\det V = \prod_{l=0}^{n-1} \lambda_l$ .  $\square$

**Corollary 3.2.1.** All circulant matrices have the same ordered set of orthonormal eigenvectors  $\{x_l\}$ .

Now we reach the main result of this section, diagonalisation of circulant matrices.

**Theorem 3.2.2.** All elements of  $\text{Circ}(n)$  are simultaneously diagonalised by the unitary matrix  $E$ ; that is, for  $V$  in  $\text{Circ}(n)$ ,

$$E^{-1}VE = D_V \tag{3.3}$$

is a diagonal matrix and the resulting map

$$\mathcal{D} : \text{Circ}(n) \rightarrow \mathbb{D}_n$$

is a  $\mathbb{C}$ -algebra isomorphism and where  $\mathbb{D}_n$  is the space of all diagonal matrices.

*Proof.* The  $n \times n$  matrix  $E$  represents the linear automorphism of  $\mathbb{C}^n$  that sends the unit vector  $e_l$  to the unit vector  $x_l$ , where  $e_l$  is the *standard orthonormal basis*;  $e_i = (\delta_{i,0}, \dots, \delta_{i,n-1})$ ,  $0 \leq i \leq n-1$ , where  $\delta_{i,j}$  is the *Kronecker delta*. If  $V$  is a circulant matrix, and  $D_V$  is the diagonal matrix with entries given by the ordered eigenvalues of  $V$ :  $\lambda_0, \dots, \lambda_{n-1}$ , then (3.3) holds.  $\square$

**Corollary 3.2.2.** *The inverse of an invertible element of  $\text{Circ}(n)$  also belongs to  $\text{Circ}(n)$ .*

*Proof.* If  $V$  is a non-singular circulant matrix, then  $D_V$  is invertible, and  $D_V^{-1} = D_{V^{-1}}$ .  $\square$

### 3.3 Leaders do not look back, or do they?

To begin, we study the points of equilibria of the two configurations in their linear form. A system of linear first-order differential equations used to describe a dynamical system allows for the calculation of the eigenvalues and eigenvectors. Points of equilibrium correspond to eigenvectors associated with the zero eigenvalue. The number of points of equilibria is equal to the multiplicity of the zero eigenvalue. The eigenvalues of such systems describe stability of points of equilibrium, and moreover, the rate at which solutions decay or grow towards or from solutions of equilibrium.

#### 3.3.1 Minimal properties of the directed chain

The simple chain is the configuration of  $n$  systems and  $n - 1$  edges, where each system has directed edge to the next, i.e., system  $i$  has directed edge to system  $i + 1$  for  $i = 1, \dots, n - 1$ . For the case of  $n$  finitely many systems coupled with arbitrary weights  $q_{ij} > 0$ ,  $q_{ij} \in \mathbb{R}$ , the system has a single asymptotically stable equilibrium. The first eigenvalue is zero, with multiplicity one, all other eigenvalues are negative.

**Theorem 3.3.1.** *Let  $T_n$  be a lower triangular matrix of order  $n$ ,*

$$T_n = \begin{pmatrix} a_{11} & 0 & \cdots & 0 \\ a_{21} & a_{22} & \ddots & \vdots \\ \vdots & & \ddots & 0 \\ a_{n1} & \cdots & & a_{nn} \end{pmatrix}. \quad (3.4)$$

*Then, the determinant of matrix  $T_n$  is equal to the entries along the main diagonal of  $T_n$ ,*

$$\det(T_n) = \prod_{i=1}^n a_{ii}. \quad (3.5)$$

To prove this results, first we must introduce the definition of a cofactor expansion of a matrix determinant and how this relates to triangular matrices

**Definition 3.3.1.** (Cofactor) Let  $A$  be a square  $n \times n$  matrix with entries  $(a_{ij})$  for  $1 \leq i, j \leq n$ . Denote  $M_{ij}$  as the minor matrix obtained by deleting the  $i$ -th row and  $j$ -th column of matrix  $A$ . Then, the  $i, j$ -th cofactor of matrix  $A$  is,

$$C_{ij} = (-1)^{i+j} a_{ij} \det(M_{ij}). \quad (3.6)$$

Using this definition, the determinant of matrix  $A$  can be expressed by the sum of cofactors

$$\det(A) = \sum_{j=1}^n C_{1j} = \sum_{i=1}^n C_{i1}. \quad (3.7)$$

For (lower) triangular matrix  $T_n$ , this becomes

$$\det(A) = C_{11} \quad (3.8)$$

since  $C_{1j} = 0$  for all  $j > 1$ .

**Lemma 3.3.1.** *For the  $i$ -th row (or  $j$ -th column), the determinant of lower (or upper) triangular matrix  $T_n$  is  $C_{ii}$  (or  $C_{jj}$ ).*

*Proof.* Theorem (3.3.1) is proven by method of induction.

Begin by taking the base case for  $n = 2$ ,

$$T_n = \begin{pmatrix} a_{11} & 0 \\ a_{21} & a_{22} \end{pmatrix}$$

and so

$$\det(T_2) = a_{11}a_{22}.$$

For finite and arbitrary  $n$ , assume that

$$\det(T_n) = \prod_{i=1}^n a_{ii}.$$

To take the inductive step, expand matrix  $T_n$  across the  $(n+1)$ -th row so that,

$$T_{n+1} = \left[ \begin{array}{ccc|c} & & & 0 \\ & [T_n] & & \vdots \\ & & & 0 \\ \hline a_{(n+1)1} & \cdots & a_{(n+1)n} & a_{(n+1)(n+1)} \end{array} \right]$$

Using the cofactor expansion to express the determinant of matrix  $T_{n+1}$ , and using Lemma (3.3.1), then

$$\begin{aligned} \det(T_{n+1}) &= \sum_{i=1}^{n+1} C_{i(n+1)} = C_{(n+1)(n+1)} \\ &= (-1)^{2(n+1)} a_{(n+1)(n+1)} \det(M_{(n+1)(n+1)}) \\ &= a_{(n+1)(n+1)} \det(T_n) \end{aligned} \quad (3.9)$$

□

Using Theorem (3.3.1), we can easily determine the eigenvalues of matrix  $K$ , where  $K$  is the directed chain. The characteristic polynomial of matrix  $K$  is

$$\det(K - \lambda I) = \prod_{i=1}^n (q_{ii} - \lambda).$$

Therefore, the first eigenvalue is zero, since  $q_{11} = 0$ , and all other eigenvalues are negative (and real), since  $q_{ii} < 0$  for  $i = 2, \dots, n$ . Hence, for all initial conditions, the states of all systems asymptotically converge to the state of system leading system.

### 3.3.2 Extremal properties of the directed cycle

The case of the directed cycle is much less trivial than the directed chain. Indeed, there is a small change in topology from the simple chain; it is the closure of the chain by the addition of an edge from the  $n$ -th vertex to the first. It is defined as a closed walk with no repetitions of vertices and edges, other than the starting (and ending) vertex. However, by no means does it lead to a small change in the stability properties of the equilibria. In this section recall the work presented in [61], in which all linear systems satisfying a simple condition are considered. All original Figures and proofs can be found in [61; 60]. In doing so, it is shown that the directed cycle with equal weights, referred to as the *simple cycle*, exhibits extremal behaviour, contrary to the asymptotic stability of the directed chain. In particular, for all matrices satisfying the condition that its column sums are all zeros, the simple cycle has the slowest decay of oscillations, i.e. perturbations take the longest time to decay. An important consequence of this extremal property of the simple cycle is that not only transients in the cycle decay very slowly but also that the overall behaviour of transients becomes extremely sensitive to perturbations.

Consider the following system of linear first-order differential equations

$$\dot{P} = KP \tag{3.10}$$

where  $P = \text{col}(p_1, p_2, \dots, p_n) \in \mathbb{R}^n$ , and a matrix  $K = (k_{ij})$ , where

$$k_{ij} = \begin{cases} q_{ij} & \text{if } i \neq j \\ -\sum_{m, m \neq i} q_{mi} & \text{if } i = j. \end{cases}, \tag{3.11}$$

Off-diagonal entries  $k_{ij}$ ,  $i \neq j$ , of  $K$  represent connection weights, from agent  $j$  to agent  $i$  in the network. The matrix  $K$  is also related to the Laplacian matrix for an associated directed adjacency matrix. Denote  $D_{\text{in}}$  as the diagonal matrix of in-degrees, such that  $D_{ii} = \sum_j a_{ij}$ , we then define the Laplacian matrix of an associated directed matrix as,

$$L = D_{\text{in}} - A. \tag{3.12}$$

Thus, for an associated directed network,  $L = -K^\top$ .

System (3.10) is known as the *master equation* and is commonly used to describe the temporal evolution of first-order kinetic systems with finite number of states. In this case the variables  $p_i$  can represent *concentration*, *probability*, or *population* of these states, in other words, a first-order differential equation that describes the probability that a system will occupy one of its states at time  $t$ .

Consider the simple simplex

$$\Delta_n = \left\{ P \mid p_i \geq 0, \sum_i p_i = 1 \right\}. \quad (3.13)$$

$\Delta_n$  is forward invariant under the dynamics (3.10) as it preserves non-negativity and observes the ‘‘conservation law’’  $\sum_i p_i = \text{constant}$ , following from the fact that  $K$  has zero column sums. Therefore, any solution  $P(\cdot; t_0, P_0)$  of (3.10) starting from  $P_0 = P(t_0) \in \Delta_n$  remains in  $\Delta_n$  for all  $t \geq t_0$ . This invariance can be used to prove certain important properties of  $K$  and its associated system (3.10), such as the existence of an equilibrium  $P^*$ .

Let  $\Phi : \Delta \rightarrow \Delta$  be a continuous mapping from  $\Delta$  to itself. According to *Brouwer’s Fixed Point Theorem*, every continuous function from a convex subset of a Euclidean space onto itself, has a fixed point [131]. Therefore, since  $\Delta$  is compact and convex, then there exists a point  $P^*$  such that  $P^*(t) = P^*(t_0)$  for all  $t \geq t_0$ .

Also, forward invariance of  $\Delta$ , in combination with fixed point  $P^*$ , asserts the existence of a zero eigenvalue. This is shown by contradiction.

**Lemma 3.3.2.** *Matrix  $K$  has a leading zero eigenvalue  $\lambda$ , i.e., eigenvalue  $\lambda$  is not purely imaginary.*

*Proof.* Using Gershgorin’s circle theorem, all eigenvalues of matrix  $K$  are contained within the union of discs  $D_i$ , where discs are defined by,

$$D_i = \{ \lambda \in \mathbb{C} \mid \| \lambda - q_{ii} \| \leq \sum_{j \neq i} |q_{ji}| \}. \quad (3.14)$$

Since matrix  $K$  has zero column sums, then,

$$\sum_{j \neq i} |q_{ji}| = |q_{ii}|, \quad i = 1, \dots, n,$$

and so we can locate the eigenvalues to be contained within the discs

$$D_i = \{ \lambda \in \mathbb{C} \mid \| \lambda - q_{ii} \| \leq |q_{ii}| \}. \quad (3.15)$$

Since off-diagonal entries of matrix  $K$  are all nonnegative,  $q_{ij} \geq 0$  for all  $i \neq j$ , then it follows that the largest eigenvalue to be contained within the union of discs  $D_i$  is  $\lambda_0 = 0$ .

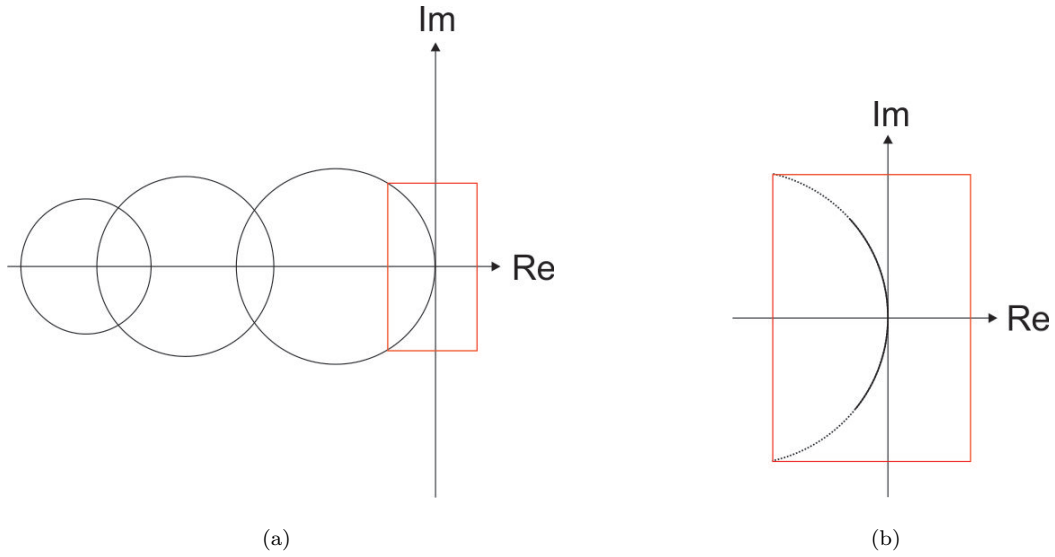


Figure 3.1: The imaginary axis (Im) in the vertical, and the real axis (Re) in the horizontal. (a) Example of Gershgorin discs where the maximum eigenvalue is zero. (b) Zoom of (a).

Moreover, assuming  $K$  is irreducible (i.e. it is strongly connected, the Perron-Frobenius theorem asserts that eigenvalue  $\lambda_0$  is unique. Therefore, all Gershgorin discs are contained in the left half-plane, with one disc touching the imaginary axis at zero, as shown in Figure 3.3.2. Therefore, there cannot exist any purely imaginary eigenvalues.  $\square$

Alternately, this result can also be deduced from the forward invariance of  $\Delta_n$  in combination with the assumption of a positive equilibrium  $P^*$ .

*Proof.* Assuming no zero eigenvalue, hence exclude its corresponding eigenvector. Then, consider  $K$  on the invariant hyperplane  $\sum_i p_i = 0$ . If  $K$  has a purely imaginary eigenvalue  $\lambda$ , then there exists a 2D  $K$ -invariant subspace  $U$ , such that in this subspace  $K$  has two conjugated eigenvalues,  $\lambda$  and  $\bar{\lambda} = -\lambda$ . Restriction of  $\exp(tK)$  on  $U$  is a one parametric group of rotations. For the positive equilibrium  $P^*$  the intersection  $(U + P^*) \cap \Delta$  is a convex polygon. It is forward invariant with respect to (3.10) since  $U$  is invariant,  $P^*$  is an equilibrium and  $\Delta$  is forward invariant. However, a polygon in a plane cannot be invariant to the one-parametric semigroup of rotations  $\exp(tK)$  ( $t \geq 0$ ). This contradiction proves the absence of purely imaginary eigenvalues.  $\square$

**Theorem 3.3.2.** *For every nonzero eigenvalue  $\lambda$  of matrix  $K$*

$$\frac{|\Im\lambda|}{|\Re\lambda|} \leq \cot \frac{\pi}{n}. \quad (3.16)$$

As this theorem is central to the results of this chapter, the proof, as originally stated in [60; 61] is also included here for the benefit of the reader; understanding the following proof will aid in understanding the underlying mechanisms for the main results of this chapter.

*Proof.* Let us assume that system (3.10) has a positive  $P^* \in \Delta_n$ : for all  $i = 1, \dots, n$ ,  $p_i^* > 0$  and

$$\sum_j q_{ij} p_j^* = \sum_i q_{ji} p_i^*. \quad (3.17)$$

Systems with non-negative equilibria may be considered as limits of the systems with positive equilibria.

Let  $\lambda$  be a complex eigenvalue of  $K$  and let  $U$  be a 2D real subspace of the hyperplane  $\sum_i p_i = 0$  that corresponds to the pair of complex conjugated eigenvalues  $(\lambda, \bar{\lambda})$ . Let us select a coordinate system in the plane  $U + P^*$  with the origin at  $P^*$  such that restriction of  $K$  on this plane has the following matrix

$$\mathcal{K} = \begin{bmatrix} \Re\lambda & -\Im\lambda \\ \Im\lambda & \Re\lambda \end{bmatrix}. \quad (3.18)$$

In this coordinate system, the solution of (3.10) is

$$P^* = \exp(t\mathcal{K})P_0^* \quad (3.19)$$

where

$$\exp(t\mathcal{K}) = \begin{bmatrix} \Re \cos(t\Im\lambda) & -\Im \sin(t\Im\lambda) \\ \Im \sin(t\Im\lambda) & \Re \cos(t\Im\lambda) \end{bmatrix}. \quad (3.20)$$

The intersection  $\mathcal{A} = (U + P^*) \cap \Delta_n$  is a polygon. Since  $\Delta_n$  has  $n$  faces, each face  $(n - 2)$ -dimensional, then  $\mathcal{A}$  has no more than  $n$  sides.

Let the polygon  $\mathcal{A}$  have  $m$  vertices  $v_j$  for  $j = 1, \dots, m$ . Move the origin of  $\mathcal{A}$  to  $P^*$  and enumerate anti-clockwise the vectors  $x_i = v_i - P^*$  Figure (3.2). Each pair of vectors  $x_i, x_{i+1}$  modulo  $m$  form a triangle with angles  $\alpha_i, \beta_i$ , and  $\gamma_i$ , where  $\beta_i$  is the angle between  $x_i$  and  $x_{i+1}$ , modulo  $m$ .

The Sine theorem provides the relation of angles

$$\frac{|x_i|}{\sin \alpha_i} = \frac{|x_{i+1}|}{\sin \gamma_i} \quad (3.21)$$

modulo  $m$ .

Several elementary identities and inequalities hold:

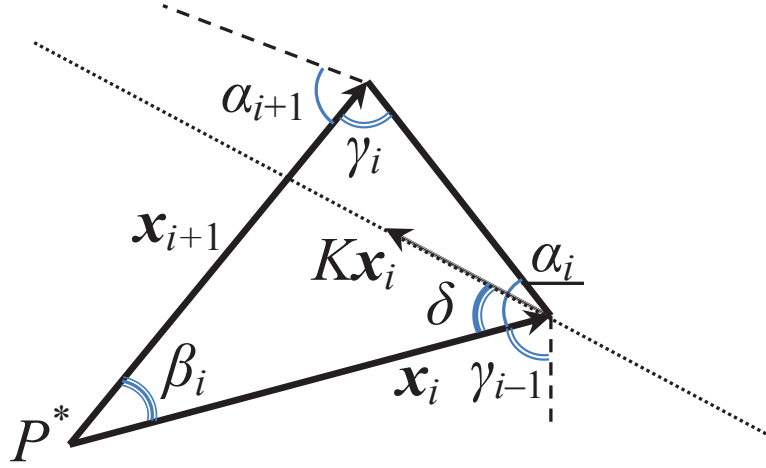


Figure 3.2: The polygon  $\mathcal{A}$  is presented as a sequence of vectors  $\mathbf{x}_i$ . The angle  $\beta_i$  between vectors  $\mathbf{x}_i$  and  $\mathbf{x}_{i+1}$  and the angles  $\alpha_i$  and  $\gamma_i$  of the triangle with sides  $\mathbf{x}_i$  and  $\mathbf{x}_{i+1}$  are shown. In the Figure, rotation goes anticlockwise, i.e.  $\Im\lambda < 0$ . In this case, the polygon  $\mathcal{A}$  is invariant with respect to the semigroup  $\exp(t\mathcal{K})$  ( $t \geq 0$ ) if and only if  $\delta \leq \alpha_i$  for all  $i = 1, \dots, m$ , where  $\delta$  is the angle between the vector field  $\mathcal{K}\mathbf{x}$  and the radius-vector  $\mathbf{x}$ .

$$0 < \alpha_i, \beta_i, \gamma_i < \pi; \sum_i \beta_i = 2\pi; \alpha_i + \beta_i + \gamma_i = \pi;$$

$$\prod_i \sin \alpha_i = \prod_i \sin \gamma_i \quad (\text{the closeness condition}) \quad (3.22)$$

These conditions (3.22) are necessary and sufficient for the existence of a polygon  $\mathcal{A}$  with these angles which is star-shaped with respect to the origin.

A star-shaped polygon is a polygonal region in the plane that contains a point from which the entire polygon boundary is visible: there exists a point  $z$  such that for each point  $p$  of  $\mathcal{A}$  the segment  $zp$  lies entirely within  $\mathcal{A}$ . The set of all points  $z$  with this property (that is, the set of points from which all of  $\mathcal{A}$  is visible) is called the kernel of  $\mathcal{A}$ .

Let us consider anticlockwise rotation ( $\Im\lambda < 0$ , Figure (3.2)). The case of clockwise rotation differs only in notations. For the angle  $\delta$  between  $\mathcal{K}x_i$  and  $x_i$ ,  $\sin \delta = -\Im\lambda$ ,  $\cos \delta = -\Re\lambda$ , and  $\tan \delta = \frac{\Im\lambda}{\Re\lambda}$ .

For each point  $\mathbf{x} \in U + P^*$  ( $\mathbf{x} \neq P^*$ ), the straight line  $\{\mathbf{x} + \epsilon\mathcal{K}\mathbf{x} \mid \epsilon \in \mathbb{R}\}$  divides the plane  $U + P^*$  in two half-plane (Fig. 3.2, dotted line). Direct calculation shows that the semi-trajectory  $\{\exp(t\mathcal{K})\mathbf{x} \mid t \geq 0\}$  belongs to the same half-plane as the origin  $P^*$  does. Therefore, if  $\delta \leq \alpha_i$  for all  $i = 1, \dots, m$  then the polygon  $\mathcal{A}$  is forward-invariant with respect to the semigroup  $\exp(t\mathcal{K})$  ( $t \geq 0$ ). If  $\delta > \alpha_i$  for some  $i$  then for sufficiently small  $t > 0$   $\exp(t\mathcal{K})\mathbf{x}_i \notin \mathcal{A}$  because  $\mathcal{K}\mathbf{x}_i$  is the tangent vector to the semi-trajectory at  $t = 0$ .

Thus, the polygon  $\mathcal{A}$  is forward-invariant with respect to the semigroup  $\exp(t\mathcal{K})$  ( $t \geq 0$ ) if and only if  $\delta \leq \alpha_i$  for all  $i = 1, \dots, m$ . The maximal  $\delta$  for which  $\mathcal{A}$  is still forward-invariant is  $\delta_{\max} = \min_i\{\alpha_i\}$ . We have to find the polygon with  $m \leq n$  and the maximal value of  $\min_i\{\alpha_i\}$ . Let us prove that this is a regular polygon with  $n$  sides. Let us find the maximizers  $\alpha_i, \beta_i, \gamma_i$  ( $i = 1, \dots, m$ ) for the optimization problem:

$$\min_i\{\alpha_i\} \rightarrow \max \text{ subject to conditions (3.22)}. \quad (3.23)$$

The solution of this problem is that all  $\alpha_i$  are equal. To prove this equality, observe that  $\min_i\{\alpha_i\} < \frac{\pi}{2}$  under conditions (3.22) (if all  $\alpha_i \geq \frac{\pi}{2}$  then the polygonal chain  $\mathcal{A}$  cannot be closed). Let  $\min_i\alpha_i = \alpha$ . Let us substitute in (3.22) the variables  $\alpha_i$  which take this minimal value by  $\alpha$ . The derivative of the left hand part of the last condition in (3.22) with respect to  $\alpha$  is not zero because  $\alpha < \frac{\pi}{2}$ . Assume that there are some  $\alpha_j > \alpha$ . Let us fix the values of  $\beta_i$  ( $i = 1, \dots, m$ ). Then  $\gamma_i$  is a function of  $\alpha_i$ ,  $\gamma_i = \pi - \beta_i - \alpha_i$ . We can use the implicit function theorem to increase  $\alpha$  by a sufficiently small number  $\varepsilon > 0$  and to change the non-minimal  $\alpha_j$  by a small number too,  $\alpha_j \mapsto \alpha_j - \theta$ ;  $\theta = \theta(\varepsilon)$ . Therefore, at the solution of (3.23) all  $\alpha_j = \alpha$  ( $j = 1, \dots, m$ ).

Now, let us prove that for solution of the problem (3.23) all  $\beta_i$  are equal. We exclude  $\gamma_i$  from conditions (3.22) and write  $\beta_i + \alpha < \pi$ ;  $0 < \beta_i, \alpha$ ;

$$m \log \sin \alpha = \sum_i \log \sin(\beta_i + \alpha). \quad (3.24)$$

Let us consider this equality as equation with respect to unknown  $\alpha$ . The function  $\log \sin x$  is strictly concave on  $(0, \pi)$ . Therefore, for  $x_i \in (0, \pi)$

$$\log \sin \left( \frac{1}{m} \sum_{i=1}^m x_i \right) \geq \frac{1}{m} \sum_{i=1}^m \log \sin x_i$$

and the equality here is possible only if all  $x_i$  are equal. Let  $\alpha^* \in (0, \pi/2)$  be a solution of (3.24). If not all the values of  $\beta_i$  are equal and we replace  $\beta_i$  in (3.24) by the average value,  $\beta = \frac{2\pi}{m}$ , then the value of the right hand part of (3.24) increases and  $\sin \alpha^* < \sin(\beta + \alpha^*)$ . If we take all the  $\beta_i$  equal then (3.24) transforms into elementary trigonometric equation  $\sin \alpha = \sin(\beta + \alpha)$ . The solution  $\alpha$  of equation (3.24) increases when we replace  $\beta_i$  by the average value:  $\alpha > \alpha^*$  because  $\sin \alpha^* < \sin(\beta + \alpha^*)$ ,  $\alpha \in (0, \pi/2)$  and  $\sin \alpha$  monotonically increases on this interval. So, for the maximizers of the conditional optimization problem (3.23) all  $\beta_i = \frac{2\pi}{m}$  and  $\alpha_i = \gamma_i = \frac{\pi}{2} - \frac{\pi}{m}$ . The maximum of  $\alpha$  corresponds to the maximum of  $m$ . Therefore,  $m = n$ . Finally,  $\max\{\delta\} = \frac{\pi}{2} - \frac{\pi}{n}$  and

$$\max \left\{ \frac{|\Im \lambda|}{|\Re \lambda|} \right\} = \cot \frac{\pi}{n}.$$

□

**Remark 3.3.1.** It is important to note that the bound given in Theorem 3.3.2 is sharp. Indeed, let  $K$  define a directed cycle with uniform weights  $q$ , e.g.

$$K = \begin{pmatrix} -q & 0 & 0 & \cdots & 0 & q \\ q & -q & 0 & \cdots & 0 & 0 \\ 0 & \ddots & \ddots & \ddots & \vdots & \vdots \\ \vdots & \ddots & \ddots & \ddots & 0 & 0 \\ 0 & & \ddots & q & -q & 0 \\ 0 & 0 & \cdots & 0 & q & -q \end{pmatrix}.$$

The eigenvalues of  $K$  are

$$\lambda_k = -q + q \exp\left(\frac{2\pi ki}{n}\right), \quad k = 0, 1, \dots, n-1,$$

cf. [37], with  $i = \sqrt{-1}$  the imaginary unit. Thus  $\lambda_1 = \cot \frac{\pi}{n}$ . Note that for large  $n$ ,

$$\cot \frac{\pi}{n} \approx \frac{n}{\pi},$$

which means that oscillations in a simple cycle with a large number of systems decay very slowly.

An important consequence of this extremal property of a simple cycle is that not only transients in the cycle decay very slowly but also that the overall behaviour of transients becomes extremely sensitive to perturbations. This, as we show in the next sections, gives rise to resonances and bistabilities if neutrally stable nodes in (3.10) are replaced with the ones exhibiting oscillatory dynamics.

## Coupled nonlinear oscillators

Linear systems give valuable insight into the local behaviour of nonlinear systems. However, they remain an approximation. Unlike linear systems, a nonlinear system may have multiple equilibrium points, some of which may be stable and some unstable. In this section we consider the problem of nonlinear oscillators coupled in the directed chain and directed cycle configurations. Indeed, the linear systems predict well the stability of equilibria in each configuration. However, as we will discuss in this section, the nonlinearity of individual oscillators can give rise to more complex solutions than described by linear systems. In particular, this section demonstrates that small changes in topology - the addition of a single edge - can give rise to entirely different solutions, and even multi-stability. In this section we review the work presented in [61]. From here on, we use as nonlinear oscillators the FitzHugh-Nagumo (FHN) neuron. The FHN neuron is one of the simplest models of spiking

dynamics of a neuron; a generalization of the Van der Pol oscillator and a two-dimensional reduction of the Hodgkin-Huxley model of spike generation in squid giant axons. The model is given by the following set of differential equations

$$\begin{cases} \dot{z}_j = \alpha(y_j - \beta z_j) \\ \dot{y}_j = y_j - \gamma y_j^3 - z_j + u_j, \end{cases} \quad (3.25)$$

$j = 1, 2, \dots, n$  with parameters  $\alpha, \beta, \gamma$  chosen as

$$\alpha = \frac{8}{100}, \quad \beta = \frac{8}{10}, \quad \gamma = \frac{1}{3}.$$

In the FHN model, the variables have no direct physiological interpretation. However, for the parameters that we use, as stated above, the qualitative behaviour of the  $y$  and  $z$  dynamics are similar to that of the voltage and gating variables, respectively, in the Hodgkin-Huxley equations.

Networks are constructed by diffusively coupling the FHN neurons

$$u_j = \sigma \sum_{l=1}^n q_{jl}(y_l - y_j) \quad (3.26)$$

with constant  $\sigma \in \mathbb{R}$ ,  $\sigma > 0$ , being the coupling strength. For convenience, let

$$y = (y_1, \dots, y_n), \quad u = (u_1, \dots, u_n), \quad x = (y, z),$$

and  $x(\cdot; x_0, \sigma)$  denote a solution of the coupled system with the coupling strength  $\sigma$  and satisfying the initial condition  $x(0) = x_0$ . The topology of network connections in (3.26) is characterized by adjacency matrix  $A$ , with entries  $q_{ij}$ . We consider two configurations, the simple chain - the directed chain with all connection weights equal to one - and the simple cycle - the directed cycle with all connection weights equal to one. We assume the interaction weights  $q_{jl}$  to be identical and, without loss of generality, we have set these weights of interaction to 1. Consider the case of the simple cycle, then the adjacency matrix appears as

$$A = \begin{pmatrix} 0 & 0 & \cdots & 0 & 1 \\ 1 & 0 & \cdots & 0 & 0 \\ 0 & 1 & \ddots & \vdots & \vdots \\ \vdots & \ddots & \ddots & 0 & 0 \\ 0 & \cdots & 0 & 1 & 0 \end{pmatrix}.$$

At the first glance, the connectivity pattern specified by  $A$  differs from that specified by matrix  $K$  in (3.11). Yet, if coupling (3.26) is rewritten in the vector-matrix notation then the following identity holds

$$u = \sigma(A - I_n)y \triangleq -\sigma Ly. \quad (3.27)$$

As remarked before, the network Laplacian matrix

$$L = \text{Diag} \left( \sum_{j \neq l} q_{jl} \right) - A = I_n - A$$

relates to  $K$  as  $L = K^T$ .

In what follows we will employ the notions of *semi-passivity* and *strict semi-passivity* as first reported in [121] and described in Chapter 2.2.

### 3.3.3 Synchronization in the simple chain

The simple behaviour of the simple chain investigated for linear first-order differential equations is extended to the more general case of nonlinear systems. We show that the property of a single asymptotically stable equilibrium is satisfied for sufficiently strong coupling.

#### Boundedness of solutions in coupled system

For the case of finitely many systems, coupled in the directed chain configuration, we show that solutions are bounded by the invariant box argument. Consider the box  $B_{z,y} = \{y, z \in \mathbb{R} \mid |z| \leq \frac{15}{8}\sqrt{3}, |y| \leq \frac{3}{2}\sqrt{3}\}$ . Denote these bounds as  $|y| \leq b_y$  and  $|z| \leq b_z$ . It can easily be calculated that at the boundaries of this box, for all coupling strengths  $\sigma > 0$ , the vectorfield of the system does not point outward. Therefore, the box is a positively invariant set, i.e. solutions of the coupled system starting within the box never leave.

In Figure 3.3, the phase portrait and corresponding nullclines for the FHN dynamics of a single neuron are shown within the invariant box  $B_{z,y}$ . At the boundaries of  $B_{z,y}$  black arrows point inward; the vector field does not point outward, it is forward invariant. This can be shown by assessing the vector field at the boundaries. Forward invariance is guaranteed if the following are satisfied:

$$\begin{aligned} \dot{z}(b_z, |y| \leq b_y) &\leq 0 \\ \dot{z}(-b_z, |y| \leq b_y) &\geq 0 \\ \dot{y}(|z| \leq b_z, b_y) &\leq 0 \\ \dot{y}(|z| \leq b_z, -b_y) &\geq 0. \end{aligned}$$

Consider the "top" of the box, i.e., upper boundary on  $z$ :

$$\dot{z}(b_z, |y| \leq b_y) = \alpha(y - \beta b_z) \leq 0 \tag{3.28}$$

is satisfied for

$$y \leq \beta b_z = \frac{3}{2}\sqrt{3} = b_y. \tag{3.29}$$

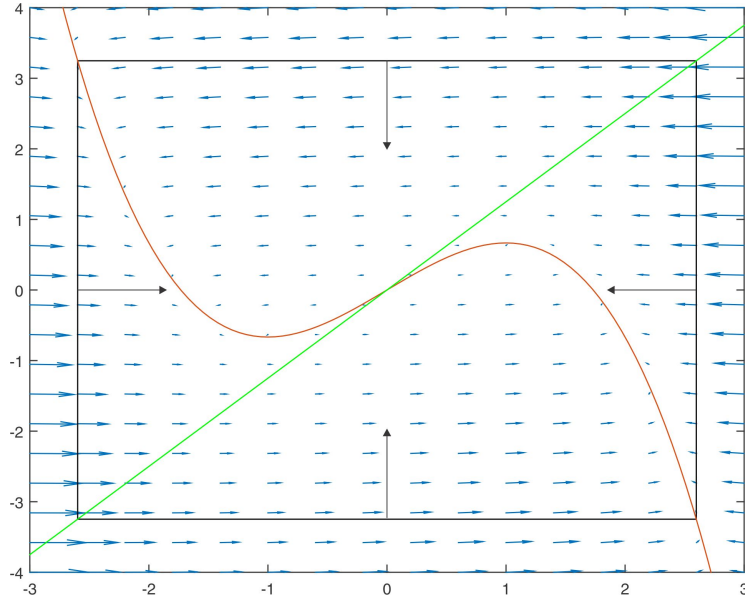


Figure 3.3: In blue are the vectors of the phase portrait; the trajectories of the system  $(\dot{z}, \dot{y})$  for initial conditions taken over a discrete grid. In red the  $z$  nullclines:  $z = \frac{1}{\beta}y$ . In green the  $y$  nullcline:  $z = y - \gamma y^3$ . In black the box  $B_{z,y} = \{y, z \in \mathbb{R} \mid |z| \leq \frac{15}{8}\sqrt{3}, |y| \leq \frac{3}{2}\sqrt{3}\}$  for which the system  $(\dot{z}, \dot{y})$  is forward invariant.

Moreover, inside the box, i.e., not including the boundaries, the vector field points away from the boundary, i.e., the vector field is strictly negative,  $\dot{z} < 0$ . Forward invariance of the box  $B_{z,y}$  is assured by repeating this for the other boundaries.

This result is easily extended to the system of two coupled FHN neurons in the directed chain configuration. Consider the dynamics of two coupled systems in the leader-follower configuration:

$$\begin{cases} \dot{z}_1 = \alpha(y_1 - \beta z_1) \\ \dot{y}_1 = y_1 - \gamma y_1^3 - z_1 \end{cases} \quad (3.30)$$

$$\begin{cases} \dot{z}_2 = \alpha(y_2 - \beta z_2) \\ \dot{y}_2 = y_2 - \gamma y_2^3 - z_2 + \sigma(y_1 - y_2) \end{cases} \quad (3.31)$$

$$(3.32)$$

As coupling is only in the  $y$  variable, we need only show that trajectories of the coupled system  $y_2$  are bounded from the right and left of  $B_{z,y}$ . The following must be satisfied:

$$\begin{aligned}\dot{y}_2(|z| \leq b_z, b_y) &\leq 0 \\ \dot{y}_2(|z| \leq b_z, -b_y) &\geq 0.\end{aligned}$$

Assuming system  $(y_1, z_1)$  begins inside the box  $B_{z,y}$ , then for  $\sigma > 0$ ,

$$\dot{y}_2(z, b_y) = (1 - \sigma)b_y - \gamma b_y^3 - z + \sigma y_1 \leq 0 \quad (3.33)$$

is satisfied for  $|z| \leq b_z$ . Similarly for the lower boundary on  $y$ ,  $y \geq -b_y$ ,  $\dot{y}_2 \geq 0$ .

The semi-passivity argument introduced earlier, and which we employ in the next section, cannot be applied to the directed chain. The reason for this, is that the directed chain is not strongly connected. Whereas the semi-passivity argument proves ultimate boundedness, i.e. convergence to some compact set, the invariant box argument does not guarantee convergence, only that solutions are bounded within. One advantage of the invariant box argument, however, is that it needs no assumption on network topology. Therefore, we can extend the property of boundedness to infinitely many systems, but this serves no purpose here.

### Sufficient conditions for synchronization

First we consider the dynamics of two coupled systems in the leader-follower configuration as described in Equation (3.30).

**Theorem 3.3.1.** *Consider the system of coupled FHN oscillators (3.30) in which the parameter  $\sigma$  is chosen so that*

$$\sigma > 1.$$

*Then solutions of the system asymptotically synchronize for all values of initial conditions.*

*Proof.* In accordance with the invariant box argument, if  $x_0 \subset B_{z,y}$  initial conditions within the invariant box, solutions of the coupled system exist and are bounded for all  $t > 0$ . Define the errors

$$\tilde{z} = z_1 - z_2, \quad \tilde{y} = y_1 - y_2,$$

so that

$$\begin{aligned}\dot{\tilde{z}} &= \alpha(\tilde{y} - \beta\tilde{z}) \\ \dot{\tilde{y}} &= \tilde{y} - \gamma(y_1^3 - y_2^3) - \tilde{z} - \sigma\tilde{y}.\end{aligned}$$

Consider the Lyapunov function

$$V = \frac{1}{2} \left( \frac{1}{\alpha} \tilde{z}^2 + \tilde{y}^2 \right),$$

then, using the equality

$$\begin{aligned} \frac{1}{4}(y_1 - y_2)^2(3(y_1 + y_2)^2 + (y_1 - y_2)^2) &= (y_1^2 + y_2^2 - 2y_1y_2)(y_1^2 + y_2^2 + y_1y_2) \\ &= y_1^4 + y_2^4 - y_1y_2^3 - y_1^3y_2 \\ &= (y_1 - y_2)(y_1^3 - y_2^3) \end{aligned}$$

we find that

$$\begin{aligned} \dot{V} &= \frac{1}{\sigma} \dot{z}\dot{z} + \tilde{y}\dot{\tilde{y}} \\ &= -\beta\dot{z}^2 + (1 - \sigma)\tilde{y}^2 + \gamma\tilde{y}(y_1^3 - y_2^3) \\ &= -\beta\dot{z}^2 + (1 - \sigma)\tilde{y}^2 + \frac{\gamma}{4}\tilde{y}^2(3(y_1 + y_2)^2 + (y_1 - y_2)^2) \end{aligned}$$

Thus if  $\sigma > 1$  we have  $\dot{V} \leq 0$  and the chain of FHN neurons synchronizes.  $\square$

Generalizing two coupled systems to a directed chain of  $n$  oscillators, we observe that the Laplacian matrix of this configuration is

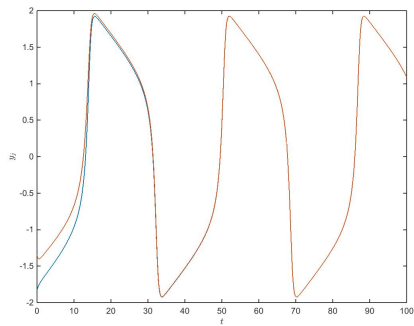
$$L = \begin{pmatrix} 0 & 0 & 0 & \cdots & 0 \\ -1 & 1 & 0 & \cdots & 0 \\ 0 & -1 & 1 & \ddots & \vdots \\ \vdots & \ddots & \ddots & \ddots & 0 \\ 0 & \cdots & 0 & -1 & 1 \end{pmatrix}.$$

The matrix  $L$  has only real eigenvalues; a simple zero eigenvalue and  $n - 1$  eigenvalues 1. The only type of stable correlated oscillations we can find in the chain are the completely synchronous oscillations. These synchronous oscillations will emerge for values of the coupling strength  $\sigma$  for which the chain of 2 FHN oscillators synchronize. Thus the conditions for synchronization are independent of the size of the network (i.e. the length of the chain). Numerical simulations below illustrate this statement.

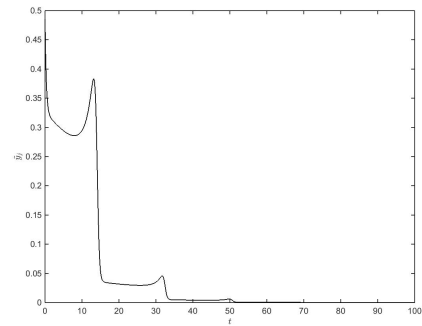
Figure 3.4 shows the outputs of two FHN oscillators and the synchronization output error for  $\sigma = 1.5$ . Figure 3.5 shows the results for longer chains; Even though the convergence to the synchronous state is slower for longer chains, the oscillators in the chains always end up in synchrony.

### 3.3.4 Synchronization in the simple cycle

As with the simple chain, the extremal property of the simple cycle investigated for linear first-order differential equations is extended to the more general case of nonlinear systems. We show that the damped oscillations and slow decay resonate with nonlinear systems. This



(a)



(b)

Figure 3.4: Synchronization of two FHN oscillators for  $\sigma = 1.5$ . a. Outputs of FHN oscillator 1 (leader, black) and FHN oscillator 2 (follower, red). b. Synchronization output error  $\tilde{y} := y_1 - y_2$ .

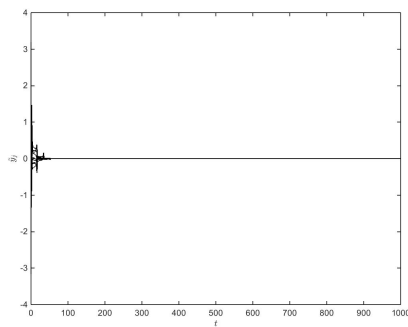
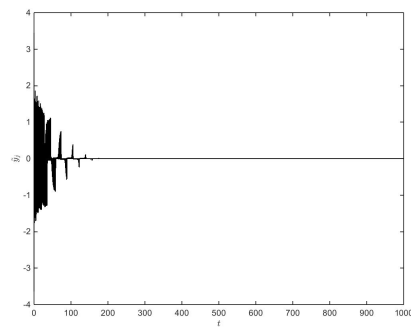
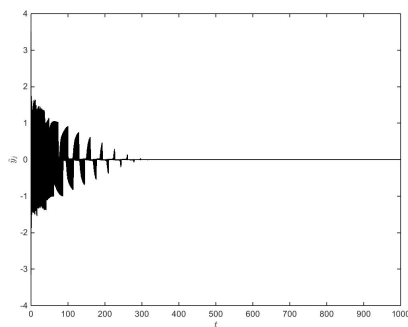
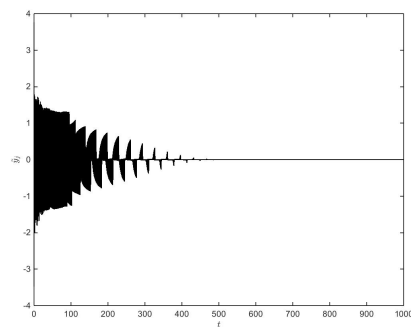
(a)  $n = 10$ (b)  $n = 50$ (c)  $n = 100$ (d)  $n = 150$ 

Figure 3.5: Synchronization output errors  $\tilde{y}_j := y_j - y_{j-2}$ ,  $j = 2, \dots, n$ , for  $\sigma = 1.5$  and different lengths of the chain.

has a profound affect; in the case of linear first-order differential systems the simple cycle is extremely sensitive to perturbations, for the case of nonlinear systems coupled in the configuration of the simple cycle, the internal dynamics of nonlinear systems resonate with small perturbations giving rise to bistabilities of system dynamics

### Boundedness of solutions in the coupled system

**Lemma 3.3.3.** *The solutions of the ring network of FHN neurons are ultimately bounded uniformly in  $x_0, \sigma \in \mathbb{R}_{\geq 0}$ . That is, there is a compact set  $\Omega \in \mathbb{R}^{2n}$  such that for all  $x_0 \in \mathbb{R}^{2n}, \sigma \in \mathbb{R}_{\geq 0}$*

$$\lim_{t \rightarrow \infty} \text{dist}(x(t, x_0, \sigma), \Omega) = 0.$$

*Proof.* We begin with establishing that the FHN neuron is strictly semi-passive (see also [142]).

Let  $S(z_j, y_j) = \frac{1}{2}(\alpha^{-1}z_j^2 + y_j^2)$  be the storage function. Then

$$\dot{S} = -H(z_j, y_j) + y_j u_j$$

with  $H(z_j, y_j) = \beta z_j^2 + y_j^2(\gamma y_j^2 - 1)$ . Noticing that

$$\begin{aligned} \beta z_j^2 + y_j^2(\gamma y_j^2 - 1) &= \beta z_j^2 + dy_j^2 + \gamma y_j^4 - y_j^2 - dy_j^2 \\ &= \beta z_j^2 + dy_j^2 + \left(\sqrt{\gamma}y_j^2 - \frac{d+1}{2\sqrt{\gamma}}\right)^2 - \frac{(d+1)^2}{4\gamma} \end{aligned} \quad (3.34)$$

we can conclude that  $H(z_j, y_j)$  is positive for all  $z_j, y_j$  such that

$$\beta z_j^2 + dy_j^2 > \frac{(d+1)^2}{4\gamma}. \quad (3.35)$$

Assigning the value of  $d = \beta$  in (3.35) ensures that  $H(z_j, y_j)$  is positive outside the ball

$$z_j^2 + y_j^2 \leq \frac{(\beta+1)^2}{4\beta\gamma}.$$

Now consider  $V(z, y) = S(z_1, y_1) + \dots + S(z_n, y_n)$ . Then the strict semi-passivity property of the FHN neurons implies

$$\dot{V} \leq -H(z_1, y_1) - \dots - H(z_n, y_n) - \sigma y^T L y.$$

Notice that the matrix  $L + L^T$  is the Laplacian matrix of the undirected ring, which is known to be positive semi-definite. Hence

$$y^T L y = \frac{1}{2} y^T (L + L^T) y \geq 0,$$

and consequently

$$\dot{V} \leq -H(z_1, y_1) - \dots - H(z_n, y_n).$$

Therefore, setting the value of  $d$  in (3.34) equal to  $\alpha\beta$  results in

$$\dot{V} \leq - \sum_{j=1}^n \beta z_j^2 + \beta \alpha y_j^2 + n \frac{(\alpha\beta+1)^2}{4\gamma} = -\beta\alpha V + n \frac{(\alpha\beta+1)^2}{4\gamma}.$$

Noticing that the function  $V$  is radially unbounded, positive-definite, we invoke the Comparison Lemma (see e.g. [83]) in order to conclude that solutions of the coupled system are bounded and converge asymptotically to a compact set of which the size is independent of the parameter  $\sigma$ .  $\square$

### Sufficient conditions for synchronization

Suppose now that the  $n$ -th oscillator is feeding back its output to the input of 1-st, that is the network topology is that of the directed ring. As we shall see later the presence of such extra connection has a drastic effect on the system's performance with respect to the coupling strength needed to maintain stable full-state synchrony. This is reflected in the statement of the theorem below.

**Theorem 3.3.2.** *Consider the system of coupled FHN oscillators (3.25), (3.26), and let  $\lambda_1 \leq \lambda_2 \leq \dots \leq \lambda_n$  be the eigenvalues of the symmetrized Laplacian of the network  $\frac{1}{2}(L + L^T)$ . Then solutions of the coupled system asymptotically synchronize providing that*

$$\sigma \lambda_2 > 1$$

*Proof.* Consider the new variables

$$\tilde{z} = Lz, \quad \tilde{y} = Ly$$

where  $L$  the Laplacian matrix of the ring, i.e.

$$\tilde{z} = \begin{pmatrix} \tilde{z}_1 \\ \tilde{z}_2 \\ \vdots \\ \tilde{z}_n \end{pmatrix} = \begin{pmatrix} z_1 - z_n \\ z_2 - z_1 \\ \vdots \\ z_n - z_{n-1} \end{pmatrix} \quad \text{and} \quad \tilde{y} = \begin{pmatrix} \tilde{y}_1 \\ \tilde{y}_2 \\ \vdots \\ \tilde{y}_n \end{pmatrix} = \begin{pmatrix} y_1 - y_n \\ y_2 - y_1 \\ \vdots \\ y_{n-1} - y_n \end{pmatrix}.$$

It is clear that the systems are synchronized if and only if

$$\tilde{z} = 0 \quad \text{and} \quad \tilde{y} = 0.$$

Observe that  $\mathbf{1} \notin \text{range}(L)$ , hence there exist no vectors  $z$  and  $y$  such that

$$Lz = \mathbf{1} \quad \text{and} \quad Ly = \mathbf{1}.$$

This means that the projections of  $(z, y)$  via  $L$  take values in the set

$$\Omega := \{(\tilde{z}, \tilde{y}) \in \mathbb{R}^{2n} \mid \tilde{z} \perp \mathbf{1}, \tilde{y} \perp \mathbf{1}\}.$$

Thus all synchronization errors  $\tilde{z}$  and  $\tilde{y}$  are orthogonal to  $\mathbf{1}$ .

Consider the function  $V : \Omega \rightarrow \mathbb{R}_+$ :

$$V = \frac{1}{2} \left( \frac{1}{\alpha} \tilde{z}^T \tilde{z} + \tilde{y}^T \tilde{y} \right).$$

From the discussion on synchronization in the chain it follows that

$$\dot{V} \leq -\beta \tilde{z}^T \tilde{z} + \tilde{y}^T (I - \sigma L) \tilde{y} - \tilde{y}^T W \tilde{y}$$

where

$$W = \frac{\gamma}{4} \begin{pmatrix} (3(y_1 + y_n)^2 + \tilde{y}_1^2) & & \\ & \ddots & \\ & & (3(y_{n+1} + y_n)^2 + \tilde{y}_n^2) \end{pmatrix},$$

which is positive semi-definite, hence

$$\dot{V} \leq -\beta \tilde{z}^T \tilde{z} + \tilde{y}^T (I - \sigma L) \tilde{y}$$

For all vectors  $\tilde{y} \perp \mathbf{1}$  the following inequality holds true:

$$\tilde{y}^T (\sigma L - I) \tilde{y} = \tilde{y}^T (\sigma \frac{1}{2} (L + L^T) - I) \tilde{y} \geq (\sigma \lambda_2 - 1) \tilde{y}^T \tilde{y}$$

where  $\lambda_2 = \lambda_2(\frac{1}{2}(L + L^T))$  is the smallest non-zero eigenvalue of  $\frac{1}{2}(L + L^T)$ . An application of LaSalle's invariance principle, cf. [94], implies that the synchronization errors  $\tilde{z}$  and  $\tilde{y}$  converge to zero asymptotically.  $\square$

**Corollary.** *For the network of  $n$  coupled FHN oscillators, solutions globally asymptotically synchronize if the following inequality holds:*

$$\sigma \left( 1 - \cos \left( \frac{2\pi}{n} \right) \right) > 1$$

*Proof.* Note that  $\frac{1}{2}(L + L^T)$  is the Laplacian matrix of the undirected ring, which has a simple zero eigenvalue with corresponding eigenvector in  $\text{span}(\mathbf{1})$ . According to the properties of the spectrum of circulant matrices, cf. [37], we know that the second smallest eigenvalue  $\lambda_2$  of the symmetrized Laplacian  $\frac{1}{2}(L + L^T)$  equals the real part of the smallest (in absolute value) non-zero eigenvalue of  $L$ , which we denote as  $\mathbb{R}(\lambda_2(L))$ . Then if

$$\sigma \lambda_2(\frac{1}{2}(L + L^T)) = \sigma \mathbb{R}(\lambda_2(L)) > 1,$$

we have  $\dot{V} < 0$ , i.e.  $V$  is a Lyapunov function on  $\Omega$ . Note that

$$\lambda_2(L) = 1 - e^{\frac{2\pi i(n-1)}{n}}$$

from which the result immediately follows.  $\square$

### 3.3.5 Numerical analysis: Synchronization and rotating waves

The results in the previous sections show that, on the one hand, when a system has a directed ring topology and the number of systems in the ring grows then their relative dynamics becomes more and more under-damped (Theorem 3.3.2). On the other hand, in accordance with Corollary 3.3.4, estimates of attraction rates of the diagonal synchronization manifold rapidly diminish to zero for increasing number of systems. The latter results are, however, sufficient and thereby conservative. To get a clearer view of the network dynamics we performed an exhaustive numerical exploration of the system dynamics for various values of coupling strengths  $\sigma$  as well as the network sizes  $n$ .

We construct a grid  $(n, \sigma)$  for number of systems  $n = 2, \dots, 20$  and coupling strength  $\sigma = \{0.05, 0.1, 0.15, \dots, 10\}$ . For each  $(n, \sigma)$  100 sets of initial conditions are drawn uniformly randomly from the domain  $|y_i(0)| \leq \frac{3}{2}\sqrt{3}$  and  $|z_i(0)| \leq \frac{15}{8}\sqrt{3}$ , which can be shown to be positively invariant for both connectivity configurations (i.e. the directed chain and the directed cycle). The *MATLAB* numerical solver *ode45* was used with relative and absolute error tolerances of order  $10^{-5}$  to integrate dynamics for a maximum of 20,000 time steps. At regular intervals of 1000, 2000, ..., 20,000 time steps, we interrupt integration to check for synchronization or rotating wave solutions. After 20,000 time steps, if neither synchronization nor a rotating wave solution is detected, we register ‘no solution’.

Synchronization is identified in terms of the absolute error between the states of neighbouring systems averaged over a 1000 time step window being less  $2 \times 10^{-5}$ . In case of no synchronization, we investigated the existence of rotating waves of Mode Type 1. Rotating waves are defined as periodic solutions where all systems take identical orbits with constant non-zero and equal phase shifts between neighbouring oscillators. The mode type describes the group velocity of the wave; for a periodic wave, Mode Type 1 describes the case where the period of a rotating wave having non-zero wave velocity equals the period of individual oscillators. Identical orbits are identified if the absolute difference between the time shifted orbits - so that orbits are in-phase - of neighbouring systems averaged over the period of the orbit is less than  $10^{-4}$ . Constant and equal phase shifts (for a Mode Type 1 rotating wave) are identified if the maximum from all absolute differences between  $n$  times the phase shifts between pairwise neighbouring systems and period  $T$  is less than a tolerance of  $10^2$ , i.e,  $\max_i |n\phi_i(t) - T| < 10^{-2}$  for phase shift  $\phi_i(t)$  between systems  $i$  and  $i + 1$  at time  $t$ .

The results of this exploration are summarized in Figure 3.6. This figure shows that in addition to regions corresponding to mere full asymptotic synchronization there is a wide range of parameter combinations (growing with the system’s size) for which the system admits an asymptotically stable rotating wave solution. The larger is the number of systems,

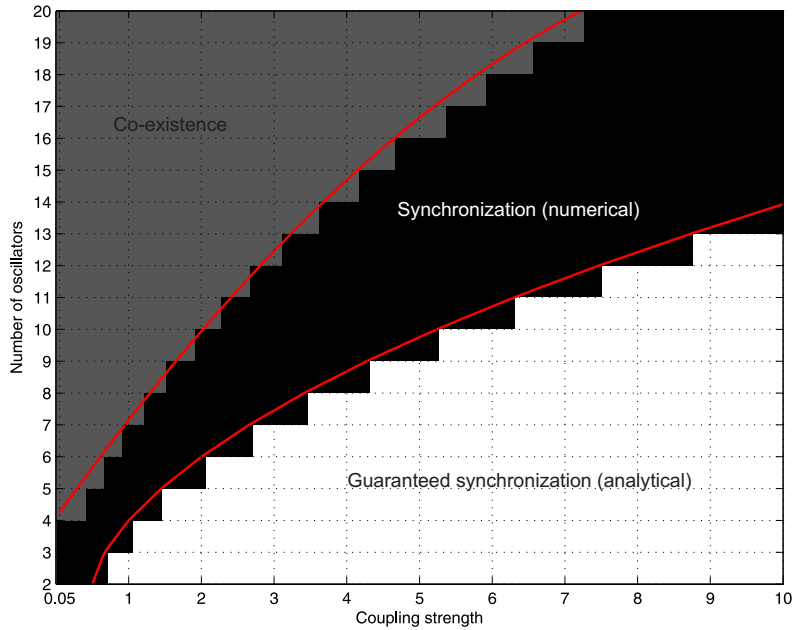


Figure 3.6: Bifurcation diagram for directed rings of FHN oscillators. The *guaranteed synchronization (analytical)* region in the parameter space corresponds to global asymptotic synchronization that is guaranteed by the semi-passivity argument, the *synchronization (numerical)* is the domain where numerical simulations found synchronization to be registered for every set of random initial conditions. The *co-existence* region shows the domain of parameter values in which both fully synchronous and rotating wave solutions have been found.

the larger values of the coupling parameter  $\sigma$  are required to maintain global stability of the fully synchronous state.

Two solid curves approximate boundaries between the parameter domains corresponding to analytically determined globally asymptotically stable full-state synchrony, and a partition of numerically determined globally asymptotically stable full-state synchrony; The first region corresponds to synchronization registered for every set of random initial conditions during numerical simulations, whilst the second region corresponds to, in addition to synchronization registered for every set of random initial conditions during numerical simulations, where Floquet stability analysis of solutions of the auxiliary system indicated existence of a locally asymptotically stable rotating wave solution

The first (lower) curve - separating analytical and numerical synchronization - was determined previously in the semi-passivity argument. The second (upper) curve - partitioning numerically determined globally asymptomatic synchronization - is determined from a local stability analysis (using Floquet theory) of the rotating wave solution. Details of the second

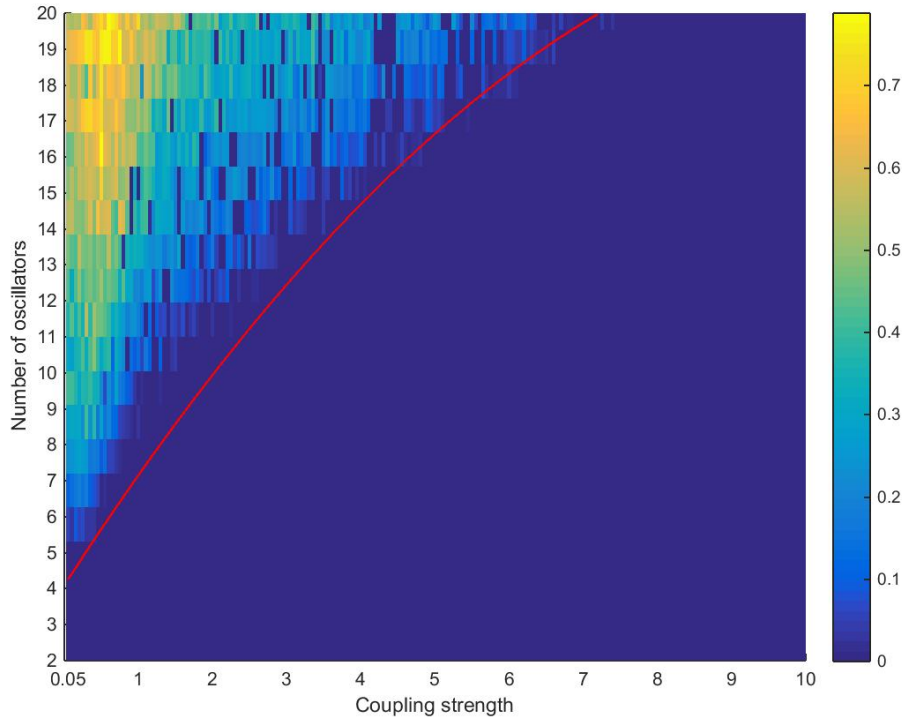


Figure 3.7: Proportion of samples that yield a rotating wave solution. Red curve shows the boundary the rotating wave is stable determined by Floquet multipliers.

are provided in the following section.

Figure (3.7) shows for each  $\sigma$  and  $n$  the proportion of initial conditions that yield a rotating wave solution of Mode Type 1 whilst Figure (3.8) shows for all mode types, i.e. rotating waves that resonate with individual systems period of oscillation. For low coupling  $\sigma$  and for increasing number of systems  $n$ , rotating wave solutions are found more often. This suggests a larger basin of attraction for the rotating wave than that for synchronization, and that this basin grows with increasing  $n$  and decreasing  $\sigma$  whilst at the same time the basin of attraction for synchronization shrinks. The relative sizes of basin of attraction result in higher or lower likelihoods for the systems to converge to a certain solution given uniformly random initial conditions.

### Local stability analysis of the rotating wave

Here, we consider only the rotating wave having mode type one - the period of the rotating wave equals the periodicity of the oscillators. Similar analysis can also be performed for other mode types.

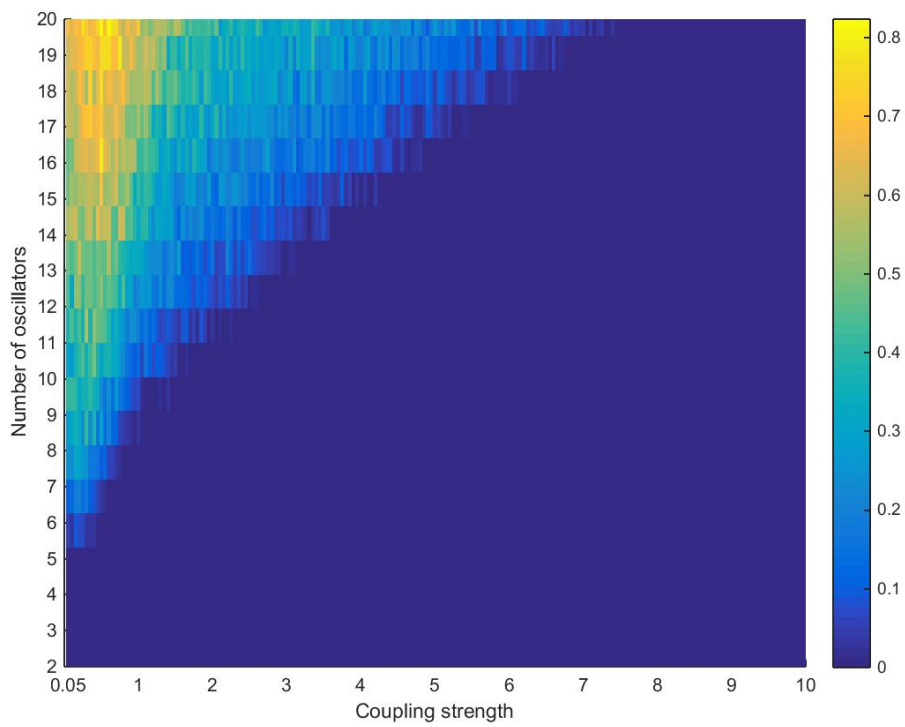


Figure 3.8: Proportion of samples that yield a rotating wave solution for all mode types.

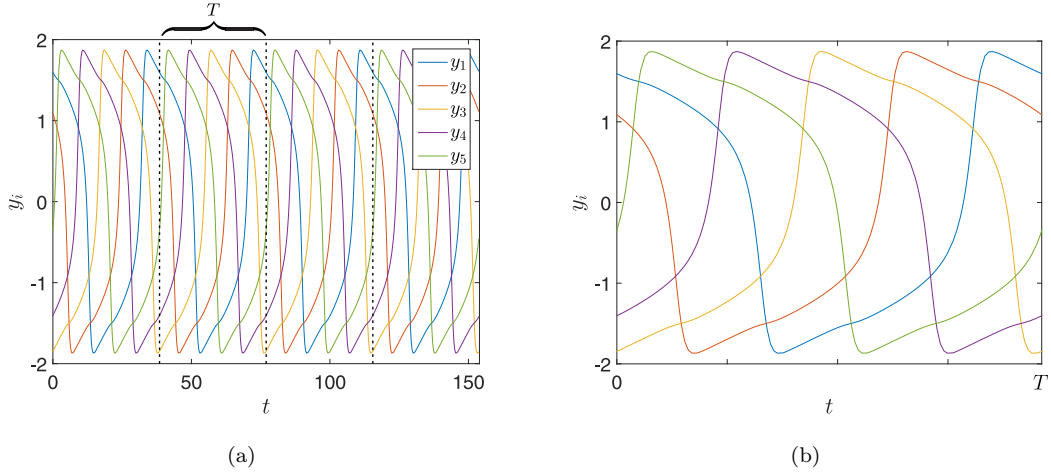


Figure 3.9: (a) The  $y$  dynamics over one oscillation. (b) The periodic  $y$  dynamics in the time interval  $[0, T]$ . The  $z$  dynamics show the same type of time shifted and periodic behavior as the  $y$  dynamics.

Suppose that  $n$  identical coupled systems have a non-constant,  $T$ -periodic solution  $x$  for constant  $T > 0$ , and for which the orbit of each subsystem is identical and time shifted by some constant  $\tau = \frac{T}{n}$ :

$$\begin{aligned} x_1(t) &= x_2(t + \tau) = x_3(t + 3\tau) = \dots \\ &\dots = x_{n-1}(t + (n-1)\tau) = x_n(t + (n-1)\tau) = x_1(t + n\tau) = x_1(t + T). \end{aligned} \quad (3.36)$$

We refer to this as the *rotating wave solution*. An example of a rotating wave solution for  $k = 5$  coupled FHN oscillators in the ring configuration is presented in Figure 3.9,

Recall Equation (3.25) with  $x_j = (y_j, z_j)$ . If we restrict the coupled dynamics of the FHN oscillators to the rotating wave manifold, then using the periodicity of the rotating wave solution, substitution of Equation (3.36) into the dynamics of each coupled FHN oscillator (3.25) yields  $n$  identical uncoupled delay differential equations (DDE's) of the form

$$\begin{aligned} \dot{x}_1(t) &= f(x_1(t)) + \sigma BC \left( x_1 \left( t - \frac{(k-1)}{k} \tau \right) - x_1(t) \right) \\ &\vdots \\ \dot{x}_n(t) &= f(x_n(t)) + \sigma BC \left( x_n \left( t - \frac{(n-1)}{n} \tau \right) - x_n(t) \right). \end{aligned}$$

Thus the rotating wave solution can only exist if the auxiliary system

$$\dot{s}(t) = f(s(t)) - \sigma BC[s(t) - s(t - \tau^*)], \quad \tau^* := T - \tau = \frac{n-1}{n}T, \quad (3.37)$$

has a non-constant,  $T$ -periodic solution:

$$s(t) = s(t + T) \forall t \in \mathbb{R}. \quad (3.38)$$

For stability analysis of the rotating wave solution, define errors around the rotating wave solution, such that all error are zero on the rotating wave manifold and non-zero elsewhere. The errors are defined between neighbouring systems as the time delayed differences,

$$e_j(t) = x_{j+1}(t + \tau) - x_j(t), \quad j = 1, 2, \dots, n, \text{ mod } n. \quad (3.39)$$

The time derivative of the error equations (3.39) provides the error dynamics: the evolution of the errors in time

$$\begin{aligned} \dot{e}_j(t) = \dot{x}_{j+1}(t + \tau) - \dot{x}_j(t) &= f(x_{j+1}(t + \tau)) - f(x_j(t)) \\ &+ \sigma(x_j(t + \tau) - x_{j-1}(t)) - \sigma(x_{j+1}(t + \tau) - x_j(t)), \end{aligned}$$

substitution of error equations yields

$$\dot{e}_j(t) = f(e_j(t) + x_j(t)) - f(x_j(t)) - \sigma(e_{j+1}(t) - e_j(t)).$$

Thus, the system of error dynamics,

$$\begin{pmatrix} \dot{e}_1(t) \\ \dot{e}_1(t) \\ \vdots \\ \dot{e}_1(t) \end{pmatrix} = \begin{pmatrix} f(e_1(t) + x_1(t)) - f(x_1(t)) \\ f(e_2(t) + x_2(t)) - f(x_2(t)) \\ \vdots \\ f(e_n(t) + x_n(t)) - f(x_n(t)) \end{pmatrix} - \sigma(L \otimes BC) \begin{pmatrix} e_1(t) \\ e_2(t) \\ \vdots \\ e_n(t) \end{pmatrix}. \quad (3.40)$$

Here  $\otimes$  is the Kronecker (tensor) product. Substitution of the rotating wave solution into equation (3.40) yields the equilibrium of all zeros. However, this solution includes time delays, and will therefore be difficult to analyse stability properties. Substitution of the rotating wave solution in terms of the auxiliary system variable  $s(t)$  into equation (3.40), on the other hand, provides an expression of the error dynamics without time delays in coupling.

Notice that

$$f(e_j(t) + x_j(t)) - f(x_j(t)) \approx e_j(t)J(f(x_j(t))) \quad (3.41)$$

where  $J(\cdot)$  is the Jacobian,

$$J(s(t)) := \begin{pmatrix} -\alpha\beta & \alpha \\ -1 & 1 - 3\gamma s_2^2(t) \end{pmatrix} \quad (3.42)$$

where  $s_2(t)$  denotes the second component of  $s(t)$ . Thus, linearisation of the error dynamics (3.40) yields

$$\begin{pmatrix} \dot{e}_1(t) \\ \dot{e}_1(t) \\ \vdots \\ \dot{e}_1(t) \end{pmatrix} = \begin{pmatrix} e_1(t)J(f(x_1(t))) \\ e_2(t)J(f(x_2(t))) \\ \vdots \\ e_n(t)J(f(x_n(t))) \end{pmatrix} - \sigma(L \otimes BC) \begin{pmatrix} e_1(t) \\ e_2(t) \\ \vdots \\ e_n(t) \end{pmatrix}.$$

$$\begin{pmatrix} \dot{e}_1(t) \\ \dot{e}_1(t) \\ \vdots \\ \dot{e}_1(t) \end{pmatrix} = \left[ \begin{pmatrix} J(f(x_1(t))) & & & \\ & J(f(x_2(t))) & & \\ & & \ddots & \\ & & & J(f(x_n(t))) \end{pmatrix} - \sigma(L \otimes BC) \right] \begin{pmatrix} e_1(t) \\ e_2(t) \\ \vdots \\ e_n(t) \end{pmatrix}.$$

Substitution of the auxiliary function  $s(t)$ , such that,

$$s(t) = x_1(t) = x_2(t + \tau) = \cdots = x_n(t + (n - 1)\tau),$$

yields the variational equation around the rotating wave solution

$$\begin{pmatrix} \dot{\xi}_1(t) \\ \dot{\xi}_2(t) \\ \vdots \\ \dot{\xi}_n(t) \end{pmatrix} = \left[ \begin{pmatrix} J(s(t)) & & & \\ & J(s(t - \tau)) & & \\ & & \ddots & \\ & & & J(s(t - (n - 1)\tau)) \end{pmatrix} - \sigma(L \otimes BC) \right] \begin{pmatrix} \xi_1(t) \\ \xi_2(t) \\ \vdots \\ \xi_n(t) \end{pmatrix}. \quad (3.43)$$

Note that  $T$ -periodicity of the system (3.37) implies the linear error system to be  $T$ -periodic.

For the local stability analysis we computed periodic solutions of the auxiliary system (3.37) for pairs  $(n, \sigma)$ . The periodic solutions are determined using *numerical continuation methods* that are available in the numerical software package *DDE-Biftool* [44]. For the interested reader, we briefly describe the non-trivial process of obtaining periodic solutions by numerical continuation.

Figure (3.10) characterizes solutions of the auxiliary system in the parameter domain  $(T, \tau, \sigma)$ . For the auxiliary system in which parameter  $T$  and  $\tau$  are allowed to vary continuously, a solution that describes the dynamics of a rotating wave solution satisfies the relation  $\frac{T}{\tau}(n - 1) = n$ . However, for the solutions we obtained, parameters  $T$  and  $\tau$  have not been varied continuously. Therefore, we choose the solution that satisfies the following the inequality

$$\left| \frac{T}{\tau}(n - 1) - n \right| < \epsilon. \quad (3.44)$$

To maintain accuracy of approximation of the auxiliary system to  $n$  coupled FHN oscillators, the error  $\epsilon$  must be small. For our stability analysis we took  $\epsilon = 0.01$ .

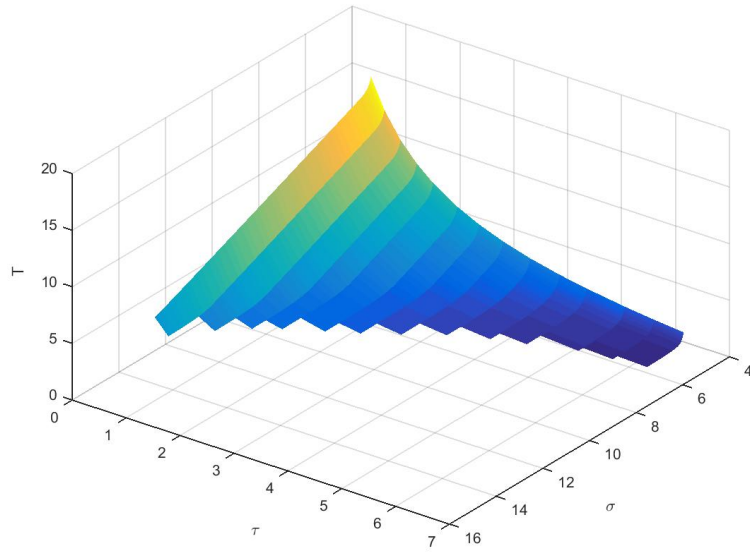


Figure 3.10: Solutions of the auxiliary system characterized in the parameter domain of period time, delay, and coupling strength  $(T, \tau, \sigma)$  presented as a surface for  $T$  a function of pairs  $(\tau, \sigma)$ .

Figures (3.3.5) and (3.3.5) show two cross sections of the surface in Figure (3.10) for coupling strengths  $\sigma = 0.95$  and  $\sigma = 6.75$ , respectively. Dashed lines identify solutions that satisfy relation (3.44) and hence map solutions of the auxiliary system to an integer number  $n$  of coupled FHN oscillators on the rotating wave manifold.

The stability of those periodic solutions of the auxiliary system are assessed by computing the Floquet multipliers of the corresponding linearised error system (3.43) (with the stability package included in *DDE-Biftool*). Recall that if all Floquet multipliers except one at 1 have modulus strictly smaller than 1, then the zero solution of the linearised error system is asymptotically stable, which implies the rotating wave solution to be locally asymptotically stable. The red line in Figure 3.6 (and Figure 3.7) is defined by the crossing of (at least) one multiplier with the boundary of the unit disc in  $\mathbb{C}$ .

## Numerical continuation

Numerical continuation is the method for determining solutions of a parametrized non-linear equation. Beginning from an initial solution, the software *DDE-Biftool* computes a solution component - a path of solutions - of a non-linear equation for changes in the free parameter.

Initial conditions include an initial solution in order to construct a path of solutions.

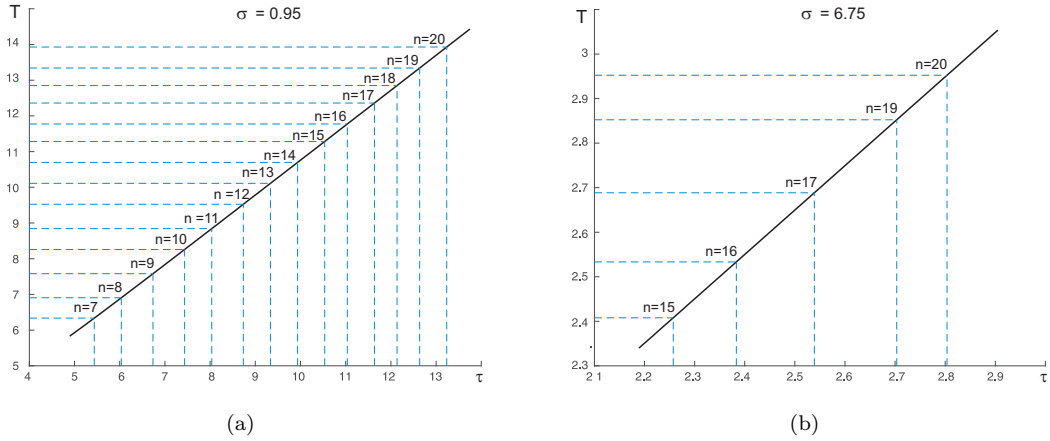


Figure 3.11: Solutions of the auxiliary system characterized in the parameter domain of period time and delay  $(T, \tau)$  for given coupling strengths: (a)  $\sigma = 0.95$ . (b)  $\sigma = 6.75$ . Dashed lines indicate solutions that satisfy relation

We choose as our initial solution the steady state solution of the auxiliary system with zero coupling strength and non-zero delay. For zero coupling strength the auxiliary system reduces to the original FHN equation. A constant  $c$  is added to the auxiliary system (3.37) such that

$$\begin{bmatrix} \dot{s}_1 \\ \dot{s}_2 \end{bmatrix} = \begin{bmatrix} \alpha(s_2 - \beta s_1) \\ s_2 - \gamma s_2^3 - s_1 + c \end{bmatrix} \quad (3.45)$$

where as before  $\alpha = \frac{8}{100}$ ,  $\beta = \frac{8}{10}$ , and  $\gamma = \frac{1}{3}$ .

A steady state solution is found by satisfying that the nullclines  $s_1 = \frac{1}{\beta}s_2$  and  $s_1 = s_2 - \gamma s_2^3 + c$  intersect on one of the outer extreme branches of the cubic  $s_2$ -nullcline (depending on the sign of the constant).

Numerical continuation of the steady state solution with the added constant  $c$  as the free parameter leads to a Hopf bifurcation. The problem therefore becomes: find  $c$  for which a Hopf bifurcation occurs. The occurrence of a Hopf bifurcation describes the emergence of a periodic solution; a local bifurcation in which a fixed point of a dynamical system loses stability, as a pair of complex conjugate eigenvalues (of the linearisation around the fixed point) cross the complex plane imaginary axis. Under reasonably generic assumptions about the dynamical system, a small-amplitude limit cycle branches from the fixed point. Equivalently, a Hopf bifurcation occurs when the Jacobian has zero trace and non-zero positive determinant. The Jacobian (3.42) has trace

$$\text{tr}J(s) = 1 - 3\gamma s_2^2 - \alpha\beta$$

which equals zero for  $s_2 = \pm\sqrt{1 - \alpha\beta}$ , and determinant,

$$\det J(s) = -\alpha\beta(1 - 3\gamma s_2^2) + \alpha$$

which is greater than zero for  $s_2 = \sqrt{1 - \alpha\beta}$ .

The Hopf point therefore occurs at the intersection of the  $s_1$  and  $s_2$  nullclines for which  $s_2 = \sqrt{1 - \alpha\beta}$ . Thus the constant  $c$  is determined,

$$c = \left(\frac{1}{\beta} - 1\right)s_2 + \gamma s_2^3 = \pm 0.5437. \quad (3.46)$$

Numerical continuation of system (3.45) with free parameter  $c$  produces a solution component for which a periodic solution exists where parameter  $c$  is equal to zero, i.e. no added constant, and hence a solution in the form of the auxiliary system (3.37).

Recall Liénard's Theorem and the Poincaré-Bendixon Theorem in Chapter 2, we know therefore that this periodic solution is unique and asymptotically stable, since it is a closed and isolated limit cycle. Since the periodic solution is asymptotically stable, small perturbations must decay. Thus, we may perform numerical continuation of the periodic solution with the coupling strength  $\sigma$  as the free parameter making it non-zero. We now have the ability to traverse the full domain of periodic solutions  $(T, \tau, \sigma)$  (period, delay, coupling strength). Finally, for any chosen periodic solution, the stability is determined by the Floquet multipliers. Performed as a separate step from the continuation method.

### Unique, stable and closed limit cycle

Let us here prove that the periodic solution for (3.45) for which parameter  $c = 0$ , and also coupling and delay are zero, i.e., the original FHN system equations (3.25), is a closed and isolated stable limit cycle and therefore a unique asymptotically stable one. We do this using Liénard's theorem for uniqueness and existence of a limit cycle, and the Poincaré-Bendixon theorem to ensure the limit cycle is closed, i.e. asymptotic stability.

Recall that

**Theorem 3.3.3.** (*Liénard's Theorem*) *Suppose that  $f(x)$  and  $g(x)$  satisfy the conditions:*

1.  $f(x)$  and  $g(x)$  are continuously differentiable for all  $x$ ;
2.  $g(-x) = -g(x)$  for all  $x$  (i.e.,  $g(x)$  is an odd function);
3.  $f(-x) = f(x)$  for all  $x$  (i.e.,  $f(x)$  is an even function);
4.  $g(x) > 0$  for all  $x > 0$ ;
5. The odd function  $F(x) = \int_0^x f(u)du$  has exactly one positive zero at  $x = a$ , is negative for  $0 < x < a$ , is positive and nondecreasing for  $x > a$ , and  $F(x) \rightarrow \infty$  as  $x \rightarrow \infty$ .

Then the system (number) has a unique, stable limit cycle surrounding the origin in the phase plane.

*Proof.* A two-dimensional system of the form

$$C \frac{dV}{dt} = -I(V, n) \quad (3.47)$$

$$\frac{dn}{dt} = \frac{n_\infty(V) - n}{\tau_n(V)} \quad (3.48)$$

describes a relaxation oscillator and can always be written in Liénard form

$$\ddot{V} + f(V)\dot{V} + g(V) = 0 \quad (3.49)$$

using a diffeomorphism.

First solve Equation (3.25) for  $z$ ,

$$z = \phi(y) - \dot{y} \quad (3.50)$$

where  $\phi(y) = y - \gamma y^3$  and substitute into the  $z$ -dynamics (3.25),

$$\begin{aligned} \dot{z} &= \alpha(y - \beta(\phi(y) - \dot{y})) \\ &= \alpha(y - \beta(y - \gamma y^3 - \dot{y})). \end{aligned} \quad (3.51)$$

Take the time derivative of the  $y$ -dynamics (3.25),

$$\ddot{y} = \phi'(y)\dot{y} - \dot{z} \quad (3.52)$$

where  $\phi'(y) = 1 - 3\gamma y^2$ , and substitute in the above expression for  $\dot{z}$

$$\begin{aligned} \ddot{y} &= (1 - 3\gamma y^2)\dot{y} - \alpha(y - \beta(y - \gamma y^3 - \dot{y})) \\ &= ((1 - 3\gamma y^2) + \alpha\beta)\dot{y} - \alpha((1 - \beta)y + \beta\gamma y^3) \end{aligned} \quad (3.53)$$

and so we obtain in Liénard's form:

$$\ddot{y} + (3\gamma y^2) - 1 + \alpha\beta)\dot{y} + \alpha((1 - \beta)y + \beta\gamma y^3) \quad (3.54)$$

where  $f(y) = 3\gamma y^2 - 1 + \alpha\beta$ , and  $g(y) = \alpha((1 - \beta)y + \beta\gamma y^3)$ .

Functions  $f(y)$  and  $g(y)$  clearly satisfy conditions (1)-(4) of Liénard's Theorem.

$$F(y) = \int_0^y (u^2 - \frac{936}{1000})du = \frac{1}{3}y^3 - \frac{936}{1000}y. \quad (3.55)$$

The function  $F(y)$  is odd.  $F(y) = 0$  for  $y = \sqrt{3(\frac{936}{1000})} = a$ .  $F(0 < y < a) < 0$ , and  $F(y > a) > 0$  and is non-decreasing. Finally,  $F(y) \rightarrow \infty$  as  $y \rightarrow \infty$ .

Therefore, the periodic solution is unique and stable. □

To show that the orbit is closed, and thus satisfy the Poincaré-Bendixon Theorem, recall the Poincaré-Bendixon Theorem.

**Theorem 3.3.4.** (*Poincaré-Bendixon Theorem*) *Suppose that:*

1.  $R$  is a closed, bounded subset of the plane;
2.  $\dot{x} = f(x)$  is a continuously differentiable vector field on an open set containing  $R$ ;
3.  $R$  does not contain any fixed points; and
4. There exists a trajectory  $C$  that is “confined” in  $R$ , in the sense that it starts in  $R$  and stays in  $R$  for all future time.

Then either  $C$  is a closed orbit, or it spirals toward a closed orbit as  $t \rightarrow \infty$ . In either case,  $R$  contains a closed orbit.

*Proof.* To show that the orbit is confined, construct a trapping region  $R$ , i.e. a closed connected set such that the vector field points inward everywhere on the boundary of  $R$ , then all trajectories of  $R$  are confined.

By the previous semi-passivity argument we know that all trajectories inside the ball

$$z^2 + y^2 \leq \frac{(\beta + 1)^2}{4\beta\gamma} \tag{3.56}$$

remain inside this ball for all future time.

Since every closed orbit must encircle a fixed point, the region  $R$  is a ring-shaped region, with this fixed point at the center of the ring, but outside of the region  $R$ . This fixed point is unstable.

This fixed point corresponds to the intersection of the two nullclines of the  $y$  and  $z$  dynamics for  $c = 0$ . This intersection occurs at the point

$$(z, y) = \left( 0, \pm \frac{1 - \frac{1}{\beta}}{\gamma} \right). \tag{3.57}$$

The fixed point  $(y, z) = (0, 0)$  has two real negative eigenvalues

$$\text{tr}(J) = 1 - y^2 - \alpha\beta = 1 - \alpha\beta > 0, \tag{3.58}$$

$$\det(J) = -\alpha\beta(1 - y^2) + \alpha = \alpha(1 - \beta) > 0. \tag{3.59}$$

$$\text{tr}(J)^2 - 4\det(J) = 1 + 2\alpha\beta + \alpha^2\beta^2 - 4\alpha > 0 \quad (3.60)$$

and hence is an unstable node.

Therefore, we have an asymptotically stable limit cycle. The fact that the limit cycle is asymptotically stable allows small perturbations. Thus, we compute the solution component for the DDE by numerical continuation of free parameter  $\sigma$ . Numerical continuation of  $\sigma$  from zero to (positive) non-zero yields a stable periodic solution that corresponds a rotating wave solution.

□

## Two coupled cycles of oscillators

Given the size of the region of where multiple solutions co-exist, and the resilience to a coherent state; does the extremal property of the simple cycle give rise to further, more complex phenomena when two simple cycles are diffusively coupled via an undirected link between an oscillator in each cycle?

For a total of  $2k$  coupled systems, two cycles are constructed with systems  $1, \dots, k$  in the first simple cycle and systems  $k+1, \dots, 2k$  in the second, and coupled via systems  $i$  and  $j$  such that  $i \in 1, \dots, k$  and  $j \in k+1, \dots, 2k$ . Clearly the synchronization manifold exists, as does the rotating wave solution in the form of two synchronized rotating waves,

$$\begin{aligned} x_1(t) &= x_{k+1}(t) = x_2(t + \tau) = x_{k+2}(t + \tau) = \dots \\ \dots &= x_{k-1}(t + (k-2)\tau) = x_{2k-1}(t + (k-2)\tau) = x_k(t + (k-1)\tau) = x_{2k}(t + (k-1)\tau). \end{aligned}$$

A full description of the phenomena of two coupled cycles is beyond the scope of this work, however, as a motivation for further study, we present a brief example.

We take  $(n, \gamma) = (10, 0.75)$ , which for a simple cycle, lies in the region of co-existence of synchronization and rotating wave solutions. We observe in Figure (3.12) a stable state in which the trajectories of all systems in the first cycle (in red) are attracted to the synchronization manifold, whilst all trajectories of systems in the second cycle (in green) are attracted to the rotating wave solution. There is a clear competition of each cycle to attract the other to its own dynamical regime. The two diffusively coupled oscillators from each cycle periodically perturb each other, which prevents asymptotic convergence of systems to either the synchronization manifold or the rotating wave solution. The basin of attraction of each of these solutions is necessarily greater than the size of perturbation, since the system trajectories appear bounded to neighbourhoods close to their respective solutions. Clearly,

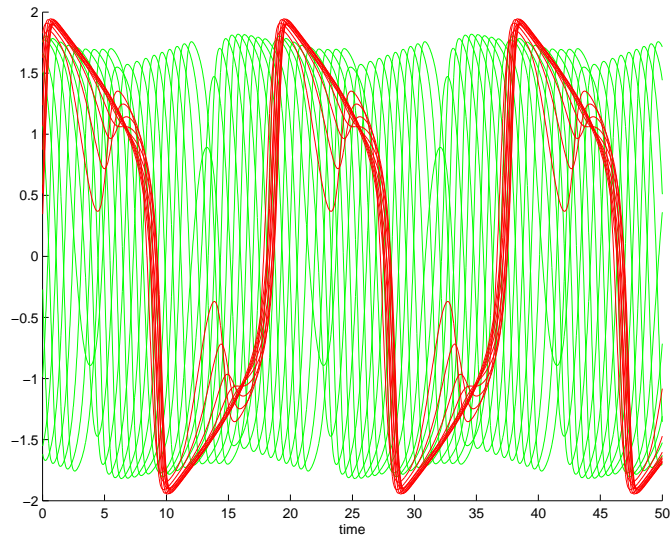


Figure 3.12: Two coupled cycles and their  $y$ -dynamics; in red the  $y$ -dynamics of the first cycle, and in green the  $y$ -dynamics of the second cycle.

the extremal properties of the simple cycle can give rise to multiple regimes of complex patterns of dynamics when embedded into larger network structures.

### 3.4 Multi-Stability of coherent dynamics in directed networks with modular topology

In this work we develop and generalize these results in the following two directions. First, instead of directed cycles we consider networks with modular structure. Such networks comprise of diffusively and undirectly coupled groups of nodes (modules). These groups are linked by directed connections forming a directed cycle. We show that, remarkably, the spectrum of the network Laplacian for such modular structures is closely related to that of individual isolated modules and the corresponding ring or cycle. Similar to our previous work [61] as discussed in the previous chapter, we hypothesise that rotating wave solutions are likely in such networks. In addition, rotating wave solutions are expected to occur for a greater domain of initial conditions and increased range of parameter values in the directed cycle of modules than in the directed cycle of simple oscillators. Numerical simulations confirm this hypothesis. Second, in addition to nodes with identical dynamics, we numerically investigate the case in which individual oscillators differ; their parameters are randomly sampled from a distribution centered at fixed nominal values. We observe that, provided that coupling within individual modules is strong enough, solutions resembling

rotating waves emerge in this system, too. In this section we review the work presented in [141].

### 3.4.1 Network definition

As previous, we consider a network of FitzHugh-Nagumo (FHN) (3.25) [46] oscillators. Now for the label of individual nodes,  $j = 1, 2, \dots, n$ ,  $n = M \times N$ ,  $M, N \in \mathbb{N}$  will be specified later. Similarly as previous, parameters  $\alpha, \beta, \gamma$  are chosen as

$$\alpha = \frac{8}{100}, \quad \beta = \frac{8}{10}, \quad \gamma = \frac{1}{3}.$$

At a later stage we will allow the case in which the values of these parameters are different for each node. Variable  $u_j$  corresponds to the network coupling.

The coupling  $u_j$  is supposed to satisfy

$$u_j = - \sum_{l=1}^n \Gamma_{jl}(\sigma, \mu) y_l \quad (3.61)$$

where the matrix  $\Gamma(\sigma, \mu) = \{\Gamma_{jl}(\sigma, \mu)\}$  is:

$$\Gamma(\sigma, \mu) = \sigma \Gamma_r(N) \otimes B + I_N \otimes \mu \Gamma_m(M). \quad (3.62)$$

In (3.62) matrix  $B$  is defined to be

$$B = \begin{pmatrix} 1 & 0 & \dots & 0 \\ 0 & 0 & \ddots & \vdots \\ \vdots & \ddots & \ddots & 0 \\ 0 & \dots & 0 & 0 \end{pmatrix},$$

$\Gamma_m(M)$  is the  $M \times M$  symmetric matrix:

$$\Gamma_m(M) = \begin{pmatrix} M-1 & -1 & \dots & -1 \\ -1 & M-1 & \ddots & \vdots \\ \vdots & \ddots & \ddots & -1 \\ -1 & \dots & -1 & M-1 \end{pmatrix} \quad (3.63)$$

corresponding to the interconnections within each module, and matrix  $\Gamma_r(N)$  is the  $N \times N$  matrix corresponding to the ring/cycle structure:

$$\Gamma_r(N) = \begin{pmatrix} 1 & 0 & \dots & 0 & -1 \\ -1 & 1 & 0 & \dots & 0 \\ 0 & \ddots & \ddots & \ddots & \vdots \\ \vdots & \ddots & -1 & 1 & 0 \\ 0 & \dots & 0 & -1 & 1 \end{pmatrix}. \quad (3.64)$$

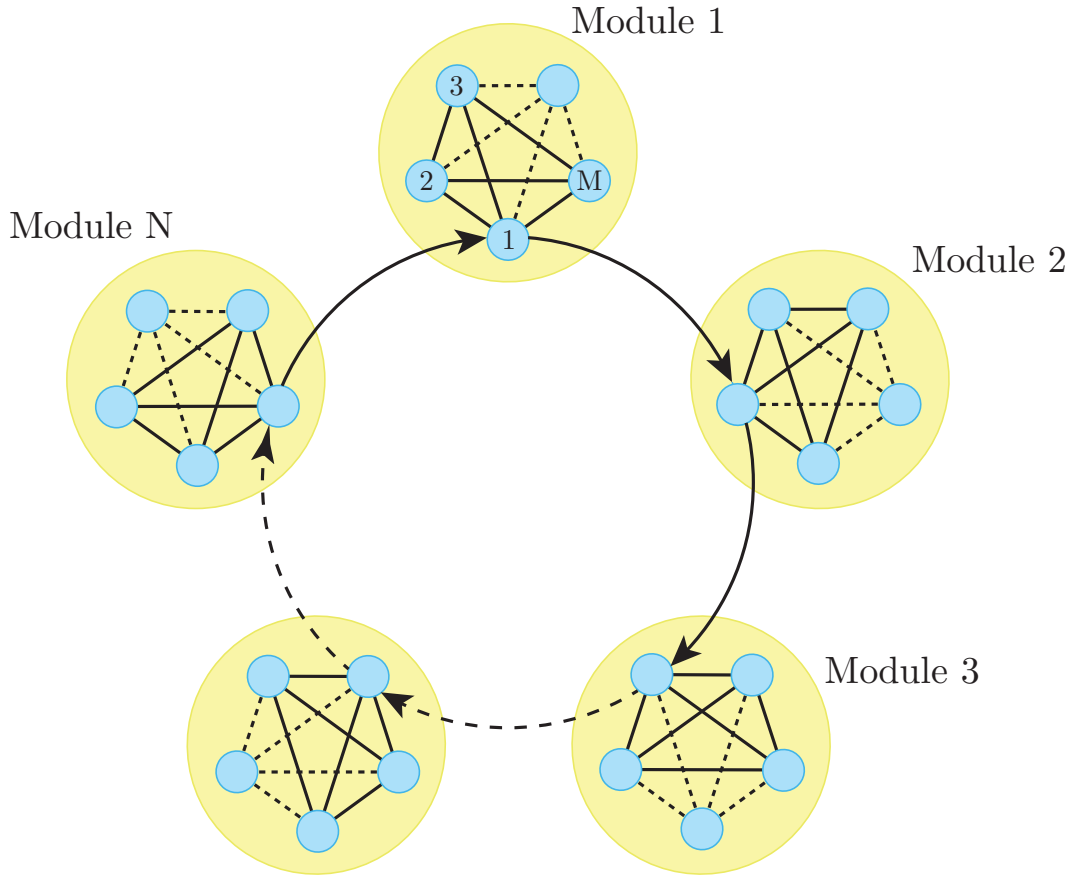


Figure 3.13: Modular network architecture specified by (3.61)

Parameters  $\sigma \in \mathfrak{R}$  and  $\mu \in \mathfrak{R}$  are the inter-modular and the intra-modular coupling strengths, respectively. The values of  $\sigma, \mu$  are supposed to be constant and non-negative.

A diagram illustrating the connectivity pattern of the class of networks considered is shown in Fig. 3.13. This network may be viewed as a simple cycle of “super-nodes”, each corresponding to fully connected modules of identical nodes. Parameters  $M$  and  $N$  in (3.63), (3.64) are hence, respectively the numbers of elements in each modules and the “length” of the cycle formed by the modules. Notice that the coupling matrix  $\Gamma(\sigma, \mu)$  is diffusive but not symmetric.

For convenience, let

$$y = (y_1, \dots, y_n), \quad u = (u_1, \dots, u_n), \quad x = (y, z),$$

and  $x(\cdot; x_0, \sigma, \mu)$  denote a solution of the coupled system with the coupling strength  $\sigma$  and satisfying the initial condition  $x(0) = x_0$ .

### 3.4.2 Extremal properties of the modular cycle

**Boundedness of solutions of the coupled system in forward time** Here we demonstrate the existence and boundedness of solutions of the coupled system and discuss observations regarding parameters  $M$ ,  $N$ ,  $\sigma$ ,  $\mu$  that can be related to coherent dynamics of the system.

As is always the case in the analysis of interconnected nonlinear systems, determining the fact that their solutions are defined for all  $t \geq 0$  and are bounded in forward time is crucial. For the class of systems considered the following statement holds:

**Lemma 3.4.1.** *Consider system (3.25)–(3.64). Solutions of the system are ultimately bounded uniformly in  $x_0$ ,  $\sigma, \mu \in \mathfrak{R}_{\geq 0}$ . That is, there is a compact set  $\Omega \in \mathfrak{R}^{2n}$  such that for all  $x_0 \in \mathfrak{R}^{2n}$ ,  $\sigma, \mu \in \mathfrak{R}_{\geq 0}$*

$$\lim_{t \rightarrow \infty} \text{dist}(x(t, x_0, \sigma, \mu), \Omega) = 0.$$

*Proof.* We first show that FHN oscillators are strictly semi-passive (see also [142]). Let  $S(z_j, y_j) = \frac{1}{2} (\alpha^{-1} z_j^2 + y_j^2)$  be the storage function. Then

$$\dot{S} = -H(z_j, y_j) + y_j u_j$$

with  $H(z_j, y_j) = \beta z_j^2 + y_j^2 (\gamma y_j^2 - 1)$ . Noticing that

$$\begin{aligned} \beta z_j^2 + y_j^2 (\gamma y_j^2 - 1) &= \beta z^2 + dy^2 + \gamma y^4 - y^2 - dy^2 = \\ \beta z^2 + dy^2 + \left( \sqrt{\gamma} y^2 - \frac{d+1}{2\sqrt{\gamma}} \right)^2 - \frac{(d+1)^2}{4\gamma} \end{aligned} \quad (3.65)$$

we conclude that  $H(z_j, y_j)$  is positive for all  $z_j, y_j$  such that

$$\beta z_j^2 + dy_j^2 > \frac{(d+1)^2}{4\gamma}. \quad (3.66)$$

Given that the value of  $d$  in (3.66) can be chosen arbitrarily then assigning  $d = \beta$ , ensures that  $H(z_j, y_j)$  is positive outside the ball

$$z_j^2 + y_j^2 \leq \frac{(\beta+1)^2}{4\beta\gamma}.$$

Hence the FHN oscillators are strictly semi-passive.

Next we consider  $V(z, y) = S(z_1, y_1) + \dots + S(z_n, y_n)$ . The strict semi-passivity property of the FHN neurons implies

$$\dot{V} \leq -H(z_1, y_1) - \dots - H(z_n, y_n) - y^T \Gamma(\sigma, \mu) y.$$

Denoting  $A = \mu \Gamma_m(M)$ ,  $D = \sigma B$ , and noticing that both  $D$  and  $A$  are symmetric, we can

conclude that

$$\Gamma(\sigma, \mu) + \Gamma(\sigma, \mu)^T = \begin{pmatrix} 2A + 2D & -D & 0 & \cdots & 0 & -D \\ -D & 2A + 2D & -D & 0 & \cdots & 0 \\ 0 & \ddots & \ddots & \ddots & \ddots & \vdots \\ \vdots & \ddots & 0 & -D & 2A + 2D & -D \\ -D & 0 & \cdots & 0 & -D & 2A + 2D \end{pmatrix}$$

which, according to the Gershgorin circle theorem, is positive semi-definite. Hence

$$y^T \Gamma(\sigma, \mu) y = \frac{1}{2} y^T (\Gamma(\sigma, \mu) + \Gamma(\sigma, \mu)^T) y \geq 0$$

and consequently

$$\dot{V} \leq -H(z_1, y_1) - \dots - H(z_n, y_n).$$

Therefore, setting the value of  $d$  in (3.65) equal to  $\alpha\beta$  results in

$$\dot{V} \leq -\sum_{j=1}^n \beta z_j^2 + \beta \alpha y_j^2 + n \frac{(\alpha\beta+1)^2}{4\gamma} = -\beta \alpha V + n \frac{(\alpha\beta+1)^2}{4\gamma}.$$

Noticing that the function  $V$  is radially unbounded and positive-definite, we invoke the Comparison Lemma (see e.g. [83]) and conclude that solutions of the coupled system are bounded and converge asymptotically to a compact set of which the size is independent of parameters  $\sigma, \mu$ .  $\square$

### Spectral properties of coupling matrix

**Lemma 3.4.2.** *Consider matrix  $\Gamma(\sigma, \mu)$  specified by (3.62) - (3.64), and let us denote*

$$a = \mu M, \quad b_j = \sigma \frac{1 - \omega_N^{j-1}}{M}, \quad \omega_N = \exp\left(\frac{2\pi i}{N}\right)$$

$$d_j = \frac{1}{2} \sqrt{a^2 + M^2 b_j^2 + (2M - 4)ab_j}.$$

*The spectrum of  $\Gamma(\sigma, \mu)$  is*

$$\begin{aligned} \lambda_1 &= 0, \\ \lambda_j &= \frac{a + Mb_j}{2} - d_j, \\ \lambda_{N-1+j} &= \frac{a + Mb_j}{2} + d_j, \\ \lambda_\ell &= a \end{aligned} \tag{3.67}$$

*where  $j = 2, \dots, N$  and  $\ell = 2N, 2N + 1, \dots, NM$ .*

*Proof.* Denote the  $k \times k$  Fourier matrix by

$$F_k^* = \frac{1}{\sqrt{k}} \begin{pmatrix} 1 & 1 & 1 & \cdots & 1 \\ 1 & \omega_k & \omega_k^2 & \cdots & \omega_k^{k-1} \\ 1 & \omega_k^2 & \omega_k^4 & \cdots & \omega_k^{2(k-1)} \\ \vdots & \vdots & \vdots & & \vdots \\ 1 & \omega_k^{k-1} & \omega_k^{2(k-1)} & \cdots & \omega_k^{(k-1)(k-1)} \end{pmatrix}$$

where

$$\omega_k = \exp\left(\frac{2\pi i}{k}\right)$$

and  $*$  denotes the complex conjugate transpose (note the left hand side of the equation defining  $F_k$ ), cf. [37]. Note that  $F$  is unitary.

Denote

$$F = F_N \otimes F_M,$$

then, by Theorem 5.6.4 of [37],

$$F^* \Gamma F = \text{diag}(W_1, \dots, W_N)$$

with  $W_j$  being  $M \times M$  matrices,  $j = 1, \dots, N$ .

We have

$$F^*(\sigma \Gamma_r(N) \otimes B)F = \sigma F_N^* \Gamma_r(N) F_N \otimes F_M^* B F_M$$

with

$$F_n^* \Gamma_r(N) F_n = \Lambda_r = \begin{pmatrix} 0 & & & & \\ & 1 - \omega_N & & & \\ & & 1 - \omega_N^2 & & \\ & & & \ddots & \\ & & & & 1 - \omega_N^{N-1} \end{pmatrix}$$

with entries of  $\Lambda$  being the eigenvalues of  $\Gamma_r(N)$ ,

$$F_M^* B F_M = \frac{1}{M} \begin{pmatrix} 1 & \cdots & 1 \\ \vdots & & \vdots \\ 1 & \cdots & 1 \end{pmatrix}$$

and

$$F^*(I_N \otimes \mu \Gamma_m(M))F = I_N \otimes \mu F_M^* \Gamma_m(M) F_M$$

with

$$F_M^* \Gamma_m(M) F_M = M \begin{pmatrix} 0 & & & \\ & 1 & & \\ & & \ddots & \\ & & & 1 \end{pmatrix}$$

being the matrix with eigenvalues of  $\Gamma_m(M)$  on its diagonal. Thus

$$W_1 = \mu M \begin{pmatrix} 0 & & & \\ & 1 & & \\ & & \ddots & \\ & & & 1 \end{pmatrix},$$

$$W_j = W_1 + \sigma \frac{1 - \omega_N^{j-1}}{M} \begin{pmatrix} 1 & \cdots & 1 \\ \vdots & & \vdots \\ 1 & \cdots & 1 \end{pmatrix}, \quad j = 2, \dots, N.$$

Denoting  $\mu M = a$  and  $\sigma \frac{1 - \omega_N^{j-1}}{M} = b_j$ , we obtain the characteristic polynomials of the blocks  $W_1, \dots, W_N$ :

$$p_1(\lambda) = \det(\lambda I_M - W_1) = \lambda(\lambda - a)^{M-1}$$

and

$$p_j(\lambda) = \det(\lambda I_M - W_j) = (\lambda^2 - (a + Mb_j)\lambda + ab_j)(\lambda - a)^{M-2}$$

for  $j = 2, \dots, N$ . Thus  $\Gamma(\sigma, \mu)$  has the following eigenvalues:

$$\begin{aligned} \lambda_1 &= 0, \\ \lambda_j &= \frac{a + Mb_j}{2} - \frac{1}{2} \sqrt{a^2 + M^2 b_j^2 + (2M - 4)ab_j}, \\ \lambda_{N-1+j} &= \frac{a + Mb_j}{2} + \frac{1}{2} \sqrt{a^2 + M^2 b_j^2 + (2M - 4)ab_j}, \\ \lambda_\ell &= a \end{aligned}$$

with  $j = 2, \dots, N$  and  $\ell = 2N, 2N + 1, \dots, NM$ . □

A statement that is very similar to Lemma 3.4.2 can be formulated for the symmetrized coupling matrix  $1/2(\Gamma(\sigma, \mu) + \Gamma(\sigma, \mu)^T)$ . In this case the values of  $b_j$  in (3.67) will be replaced with  $\Re(b_j)$ .

According to Lemma 3.4.2 the spectrum of  $\Gamma(\sigma, \mu)$  contains one zero eigenvalue, the eigenvalues  $\mu M$  of isolated modules, and complex eigenvalues

$$\frac{a + Mb_j}{2} \pm \frac{1}{2} \sqrt{a^2 + M^2 b_j^2 + (2M - 4)ab_j}.$$

Let us consider the eigenvalue  $\lambda_N$ :

$$\frac{a + Mb_N}{2} - \frac{1}{2} \sqrt{a^2 + M^2 b_N^2 + (2M - 4)ab_N}.$$

Note that

$$\begin{aligned} b_N &= \frac{\sigma}{M} (1 - \omega_N^{N-1}) = \\ &= \frac{\sigma}{M} \left( 1 - \cos \left( 2\pi \frac{N-1}{N} \right) - i \sin \left( 2\pi \frac{N-1}{N} \right) \right). \end{aligned}$$

That is, for  $N$  large the absolute value of  $b_N$  approaches zero, and hence  $\lambda_N$  approaches zero, too. Expressing  $\lambda_N$  as a function of  $b_N$  results in

$$\lambda_N = b_N + O(\|b_N\|^2) \quad (3.68)$$

and hence for  $N$  sufficiently large

$$\frac{\Im(\lambda_N)}{\Re(\lambda_N)} \simeq \frac{\Im(b_N)}{\Re(b_N)} = \frac{\sin\left(2\pi\frac{N-1}{N}\right)}{1 - \cos\left(2\pi\frac{N-1}{N}\right)} = \cot\left(\frac{\pi}{N}\right).$$

This observation, for modular networks of which the connectivity is determined by (3.62)–(3.64), is strikingly consistent with the extremal properties of simple cycles [61]. This motivates our expectation that behaviour previously observed for simple cycles (such as prevalence of rotating wave solutions) will also be observed for networks with the modular architecture discussed here.

Note also that according to (3.68) the values of  $\lambda_N$  and  $\Re(\lambda_N)$ , for  $N$  sufficiently large, scale with  $M$ . This suggests that achieving fully synchronous state in modular systems may require proportionally larger values of coupling strength  $\sigma$  as compared with the simple cycles of the same lengths. This is exactly what we observed in our numerical experiments of which the summary is presented below.

**Co-existence of synchronization and rotating waves** The previous sections show that, on the one hand, when the number of modules in the network grows, their relative dynamics becomes more and more under-damped. In order to confirm our intuition and at the same time to explore the behaviour of the system for heterogeneous nodes, we performed an exhaustive numerical exploration of the system dynamics for various values of coupling strengths  $\sigma, \mu$  and  $N, M$ .

We considered networks with both identical and non-identical nodes. For networks with identical nodes we investigated the influence of the number of elements in each module,  $M$ , on the prevalence of rotating wave solutions. The methodology of numerical analysis was similar to the one reported in [61]. Results are provided in Fig. 3.14. Red lines show the values of critical coupling strength corresponding to rotating wave solutions in simple cycles [61]. Note that the boundaries of rotating wave solutions in these diagrams appear to stretch along the  $\sigma$ -axis with  $M$ .

For the case of heterogeneous dynamics we numerically determined the regions of practical stability of the two solution types: rotating waves, and synchronization. Note that the systems are not identical, hence one can only expect the systems to converge to a solution that is resembling that of a rotating wave or a synchronized state. For fixed parameters  $M$ , the size of each module, and intra-modular coupling strength  $\mu$ , the parameters  $N$ , the

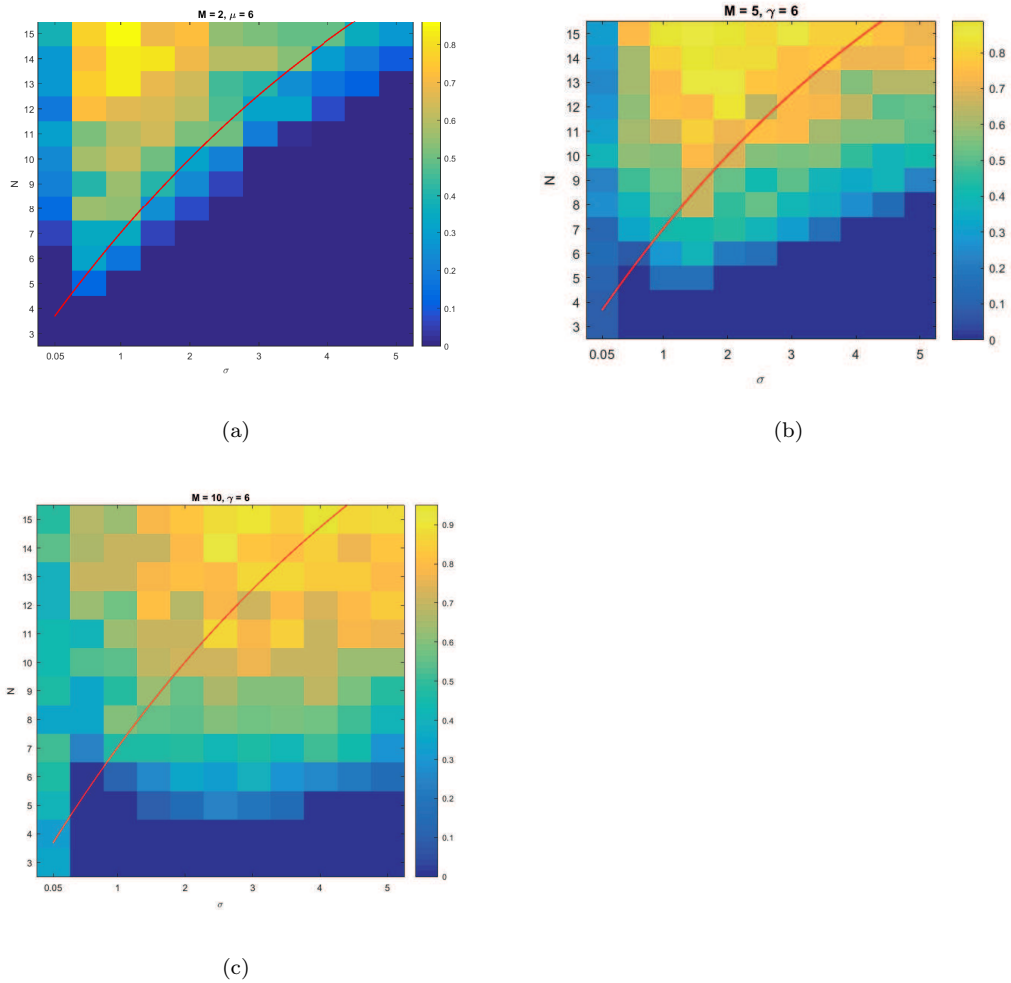


Figure 3.14: Proportion of samples yielding rotating wave solutions in the  $(N, \sigma)$  plane (identical oscillators). The horizontal axis shows the values of  $\sigma$ ; the vertical axis shows the values of  $N$

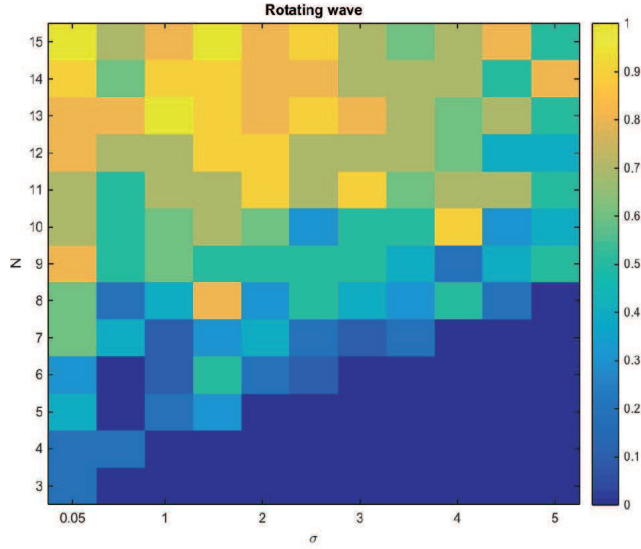


Figure 3.15: Proportion of samples that yield solutions resembling rotating waves in the  $(N, \sigma)$  plane (heterogeneous oscillators). The horizontal axis corresponds to the values of  $\sigma$ , vertical axis stands for the values of  $N$

size of the cycle, and  $\sigma$ , the inter-modular coupling strength were varied. Parameters  $M$  and  $\mu$  are chosen as:  $M = 2, 5, 10$ , and  $\mu = 6$ . For each pair of these parameter values, the parameters  $N = 3, 4, \dots, 15$  and  $\sigma = 0.05, 0.5, 1, 1.5, \dots, 5$  are considered. For each possible pair of parameter values  $(N, \sigma)$ , the dynamics of coupled FHN oscillators are initiated independently, 25 times. Results of our numerical investigation for  $M = 5$  and  $\mu = 6$  are summarized in Figs. 3.15 – 3.17. Simulations performed for other parameter values were similar to the ones presented.

We considered the effect of how parameters of the network topology such as modularity and the presence of cycles, influences the dynamics of collective behaviour in the system. We showed that if connectivity within isolated modules is diffusive with relatively strong coupling, multiple coherent and orderly dynamic regimes co-exist in the system state space. In addition to a nearly fully synchronous state, an attracting rotating wave solution occurs. Prevalence of one solution type over the other is determined by the combination of the cycle length, inter- and intra-modular coupling strengths, and the number of elements in each modules. The results persist even when the dynamics of individual nodes are not identical.

### 3.5 Conclusion

In the first part of this chapter, *Leaders do not look back, or do they?*, we considered the problem of how network topology influences the dynamics of collective behaviour in the

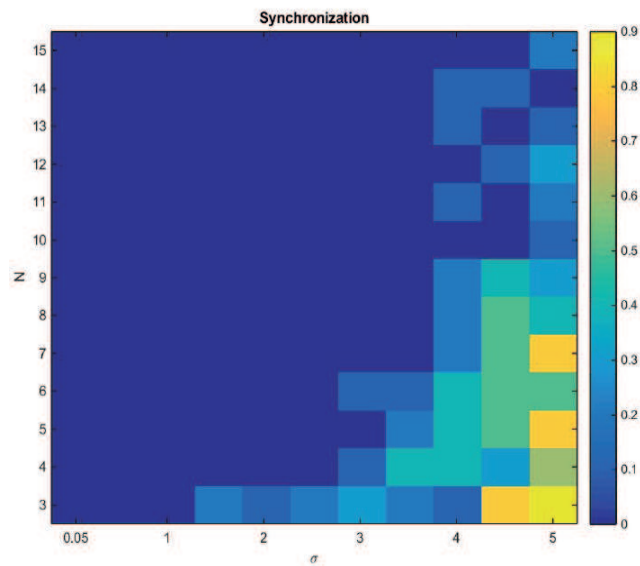


Figure 3.16: Proportion of samples that yield a nearly fully synchronous solution in the  $(N, \sigma)$  plane (heterogeneous oscillators). The horizontal axis corresponds to the values of  $\sigma$ ; the vertical axis stands for the values of  $N$

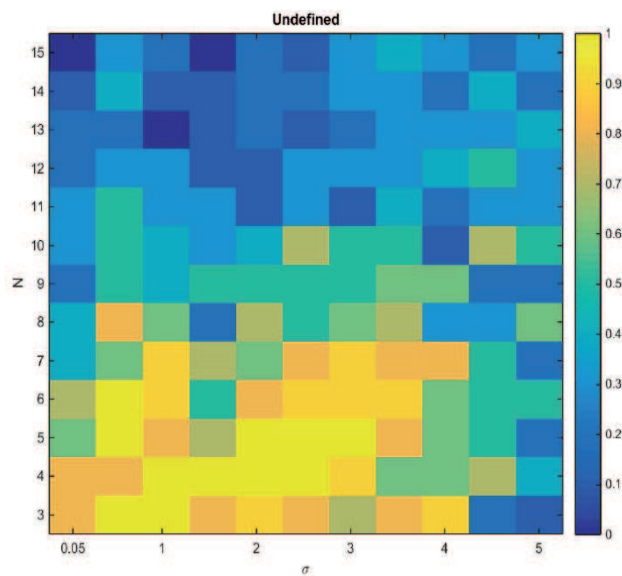


Figure 3.17: Proportion of samples that we were unable to relate to either of the classes (rotating wave or fully synchronous state). The horizontal axis corresponds to the values of  $\sigma$ ; the vertical axis stands for the values of  $N$

system. We approached the problem by studying how “closing” a chain of interconnected systems with directed coupling by a directed feedback from the last element in the chain to the first may affect the dynamics of the system. Two general settings have been investigated. In the first we analysed the behaviour of a simple linear system. We showed that the simple cycle with equal interaction weights has the slowest decay of the oscillations among all linear systems with the same number of states. In the second setting we considered directed rings and chains of identical nonlinear oscillators. For directed rings, a lower bound  $\sigma_c$  for the connection strengths that guarantee asymptotic synchronization in the network is found to follow a pattern similar to that of a simple cycle. Furthermore, numerical analysis revealed that, depending on the network size  $n$ , multiple dynamic regimes co-exist in the system’s state space. In addition to the fully synchronous state, for sufficiently large networks an asymptotically stable rotating wave solution emerges. The emergence of the rotating wave is a phenomenon that persists over a broad range of coupling strengths and network sizes, and can be viewed as a form of extreme sensitivity of the network dynamics to removal or addition of a single connection. The result confirms the significance of shortcuts in networks with large numbers of nodes.

Getting back to the question if leaders should look back. To stay in sync we advise a leader either not to look back at all or to look back just a few links; Looking back too far induces oscillations that destroy the coherent state.

In the second part of this chapter, *Multi-Stability of coherent dynamics in directed networks with modular topology*, we considered the effect of how parameters of the network topology such as modularity and the presence of cycles, influences the dynamics of collective behaviour in the system. We showed that if connectivity within isolated modules is diffusive with relatively strong coupling, multiple coherent and orderly dynamic regimes co-exist in the system state space. In addition to a nearly fully synchronous state, an attracting rotating wave solution occurs. Prevalence of one solution type over the other is determined by the combination of the cycle length, inter- and intra-modular coupling strengths, and the number of elements in each modules. The results persist even when the dynamics of individual nodes are not identical.

## Chapter 4

# Emergence of Complex Network Structures

### 4.1 Introduction

In this chapter, we turn our attention to network structures more complex than previously discussed, and how they arise as a process of self-organisation. Particular attention is paid to the emergence of small-world network (SWN) structures. In addition, modular, centralised, and hierarchical structures are also considered.

Before considering such complex structures, as we have done in the previous chapter, it is helpful to first understand more basic ones. Two such basic network structures - often used to characterise more complex ones - are the regular and random networks.

A regular network is one that possesses a form of isotropy; vertices have equal degree and typically local connectivity structures for each vertex are identical. For example, the 4-regular lattice is the network in which vertices are embedded on a grid, and each vertex connects to its four nearest neighbours. Such a graph possesses a high degree of segregation - densely connected cliques of vertices -, yet a poor degree of integration - the likelihood is low that there exists a relatively short sequence of edges connecting any two randomly chosen vertices.

In contrast, a strongly opposing network structure is the random network. The classical Erdős-Rényi [45] network is constructed from the set of vertices  $V$  by adding each pair  $i, j \in V$  to the edge set with some probability  $p$ , i.e., with probability  $p$ ,  $(i, j) \in E$ . Such a random graph possesses a high degree of integration, yet a low degree of segregation.

A complex network structure, the SWN, is considered as the reconciliation of such regular and random ones. In the classic Watts and Strogatz (WS) algorithm [154], a SWN is obtained

by randomly rewiring a certain proportion of edges of an initially regular network. Thereby, the network largely maintains segregation, while the rewiring creates shortcuts that enhance the networks integration.

SWN structures are ubiquitous in nature and man-made systems; SWNs can be found in protein [4] and ecological networks [105], social networks [149], the mammalian brain [63; 139; 25], and the World Wide Web [147]. As the WS algorithm demonstrates how these properties may be reconciled in a very basic manner, the WS algorithm may have a justifiable claim to be considered a common principle underlying the emergence of SWNs in these different physical contexts. However, the rewiring of the WS algorithm compromises any existing order, rather than to develop order over time. Hence, the WS algorithm does not fit easily to the self-organisation and maintenance found in adaptive systems.

It remains that the emergence of SWNs in nature and man-made systems is not yet fully understood. In this chapter, we aim to provide further insight into the process of self-organisation of SW, modular, centralised, and hierarchical network structures. In Section 4.3 we consider the role that space plays in network self-organisation. Using coupled logistic maps to model large populations of neurons, network connectivity evolves in response to both patterns of activity and the distance separating them. The effect of spatial bias is shown to promote emergence of modular and SW structures, and moreover, emergent order is organised in space, for instance, segregated cliques of vertices are spatially local. In addition, spatial bias reveals that the spatial organisation and the cost of long distance connections improves the robustness of self-organising processes; self-organisation is shown to be robust to low connectivity densities (edge sets with small cardinality).

In Section 4.4 we aim to generalise network self-organisation by removing explicit dynamics. In previous studies, SWN structures have been shown to robustly emerge through rewiring according to the ongoing dynamics on the network, however, the claim to universality has been frustrated by need to explicitly specify the dynamics. Here we take a more general approach and replace explicit dynamics with an abstract representation of network diffusion using heat kernels. Heat kernels capture network-specific interaction between vertices and as such they are, for the purpose of this article, a generic model of network diffusion. We therefore propose, essentially, that patterns of activity play a “lesser” role in network structure evolution than previously thought. In particular, that patterns of activity are the product of the underlying connectivity (network diffusion) and noise. Accordingly, in a computational model, network structure evolution is in response to the product of *patterns of connectivity*, and varying degrees of noise. In contrast with the random rewirings in the WS algorithm, here, noise (random rewirings) have the function of perturbing possible equilibrium network states, akin to the Boltzmann machine.

## 4.2 Preliminaries: Characterising graph structure

In this Section we review some of the network measures used to characterise specific properties of a given networks structure. Often a collection of measures are needed in order to understand the structure of a network. (Almost all) Measures used in this thesis are discussed in [127] and implemented using the MATLAB scripts they provide.

### Notation

In what follows we consider graphs that are undirected. A graph is an ordered pair  $G = (V, E)$  where  $V$  is the set of vertices and  $E$  is a subset of  $V \times V$  called the edges. If  $X$  is a finite set, then  $|X|$  denotes its cardinality. The total number of vertices and edges in the graph are  $|V| = n$  and  $|E| = m$ , respectively. Two vertices  $u, v \in V$  are called *adjacent* if  $(u, v) \in E$ . The *adjacency matrix* of a graph  $G$  is a square  $n \times n$  matrix  $A$  with entries  $a_{uv} = 1$  if  $(u, v) \in E$ , and  $a_{uv} = 0$  otherwise. For undirected graphs  $A$  is symmetric. It is typically the case that  $a_{uu} = 0$ , i.e. no self-loops. The *degree*  $d_v$  of a vertex  $v$  is the number of vertices adjacent to vertex  $v$ :  $d_v = \sum_{u \in V, u \neq v} a_{vu}$ . The matrix  $D$  is the diagonal matrix of degrees having entries  $D_{uv} = d_u$  if  $u = v$  and 0 otherwise. For a given set of  $n$  vertices  $V$  the complete graph is denoted as  $K_n$  and its edge set is denoted as  $E^{K_n}$ . The complement of an edge set  $E$ , denoted as  $E^c$ , is  $E^c = E^{K_n} \setminus E$ .

A graph  $G = (V, E)$  is called *directed* if for at least one pair of vertices  $i, j \in V$ ,  $(i, j) \neq (j, i)$ , i.e., if  $(i, j) \in E$  then  $(j, i) \notin E$ , or *vice versa*. Here, without loss of generality we use the convention that row-wise entries of the adjacency matrix  $A$  correspond to out-going edges, while column-wise entries correspond to in-coming edges. To take the converse, take the transpose of matrix  $A$ . Directed graphs have two degrees, the in-degree and the out-degree, that are not necessarily equal. The in-degree of vertex  $v$  is  $d_v^{\text{in}} = \sum_{u \in V, u \neq v} a_{vu}$  while its out-degree is  $d_v^{\text{out}} = \sum_{u \in V, u \neq v} a_{uv}$ .

### Statistical characterisation of graph structure

**Clustering coefficient** ( $C$ ) provides a measure of network segregation. It is calculated for each vertex as the fraction of its adjacent vertices that are also pairwise adjacent, i.e. where a triangle is the fully connected sub-network of three vertices, it is the number of triangles that share a vertex, divided by the degree of that vertex. The mean clustering coefficient for the network hence reflects, on average, the prevalence of clustered connectivity around individual nodes [127].

Denote as a *candidate triangle* pivoting on node  $i$  each pair of nodes adjacent to  $i$ , and as an *actual triangle* pivoting on  $i$  each pair of nodes adjacent to  $i$  that are themselves

connected. The clustering coefficient  $C_i$  for vertex  $i$  is then the ratio of the number of actual triangles pivoting on  $i$  to the number of candidate triangles pivoting on  $i$ .

The number of triangle sub-networks pivoting on node  $i$  - pairwise vertices adjacent to node  $i$  that are themselves connected - is calculated as

$$t_i = \frac{1}{2} \sum_{j,h \in \mathcal{N}} a_{ij} a_{ih} a_{jh}.$$

The clustering coefficient  $C$  for the network is the average of  $C_i$  over vertices  $i$ ,

$$C = \frac{1}{n} \sum_{i \in \mathcal{N}} C_i = \frac{1}{n} \sum_{i \in \mathcal{N}} \frac{2t_i}{k_i(k_i - 1)}. \quad (4.1)$$

**Weighted clustering coefficient** ( $C^w$ ) provides a geometrical measure of segregation (also referred to in Chapter 4 as spatially localised clustering or spatial clustering) by combining edge weights - possibly spatial distance - with clustering. It uses a weighted adjacency matrix in which weight is inversely proportional to distance. the weight of an edge is a linearly decreasing function of edge lengths in  $[0, \pi]$  normalised to the range  $[0, 1]$ .

The weighted clustered coefficient  $C_i^w$  for vertex  $i$  is calculated as the sum over all triangles centred on  $i$  of the geometric mean of the three edge weights, divided by the degree of vertex  $i$ . The weighted clustering coefficient  $C^w$  for the network is the average of  $C_i^w$  over  $i$ .

A weighted triangle is determined as the cubic root of the product of the three weighted edges that make a triangle centred on a given vertex. The sum of all triangles pivoting on a given node  $i$  is

$$t_i^w = \frac{1}{2} \sum_{j,h \in \mathcal{N}} (w_{ij} w_{ih} w_{jh})^{1/3}$$

for edge weights  $w_{ij}$ .

Thus, the weighted clustering coefficient is calculated as

$$C^w = \frac{1}{n} \sum_{i \in \mathcal{N}} C_i^w = \frac{1}{n} \sum_{i \in \mathcal{N}} \frac{\sum_{j,h \in \mathcal{N}} 2t_i^w}{k_i(k_i - 1)} \quad (4.2)$$

**Average shortest path length** ( $L$ ), also known as the characteristic path length, provides a measure of network integration. A path of length  $l$  connecting two given vertices  $i$  and  $j$  is a sequence of vertices  $i = i_0, i_1, \dots, i_l = j$  with edges  $e_k = (i_k, i_{k+1})$  connecting successive pairs of vertices. The average shortest path length of the network is the average over all pairs  $i$  and  $j$  ( $i \neq j$ ) of the length of the shortest path connecting  $i$  and  $j$ . For disconnected pairs of nodes the path length is infinite. Such pairs are excluded from calculation of the average shortest path length. However, the connectivity densities we have

used are above the corresponding percolation threshold and thus guarantee that all vertices belong to a single connected component.

A path of length  $l$  between nodes  $i$  and  $j$  is a sequence of vertices  $\eta_{i \leftrightarrow j} = (i = i_0, \dots, i_l = j)$  with  $a_{i_k, k+1} = 1$ . Let  $l_{ij}$  be the length of the shortest path between  $i$  and  $j$ . The average shortest path length is the mean value over all pairwise nodes, calculated as

$$L = \frac{1}{n(n-1)} \sum_{i \in \mathcal{N}} \sum_{j \in \mathcal{N}_i} l_{ij}. \quad (4.3)$$

For disconnected pairs of nodes  $l_{ij}$  is undefined, however, such pairs are excluded in the MATLAB program computation to allow a result.

**Global efficiency** ( $E$ ), closely related to the average shortest path length, provides the average inverse shortest path length between all pairs of vertices in the network [95]. Unlike the average shortest path length, the global efficiency may be meaningfully computed on disconnected networks, as paths between disconnected nodes are defined to have infinite length, and correspondingly zero efficiency. More generally, the characteristic path length is primarily influenced by long paths (infinitely long paths are an illustrative extreme), while the global efficiency is primarily influenced by short paths. Some authors have argued that this may make the global efficiency a superior measure of integration [2].

For all pairwise shortest paths  $d_{ij} = \sum_{a_{uv} \in g_{i \leftrightarrow j}} a_{uv}$ , define the global efficiency  $E$  as

$$E = \frac{1}{n} \sum_{i \in \mathcal{N}} E_i = \frac{1}{n} \sum_{i \in \mathcal{N}} \frac{\sum_{j \in \mathcal{N}, j \neq i} d_{ij}^{-1}}{n-1} \quad (4.4)$$

**Modularity** ( $Q$ ) describes the degree to which a network may be partitioned into non-overlapping communities of vertices [109]. An optimization problem, solutions are not necessarily unique. Partitions are defined such that non-overlapping communities maximize the number of within-community edges and minimize the number of between-community edges. Various algorithms have been suggested for finding optimal or near-optimal partitions. We use Newman's community structure detection algorithm [110]:

For a given network partition of modules  $M$ , the modularity index  $Q$  is given by

$$Q = \sum_{u \in M} \left[ e_{uu} - \left( \sum_{v \in M} e_{uv} \right)^2 \right] \quad (4.5)$$

where  $e_{uu}$  is the proportion of all edges that connect vertices within a module and  $e_{uv}$  is the expected proportion edges that connect vertices in module  $u$  with vertices in module  $v$  for an equivalent random network. An optimal modular structure for a given network is one that maximizes the value  $Q$ .

**Small-worldness** ( $\Sigma$ ) provides a single value involving both clustering coefficient and average shortest path length. The measure of small-worldness is calculated as the normalised

ratio of clustering coefficient and average shortest path length, where  $C$  and  $L$  are normalised by the values of clustering coefficient  $C_{\text{rand}}$  and average shortest path length  $L_{\text{rand}}$  calculated for a random network. The measure of small-worldness was proposed by [67] as a method for determining network canonical equivalence; however, this measure has been criticised by [127] for yielding false positives with highly segregated but poorly integrated networks. However, in combination with other measures, we can safely use this simple measure.

Calculated as the normalised ratio of the clustering coefficient to the average shortest path length:

$$\Sigma = \frac{C/C_{\text{rand}}}{L/L_{\text{rand}}}, \quad (4.6)$$

for  $C$  the clustering coefficient and  $L$  average shortest path length of a network, normalised respectively by the corresponding quantities  $C_{\text{rand}}$  and  $L_{\text{rand}}$  for a corresponding random network.

Alternatively, the measure of small-worldness [67] may be modified by replacing the average shortest path length with the global efficiency, such that  $\Sigma$  becomes

$$\Sigma_E = \frac{C}{C_{\text{rand}}} \times \frac{E}{E_{\text{rand}}}$$

where  $E$  and  $E_{\text{rand}}$  are the global efficiency of a given network and of a corresponding equivalent random network, respectively. By this definition, the small-worldness index is robust to isolated vertices. Moreover, it is influenced more by shorter path lengths, whereas  $\Sigma$  is more influenced by longer path lengths.

**Edge betweenness (EB)** provides a measure of the centrality of a given edge in a network. Each edge is assigned a value equal to the fraction of all shortest paths in the network that include that edge. High betweenness edges have a considerable effect on the integration of the network through their effect on the average shortest path length.

Calculated for each edge as the fraction of shortest paths in the network which pass through the edge. Let  $H_{uv}$  be the number of shortest paths that connect nodes  $u$  and  $v$ , and let  $H_{uv}(i, j)$  be the number of shortest paths between nodes  $u$  and  $v$  that includes the edge between  $i$  and  $j$ .

Then, the edge betweenness value for the edge between  $i$  and  $j$  is calculated as

$$\text{EB} = \sum_{\substack{u, v \in \mathcal{N} \\ u \neq v}} \frac{H_{uv}(i, j)}{H_{uv}}. \quad (4.7)$$

**Network wiring cost ( $M$ )** is a measure we define and use in Section 4.3 to measure the spatial localisation of edges. It is calculated as the normalised average edge length. Small  $M$  corresponds to high spatial localisation and vice versa.

The normalised average edge length for all edges of the network is

$$M = \frac{1}{\pi \sum_{i \in \mathcal{N}} k_i} \sum_{i \in \mathcal{N}} \sum_{j \in \mathcal{N}_i} d_{ij} \quad (4.8)$$

where  $\pi$  is the maximum edge length that connects two vertices on the shortest arc along the great circle for the network embedded on a unit sphere. A network wiring cost value of 1 indicates an average edge length of  $\pi$ , of zero indicates an average edge length of zero, and of  $\frac{1}{2}$  indicates the expected value for randomly distributed edge lengths.

**Assortativity coefficient** ( $a$ ) describes the ‘‘assortative mixing’’ of vertex degrees, i.e. the preference for high-degree vertices to attach to other high-degree vertices.

The assortativity coefficient [108]

$$a = \frac{l^{-1} \sum_{(i,j) \in L} k_i k_j - \left[ l^{-1} \sum_{(i,j) \in L} \frac{1}{2} (k_i + k_j) \right]^2}{l^{-1} \sum_{(i,j) \in L} \frac{1}{2} (k_i^2 + k_j^2) - \left[ l^{-1} \sum_{(i,j) \in L} \frac{1}{2} (k_i + k_j) \right]^2} \quad (4.9)$$

**Maximised coreness statistic** ( $c$ ) measures the extent to which a network may be well-partitioned into two non-overlapping groups of vertices, a core and a periphery group. The original conception of this measure can be found in [20]. The intuition of the core-periphery partition is to label the network into two subgroups; the core group cannot be divided into exclusive subgroups, while the whole network can be seen as just one group, to which all vertices belong to the core group, but to greater and lesser extents. The coreness statistic  $c$  is the optimization of  $\rho$ ,

$$\rho = \sum_{i,j} a_{ij} \delta_{ij}$$

$$\delta_{ij} = \begin{cases} 1 & \text{if } c_i = \text{CORE or } c_j = \text{CORE} \\ 0 & \text{otherwise} \end{cases}$$

where  $a_{ij}$  represents an edge,  $c_i$  refers to the label of vertex  $i$ , and  $\delta_{ij}$  represents an edge in the idealised core/periphery structure, where the idealised core/periphery partition is computed using a version of Kernighan-Lin algorithm for graph partitioning in community detection [110].

**PageRank centrality** vector ( $\pi$ ), is a variant of eigenvector centrality. It is defined as the stationary distribution achieved by instantiating a Markov chain on a graph. The PageRank centrality of a given vertex, then, is proportional to the number of steps (or amount of time) spent at that vertex as a result of such a process [127]. PageRank centrality takes into account global communication patterns, mediated by longer path lengths and patterns of convergence and divergence, whereas some of the more common centrality measures, such as closeness and betweenness centrality, do not [138].

A defining feature of the PageRank centrality is how it differs from the eigenvector centrality: PageRank centrality allows for random ‘jumps’ in the network. Motivated by a person navigating web pages, they follow directed edges - web page links - to progressive web pages. Spontaneously that person may ‘jump’ to another web page without following a web page link, i.e. they navigate from one vertex to another where there may be no edge connecting them. For derivation of the PageRank vector consider the original Google Pagerank [23].

In Section 4.4 we denote as  $\pi$  the (normalised) maximum component of the PageRank vector. The mean value of the components of a PageRank vector for a given network of  $n$  vertices is  $\frac{1}{n}$ . For convenience we normalise  $\pi$  by this mean value.

### 4.3 Spatially constrained adaptive rewiring in cortical networks creates spatially modular small-world structures

In a highly simplified model of cortical network, [59] showed that rewiring of an initially random network in response to a model of spontaneous cortical activity - adaptive rewiring - gives rise to a modular small-world structures. This effect was further explored in a series of studies [128] that demonstrated a symbiotic relationship between structure and function. This means that not only the structure is created by the activity patterns, but the structure created by the patterns is optimal for sustaining them. On a random underlying connectivity structure, nonlinear neural mass models have been shown to exhibit modular functional connectivities. The presence of functional modules will gradually, through activity-dependent synchrony-favouring rewiring, enable the emergence of similar modules in the underlying structural connectivity.

The advantage of simple models is their application to uncovering universal principles. A simple model is “detail invariant” - that is, robust across a range of potential constraints, whereas findings arising in detailed models may not be robust to changes in those details.

Following the success of adaptive rewiring, over a period of 10 years further steps have been taken to improve the realism through a series of computational studies. These include model neurons [91], pruning [150], and growth by preferential attachment [58]. The resulting rewiring scenarios showed, not only greater realism but also increased efficiency and robustness of the symbiosis of activity and structure. Despite previous developments of the adaptive rewiring model, there remains an important limitation to the applicability as a model of real, biological cortices: adaptive rewiring is missing any notion of metric

space. Embedding this process into a metric space may allow models to incorporate realistic characteristics of cortical networks, such as metabolic cost and wiring length [97].

### 4.3.1 Dynamics: Coupled maps

The evolving networks we study in this section have  $n = 500$  nodes and  $E$  undirected edges, with  $E = \kappa \frac{n(n-1)}{2}$  where  $\kappa \in (0, 1]$  is the connection density;  $\kappa$  takes the value of 0.1, i.e. 10% connectivity density, except for our study of dependence on connection density where it ranges from 2.5% to 5%. Previous non-spatial implementations of the adaptive rewiring process with  $\kappa = 0.1$  were found to yield small-world structure [59; 58; 128; 150].

The  $n$  nodes of the network are assigned positions on a unit sphere that are approximately evenly distributed over the surface with sufficient accuracy for our purpose. To distribute the  $n$  points on a sphere, we use a simple iterative algorithm based on repulsion. Beginning from an initial set of points drawn randomly from a uniform distribution over the sphere, on each iteration the point “most central” is selected, all other points are then repelled by a linearly dampening force function. Individual approximations of evenly distributed points on the sphere are used for independent runs.

As reference points for network structure, we also apply the above network measures to a random network and a regular type network on the sphere, with the same  $n$  and  $\kappa$  as our evolving networks. The random graph is generated by selecting  $E$  pairs of vertices uniformly at random from all possible pairs and connecting each pair with an edge [111]. Note that the graph will (with very high probability) be connected if  $E \gg \frac{\log(n)}{n}$  [18], which is the case for all networks we study here. The regular type network is constructed such that each node is connected to its  $k = \kappa n$  nearest neighbours on the unit sphere. Note that, unlike the ring-like regular networks used by [154], it is not the case that  $L_{\text{regular}} \gg L_{\text{random}}$  for our regular networks because of the spherical geometry and the relatively high connectivity density of our networks.

The dynamics upon which rewiring is based is a well-established class of dynamical systems, that of coupled maps [79; 5]. On these networks, the nodes are assigned identical nonlinear maps  $f : [-1, 1] \rightarrow [-1, 1]$ . The states of the nodes are updated iteratively using the following diffusive coupling scheme:

$$x_i(t+1) = f(x_i(t)) + \frac{\epsilon}{|\mathcal{N}_i|} \sum_{j \in \mathcal{N}_i} [f(x_j(t)) - f(x_i(t))], \quad (4.10)$$

for  $i = 1, 2, \dots, n$ ,  $\epsilon$  is the coupling strength,  $\mathcal{N}_i$  denotes the set of neighbours of node  $i$ , i.e. the set of all nodes that connect to node  $i$ , and  $|\mathcal{N}_i|$  is the cardinality of the set  $\mathcal{N}_i$ , i.e. the number of neighbours to node  $i$ . Connections are undirected, i.e.  $i$  connects to  $j$  if and only

if  $j$  connects to  $i$ . Function  $f$  is the logistic map

$$f(y) = 1 - \alpha y^2$$

with parameter  $\alpha \in [0, 2]$ . As demonstrated in Figure 2 of [128], the logistic map can be considered as a reduced model, constructed using a Poincaré section, of a chaotic model of neuronal population activity [22]. Since we are interested in population activity, this map was preferred as a model over others, such as [130], that represent individual neuron spiking activity. It is easy to verify that for  $\epsilon \in [0, 1]$ ,  $x(0) = (x_1(0), \dots, x_n(0)) \in [-1, 1]^n$  implies  $x(t) \in [-1, 1]^n$  for all  $t \geq 0$  so the dynamics are well-defined in forward time. The parameters used in this study are  $\alpha = 1.7$ , for which the dynamics  $y(t + 1) = f(y(t))$  are chaotic, and  $\epsilon = 0.4$  which previous studies have shown to yield modular small-world structure in non-spatial networks of this size [150].

### 4.3.2 Stability of synchronization

The stability of the synchronization manifold for coupled logistic maps can be assessed by linearising the transverse stability of the synchronization manifold

Rewrite Equation (4.10) as

$$x_i(t + 1) = (1 - \epsilon)f(x_i(t)) + \frac{\epsilon}{|\mathcal{N}_i|} \sum_{j \in \mathcal{N}_i} f(x_j). \quad (4.11)$$

Denote the vector  $x(t) = (x_1(t), \dots, x_n(t))^T$ , then Equation (4.11) can be written as

$$x(t + 1) = (1 - \epsilon)F(x(t)) + \epsilon \mathcal{N}F(x(t)) \quad (4.12)$$

where  $F(x(t)) = (f(x_1(t)), \dots, f(x_n(t)))^T$ ,  $\mathcal{N} = AD^{-1}$  for  $A$  the adjacency matrix, and  $D$  the diagonal matrix of vertex degrees. Assuming that the network is connected, i.e., there exists a path between any pairwise vertices, then matrix  $\mathcal{N}$  has the following properties:

- 1) Matrix  $\mathcal{N}$  has all row sums equal to one, i.e.,  $\mathcal{N}\mathbf{1} = \mathbf{1}$  for  $\mathbf{1} = (1, \dots, 1)^T$  the  $n$ -vector of all ones.
- 2) All eigenvalues of  $\mathcal{N}$  are contained within a unit disc in the complex plane. This can be shown using Gershgorins circle theorem [55].
- 3) There exists a zero eigenvalue, such that its corresponding eigenvector is in the set  $\text{span}(1, \dots, 1)$ , i.e.,  $\mathcal{N}\mathbf{1} = \mathbf{0}$ .
- 4) The zero eigenvalue of matrix  $\mathcal{N}$  is unique, and all other eigenvalues are strictly greater than 0.

The eigendecomposition of matrix  $\mathcal{N}$  is  $\mathcal{N}U = U\Lambda$ , where  $U$  is the  $n \times n$  matrix whose columns contain the eigenvectors of  $\mathcal{N}$  and  $\Lambda$  is the diagonal matrix of eigenvalues having entries  $\Lambda_{ii} = \lambda_i$ . Order the entries of matrix  $\Lambda$  such that  $0 = \lambda_1 < \lambda_2 \leq \lambda_n$ . Assuming matrix  $U$  is nonsingular (invertible), then substitute in the eigendecomposition representation of matrix  $\mathcal{N}$  into Equation (4.12),

$$x(t+1) = (1 - \epsilon)F(x(t)) + \epsilon U \Lambda U^{-1} F(x(t)). \quad (4.13)$$

Define new coordinates  $z(t) = U^{-1}x(t)$  to obtain

$$z(t+1) = (1 - \epsilon)U^{-1}F(Uz(t)) + \epsilon \Lambda U^{-1}F(Uz(t)). \quad (4.14)$$

To assess stability of the synchronization manifold, like in Section 2.2, consider those perturbations transverse to the synchronization manifold. In that respect, if systems are synchronized, then denote  $s(t) = x_1(t) = x_2(t) = \dots = x_n(t)$  as the synchronized solution. In other words, it is the solution of the system,

$$\begin{pmatrix} s(t+1) \\ \vdots \\ s(t+1) \end{pmatrix} = \begin{pmatrix} f(s(t)) \\ \vdots \\ f(s(t)) \end{pmatrix}. \quad (4.15)$$

In addition, since  $\Lambda_{11} = 0$ , then the first column of  $U$  is the eigenvector  $\mathbf{1}$ . Therefore,

$$U^{-1} \begin{pmatrix} s(t) \\ \vdots \\ \vdots \\ s(t) \end{pmatrix} = \begin{pmatrix} s(t) \\ 0 \\ \vdots \\ 0 \end{pmatrix}. \quad (4.16)$$

Linearisation of Equation (4.14) around the synchronization manifold

$$\begin{pmatrix} s(t) \\ \vdots \\ s(t) \end{pmatrix} =: S(t) \quad (4.17)$$

yields

$$\tilde{z}(t+1) = (1 - \epsilon)(I \otimes Df(s(t)))\tilde{z}(t) + \epsilon(\Lambda \otimes Df(s(t)))\tilde{z}(t) \quad (4.18)$$

where  $\otimes$  is the Kronecker product, and  $Df$  is the Jacobian of  $f$ .

Since we have ordered the entries of matrix  $\Lambda$ , such that

$$\Lambda = \begin{pmatrix} 1 & & & \\ & \lambda_2 & & \\ & & \ddots & \\ & & & \lambda_n \end{pmatrix} \quad (4.19)$$

then it follows that

$$\tilde{z}_1(t+1) = Df(s(t))\tilde{z}_1(t) \quad (4.20)$$

are deviations in the direction of the synchronization manifold, and

$$\tilde{z}_k(t+1) = (1 - \epsilon + \epsilon\lambda_k)Df(s(t))\tilde{z}_k(t) \quad (4.21)$$

for  $k = 2, \dots, n$ , are deviations transverse to the synchronization manifold.

Stability, then, is determined by the values  $\epsilon$  and  $\lambda_n$  (since  $\lambda_n \geq \lambda_k$ ,  $k = 2, \dots, n-1$ ).

However, stability analysis is not performed in the following description of simulations. In the following computational simulations, graph topologies change many thousands of times. It is therefore not computationally plausible to calculate the eigenvalues for each new graph topology.

### 4.3.3 Adaptive rewiring: Spatial bias

The network rewiring procedure uses a cost function so as to favour edges of low cost over edges of high cost when rewiring. This cost function,

$$R(i, j, t) = \gamma_{ij}(t)S(d_{ij}),$$

is the product of an activation cost  $\gamma_{ij}(t)$  and a spatial cost function  $S(d_{ij})$ . The activation cost,  $\gamma_{ij}(t)$ , is the distance between the states of two nodes  $i$  and  $j$  at time  $t$ .

$$\gamma_{ij}(t) = |x_i(t) - x_j(t)|.$$

The spatial cost,  $S(\cdot)$ , is a monotonic function of  $d_{ij}$ , the distance between nodes  $i$  and  $j$  defined as the length of the shortest arc on the sphere connecting  $i$  and  $j$ . We consider the following spatial cost functions:

$$S(D) \subset \begin{cases} D & \text{linear} \\ \exp(D) - 1 & \text{exponential} \\ & \text{(concave up)} \\ \log\left(\frac{D}{D_{\min}} + 1\right) & \text{logarithmic} \\ & \text{(concave down)} \end{cases}$$

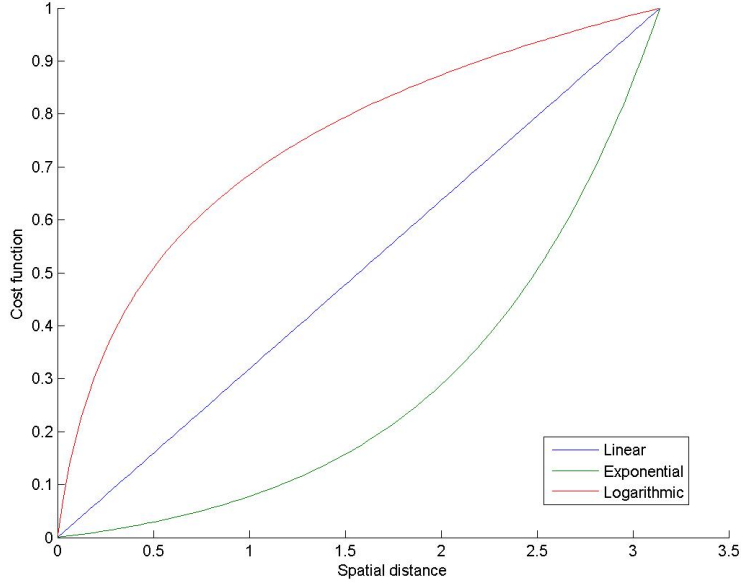


Figure 4.1: Cost functions of spatial distance: linear in blue, exponential in green, logarithmic in red.

for  $D_{\min} = \min_{i,j \in \mathcal{N}, i \neq j} d_{ij}$ , the minimal pairwise distance amongst all nodes on the sphere. We will refer to the adaptive rewiring function, and the corresponding process of rewiring, by the spatial cost function used, e.g. *logarithmic cost function* will refer to the adaptive rewiring function with a logarithmic cost function of distance. Likewise, the *logarithmic rewiring process* will refer to the rewiring process equipped with a logarithmic cost function.

For ease of comparison, Figure 4.1 is presented with  $S$  scaled such that the ranges of the spatial cost functions are equal. The ordering of node pairs induced by  $R$ , and hence the outcomes of Steps 2.2 and 2.3, are invariant to scaling of the image of  $S$ .

For  $\mathcal{N} = \{1, 2, \dots, n\}$  the set of nodes,  $R : \mathcal{N} \times \mathcal{N} \rightarrow \mathbb{R}_{0+}$ , ( $\mathbb{R}_{0+}$  the set of non-negative real numbers), we define the following rewiring process:

Step 0: Generate a random graph with  $n$  nodes and  $E$  edges.

Step 1: Take  $x(0) \in [-1, 1]^n$  randomly from a uniform distribution and iterate the dynamics described in Equation (4.10) for  $t = 0, 1, 2, \dots, T - 1$ .

Step 2: Rewiring:

- i. select a pivot node  $p \in \mathcal{N}$  randomly from a uniform distribution
- ii. determine the rewiring candidate
 
$$c = \arg \min_{j \in \mathcal{N} \setminus \{p\}} R(p, j, T)$$

- iii. go to Step 3 if  $c \in \mathcal{N}_p$ . If  $c \notin \mathcal{N}_p$ , update the graph by creating an edge between  $p$  and  $c$  and removing the edge between  $p$  and  $\bar{c} = \arg \max_{j \in \mathcal{N}_p} R(p, j, T)$ .

Step 3: Repeat from Step 1 until  $3 \times 10^5$  iterates have been reached.

In the case of ties in Steps 2.2 and 2.3, i.e. multiple candidates to rewire to or disconnect from, the rewiring candidate is chosen at random.

A minimal number of time steps  $T$  is needed in order to minimise the effect of initial transient activity after rewiring;  $T$  needs to be sufficiently large such that the choice of  $x(0)$  has minimal bias on the results. The relation between dynamics and structure during the rewiring stage is thus, effectively, independent of initial conditions. The value of  $T = 1000$  as used in this study has previously shown to be sufficient for this purpose [128].

For comparison we include as a baseline the previously mentioned rewiring process of [59], i.e. the *non-spatial* cost function in which spatial distance has no influence on the costs of rewiring and thus  $S(D)$  is constant. Without loss of generality we take  $S(D) \equiv 1$ .

Across all versions of adaptive rewiring, rewiring is based on non-spatial preferences; it was conceived in analogy to Hebbian learning. Hebbian learning relies on two mechanisms; the first is that synapses are strengthened according to correlated deviations from the mean firing rate [134]. The second is that synaptic plasticity is competitive, where some synapses are strengthened, others are weakened [137]. Our rewiring function uses similar mechanisms. The mechanism for rewarding synchrony is the activation cost  $\gamma_{ij}(t)$ . Even though, rather than synchrony over a window of time, this mechanism follows instantaneous synchrony, it was shown in [128] that according to this mechanism, the evolving architecture reflects the long-term patterns of activity. The method of conservative rewiring then allows for competition among nodes.

#### 4.3.4 Results

The network measures are reported for rewiring processes under the given cost functions. The network structure is sampled every 500 iterations of the algorithm, starting from the initial random network and ending after  $3 \times 10^5$  iterations. We conduct five such runs for each cost function (linear, exponential, logarithmic, and non-spatial). Independent instances of the random and regular type networks are constructed for each of the five runs.

This section is organised as follows: First we discuss the obtained topological structure and show all rewiring processes to yield small-world architecture, and then the effect of cost functions on spatial localisation of edges and clustering. This is followed by an examination of the relationship between edge betweenness and edge length. Then we report on the

degree of spatial modularity of the emergent small-world network. Finally, we report on the dependence of small-world emergence on connectivity density.

### Topological small-worldness

Figures (4.2(a)) and (4.2(b)) show the evolution of the clustering coefficient  $C$  and average shortest path length  $L$  for the non-spatial and spatial rewiring processes averaged over five runs. As shown in Figure (4.2(a)), the non-spatial and all spatially constrained adaptive rewiring processes yield a network that is clustered: for the final network structure, adaptive rewiring processes yield values of  $C$  that are greater than that of the regular lattice. Figure (4.2(b)) shows that the values of  $L$  for final network structure for the non-spatial and spatially constrained adaptive rewiring processes are less than that of the regular lattice, whilst exhibiting a modest increase over that of the random network. There is, on the whole, little difference between the final  $C$  and  $L$  values for the non-spatial and spatial processes. We may therefore conclude that, like the non-spatial rewiring process, the spatially biased rewiring ones successfully reach small-world topology. Furthermore, considering the evolution of the average values of  $C$  and  $L$ , the linear and exponential rewiring processes show faster initial rates of increase than the non-spatial and logarithmic ones. This suggests that factoring in specific spatial constraints of a linear or exponential type may facilitate reaching a small-world topology in the system.

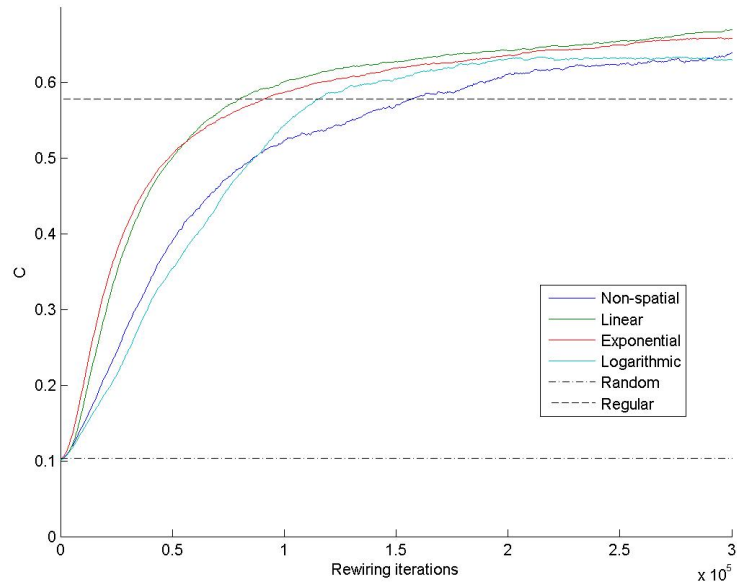
Figures (4.3(a)) and (4.3(b)) show the evolution of  $C$  and  $L$  for individual runs of the rewiring processes. The linear and exponential cost functions lead to rewiring processes that exhibit less variability between runs than the logarithmic and non-spatial ones throughout the full course of rewiring. Factoring in spatial constraints of a linear or exponential type therefore enhances the consistency of the small-world construction.

### Spatial localization

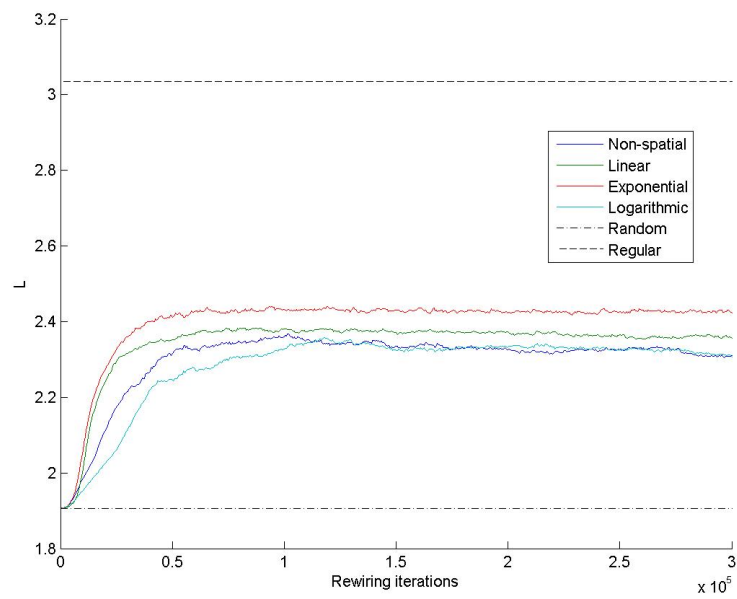
Figures (4.4(a)) and (4.4(b)) show the evolution of the spatially weighted clustering coefficient  $C^w$  and the network wiring cost  $M$  for the non-spatial and spatial rewiring processes averaged over the five runs. The edge weight set is defined by a linear relation:

$$w_{ij} = \begin{cases} 1 - \frac{d_{ij}}{\pi}, & \text{if } a_{ij} = 1, \\ 0, & \text{otherwise.} \end{cases}$$

Zero distance corresponds to a weight of 1 and the maximum distance  $\pi$  corresponds to a zero weight. We see from Figure (4.4(a)) that all spatially biased rewiring processes yield values of weighted clustering coefficient  $C^w$  for final network structure that are well above the value of the non-spatial process, which in turn is still considerably greater than the

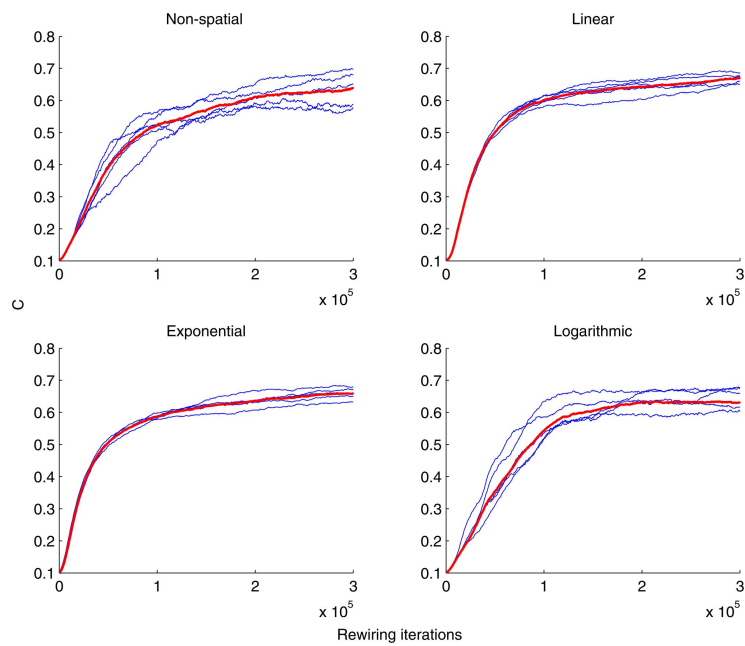


(a)

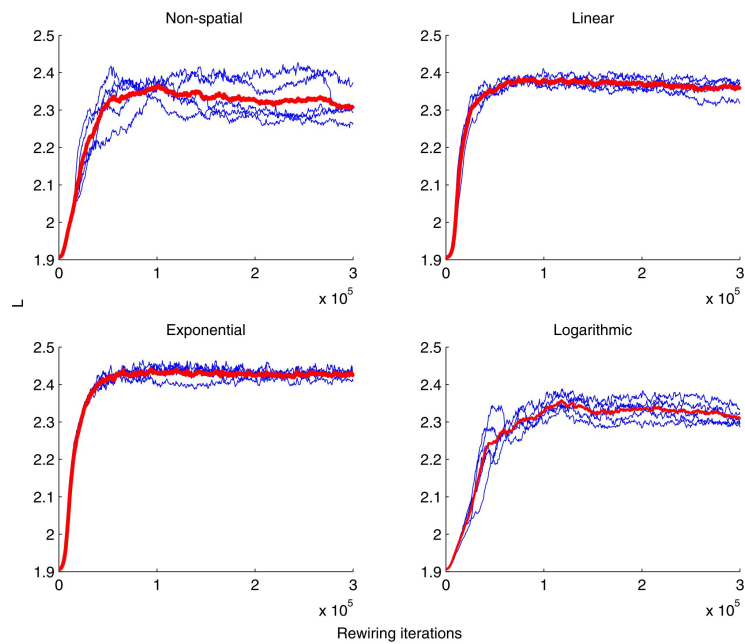


(b)

Figure 4.2: Evolution of  $A$ , the clustering coefficient values  $C$  averaged over five runs; and  $B$ , the average shortest path length values  $L$  averaged over five runs; for the non-spatial and spatial rewiring processes, regular lattice on the sphere, and random network.



(a)



(b)

Figure 4.3: (a) Evolution of the clustering coefficient; and (b), the average shortest path length; for the non-spatial and spatial rewiring processes, regular lattice on the sphere, and random network. Individual runs in blue and their average value in red.

random network on the sphere. In particular, the linear and exponential rewiring processes yield values of  $C^w$  for final network structure that are greater than the regular lattice and, thus, yield small-worlds with higher degrees of spatial clustering than the regular lattice. The final value of  $C^w$  for the logarithmic rewiring process, however, is slightly less than that of the regular type lattice. In Figure (4.4(b)), as one would expect, since connections in a regular lattice are optimal for spatial localisation, the regular lattice has the lowest value of  $M$  amongst all the spatial rewiring processes. However, those of the linear and exponential rewiring processes are close to that of the regular lattice. On the other hand, the logarithmic rewiring process yields values of  $M$  for final network structure that are well above the values for linear and exponential ones. The value of  $M$  for the non-spatial process is approximately equal to that of the random one, and corresponds to an average edge length of  $\frac{\pi}{2}$ , as one would expect, this being the average distance between randomly chosen points on the sphere.

Spatially biased rewiring processes that have a linear or exponential cost function of distance, therefore, facilitate spatial localisation and spatial clustering better than ones with a logarithmic cost function. Furthermore, considering the evolution of the average value of  $C^w$  and  $M$ , the linear and exponential rewiring processes exhibit similar initial rates of change and drive the network to a spatial small-world more rapidly than the logarithmic one.

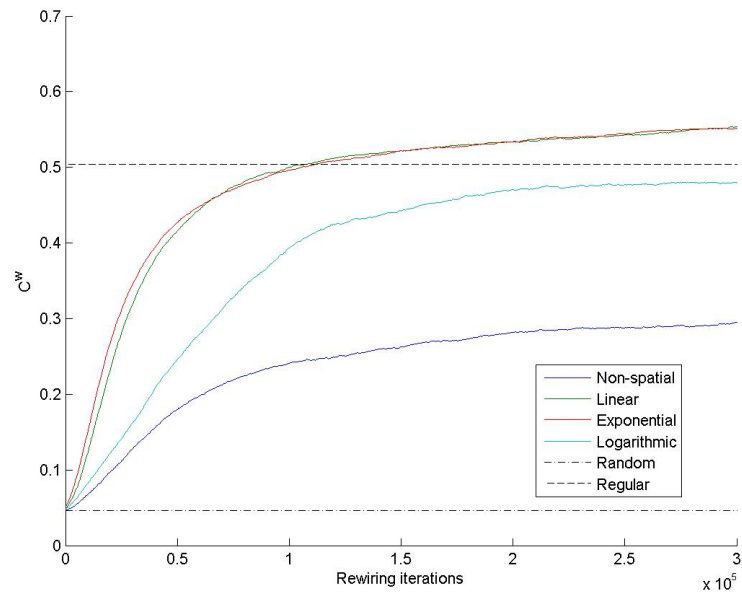
Figures (4.5(a)) and (4.5(b)) show the evolution of  $C^w$  and  $M$  for individual runs of the rewiring process. Similar to Figures (4.3(a)) and (4.3(b)), the linear and exponential rewiring processes exhibit less variation for values of  $C^w$  and  $M$  than the logarithmic and non-spatial ones. Therefore, arguably the linear and exponential rewiring processes are most consistent in reaching a spatially localised and spatially clustered small-world topology.

We may conclude that spatially biased rewiring processes with linear or exponential cost functions produce spatially localised and clustered small-world topologies and achieve this more effectively, quickly, and consistently than the logarithmic-based process.

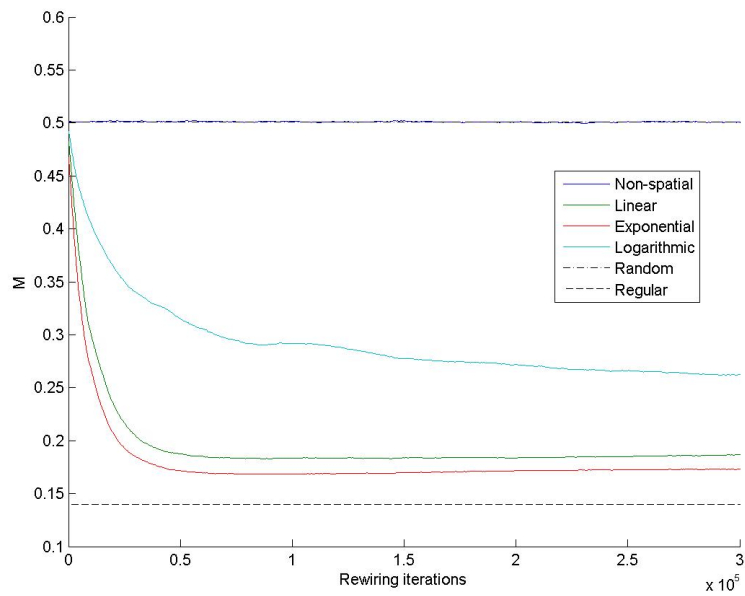
### **Edge betweenness and distance relationship**

To investigate the relation between topological and spatial structure of the network, we focused on the evolving relationship between edge betweenness and spatial distance.

Figure (4.6(a)) shows the linear correlation coefficients  $\rho$  between edge betweenness and edge length for all edges generated by our models. For the non-spatial rewiring process, as one would expect, there is no correlation between edge betweenness and spatial distance. As for the spatially biased rewiring processes, the linear and exponential cost functions yield similar time-courses for  $\rho$  throughout the full course of rewiring. The time-course shows

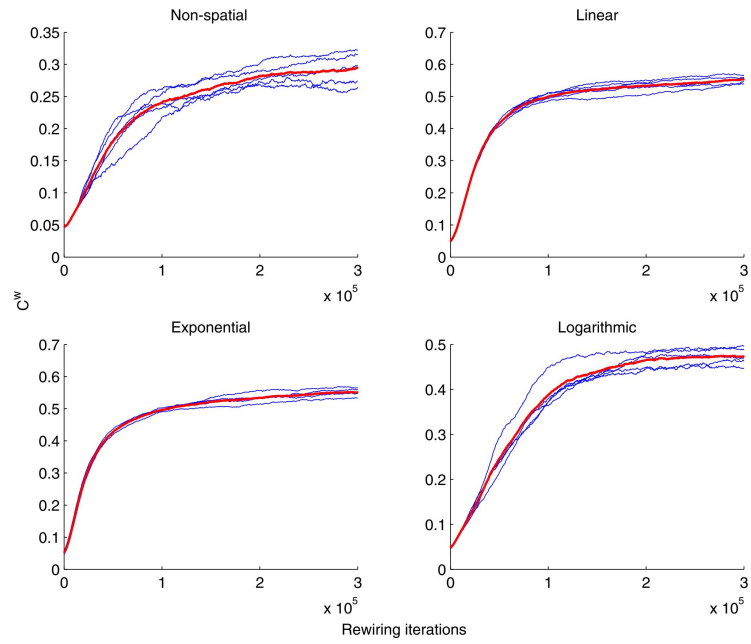


(a)

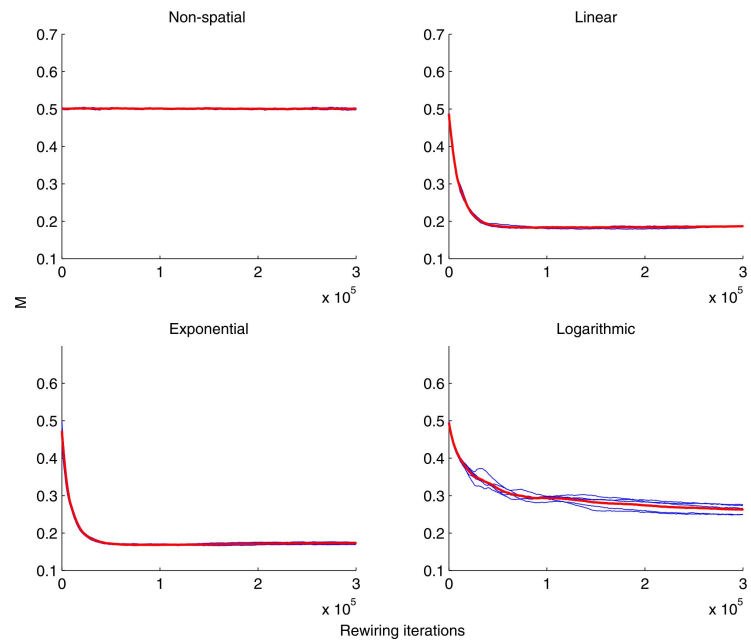


(b)

Figure 4.4: (a) Evolution of the spatially-weighted clustering coefficient values  $C^w$  averaged over five runs; and (b), the network wiring cost values  $M$  averaged over five runs; for the non-spatial and spatial rewiring processes, regular lattice on the sphere, and random network.



(a)



(b)

Figure 4.5: (a) Evolution of the spatially-weighted clustering coefficient values  $C^w$ ; and (b), the network wiring cost values  $M$ ; for the non-spatial and spatial rewiring processes, regular lattice on the sphere, and random network. Individual trials in blue and averaged value of five runs in red.

an initial peak followed immediately by a trough and then a plateau. For the logarithmic rewiring process the correlation between edge betweenness and distance is much weaker and even exhibits a slightly negative trough prior to a gradual increase to a small positive value.

Scatter plots of edge betweenness and spatial distance at selected rewiring iterations reveal in more detail the evolving relation between topological and spatial structure. We uniformly randomly selected 4% of the nodes from the combined five runs and plotted for all of their connections their values of edge betweenness against spatial distance at five different moments during the rewiring process: the initial moment; the moment when the peak occurs for the linear and exponential rewiring processes; the moment when the trough occurs for the linear and exponential rewiring processes; at the start of the plateau of the linear and exponential rewiring processes; and the final moment. The 2<sup>nd</sup>, 3<sup>rd</sup>, and 4<sup>th</sup> moments sampled are indicated in Figure (4.6(b)) by vertical lines.

In Figure 4.7:

- Row 1 depicts the initial random structure.
- In Row 2 the linear and exponential rewiring processes exhibit a positive slope in their scatter plots whilst the non-spatial and logarithmic rewiring processes do not; all rewiring processes show the emergence of a small number of edges with somewhat higher values of edge betweenness.
- In Row 3 edges of even higher betweenness appear; for the linear and exponential rewiring processes, predominantly the short-range edges yield the greatest values of betweenness, while for the non-spatial and logarithmic rewiring processes, edges with high betweenness are present over the full range of edge lengths.
- In Row 4 the linear and exponential rewiring processes show what appears to be a newly emerged order; edges of still higher betweenness appear that are long-range, while long-range edges that are of low betweenness disappear. For the non-spatial and logarithmic rewiring processes, edges with high betweenness mostly remain of random edge length. (An apparent excess of high betweenness edges at mid-range lengths for the non-spatial process is merely because, given the geometry of the sphere, such distances are most common).
- In Row 5 the scatter plots show a strong resemblance to those in Row 4. Only the logarithmic rewiring process shows noticeable change: there are now more long-range high betweenness edges but still many short-range ones, and still many long-range edges of low betweenness.

We see that for the non-spatial case, there is, as one would expect, no trend in the correlation between edge betweenness and edge length. The linear and exponential rewiring processes show that after the initial trough, edges of high betweenness and large distance are present throughout the remaining course of rewiring (but not necessarily the same edges throughout). For the linear and exponential rewiring processes the network is strongly affected by the spatial constraint and quickly comprises mostly short-range edges of low betweenness along with a few long-range edges of high betweenness. By contrast, in the logarithmic rewiring process, network structure is not affected by spatial constraints to such an extent and spatial localisation proceeds more slowly.

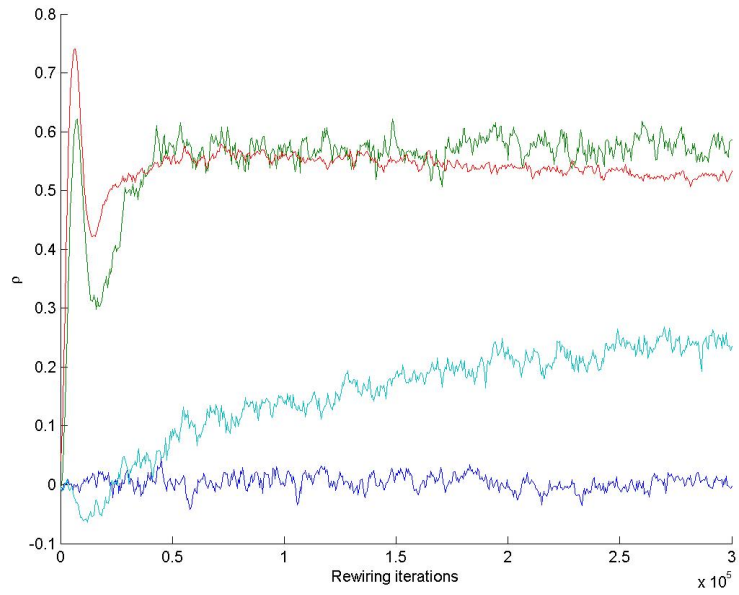
### Spatial modularity

We now examine the degree of modularity in our networks and the spatial organisation of the modules.

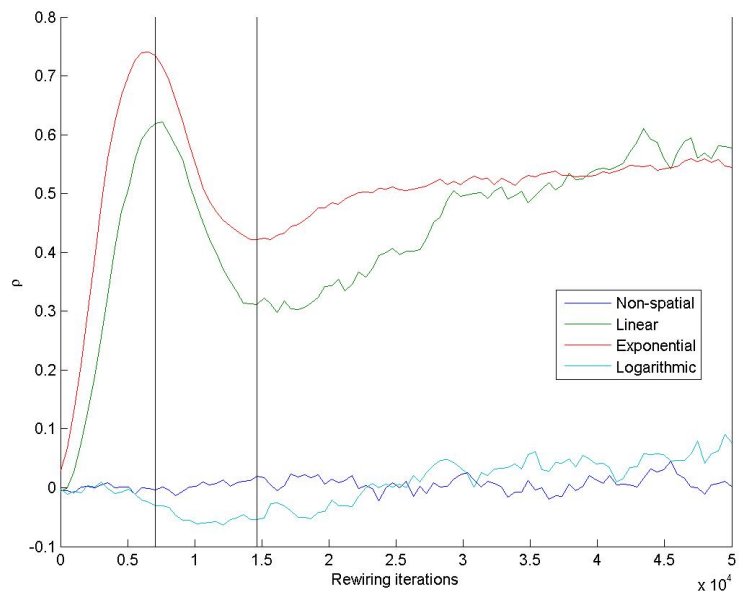
Figures (4.8(a)) and (4.8(b)) show the evolution of the modularity values  $Q$  for the non-spatial and spatial rewiring processes averaged over five runs, and for individual runs, respectively. As shown in Figure (4.8(a)), all rewiring processes yield a highly modular network. The spatially biased rewiring processes yield values of  $Q$  for final network structure that are greater than that of the non-spatial one. In addition, the initial rates of  $Q$  for the linear and exponential rewiring processes are greater than those of the non-spatial and logarithmic ones. Figure (4.8(b)) shows the evolution of  $Q$  for individual runs of the rewiring processes. As with previous measures we see that the linear and exponential rewiring processes exhibit less variability than the non-spatial and logarithmic ones. Linear or exponential cost functions therefore provide a mechanism that achieves a modular network structure to a greater extent, more rapidly, and with less variability compared to the non-spatial or logarithmic rewiring processes.

Figure 4.9 shows the adjacency matrices of the final network structure when columns and rows are permuted such that the connections between nodes within the same module are represented as blocks along the diagonal. We see that for all cases a modular network structure emerges: densely connected subsets of nodes and a sparse connectivity between those subsets. For individual runs, both the linear and exponential rewiring processes are more consistent between runs than the non-spatial and logarithmic ones. For all spatial rewiring processes, but more so for linear and exponential than for logarithmic ones, there exist more modules and there is less variation between the sizes of modules, compared to the non-spatial rewiring process.

To show how the modular structure corresponds to the spatial organisation of the network, Figures 4.10 and 4.11 represent typical networks resulting from the linear and log-



(a)



(b)

Figure 4.6: Linear correlation coefficient  $\rho$  between edge betweenness and spatial distance averaged over five runs versus rewiring iterations. (a) The full course of rewiring; and (b), early course of rewiring.

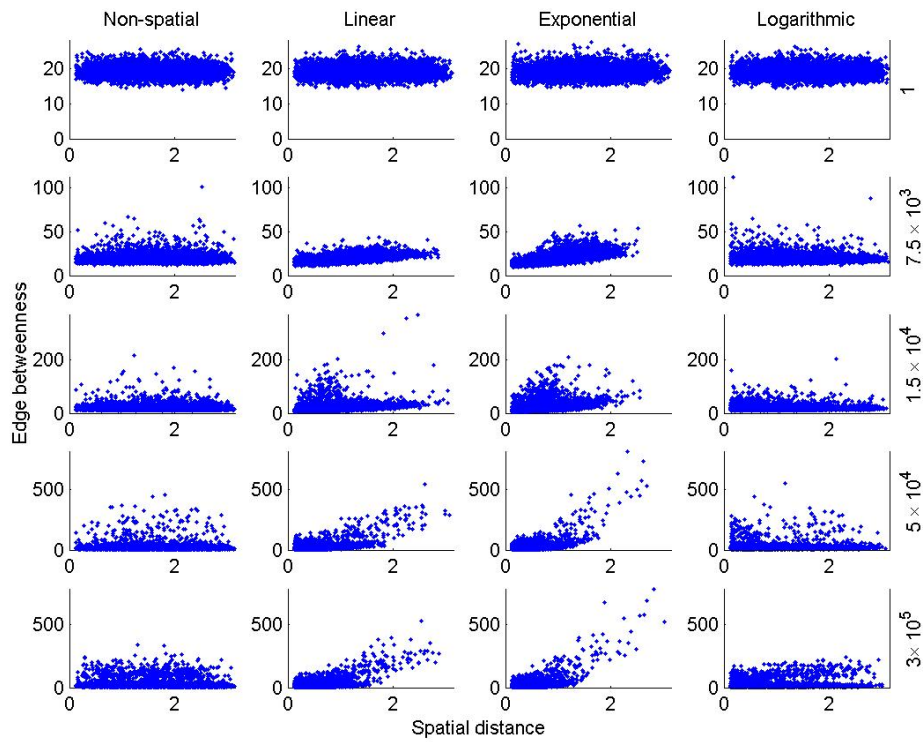
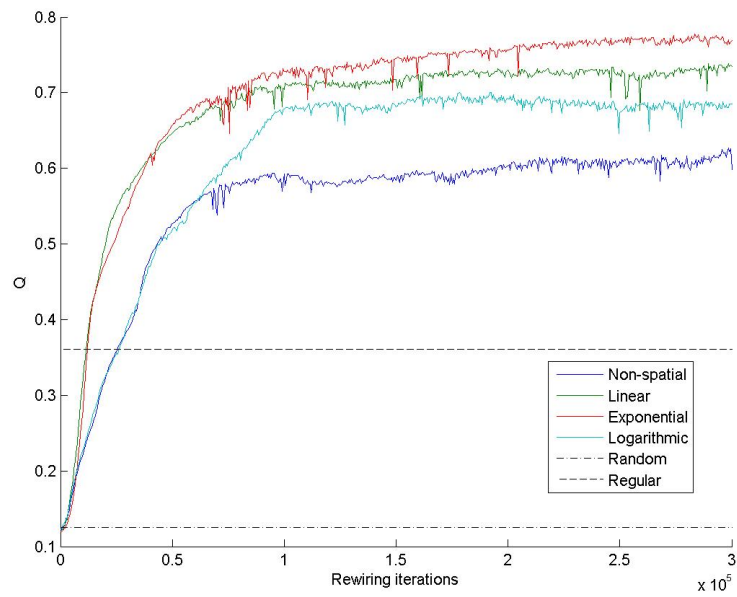
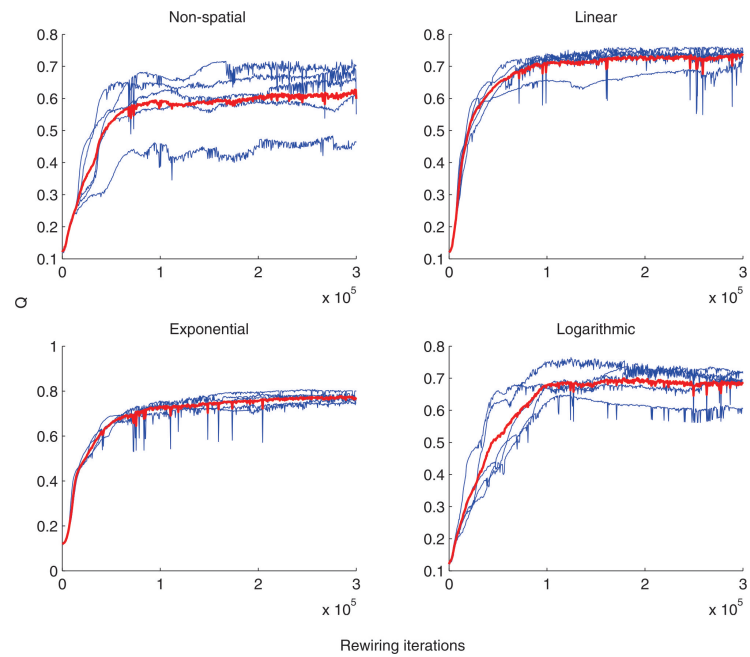


Figure 4.7: Scatter plots of edge betweenness versus spatial distance. Betweenness values presented here were obtained by uniformly randomly selecting 4% of nodes from the combined five runs and plotting the betweenness values of all their connections. Rows top to bottom for rewiring steps, 1,  $0.75 \times 10^3$ ,  $1.5 \times 10^4$ ,  $5 \times 10^4$ ,  $3 \times 10^5$ , columns are for different rewiring processes.

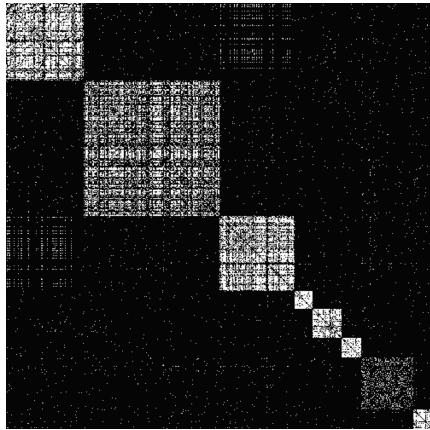


(a)

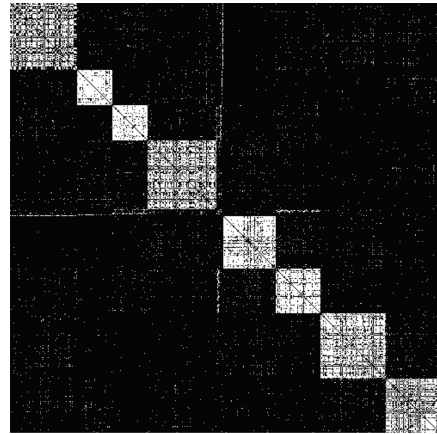


(b)

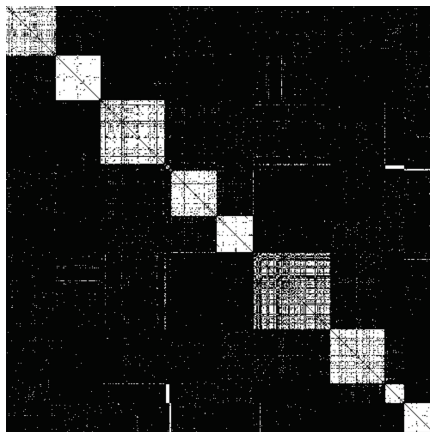
Figure 4.8: Evolution of the value of the modularity  $Q$ . (a) The average of five runs; and (b), the individual runs; for the non-spatial and spatial rewiring processes, regular lattice on the sphere, and random network. Individual runs in blue and their average values in red.



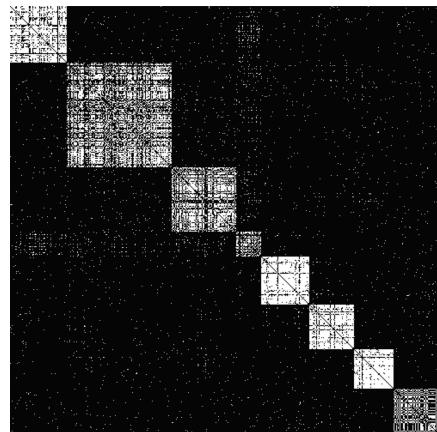
(a) Non-spatial.



(b) Linear.



(c) Exponential.



(d) Logarithmic.

Figure 4.9: Permutated adjacency matrices that correspond to the module structure of the non-spatial, linear, exponential, and logarithmic rewiring processes. A point with coordinates  $(i', j')$  is white if  $i', j'$  are the permuted indices of nodes  $i, j$  that are connected; otherwise it is black.

arithmetic rewiring processes with nodes coloured according to the module they belong to. The exponential case yields results very similar to the linear one, hence for illustration we only present the case of the linear rewiring process. For the case of the linear rewiring process we see very little spatial overlap of communities of nodes. This is contrasted with the logarithmic rewiring process where modules are less clearly separated. Therefore, for the linear and exponential rewiring processes, modular topology indeed corresponds to a spatially modular structure, while this is not so clear cut for the logarithmic one.

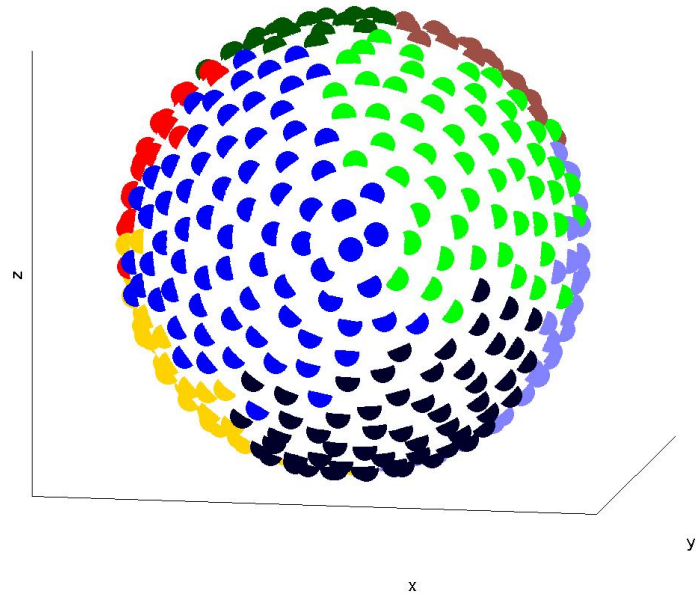
These results show that the linear and exponential rewiring processes give rise to spatially modular small-worlds, while the logarithmic small-worlds are less spatially modular. We remark that the modularity algorithm [110] does not always find the partition into modules that maximises  $Q$ . However we trust the modularity results for the rewiring processes because, as Figure 4.9 shows, the adjacency matrices have a clear block-diagonal structure. In addition, we used an alternative algorithm for modularity, the Louvain algorithm [16], and obtained similar results. A case where the algorithm [110] performs poorly, however, is the regular graph. While the algorithm consistently gave a modularity value of around 0.3610, calculation of  $Q$  using spatially modular partitions shown in Figures (4.9(b)) and (4.9(c)) gave values of 0.4538 and 0.4219 respectively for the regular graph; substantially higher than the value of 0.3610 found by the algorithm.

### **Dependence of small-world emergence on connection density**

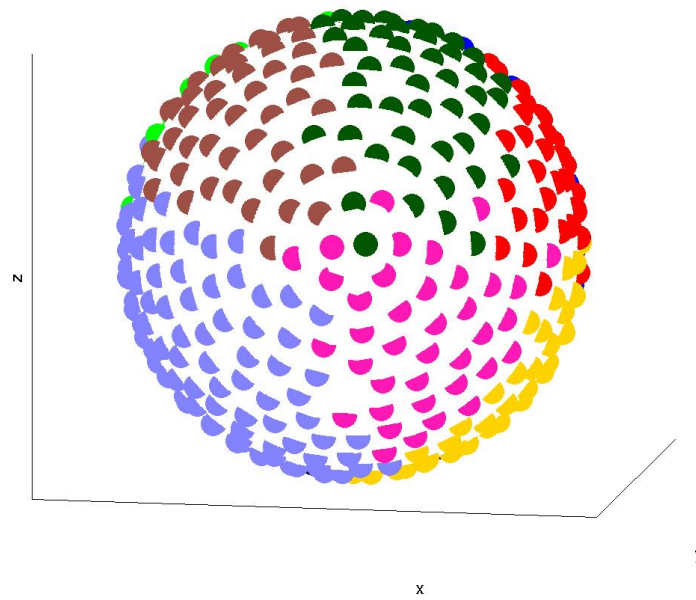
Edge density had been found in non-spatial networks to have a critical threshold; as edge density falls below this threshold the development of a high clustering coefficient becomes first unreliable and then fails altogether [150]. Since adding spatial constraints was shown to reduce the variability of the rewiring process, we hypothesize that the localizing tendency of the spatial cost functions shall reduce this threshold by promoting spatially localised clusters as occurs in the regular network limiting case. Accordingly, we investigated the dependence of rewiring processes on the parameter of edge density.

We performed simulations of the linear, exponential, and non-spatial rewiring processes with connectivity densities in the set  $\{2.5, 2.75, 3, \dots, 5\}$ , using the same procedure as previous. The minimum, maximum, and average values of  $C$  and  $L$  after  $3 \times 10^5$  rewiring iterations are presented in Figure 4.12 as functions of connectivity density.

For non-spatial rewiring, a connectivity density threshold of approximately 4% was required for networks of this size to achieve self-organised clustering (Figure (4.12(a))). Below this, the clustering coefficient drops off, until, at a connectivity density of approximately 3%, it reaches that of a random network. This result confirms what was previously observed [128]. The average shortest path length increases gradually as edge density decreases and at

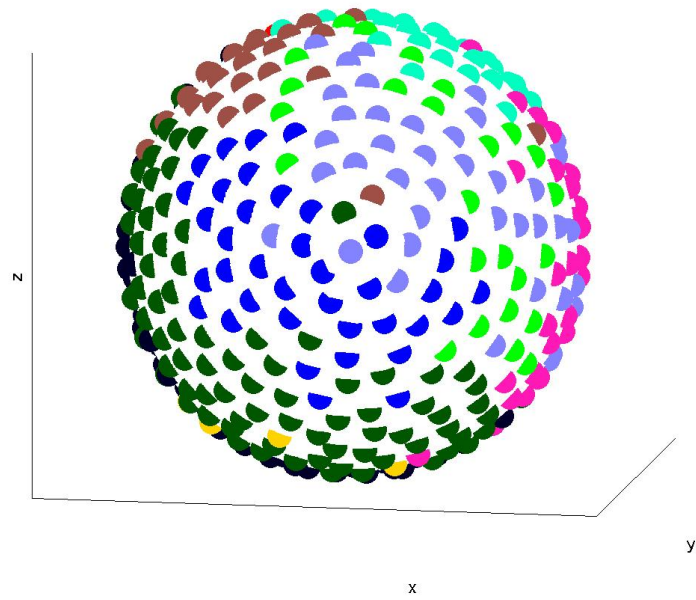


(a)

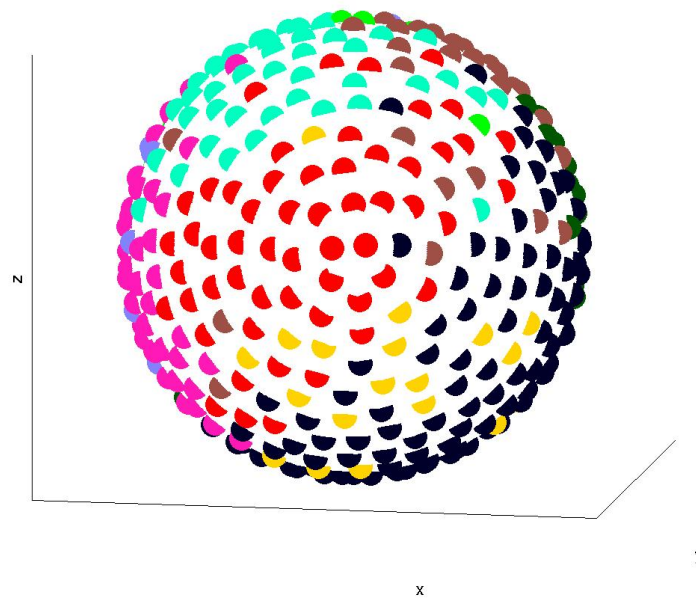


(b)

Figure 4.10: Final community structure of one run of the linear rewiring process. (a) and (b) show opposite hemispheres. Nodes are coloured according to the module to which they belong.



(a)



(b)

Figure 4.11: Final community of the logarithmic rewiring process. (a) and (b) show opposite hemispheres. Nodes are coloured according to the module to which they belong.

the same rate as that of the random network but offset to a somewhat higher level. Below 3% the non-spatial rewiring process remains, essentially random (Figure (4.12(b))).

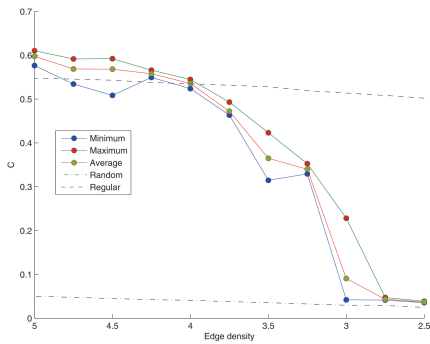
On the other hand, the linear and exponential rewiring processes share a threshold for self-organised clustering that is considerably lower than the non-spatial one. Similarly, reduced threshold is also observed for the average shortest path length of the linear and exponential rewiring processes (Figures (4.12(c))-(4.12(f))); at 2.5% connectivity these processes still yield small-world networks. Furthermore, preliminary data for  $\kappa \in \{0.01, 0.0125, 0.015, \dots, 0.025\}$  indicates that  $C$  for the linear and exponential rewiring processes decreases gradually while remaining above that of the random network; there is no sudden phase transition of network structure toward random structure. Therefore, the linear and exponential adaptive rewiring processes yield small-world architecture for connectivity densities well below that required by the non-spatial adaptive rewiring process.

Thus, the linear and exponential adaptive rewiring processes yield small-world networks for connectivity densities well below that required for the non-spatial adaptive rewiring process. For  $\kappa = 0.1$ , our small-world networks differed from the classic small-world example of WS based on the ring lattice in that it was not the case that  $L_{\text{regular}} \gg L_{\text{random}}$ . However as  $\kappa$  approaches 0.025 we have  $L_{\text{regular}} \gg L \gtrsim L_{\text{random}}$  since  $L_{\text{regular}}/L_{\text{random}}$  increases more than  $L/L_{\text{random}}$ , and hence our small-world networks more resemble the classic example of WS.

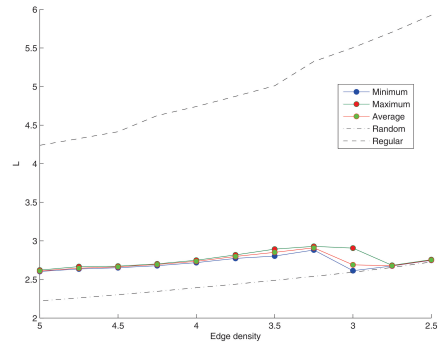
This point is illustrated in Figure 4.13 by the small-worldness measure  $\Sigma$ , as a function of connectivity density. The initial trend of  $\Sigma$  for the three rewiring processes for decreasing connectivity density is the same with  $\Sigma$  increasing. However, below a connectivity density of 4.25%, the value of  $\Sigma$  for the linear and exponential rewiring processes continues to increase while that for the non-spatial rewiring process begins to decrease until it reaches the value of one, that of the random network. In sum, for locally biased rewiring, the small-world effect is more pronounced in sparser networks. The critical threshold of edge density for self-organised clustering in a non-spatial adaptive rewiring regime is indeed reduced when adaptive rewiring becomes locally biased.

## 4.4 “Go with the flow”; Self-organisation of small-world network

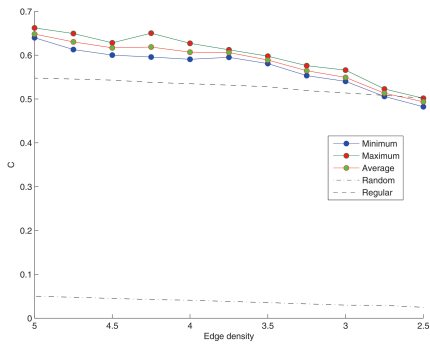
In the myriad contexts for which SWN structures are observed, the patterns of activity on those networks can vary greatly - the activity of a community of neurons translates poorly to the activity of a community of people. If indeed there exist underlying principle(s), then



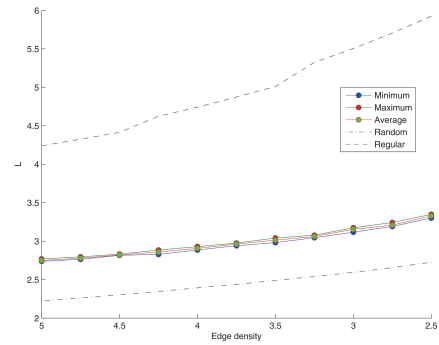
(a) Clustering coefficient for non-spatial cost function.



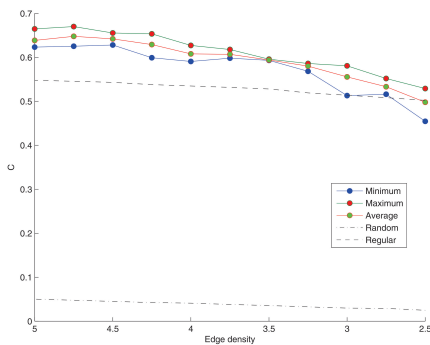
(b) Average shortest path length for non-spatial rewiring process.



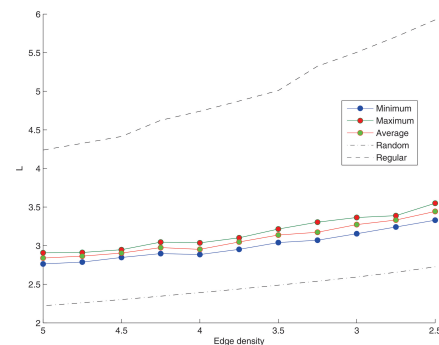
(c) Clustering coefficient for linear rewiring process.



(d) Average shortest path length for linear rewiring process.



(e) Clustering coefficient for exponential rewiring process.



(f) Average shortest path length for exponential rewiring process.

Figure 4.12: Clustering coefficient,  $C$ , and average shortest path length  $L$ , for (a), (b), non-spatial; (c), (d), linear; and (e), (f), exponential cost functions as function of edge density. Maximum, average, and minimum values from the five independent runs are shown, along with values for the corresponding random and regular graphs.

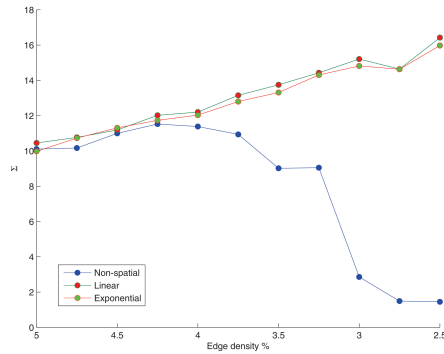


Figure 4.13: Small-worldness measure  $\Sigma$  averaged over five runs for non-spatial, linear, and exponential rewiring processes as a function of edge density.

we may safely assume that such principle(s) are robust to particular patterns of activity.

It is well established that patterns of dynamics on networks, such as synchronization or rotating waves as discussed in the previous chapter, may be determined from the underlying connectivity structure. Approached in its full generality, determining patterns of dynamics is too complex for current methods. It remains that if individual dynamics are well defined and for all time, and all information of connectivity is given, then it follows that it is possible to determine even the most complex patterns of dynamics.

Applying this rationale to the model of adaptive rewiring provokes the notion that activity and structure play a mutual role, a symbiotic relationship [128]. If patterns of activity are a determined solution on a given connectivity structure, then structural evolution in response to adaptive rewiring is also determined. The emergence of modular SWN structures as reported in [59; 75] can then be seen as a type of attracting network structure.

We motivate a model of SWN self-organisation by the principle of adaptive rewiring [59], however, we aim to achieve a greater level of simplicity and abstractness void of specific patterns of activity that allows it to be made applicable to a universal class of systems. In [59] synchronization of agents governs network evolution; agents that are synchronised become connected, while asynchronised agents become disconnected. We hypothesize that in the [59] dynamics regime, the likelihood of any given pairwise agents being synchronised is related to the diffusion properties in the graph. Graph (or network) diffusion may be considered to represent “convergence rates” between pairwise vertices at a given time. We hypothesize that pairwise agents having higher convergence rates also have a higher likelihood that they are in the same state, i.e. synchronised. Therefore, the process of adaptive rewiring can be applied to these likelihoods of vertices being synchronised, as opposed to the actual patterns of dynamics.

We propose that in self-organising systems the network structure adapts to its use, creating shortcuts where network diffusion (traffic flow or information transfer) is intensive while annihilating underused connections - like pedestrians define walkways in parks. As in the Watts–Strogatz algorithm, rewirings will be random for some proportion  $p$ , representing noise perturbation of the rewiring process, but for the proportion  $1 - p$ , they will be in adaptation to the ongoing diffusion process in the network. We show that with progressive adaptive rewiring, SWNs always emerge from initially random networks for almost any value of  $p$ : diffusion solutions cause the contraction of clusters while a random factor integrates clusters.

In networks adapting to their diffusion, changes in structure generally occur at a slower rate than the diffusion itself. The proportion of these two rates is expressed by  $\tau$ , which we call the *diffusion rate*. As with  $p$ , SWNs emerge for almost any value of  $\tau$ . The diffusion rate biases local or global connectivity structures. Depending on this bias, either modular or centralised SWN structures emerge. Moreover, at the critical point of phase transition, there exists a network structure in which the two opposing properties of modularity and centrality are balanced. This characteristic is observed, for instance, in the human brain [6; 39; 135]. We call such a structure *hierarchical*. In sum, adaptation to network diffusion represents a universal mechanism for the self-organisation of a family of SWNs, including modular, centralised, and hierarchical ones.

#### 4.4.1 Preliminaries: Network diffusion

Here we will provide a formal definition of network diffusion, an algorithm for adaptive rewiring, and a description of a set of computational simulations to demonstrate the role of adaptive rewiring in the generation of small-world networks.

##### Normalised Laplacian matrix

The Laplacian matrix of the graph  $G$  is  $L = D - A$ . The normalised Laplacian matrix,  $\mathcal{L}$ , is more appropriate for dealing with irregular graphs,

$$\mathcal{L} = D^{-1/2}LD^{-1/2} = I - D^{-1/2}AD^{-1/2} \quad (4.22)$$

with the convention that  $D_{uu}^{-1} = 0$  for  $d_u = 0$ .

All eigenvalues of  $\mathcal{L}$  are real (since  $\mathcal{L}$  is symmetric real) and confined to the interval  $[0, 2]$ , in accordance with Gershgorin circle theorem [55], and relate well to other graph invariants, such as random walks (or Markov chains), in a way that the eigenvalues of the Laplacian matrix and adjacency matrices often fail to do [33].

**Definition 4.4.1.** (Transition matrix) For a graph  $G$ , the transition matrix  $P$  contains the probabilities of traversing to any given vertex from some initial vertex:

$$P_{ij} = \begin{cases} 1/d_i & \text{if } (j, i) \in E \\ 0 & \text{otherwise} \end{cases} \quad (4.23)$$

or, more compactly,

$$P = AD^{-1} \quad (4.24)$$

where  $D$  is the diagonal matrix of out-degrees,  $D_{uv} = d_u^{\text{out}}$  if  $u = v$  and 0 otherwise.

Using the compact representation of the transition matrix  $P$  (4.24), we formulate the following lemma.

**Lemma 4.4.1.** *Consider a connected undirected graph  $G$ . Let  $P$  be the corresponding transition matrix (random walk matrix or Markov chain), and let  $\mathcal{L}$  be the corresponding normalised Laplacian matrix. Then, matrices  $P$  and  $\mathcal{L}$  share the same, albeit shifted by 1, spectrum of eigenvalues and closely related eigenvectors.*

*Proof.* Let matrix  $P$  have eigenvalues  $\omega_i$  and eigenvectors  $u_i$ . Consider the normalised Laplacian matrix  $\mathcal{L}$  of graph  $G$ , and substitute in the transition matrix  $P$  such that,

$$\mathcal{L} = I - D^{-1/2}AD^{-1/2} = I - D^{-1/2}PD^{1/2}. \quad (4.25)$$

Let  $\lambda_i$  be an eigenvalue of  $\mathcal{L}$  with eigenvector  $v_i$  such that

$$(I - D^{-1/2}PD^{1/2})v_i = \mathcal{L}v_i = \lambda_i v_i, \quad (4.26)$$

then, multiplication on both left hand sides yields

$$\begin{aligned} (D^{1/2} - PD^{1/2})v_i &= \lambda_i D^{1/2}v_i \\ PD^{1/2}v_i &= (1 - \lambda_i)D^{1/2}v_i. \end{aligned} \quad (4.27)$$

Therefore,  $1 - \lambda_i$  is an eigenvalue of  $P$  with eigenvector  $D^{1/2}v_i$ . Moreover,  $\omega_i = 1 - \lambda_i$  and  $u_i = D^{1/2}v_i$ .  $\square$

While  $\mathcal{L}$  incorporates information of the connectivity of vertices, this information is only local; it fails to provide any global connectivity metric.

### Graph kernels: Network diffusion

The introduction of a *graph kernel*  $h$  solves this problem by providing a similarity metric between all pairwise vertices of a given graph:  $h$  describes the degree of similarity between any two vertices  $v_1, v_2 \in V$  with fine distinctions in the degree to which  $v$  and  $v_1$  are distant

from each other in the graph. A crucial condition for the existence of a graph kernel is that  $h$  must be positive definite and symmetric. A more detailed description of graph kernels may be found in [87].

The simplest measure of similarity on a graph  $G$  is the shortest path length  $d(i, j)$ . The shortest path length, however, does not define a positive definite kernel since it violates positive definiteness for non-adjacent vertices having zero path length [87]. The global efficiency is robust to non-adjacent vertices, however as with the shortest path length, the global efficiency is sensitive to the insertion and/or deletion of individual edges. A more robust similarity measure is needed.

Random walks are more robust to changes in the graph edge set. In a random walk a path is generated such that each successive edge traversed is chosen uniformly randomly. More specifically, the sequence of vertices  $v_k, v_{k+1}$  is achieved by traversing the edge  $e_k$  with probability  $1/d_k$ , the inverse of the degree of vertex  $v_k$ . A compact representation of this process is provided by the *transition matrix*. Raising the transition matrix to the power  $T$ , gives the matrix, denoted as  $P_T$ , whose  $i, j$  element describes the probability of a random walker starting from  $j$  being found at  $i$  at time  $T$ . Unfortunately,  $P_T$  is not guaranteed to be positive definite or symmetric, and hence fails to qualify as a graph kernel.

A class of kernels, *diffusion kernels*, address these problems. A particular case of the Gaussian Radial Basis Function kernel, the *diffusion kernel* is positive definite and symmetric, and is constructed in such a way to be robust to changes in the edge set. It is the solution of the diffusion equation, where space is defined by the graph Laplacian - the discretisation of the Laplacian operator, the second order differential operator.

The physical meaning of the diffusion kernel  $h$  is clear:  $h$  describes how heat, gases, etc., introduced at vertex  $v_0$ , diffuse with time in a homogeneous, isotropic medium. However, a graph is typically not an isotropic medium. This motivates the use of the normalised Laplacian, as opposed to the unnormalised Laplacian, as described above.

Network diffusion is formally represented by the *exponential heat kernel* of the graph (cf. Theorem 10.11 in [33]).

**Definition 4.4.1.** Let  $\mathcal{L}$  be the normalised Laplacian matrix for an  $n \times n$  real symmetric matrix and  $t \geq 0$ . The exponential heat kernel of  $\mathcal{L}$ , denoted by  $h(t)$ , is the symmetric and positive definite  $n \times n$  matrix,

$$h(t) = e^{-t\mathcal{L}} = \sum_{k=0}^{\infty} \frac{(-t)^k}{k!} \mathcal{L}^k. \quad (4.28)$$

In particular  $h(0) = I$ , the identity matrix.

### Properties of the exponential heat kernel

One of the most important properties of the heat kernel is the role of which the time parameter  $t$  plays.

**Lemma 4.4.2.** *For a graph  $G$  with vertex set  $V = \{1, 2, \dots, n\}$ , the entry  $a_{ij}^k$  of the matrix  $A^k$  obtained by taking the  $k$ -th power of the adjacency matrix  $A$  equals the number of walks of length  $k$  between pairwise vertices  $i$  and  $j$ .*

*Proof.* By method of induction, take as the base case  $k = 1$ , and thus  $a_{ij}$  is 1 if  $\{i, j\} \in E$ . So the statement is true for  $k = 1$ . Now assume the statement holds true for  $k$  and then prove for the case  $k + 1$ . Since  $A^{k+1} = A^k \cdot A$ , then,  $a_{ij}^{k+1} = \sum_{l=1}^n a_{il}^k \cdot a_{lj}$ . Whenever  $\{i, j\} \notin E$ ,  $a_{ij} = 0$  and vice versa, and so it follows that  $a_{il}^k \cdot a_{lj}$  represents the number of length  $k + 1$  walks between vertices  $i, j$  that are constructed from length  $k$  walks between pairwise vertices  $i, l$  joined by the edge  $\{l, j\}$ . In particular, all walks of length  $k + 1$  between pairwise vertices  $i, j$  are of this form for some vertex  $l$ . Thus,  $a_{ij}^{k+1} = \sum_{l=1}^n a_{il}^k \cdot a_{lj}$  indeed represents the total number of length  $k + 1$  walks between pairwise vertices  $i, j$ . This proves the statement for  $k + 1$ , and by the principle of induction, therefore proves the statement for all natural numbers  $k$ .  $\square$

Coefficients  $\frac{(-t)^k}{k!}$  in Equation (4.28) therefore allow for biasing of path lengths in the construction of  $h(t)$ , where for small  $t$  shorter paths carry greater weight and longer paths carry lesser weight, and *vice versa* for large  $t$ . In our simulations we use the parameter  $\tau = t$ .

The exponential growth of a matrix  $A^k$  as  $k \rightarrow \infty$  is controlled by the eigenvalue of  $A$  with greatest absolute value. The Perron-Frobenius theorem describes the properties of the leading eigenvalue and of the corresponding eigenvectors when  $A$  is a non-negative square real matrix.

**Lemma 4.4.3.** *Assuming the square  $n \times n$  real and symmetric matrix  $X$  is diagonalisable by some orthogonal matrix  $Q$ , such that  $X = Q\Lambda Q^{-1}$ , then*

$$h = e^{-tX} = Qe^{-t\Lambda}Q^{-1}$$

where  $e^{(\cdot)}$  is the matrix exponential operator and  $t \in \mathbb{R}$ .

*Proof.* Consider the Taylor series expansion of the matrix exponential operator  $e^{(\cdot)}$  acting

on matrix  $X$ ,

$$\begin{aligned}
e^{-tX} &= \sum_{k=0}^{\infty} \frac{(-t)^k}{k!} X^k \\
&= I - tX + \frac{t^2}{2!} X^2 - \dots \\
&= I - tQ\Lambda Q^{-1} + \frac{t^2}{2!} (Q\Lambda Q^{-1})^2 - \dots + \frac{(-t)^k}{k!} (Q\Lambda Q^{-1})^k + \dots \\
&= I - tQ\Lambda Q^{-1} + \frac{t^2}{2!} Q\Lambda^2 Q^{-1} - \dots + \frac{(-t)^k}{k!} Q\Lambda^k Q^{-1} + \dots \\
&= Q \left[ I - t\Lambda + \frac{t^2}{2!} \Lambda^2 - \dots + \frac{(-t)^k}{k!} \Lambda^k + \dots \right] Q^{-1} \\
&= Qe^{-t\Lambda} Q^{-1}.
\end{aligned}$$

□

**Theorem 4.4.1.** *The matrix  $h(t)$  as  $t \rightarrow \infty$  can be expressed by the leading eigenvector associated with the zero eigenvalue of  $\mathcal{L}$ :*

$$\lim_{t \rightarrow \infty} h(t) = qq^\top.$$

*Proof.* Since  $\mathcal{L}$  is real and symmetric, there exists an orthonormal matrix  $Q$  such that  $\mathcal{L} = Q\Lambda Q^{-1}$  where  $Q$  is the matrix of eigenvectors and  $\Lambda$  is the diagonal matrix of eigenvalues. From Lemma 4.4.3, substitution of this eigendecomposition into the Taylor expansion yields  $h(t) = Qe^{-t\Lambda} Q^{-1}$ . Let  $\Lambda_{ii} = \lambda_i$  and order the eigenvalues such that  $0 = \lambda_0 \leq \lambda_1 \leq \dots \leq \lambda_{n-1}$ . If  $G$  is connected, then  $\mathcal{L}$  has one simple zero eigenvalue  $\lambda_0$ . Thus, in the infinite limit

$$\lim_{t \rightarrow \infty} e^{-t\Lambda} = B$$

where matrix  $B$  is

$$B = \begin{pmatrix} 1 & & & \\ & 0 & & \\ & & \ddots & \\ & & & 0 \end{pmatrix},$$

since  $e^{-t\lambda_0} = 1$  for all  $t \in \mathbb{R}$  and  $\lim_{t \rightarrow \infty} e^{-t\lambda_k} = 0$  for  $k = 1, \dots, n-1$ .

Therefore,

$$\lim_{t \rightarrow \infty} h(t) = QBQ^{-1} = qq^\top$$

where  $q$  is the first column of  $Q$ , called the leading (or principle) eigenvector associated with the zero eigenvalue. Note that matrix  $Q$  is *unitary*, i.e.,  $Q^{-1} = Q^\top$ , thus yielding the result  $qq^\top$ . □

The matrix  $qq^\top$  allows one to express analytically the behaviour of  $h(t)$  as  $t \rightarrow \infty$ ; it is the projection onto the eigenspace corresponding to  $\lambda$ , called the *Perron projection*.

If  $G$  is regular - all vertices have equal degree  $d = d_v$  for all  $v \in V$  - then,  $\mathcal{L} = \frac{1}{d}L$ .

**Corollary 4.4.1.** *If  $G$  is regular, then  $q \in \text{span}\{1, \dots, 1\}$ , hence  $\lim_{t \rightarrow \infty} h_L(t) = \frac{1}{n} \mathbf{1} \mathbf{1}^\top$ , where  $h_L(t) = e^{-tL}$ .*

*Proof.* Consider the combinatorial Laplacian  $L$  and notice that  $D = \text{diag}(A\mathbf{1}^\top)$ . Denote  $q$  as the eigenvector associated with the zero eigenvalue  $\lambda_0$ . Let  $q = \text{span}\{1, \dots, 1\}$ , then

$$Lq = \text{diag}(A\mathbf{1}^\top)\mathbf{1}^\top - A\mathbf{1}^\top = 0.$$

Thus, in the infinite limit of  $t$ ,

$$\lim_{t \rightarrow \infty} h_L(t) = qq^\top = \begin{pmatrix} 1 & \cdots & 1 \\ \vdots & & \vdots \\ 1 & \cdots & 1 \end{pmatrix}.$$

□

Assuming  $G$  is irregular, as is often the case in evolving networks, then the leading eigenvector  $q$  is not consistent for the heat kernel constructed using the combinatorial Laplacian matrix  $L$  and normalised Laplacian matrix  $\mathcal{L}$ .

**Corollary 4.4.2.** *if  $G$  is irregular, then  $q \in \text{span}\{\sqrt{d_1}, \dots, \sqrt{d_n}\}$ , thus  $\lim_{t \rightarrow \infty} h_{\mathcal{L}}(t) = \frac{1}{\mathbf{1}^\top D \mathbf{1}} D^{1/2} \mathbf{1}^\top \mathbf{1} D^{1/2}$ , where  $h_{\mathcal{L}}(t) = e^{-t\mathcal{L}}$ .*

*Proof.* For the normalised Laplacian matrix  $\mathcal{L}$ , denote its leading eigenvector as  $q$  associated with the zero eigenvalue  $\lambda_0$ . Let  $q = D^{1/2} \mathbf{1}^\top$ , then

$$\mathcal{L}q = D^{-1/2} L D^{-1/2} q = D^{-1/2} L \mathbf{1}^\top = 0$$

since  $\mathbf{1}^\top$  is the eigenvector of  $L$  associated to  $\lambda_0$ .

Alternately, noting that since  $D = \text{diag}(A\mathbf{1}^\top)$  and  $D\mathbf{1}^\top = A\mathbf{1}^\top$ , then

$$\begin{aligned} \mathcal{L}q &= (I - D^{-1/2} A D^{-1/2}) D^{1/2} \mathbf{1}^\top \\ &= D^{1/2} \mathbf{1}^\top - D^{-1/2} A \mathbf{1}^\top \\ &= D^{1/2} \mathbf{1}^\top - D^{-1/2} D \mathbf{1}^\top \\ &= D^{1/2} \mathbf{1}^\top - D^{1/2} \mathbf{1}^\top \\ &= 0. \end{aligned}$$

Hence,  $q = \text{span}\{\sqrt{d_1}, \dots, \sqrt{d_n}\}$ .

To describe  $h_{\mathcal{L}}(t)$  in the infinite limit of  $t$ , one must normalise the eigenvector  $q$ :  $q = \frac{q}{\mathbf{1}q} = \frac{D^{1/2}\mathbf{1}^\top}{\sqrt{\mathbf{1}D\mathbf{1}^\top}}$ .

Therefore,

$$\begin{aligned} \lim_{t \rightarrow \infty} h_{\mathcal{L}}(t) &= qq^\top \\ &= \frac{1}{\mathbf{1}D\mathbf{1}^\top} D^{1/2} \mathbf{1}^\top \mathbf{1} D^{1/2} \\ &= \frac{1}{\sum_j d_j} \begin{pmatrix} d_1 & \sqrt{d_1 d_2} & \cdots & \sqrt{d_1 d_n} \\ \sqrt{d_2 d_1} & d_2 & & \vdots \\ \vdots & & \ddots & \\ \sqrt{d_n d_1} & \cdots & & d_n \end{pmatrix}. \end{aligned}$$

□

The use of  $\mathcal{L}$  over  $L$  in construction of the heat kernel becomes apparent for  $G$  irregular. Assuming  $G$  is irregular, then the off-diagonal entries of  $h(t)$  as  $t \rightarrow \infty$  are proportional to the square root of the vertex degrees. Thus, for  $t$  taken arbitrarily large, irregularities in  $\mathcal{L}$  also appear in  $h(t)$ , i.e. information of network structure is still contained in  $h(t)$ . This property does not hold if we were to replace  $\mathcal{L}$  with  $L$  in the construction of  $h(t)$ . Indeed, denote the heat kernel constructed using  $L$  as  $h_L(t)$ , then for  $G$  regular,  $\lim_{t \rightarrow \infty} h_L(t) = \frac{1}{n} \mathbf{1}\mathbf{1}^\top$ . Note also, that for  $\alpha > 0$  where  $\alpha$  may be taken arbitrarily small,  $h(\alpha) \neq I$ , i.e. off-diagonal entries of  $h(\alpha)$  are nonzero, and hence  $h(\alpha)$  contains information of network structure. This property holds for both the use of  $\mathcal{L}$  and  $L$  in construction of the heat kernel.

#### 4.4.2 Adaptive rewiring: In response to network diffusion

Consider an undirected graph with number of vertices  $n$  and number of edges  $m$ . For convenience we take  $m = 2\rho n(n-1)$ , where  $\rho = \frac{\log(n)}{n}$ , i.e. twice the critical connection density for which a random Erdős–Rényi (ER) graph is connected with probability one [45; 18].

We consider self-organisation starting from a random network. The network is progressively rewired, with probability  $p$  at random and with probability  $1-p$  according to the current network diffusion. The process can be described in algorithmic form:

Step 0: Generate an undirected random graph  $G$  of the Erdős–Rényi type.

Step 1: Select a vertex  $v$  uniformly randomly from all non-zero degree vertices  $v \in \{u \in V | d_u \neq 0 \text{ and } d_u \neq n-1\}$ .

Step 2: Delete the edge  $(v, u_1)$  and add the edge  $(v, u_2)$  where vertices  $u_1$  and  $u_2$  are selected by the following criteria: With probability  $p$  go to 2i, otherwise go to 2ii,

- i. Vertices  $u_1$  and  $u_2$  are uniformly randomly selected from the sets  $u_1 \in \{u \in V | (v, u) \in E\}$  and  $u_2 \in \{u \in V | (v, u) \in E^c\}$ .
- ii. For adjacency matrix  $A$  (of graph  $G$ ), calculate the heat kernel  $h(t)$  for  $t = \tau$ , where  $\tau$  is a chosen parameter. Vertices  $u_1$  and  $u_2$  are chosen such that, for all  $u \in V$  and  $u \neq v$ ,

$$u_1 : h_{vu_1}(t) \leq h_{vu}(t) \text{ for all } (v, u) \in E$$

$$u_2 : h_{vu_2}(t) \geq h_{vu}(t) \text{ for all } (v, u) \in E^c$$

where  $h_{uv}(t)$  is the  $u, v$  entry in matrix  $h(t)$ . In case of ties  $u_1, u_2$  are chosen arbitrarily.

Step 3: Repeat from Step 1 until  $k$  edge rewirings have been made.

All simulations are performed using MATLAB R2014. In Step 3 we take  $k = 4m$ ; simulations without upper limit on  $k$  show sufficient convergence after only  $m$  rewirings. We simulate 100 independent trials for each pair  $(\tau, p)$ . In analysing the networks generated by the algorithm all measures used are provided by the *Brain Connectivity Toolbox* [127]. Note that for  $\tau \gg 1$  the heat kernel approaches the matrix  $\frac{1}{\mathbf{1}^T D \mathbf{1}} D^{1/2} \mathbf{1} \mathbf{1}^T D^{1/2}$  and so rewiring biases toward high degree vertices, hence, adaptive rewiring approaches a process of preferential attachment.

### 4.4.3 Results

Networks obtained by adaptive rewiring are described according to measures of small-world structure, modularity, centrality, and criticality.

#### Small-World Structure

The *small-worldness* index  $S$  provides a canonical measure of the degree to which a network is small-world [67]. Here, we take a slightly modified version, in which the normalised clustering coefficient ( $C$ ) is multiplied by the normalised global efficiency ( $E$ ), such that  $S = \frac{C}{C_r} \times \frac{E}{E_r}$ , where  $C_r$  and  $E_r$  are measures of  $C$  and  $E$  for an equivalent Erdős-Rényi (ER) random graph, i.e. with equal  $n$  and  $m$ . In doing so,  $S$  is also defined on disconnected networks.

For random graphs,  $S = 1$  and so the greater the (positive) deviation of  $S$  from one, the greater the degree of small-worldness. For comparison, we include the average small-worldness values for networks constructed by the Watts-Strogatz algorithm (100 independently constructed networks for each  $p = 0, \frac{1}{500}, \frac{2}{500}, \dots, 1$ ).

In Figure (4.4.3) we observe for networks the average small-worldness index  $S$  as a function of random rewiring probability  $p$ . A striking result is that SWN emergence is

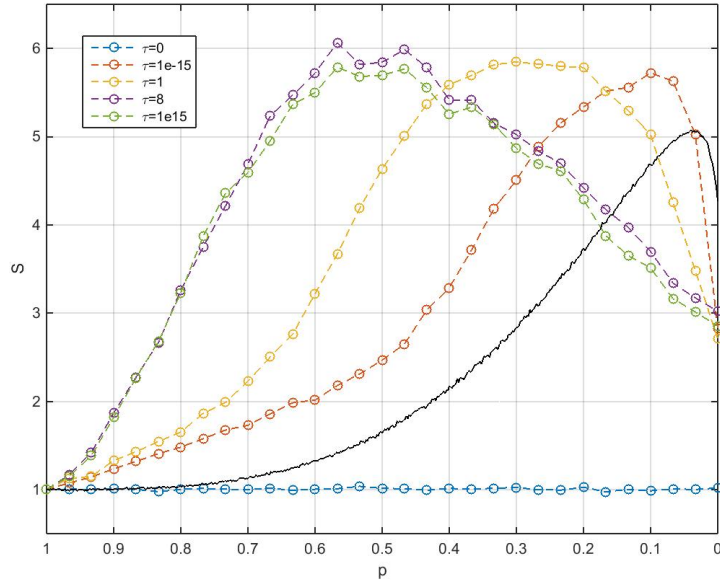


Figure 4.14: The small-world index  $S$  as a function of decreasing random rewiring probability  $p$ : Coloured lines indicate values of heat kernel parameter  $\tau$ , black line indicates the Watts-Strogatz algorithm.

observed for all sample values of  $\tau$  nonzero, no matter how small or large. Moreover, for all nonzero  $\tau$  a greater maximum small-worldness is achieved than with the Watts-Strogatz algorithm.

The degree of network adaptation to network diffusion,  $1 - p$ , for which maximum small-worldness is obtained depends on the rate of diffusion: local diffusion,  $\tau = \epsilon, 1$ , requires small  $p$ , i.e. small degree of random rewiring, while more global diffusion,  $\tau = 8, \delta$ , requires larger  $p$ .

### Clustering and Path length

The emergence of small-world structure can be seen as the result of significant increases in clustering, seen in Figure (4.15(a)), while simultaneously, a comparably disproportionately less decrease in efficiency, Figure 4.15(b). As the random rewiring probability  $p$  approaches 0, there is a breakdown in integration, as seen by a final low value of global efficiency in Figure 4.15(b). This is reflected in the values of small-worldness for which the values of  $S$  for all  $\tau$  nonzero decay as  $p$  goes to zero.

Interestingly, In Figure 94.15(b)) for  $\tau = 8, \delta$  and  $p$  between 0.6 and 1 the network achieves a greater degree of efficiency than an equivalent random ER one. This is despite

an increase in segregation, seen by the clustering coefficient, over the same interval. Importantly, this indicates that random ER networks are not optimally efficient networks, as they may be improved by a small degree of ordering. Intuitively, a random ER network may be made more efficient with relative ease if connections are intelligently rewired with the aim of improving efficiency, however, here connections are rewired in a process of self-organization, based on generic factors of the network. Therefore, improved efficiency is an attracting structure of self-organization for those pairs of  $(\tau, p)$ .

### Modular Structure

The modularity index  $Q$  is an optimised statistic of network partitioning into non-overlapping communities. The value  $Q$  is calculated as the proportion of intra-modular connections minus the expected proportion of inter-modular connections for an equivalent ER random network under the same community structure.

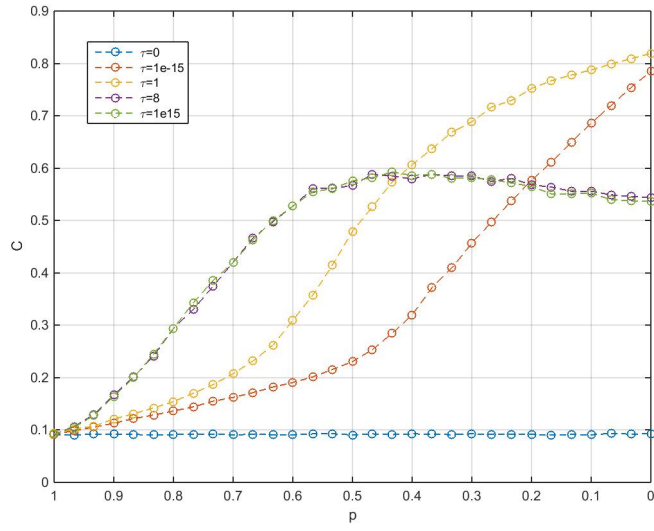
In Figure (4.4.3). we observe the average modularity index  $Q$  as a function of random rewiring probability  $p$ . We observe that modularity can be switched *on* or *off* by choice of pair  $(\tau, p)$ . This is discussed in further detail in the section *Critical Network Structure*. For  $\tau = \epsilon, 1$  networks emerge with near-maximal degrees of modularity as  $p \rightarrow 0$ . On the other hand, for  $\tau = 8, \delta$  and over all  $p \in [0, 1]$  emergent networks possess no community structure, i.e. modularity is switched off. In fact, we see a lesser degree of modularity than in an equivalent random ER network.

In Figure (4.18) we present the adjacency matrices from a randomly chosen trial with pairs  $(\tau, p)$ , where  $p$  is chosen dependent on  $\tau$  so that the values of small-worldness  $S$  are at maximum. In both Figure (4.18(a)) and Figure (4.18(b)) where  $(\tau, p) = (\epsilon, 0.1)$  and  $(\tau, p) = (1, 0.3)$ , respectively, emergent modules are relatively uniform with a dense intra-connectivity and sparse inter-connectivity.

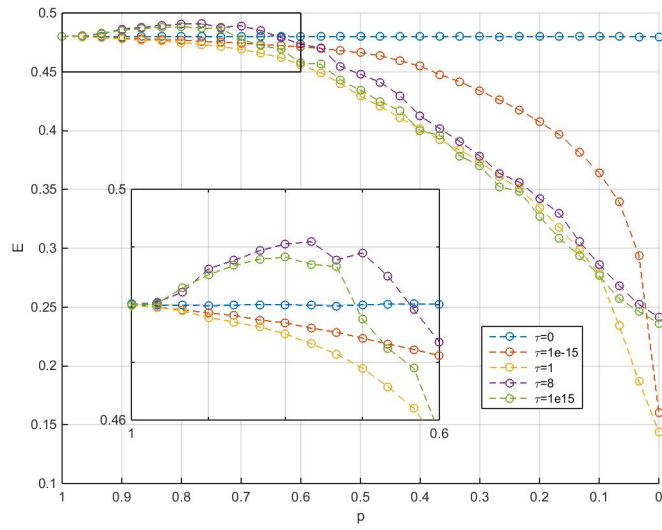
### Centralised Structure

Properties of centrality are characterised using the measures of Page-Rank, and for pairs  $(\tau, p)$  where  $p$  is chosen dependent on  $\tau$  such that  $S$  is at maximum, the degree, assortativity, and maximised coreness statistic.

The *PageRank centrality* vector, a variant of eigenvector centrality, is defined as the stationary distribution achieved by instantiating a Markov chain on a graph. The PageRank centrality of a given vertex, then, is proportional to the number of steps (or amount of time) spent at that vertex as a result of such a process [127]. PageRank centrality takes into account global communication patterns, mediated by longer path lengths and patterns of convergence and divergence, whereas some of the more common centrality measures, such



(a)



(b)

Figure 4.15: As functions of decreasing  $p$  along the horizontal axis: A clustering coefficient  $C$ ; B global efficiency  $E$ , with upper right region magnified in subplot.

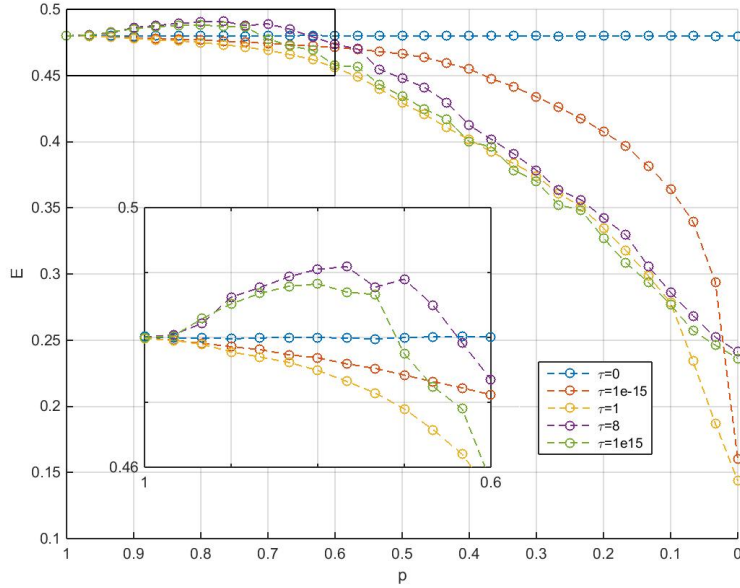


Figure 4.16: Along the vertical axis is the global efficiency  $E$  as a function of random rewiring probability  $p$  along the horizontal axis: Coloured lines indicate values of heat kernel parameter  $\tau$ .

as closeness and betweenness centrality, do not [138]. We denote as  $\pi$  the (normalised) maximum component of the PageRank vector. The mean value of the components of a PageRank vector for a given network of  $n$  vertices is  $\frac{1}{n}$ . For convenience we normalise  $\pi$  by this mean value.

In Figure (4.4.3) we observe the average PageRank value  $\pi$  as a function of random rewiring probability  $p$ . As with modularity, we see that centrality can be switched on or off depending on the choice of  $\tau$ . For  $\tau = 8, \delta$  emergent network structures exhibit values of  $\pi$  considerably (positively) far from that of the ER networks, indicating large deviations of the maximum component from the mean of the PageRank vector. Therefore, there exists at least one vertex having a significantly higher likelihood of being traversed in a random Markov chain than all others. On the other hand, for  $\tau = \epsilon, 1$  and over all  $p \in [0, 1]$  emergent networks possess no such central vertices, i.e. centrality is switched off. In fact, we see a lesser degree of centrality than in an equivalent random ER network.

In accordance with Figure (4.4.3), by choice of pair  $(\tau, p)$  emergent networks are either modular or centralised. The phase transition of network structure is discussed in the section *Critical Network Structure*.

In Figure (4.4.3) the *degree distribution* of vertices is Gaussian for  $\tau = \epsilon, 1$  and log-normal

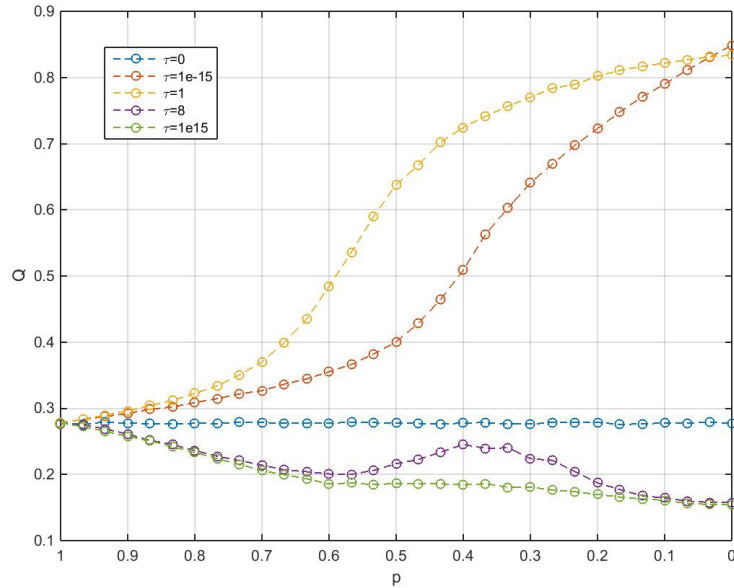


Figure 4.17: The average modularity  $Q$  as a function of decreasing random rewiring probability  $p$ : Coloured lines indicate values of heat kernel parameter  $\tau$ .

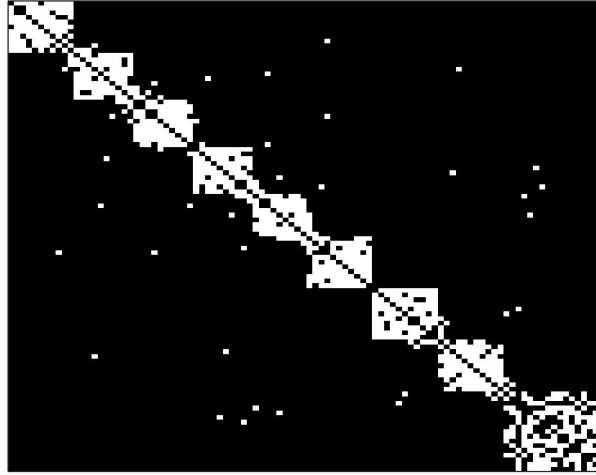
for  $\tau = 8, \delta$ . Moreover, for  $\tau = 8, \delta$  there emerge vertices having remarkably high degrees ( $> 70$ ).

In Figure(4.21) we present the adjacency matrices from a randomly chosen trial with pairs  $(\tau, p)$ , where  $p$  is chosen dependent on  $\tau$  so that the values of  $S$  are at maximum. In both Figure (4.21(a)) where  $(\tau, p) = (8, 0.5667)$ , and Figure (4.21(b)) where and  $(\delta, 0.5667)$ , we observe a small subset of hub vertices connecting to many peripheral vertices.

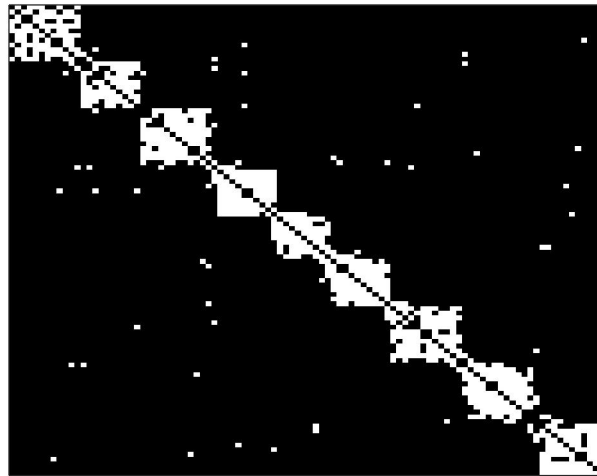
The *assortativity coefficient*  $a$  describes the “assortative mixing” of vertex degrees, i.e. the preference for high-degree vertices to attach to other high-degree vertices. In Table (4.1) row  $a$ , a strong negative correlation for  $\tau = 8, \delta$  indicates that vertices of a high degree typically connect to vertices of a low degree. For  $\tau = \epsilon, 1$  an approximately zero correlation indicates no preference of connections between vertices of varying degrees.

The *maximised coreness statistic*  $c$  measures the extent to which a network may be well-partitioned into two non-overlapping groups of vertices, a core and a periphery group. In Table (4.1) row  $c$ , for  $\tau = 8, \delta$  values close to one indicate that the network may be well-partitioned into non-overlapping groups of core and peripheral vertices. For  $\tau = \epsilon, 1$  values close to zero indicate no such core-periphery partition.

In sum, we note that for  $\tau = 8, \delta$  networks emerge as centralised, with a strong core, and that those core vertices connect to a high number of peripheral vertices. For  $\tau = \epsilon, 1$ ,



(a)



(b)

Figure 4.18: Single trial. Example modular SWN. Adjacency matrices mapped to an  $n$ -by- $n$  grid where rows (and columns) represent vertices and white indicates the existence of an edge. Rows and columns of adjacency matrices have been permuted to visualise the modules, in accordance with [127]. **a**:  $(\tau, p) = (\epsilon, 0.1)$ ; **b**:  $(\tau, p) = (1, 0.3)$ .

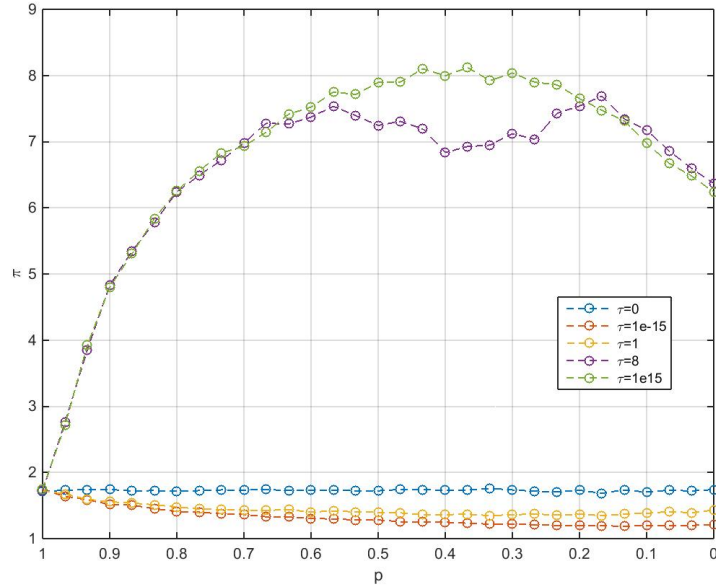


Figure 4.19: The average  $\pi$  - maximum component of PageRank vector normalised by its mean - as a function of decreasing random rewiring probability  $p$ : Coloured lines indicate values of heat kernel parameter  $\tau$ .

networks exhibit none of these properties.

$\tau$	0	$\epsilon$	1	8	$\delta$
$a$	-0.0219	0.0259	0.0905	-0.4689	-0.5094
$c$	0.2482	0.0491	0.1317	0.8770	0.9066

Table 4.1: Column wise  $\tau$ . Row wise:  $a$  assortativity coefficient;  $c$  maximised core-periphery statistic. Values presented are averages over trials.

### Critical Network Structure

Now let us take a closer look at the transition between modularity and centrality, and show that at the phase transition of network structure, the two seemingly opposing properties are reconciled. Properties of modularity are characterised by  $Q$  while properties of centrality are characterised by  $\pi$ .

In Figure (4.22), for parameters  $\tau$  in  $[4.5, 5.5]$  with increments of 0.05 and  $p$  as previous, we present  $Q$  (Figure (4.22(a))), and  $\pi$  (Figure (4.22(b))). In the domain  $(\tau, p)$  there is a broad region of high modularity where both  $\tau$  and  $p$  are low, and a broad region of high centrality in the remainder. Where the domain of modularity ends, the domain of centrality

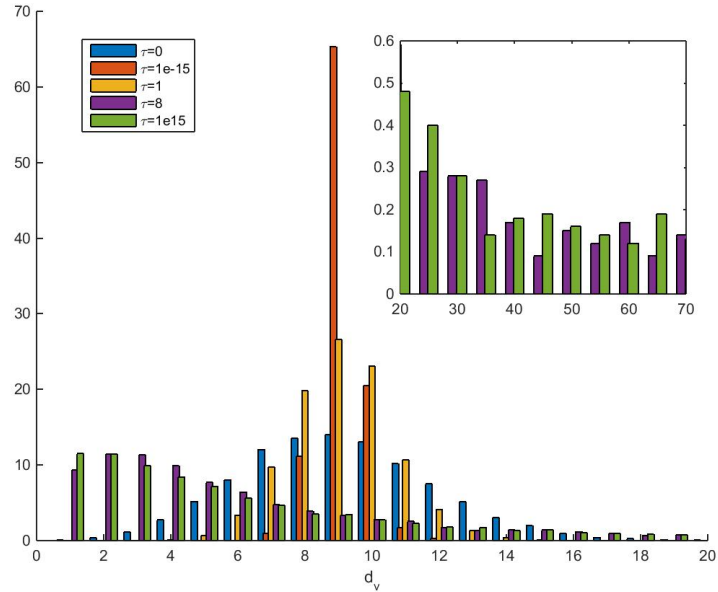
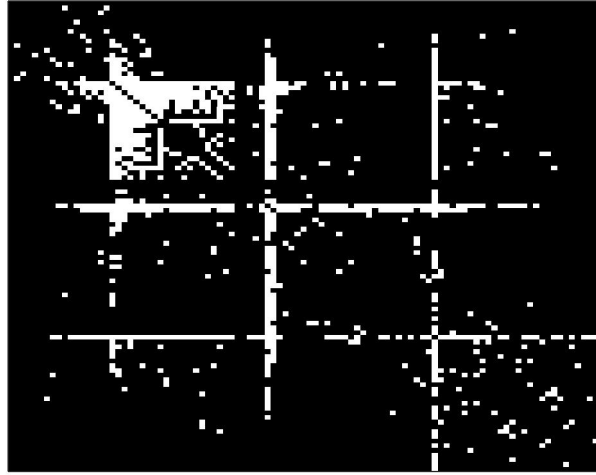


Figure 4.20: A bar-plot graph where the height of individual bars are the average number of vertices having degree  $d_v$ . Coloured bars indicate values of heat kernel parameter  $\tau$ .

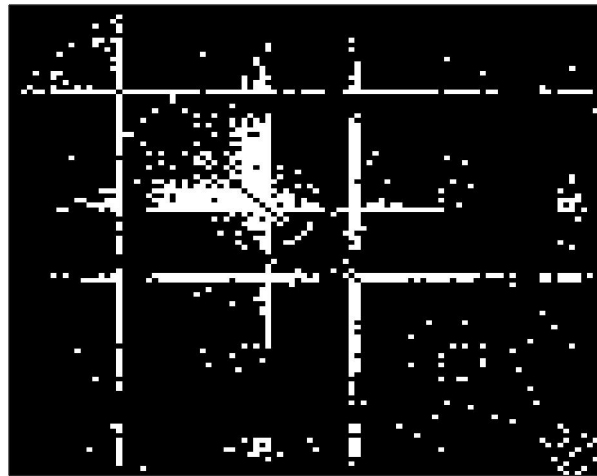
begins: The system exhibits a critical transition from decentralised (modular) to centralised structure as a function of the pair  $(\tau, p)$ . The phase transition region between the two is relatively sharp with respect to both  $\tau$  and  $p$ .

In Figure (4.23(a)) we fix  $\tau = 0.5$  and take  $Q$  and  $\pi$  as a function of  $p \in [0.4, 0.6]$  with uniform spacing 0.002. As previous we take the average of 100 trials. It is clear that modularity and centrality are opposing properties, however, at the boundary of modularity and centrality, where they intersect at around  $p = 0.52$ , there is a small domain of  $p$  for which networks are a blend of both modular and central structure: each of  $Q$  and  $\pi$  are considerably large, indicating the presence of both network properties. Furthermore, the value of small-worldness for pair  $(\tau, p) = (5, 0.522)$  is  $S = 5.32$ , indicating the network is also small-world.

In Figure(4.23(b)) we present from one trial with pair  $(\tau, p) = (5, 0.522)$  the adjacency matrix permuted to visualise the modules. We observe a competition between modular and centralised structure: The simultaneous existence of densely connected communities (decentralised) and a core of high degree vertices connecting to many low degree peripheral vertices (centralised). In Figure (4.24) we present four additional randomly sampled networks for pair  $(\tau, p) = (5, 0.522)$ . These additional figures support the notion that centrality and modularity are opposing, that at the point of phase transition they are reconciled, and that



(a)



(b)

Figure 4.21: Single trial. Example centralised SWN. Adjacency matrices mapped to an  $n$ -by- $n$  grid where rows (and columns) represent vertices and white indicates the existence of an edge. Rows and columns of adjacency matrices have been permuted to visualise the modules, in accordance with [127]. **a**: depicts  $(\tau, p) = (8, 0.5667)$ ; **b**: depicts  $(\tau, p) = (\delta, 0.5667)$ .

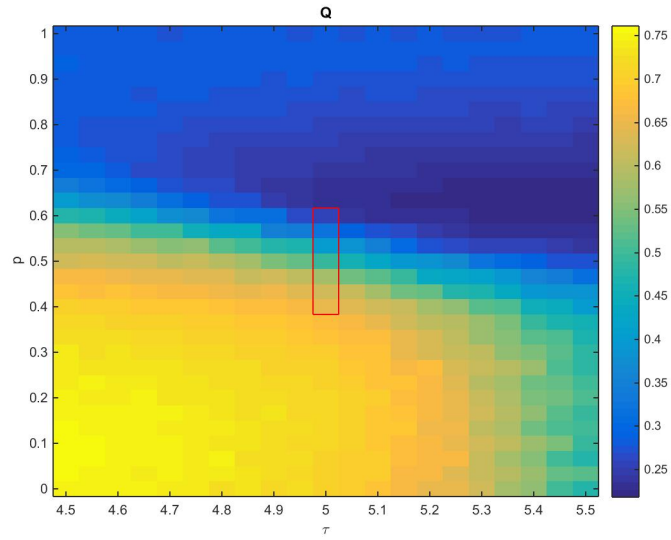
this is critical, i.e. they are competitive. Under the same parameters, all adjacency matrices exhibit some degree of both centrality and modularity: emergent networks may appear as more centralised (Figures (4.24(a)) and (4.24(b))), or more modular (Figure (4.24(c))), or a blend of the two (Figure (4.24(d))).

## 4.5 Conclusion

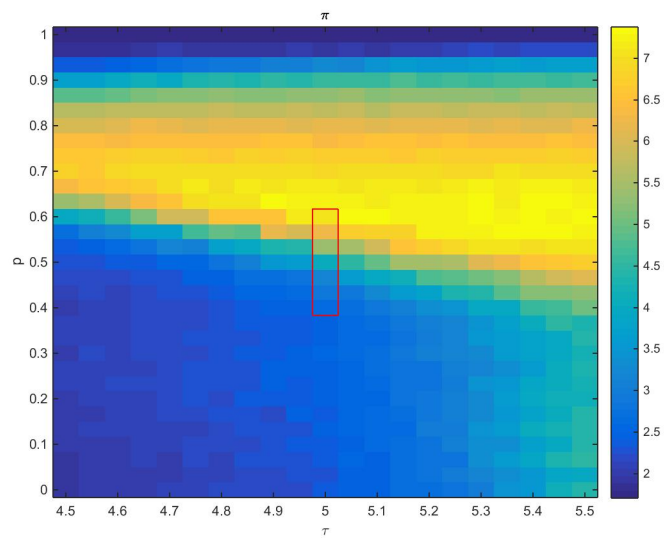
In the first part of this chapter, *Spatially constrained adaptive rewiring in cortical networks creates spatially modular small-world structures*, we aimed to understand the principles whereby the large-scale information processing architecture of the cortex takes shape – in particular, the observation that this structure consists of a large number of efficiently connected clusters: a modular small-world. In the cortex, this architecture exists within an essentially sheet-like structure, in which the modules are spatially segregated, and their links are long-range connections. We propose that this network structure, and its spatial layout, take shape in a process through which neural connections are rewired in response to the patterns of dynamic synchronization in ongoing neural activity. In a highly simplified model of the functional architecture, starting from a random initial network structure, a modular small world network gradually emerges when connections are attached and detached, depending on the presence or absence of pairwise synchrony between activity in the nodes.

Previous adaptive rewiring models have considered synchrony as the only rewiring criterion irrespectively of the information processing architecture of the brain [59; 91; 75; 128]. Here we consider networks endowed with metrics, a definition of distance between nodes, and study the effect on the outcome of adaptive rewiring. We study the effect of local bias on the rewiring of connections in a highly simplified model process. Doing so allows us to consider the effect of biological constraints such as metabolic costs and wiring length. Factoring in a preference for spatially local rewiring is cause for the modular small world structure to be reached with greater robustness, compared to rewiring based on synchrony alone. The resulting network, moreover, consists of spatially segregated modules, in which within-module connections are predominantly of short range and their interconnections are of long range. The spatially biased rewiring process, therefore, might be considered as a principle for how the large-scale architecture of the cortex is formed.

In our current, highly abstract model, a locally biased Hebbian-like adaptive rewiring process is applied to a network consisting of 500 nodes evenly distributed on a sphere. Rewiring depended on the factors of synchrony between pairwise unit activity and the spatial distance between nodes. The procedure extends the adaptive dynamical rewiring process of

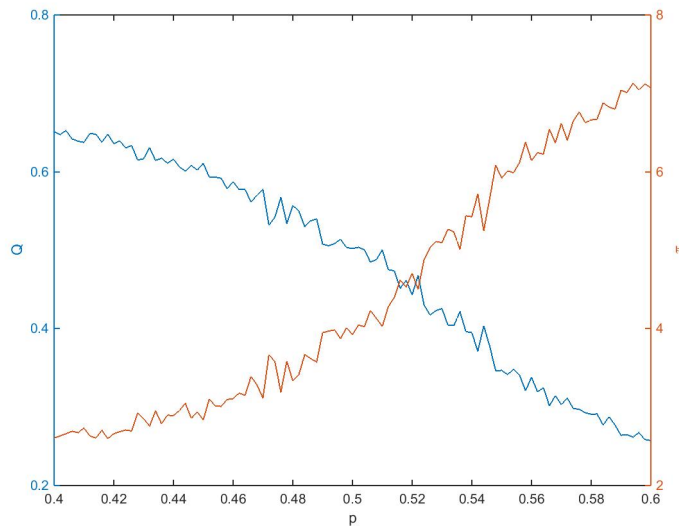


(a)



(b)

Figure 4.22: In the plane  $\tau$  along the horizontal axis and random rewiring probability  $p$  along the vertical axis: **a**: depicts the modularity index  $Q$ ; **b**: depicts  $\pi$ , the maximum component of PageRank vector normalised by its mean value.



(a)



(b)

Figure 4.23: **a:** For  $\tau = 0.5$ . Along the horizontal axis random rewiring probability  $p$ . Along the vertical axis are  $Q$  the modularity index (left), and  $\pi$  is the maximum component of PageRank vector normalised by its mean value (right). **b:** Single trial. Example centralised SWN. Adjacency matrix mapped to an  $n$ -by- $n$  grid where rows (and columns) represent vertices and white indicates the existence of an edge. Rows and columns of adjacency matrices have been permuted to visualise the modules, in accordance with [127]. Pair  $(p, \tau) = (5, 0.522)$ .



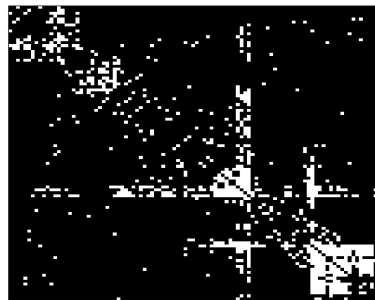
(a)



(b)



(c)



(d)

Figure 4.24: For four single trials, (a)–(d), where in each the pair  $(p, \tau) = (5, 0.522)$ , the adjacency matrix permuted to visualise the modules, in accordance with [127].

[59] with a function that biases rewiring such that spatially local connections are more likely. We considered three functions to specify the costs of a given wiring length: logarithmic, linear, and exponential.

For 10% connectivity, all versions of the locally biased rewiring process preserve the phenomenon of small-world emergence found in the non-spatial one. Furthermore, the linear and exponential ones yielded networks that are spatially organised such that topologically segregated regions correspond to spatially segregated regions, with these regions being linked by long-range connections; that is to say, a spatially modular small-world.

Locally biased adaptive rewiring improves the robustness of network evolution from random to small-world topology. Non-spatial adaptive rewiring processes are subject to a minimum connectivity density threshold, below which the rewiring process does not achieve self-organised clustering [150]. Locally biased adaptive rewiring processes that have a linear or exponential cost function, however, achieve self-organised clustering for connectivity densities considerably lower than this threshold.

The measure of edge betweenness in relation to spatial distance enables us to relate hub nodes - nodes that participate in a relatively high proportion of shortest paths - with connections that are spatially long-range (since hub nodes can be inferred from high betweenness edges). Previously, anatomical network hub nodes appeared random in functional networks due to observed disparity between structural and functional connectivity [150]. Now, however, we see hub nodes connect spatially distant regions.

We conclude that a locally biased adaptive rewiring function equipped with a linear or exponential cost function is capable of generating a spatially modular small-world network. Thus, spatially constrained adaptive rewiring schemes are sufficient to explain both the emergence of topological connectivity structure and spatial distribution of large-scale cortical architecture.

In the second part of this chapter, *“Go with the flow”; Self-organisation of small-world network*, we proposed a principle of network self-organisation that relies only on ongoing network diffusion; over time, the network is rewired adaptively, rendering it conform to the patterns of diffusion. With some probability  $p$ , this process is perturbed by random rewiring. For almost any proportion of random noise rewiring small-world structure emerged. For a broad range of  $p$ , the networks reached higher degrees of SWN structure than those in the Watts and Strogatz algorithm [154].

The optimal proportion of noise rewiring depends on the diffusion rate  $\tau$ . The value of  $\tau$  biases for local or global connectivity structures in the network. Depending on this bias, a family of SWNs emerges. For small  $\tau$ , i.e. local diffusion, networks emerge as modular. For large  $\tau$ , i.e. global diffusion, emergent network structures are centralised. For intermediate

values of  $\tau$  and  $p$  there is a critical transition point at which network structures emerge that blend modularity and centrality. We may call these “hierarchical” [103].

Such networks are desirable for natural information processing systems like the human brain, in which a core of centralised components represents a global workspace and the decentralised modules represent autonomous client systems [6; 39; 135]. The criticality of these architectures renders them all but robust. At the level of the neuro-anatomy of the brain, it would probably involve dynamic maintenance to keep these architectures at the critical point. As a property of functional architecture, the criticality would render cognition extremely flexible, enabling rapid switching between centralised and modular processes [101].

## Chapter 5

# Conclusion

The purpose of this thesis was to further understand self-organisation in network structure, in particular, in the context of the brain.

Functional and anatomical structures in the brain are non-trivial [63; 139; 25; 53]. A structure we have assigned particular attention to is the small-world network, classically known for reconciling opposing properties of segregation and integration [154]. Complex network structure is highly unlikely to emerge by chance. Moreover, small-world networks are observed in myriad contexts besides the brain, such as ecological networks [105], social networks [149], protein networks [4], the Boston subway [96], and the World Wide Web [147]. This suggests that there may exist some universal underlying principle for their emergence.

In the quest for a universal principle, we consider two very different approaches: the mathematical analysis of dynamics on a given network, and the computational modelling of network structure evolution. Network dynamics and structural evolution have been shown to play a mutual role in network self-organisation [127], i.e. activity and structure are symbiotically related.

In Chapter 2 we introduced some basic concepts of nonlinear systems theory [40]. This foundation is necessary for the study of stability of solutions of a dynamical system. Understanding the dynamics of interconnected systems of nonlinear ordinary differential equations is arguably amongst the oldest and inspiring problems. Objects of this type occur in a broad range of fields of engineering and science [119]. We reviewed methods for stability analysis, in particular, for synchronous solutions the Connection Graph Stability method [14], Wu-Chua conjecture [159], Master stability function [117], semi-passivity argument [121], and for periodic solutions the Floquet multipliers [88; 83]. In the following Chapter we apply methods of semi-passivity and Floquet multipliers to a study of change in network topology. This is complemented with numerical simulations. While analytical solutions for stability

analysis provide a great deal of insight, they may at times be conservative, i.e., provide bounds for which synchronization is guaranteed, however the true bounds may exist for a larger domain of parameter space. This is when numerical simulations become useful, even when analytical solutions exist.

In Chapter 3 we study how small changes in network structure can effect stability properties in a system of coupled oscillators. We chose as nonlinear dynamics the FitzHugh-Nagumo oscillator [46], a generalisation of the van der Pol equation for a relaxation oscillator. Individual oscillators were then diffusively coupled into two configurations, the directed chain and directed cycle. The directed chain and the directed cycle differ by just one connection; the directed cycle is obtained by the addition of an edge that closes the directed chain. The choice of directed cycle is motivated by its extremal properties. Among all linear systems satisfying the condition that the transposed Laplacian matrix has all zero column sums, the directed cycle with equal connection weights is the most sensitive to disturbances, i.e. perturbations take the longest time to decay. We applied from Chapter 2 previously discussed stability analysis methods of semi-passivity and Floquet multipliers in addition to numerical simulations. In doing so, in changing from one configuration to the other we see a profound bifurcation of equilibria. For the case of the directed chain there exists an asymptotically stable fixed point, the synchronization manifold. The directed cycle, however, exhibits multi-stability; both a fixed point - synchronization - and a periodic solution, called a rotating wave, are stable. The extremal properties of the directed cycle configuration therefore create resonances with nonlinear systems. The emergence of periodic behaviour is thus the result of initial perturbations from the synchronous manifold (initial conditions) not decaying, but instead resonating, eventually into a stable periodic solution. In natural systems, such a multistability may have use as a switch, from periodic motion to stationary motion, and vice versa. One such example of feedback mechanisms generating periodic motion is the generation of quadrupedal gaits, the order of movement of four legs [51].

In the second part of Chapter 3 (*Multi-Stability of coherent dynamics in directed networks with modular topology*), we generalise the directed cycle configuration to one of modules directionally coupled in a cycle. We show that if connectivity within isolated modules is diffusive with relatively strong coupling, multiple coherent and orderly dynamic regimes co-exist in the system state space. In addition to a nearly fully synchronous state, an attracting rotating wave solution occurs. Moreover, the rotating wave solutions are shown by numerical simulation to occur with greater frequency than in the previous case of individual oscillators in the directed cycle.

In Chapter 4 we turn our attention toward a more general setting. In Section 4.3 we

consider a computational model of a network of brain regions. Regions are modelled by the chaotic dynamics of the logistic map. The logistic map is an interesting dynamical system, since diffusively coupled arrays exhibit more complex patterns of dynamics than a single map is capable [78]. The logistic map may also represent a model of neural population dynamics, as demonstrated in Figure 2 of [128]. The key aim of this section was to expand upon previous studies of adaptive rewiring [59], in particular, to incorporate space into a model of adaptive rewiring. Adaptive rewiring was conceived as an abstract model of brain evolution and the mutual role of activity and structure [128]; structure adapts to activity, while activity is influenced by structure. Many studies have strengthened this model [91; 128; 59; 150]. Missing from this model was any notion of space, arguably a very important factor in brain network structure, in particular in minimisation of wiring cost [32], organisation [26], and trade-offs between spatial cost and function [24].

By incorporating space as a cost function of distance in the adaptive rewiring a number of interesting results were found. To begin, we investigated several cost functions of distance, over increasing distance the cost increased exponentially, linearly, and logarithmically. Network measures clearly demonstrated that a logarithmic cost of distance failed to yield similar complex structures as seen in the brain, i.e. the failure for modular and small-world network structure to emerge. Linear and exponential cost functions of distance on the other hand showed improved emergence of these network structures; networks more consistently and with greater pronunciation emerged as modular and small-world as compared to the original adaptive rewiring model without any dependency on space.

Possibly the most interesting result, was the improved robustness of network self-organisation under the constraint of reduced connectivity density, i.e. fewer edges. In [150], network connectivity was investigated, and it was shown that for reduced connectivity there existed a threshold for which emergence of modular small-world structure failed, and the network remained random. It was suggested in [150] that this fragmentation of network structure may explain schizophrenia; schizophrenia is often characterized as a reduced clustering and increased integration. With the addition of spatial cost on adaptive rewiring, this threshold was found to be significantly lower, allowing for modular small-world networks to self-organise for networks having much fewer edges. This suggests an alternative explanation for the occurrence of schizophrenia: a disruption to the metabolic cost of connections in the brain such that connection organisation is to a lesser degree influenced by spatial distance.

Following this, in Section 4.4 we present the key result of this thesis: the synthesis of mathematical formalization and computational modelling to understanding network self-organisation. As we have demonstrated in Chapter 3, due to dynamic sensitivities to the underlying connectivity structure, it is not (yet) feasible to analytically characterize general

patterns of dynamics on an evolving network. This issue is in part addressed in this section, in which this very complex problem is reduced to a problem of estimating the likelihood of solutions: we consider the solution of synchronization and estimate the likelihood of systems synchronizing by considering the degree of graph diffusion (traffic flow or information transfer) between all pairwise vertices. Systems with higher degrees of diffusion are deemed to have a higher likelihood, and vice versa. This estimation for systems to synchronize is applied to the adaptive rewiring rule described in Section 4.3 in the way that vertices with a higher likelihood of synchronizing are wired together and those with a low likelihood have their edge removed.

The model has two key parameters: a time parameter representing the diffusion rate that can bias between local and global connectivity structures, and a random parameter used in the rewiring process that determines if the network rewires according to diffusion patterns or randomly. Numerical simulations showed that biasing toward local structures in the rewiring process produce modular structures, while biasing toward more global structures produce centralised structures. The degree of randomness in the rewiring process was shown to be related to the diffusion rate, in that optimal small-world structures were for pairs of diffusion rate and random rewiring. Interestingly, there exists a phase transition of network structure, from modular to centralised. At the transition between these two structures there exists a critical network structure in which the network was a blend of both. Such a structure can be considered “hierarchical” [103], and may be desirable for natural information processing systems like the human brain [6; 39; 135].

While we only considered one class of solutions as a criteria for rewiring - synchronization -, we were able to achieve self-organisation of highly complex network structures. In reducing the complexity of a problem, it may become detail invariant, and one can better understand the basic principles that underlie the process in its many manifestations. To this end, we can conclude that *optimization of patterns of communication* is a basic and universal principle of complex network structure emergence.

The study of brain network self-organisation is one that can be approached from many directions. To name a few: biological, chemical, physical, psychological, mathematical, and computational. This makes the problem both highly challenging but also very interesting. One may wish to put their effort into just one field, however, they may limit themselves in their scope of addressing the problem of self-organisation. These different fields can at times find emphasis to particular scales of space, time, and realism in brain network growth and development. On the smallest spatial scale, a chemical approach may be limited to the molecular level, such as the ion diffusion through gates in the cell membrane and the feedback processes leading to spike generation. A biological approach may be of a higher

spatial scale, such as the anatomy of axons and the growth cones that guide them, yet this is a slow temporal scale. A psychological scale may record activity patterns on the millisecond scale, yet on the global brain spatial scale. Considering the realism, mathematics may reduce a process to an abstract one that characterises bifurcations of nonlinear dynamics describing cell action potentials [71]. While on the other hand, computational modelling of a large array of simple neurons, such as integrate and fire, can capture the large scale activity patterns observed in real networks.

## 5.1 Future work

Let us briefly describe studies for future work.

**Adaptive rewiring and brain pathology** One study concerns the application of spatially biased adaptive rewiring to brain pathology. Consider the computational model described in Section 4.3. It would be interesting, and rewarding, to connect spatial cost functions of distance to brain pathologies. The results presented suggest that schizophrenia may arise from a weaker than normal metabolic cost over distance. Other such pathologies that may be targeted in this study include autism, which is understood to arise as the result of over-localisation; compared to normal brain structure, one with autism exhibits increased segregation and weakened integration, resulting in improved processing of information at the expense of poor communication.

**Adaptive rewiring in weighted networks** This project is currently in the writing stage with the aim to publish in 2017. This study is an extension of the original adaptive rewiring model [59]. It concerns the evolution of networks having weighted edges, and how the set of weights affects the structures that emerge. A wide range of distributions are considered, including exponential, normal, log-normal, and power-law, from which a set of weights are drawn. In previous studies, coupling has been uniform, and in the model presented in Section 4.3, spatial distance is incorporated into the rewiring phase of the model. In this model, however, edge weighting is incorporated in the evolution of dynamics.

**Adaptive rewiring and the heat kernel for directed and weighted networks** A study, with the aim of two publications in 2017, is to extend the model of adaptive rewiring in response to graph diffusion presented in Section 4.4 to one of directed and one of weighted networks. In particular, in Section 4.4 we considered the heat kernel for undirected and binary graphs. However, many real world networks are better described by directed and/or

weighted graphs. For instance, the neural network of the mammalian brain has many different means of communication, among which but not limited to, are directed axonal-synaptic connections. Such connections are not binary, nor are they necessarily bi-directional. In addition, connection weights may also be considered negative, describing inhibitory synapses.

The aim of this study is to extend the result of self-organisation by diffusion to directed and weighted networks, however, we begin by addressing each individually.

The study of weighted networks is a relatively simple extension of the model since the definition of the heat kernel is almost unchanged. Since the weight matrix is symmetric, definitions of the normalised graph Laplacian remains almost unchanged:

$$\mathcal{L} = I_n - D_w^{-1/2} W D_w^{-1/2} \quad (5.1)$$

where  $I_n$  is the identity matrix,  $W$  is the weight matrix such that  $W_{ij} = w_{ij}$  if  $A_{ij} = 1$  where  $w_{ij}$  is a nonzero weight drawn randomly from some distribution and  $W_{ij} = 0$  otherwise, and  $D_w^{-1/2}$  is the diagonal matrix of degrees  $D_{ii} = \sum_j W_{ij}$ . We hypothesise that for certain pairs of parameters  $(\tau, p)$  (the diffusion rate and probability of random rewiring) emergent structures should reflect the previously described model for weighted adaptive rewiring. However, it is not yet understood how changes in the pair  $(\tau, p)$  will effect network evolution for the different connection weight distributions.

In the study of directed networks, the normalised Laplacian matrix takes a different form. Considering the definition for the normalised Laplacian in [33], we formulate the normalised Laplacian for directed adjacency graph  $G$  with non-symmetric adjacency matrix  $A$

$$L = I_n - D_{\text{in}}^{-1/2} A D_{\text{out}}^{-1/2}$$

where  $D_{\text{in}}$  and  $D_{\text{out}}$  are the diagonal matrices of in- and out-degrees, respectively. For undirected  $k$ -regular graph  $L$  is equal to the ordinary graph Laplacian. One may then calculate the heat kernel - the solution for heat diffusion on the graph -, denoted as  $h(t)$ , as

$$h(t) = \exp^{(-tL)}. \quad (5.2)$$

The next step is the rewiring criteria: since  $L$  is non-symmetric, then so is  $h(t)$ . The column-wise entries of  $h(t)$  correspond to the diffusion flow from a given vertex to another. In the emergent network structures we consider the motifs, specific patterns of connectivity. Preliminary results suggest that this may provide an answer for the emergence of feedforward loops, a widely observed network motif in brain networks [104].

**Adaptive rewiring and memory: Rewiring Izhikevich's polychronous neuronal groups** It is hypothesized in [42; 74] that higher-order processing in the brain, such as

memories or experience, may be represented by patterns of temporal coding. In a small-scale network model, comprising excitatory and inhibitory neurons with delay synaptic coupling and synaptic weight update by Spike-Time Dependent Plasticity (STDP) [137], [73] proposes as a model of temporally coded memory, computational units called Pynchronous Neuronal Groups (PNG's): certain persistent spike-timing patterns that emerge and re-occur with millisecond precision, despite statistically highly unlikely probability of repetition.

The principal result of [73] are the number of emergent PNG's; the number of PNGs that emerge far exceeds the number of neurons in the network, possibly explaining the rich diversity of activity and memory capacity in the cortex. This is the result of competitive synaptic plasticity. STDP can select matching conduction delays and give rise to the spontaneous formation of neuronal groups, i.e. self-organization of neurons into neuronal groups [74].

A limitation of this study however is the choice of neuron model. Individual neurons are modelled by the Izhikevich spiking neuron model [71; 72], capable of producing 20 fundamental neuro-computational features of biological neurons while at a computational cost comparable to that of an integrate-and-fire neuron. Despite these advantages, the neuron model is a piecewise continuous one, and therefore, standard stability analysis of nonlinear systems, as discussed in this thesis, do not apply.

A drawback of the model lies in the rigidity of the network structure. STDP must select the 'best fitting' set of connections - which neurons have a connection and their specific delay value - from an initially random configuration. For future study we aim to demonstrate that if network structure is allowed to change in response to activity, if the network is adaptively rewired, that a more efficacious structure may self-organize, i.e. one that has an increased capacity for PNG's without requiring more resources. We aim to characterize the improved efficiency of the network structure through a series of network measures and understand how, and which, topological properties of a network structure self-organize to promote the emergence of PNG's. Achieving this goal will provide valuable insight into the network properties optimal for memory formation and storage.

To address this problem, we introduce structural plasticity in the form of connection rewiring. Studies include pruning of connections whose weight depresses to zero. When a connection is pruned, a new connection replaces it. We hypothesise that over time network structure and delay values self-organize in such a way to maximise the number of emergent PNG's.

Preliminary results have already given many answers to this problem. One result in particular is interesting, since it relates well to our study of spatially dependent adaptive

rewiring, as discussed in Section 4.3. When forming a new connection the question arises of what delay value should the new connection take? We have found that compared to assigning random delay values to new connections, the process of adaptively rewiring of connections is more efficient, in terms of the total number of edge rewirings and the number of emergent PNG's, when delays are spatially dependent.

# Bibliography

- [1] ABELES, A., PRUT, Y., BERGMAN, H., AND VAADIA, E. Synchronization in neuronal transmission and its importance for information processing. *Progress in Brain Research* 102 (1994), 395–404.
- [2] ACHARD, S., AND BULLMORE, E. Efficiency and Cost of Economical Brain Functional Networks. *PLoS Comput Biol* 3, 2 (Feb. 2007), e17+.
- [3] ASL, M., VALIZADEH, A., AND TASS, P. Dendritic and axonal propagation delays determine emergent structures of neuronal networks with plastic synapses. *Scientific Reports* 7, 39682 (2017), 1–12.
- [4] ATILGAN, A. Small-World Communication of Residues and Significance for Protein Dynamics. *Biophysical Journal* 86, 1 (2004), 85–91.
- [5] ATMANSPACHER, H., AND SCHEINGRABER, H. Inherent global stabilization of unstable local behaviour in coupled map lattices. *International Journal of Bifurcation and Chaos* 15 (2005), 1665–1676.
- [6] BAARS, B. J. Metaphors of consciousness and attention in the brain. *Trends in Neurosciences* 21, 2 (1998), 58–62.
- [7] BAIER, H., AND BONHOEFFER, F. Axon guidance by gradients of a target-derived component. *Science* 255, 5043 (1992), 472–475.
- [8] BAO, J., AND LEE, P. *Dissipativity and Passivity*. Springer London, London, 2007.
- [9] BASSETT, D. S., MEYER-LINDENBERG, A., ACHARD, S., DUKE, T., AND BULLMORE, E. Adaptive reconfiguration of fractal small-world human brain functional networks. *Proceedings of the National Academy of Sciences of the United States of America* 103, 51 (2006), 19518–23.
- [10] BEAN, B. The action potential in mammalian central neurons. *Nature Reviews Neuroscience* 8 (2007), 451–465.

- [11] BELMONTE, M. K. Autism and Abnormal Development of Brain Connectivity. *The Journal of neuroscience : the official journal of the Society for Neuroscience* 24, 42 (2004), 9228–9231.
- [12] BELYKH, I., HASLER, M., LAURET, M., AND NIJMEIJER, H. Synchronization and graph topology. *International Journal of Bifurcation and Chaos* 15, 11 (2005), 3423 – 3433.
- [13] BELYKH, V. N., BELYKH, I. V., AND HASLER, M. Hierarchy and stability of partially synchronous oscillations of diffusively coupled dynamical systems. *Physical Review E* 62, 5 (2000), 6332–6345.
- [14] BELYKH, V. N., BELYKH, I. V., AND HASLER, M. Connection graph stability method for synchronized coupled chaotic systems. *Physica D: Nonlinear Phenomena* 195, 1-2 (2004), 159–187.
- [15] BENJAMIN, O., FITZGERALD, T. H., ASHWIN, P., TSANEVA-ATANASOVA, K., CHOWDHURY, F., RICHARDSON, M. P., AND TERRY, J. R. A phenomenological model of seizure initiation suggests network structure may explain seizure frequency in idiopathic generalised epilepsy. *The Journal of Mathematical Neuroscience* 2, 1 (2012), 1.
- [16] BLONDEL, V. D., GUILLAUME, J. L., LAMBIOTTE, R., AND LEFEBVRE, E. Fast unfolding of communities in large networks. *Journal of Statistical Mechanics: Theory and Experiment* 8, 10 (2008), 1–12.
- [17] BOCCALETTI, S., LATORA, V., MORENO, Y., CHAVEZ, M., AND HWANG, D.-U. Complex networks: Structure and dynamics. *Physics Reports* 424, 4-5 (2005), 175–308.
- [18] BOLLOBÁS, B. *Random graphs*, 2 ed. Cambridge University Press, Oct. 2001.
- [19] BONNARD, M., CHEN, S., GAYCHET, J., CARRERE, M., WOODMAN, M., GIUSIANO, B., AND VIKTOR, J. Resting state brain dynamics and its transients: a combined tms-eeeg study. *Scientific Reports* 6, 31220 (2016), 1–9.
- [20] BORGATTI, S. P., AND EVERETT, M. G. Models of core/periphery structures. *Social Networks* 21, 4 (2000), 375–395.
- [21] BPYDEN, E., ZHANG, F., BAMBERG, E., AND NAGEL, G. ANND DEISSEROTH, K. Millisecond-timescale, genetically targeted optical control of neural activity. *Nature Neuroscience* 8, 9 (2005), 1263–1268.

- [22] BREAKSPEAR, M., TERRY, J. R., AND FRISTON, K. J. Modulation of excitatory synaptic coupling facilitates synchronization and complex dynamics in a biophysical model of neuronal dynamics. *Network* 14 (2003), 703–732.
- [23] BRIN, S., AND PAGE, L. The anatomy of a large scale hypertextual Web search engine. *Computer Networks and ISDN Systems* 30, 1/7 (1998), 107–17.
- [24] BUDD, J. M. L., AND KISVÁRDAY, Z. F. Communication and wiring in the cortical connectome. *Frontiers in neuroanatomy* 6, October (2012), 42.
- [25] BULLMORE, E. T., AND BASSETT, D. S. Brain graphs: Graphical models of the human brain connectome. *Annual review of clinical psychology* 7 (2011), 113 – 140.
- [26] BULLMORE, E. T., AND SPORNS, O. The economy of brain network organization. *Nature Reviews Neuroscience* 13, 5 (2012), 336–49.
- [27] BUZSÁKI, G., AND CHROBAK, J. J. Synaptic plasticity and self-organization in the hippocampus. *Nature Neuroscience* 8, 11 (2005), 1418–1420.
- [28] BYRNES, C. I., ISIDORI, A., AND WILLEMS, J. C. Passivity, Feedback Equivalence, and the Global Stabilization of Minimum Phase Nonlinear Systems. *IEEE Transactions on Automatic Control* 36, 11 (1991), 1228–1240.
- [29] CANOLTY, R. T., AND KNIGHT, R. T. The functional role of cross-frequency coupling. *Trends in Cognitive Science* 14, 11 (2012), 506–515.
- [30] CHECHIK, G., MEILIJSON, I., AND RUPPIN, E. Synaptic Pruning in Development: A Computational Account. *Neural Computation* 10, 7 (1998), 1759–1777.
- [31] CHKLOVSKII, D. B., MEL, B. W., AND SVOBODA, K. Cortical rewiring and information storage. *Nature* 431, 7010 (2004), 782–788.
- [32] CHKLOVSKII, D. B., SCHIKORSKI, T., AND STEVENS, C. F. Wiring optimization in cortical circuits. *Neuron* 34, 3 (2002), 341–347.
- [33] CHUNG, F. R. K. *Spectral Graph Theory*, vol. 92 of *CBMS Regional Conference Series in Mathematics*. American Mathematical Society, Feb. 1996.
- [34] CICCETTI, D., AND COHEN, D. *Developmental Psychopathology: Developmental Neuroscience*. Wiley; Volume 2 edition, 2006.
- [35] CUOMO, K., OPPENHEIM, A. V., AND STROGATZ, S. Synchronization of lorenz based chaotic circuits with applications to communications. *IEEE Transactions on Circuits and Systems-11: Analog and Digital Signal Processing* 40, 10 (1993), 626–633.

- [36] CVITANOVIC, P. [www.chaosbook.org/course1](http://www.chaosbook.org/course1), 2016.
- [37] DAVIS, P. *Circulant Matrices*. AMS Chelsea Publishing Series. Chelsea, 1994.
- [38] DAYAN, P., AND ABBOTT, L. F. *Theoretical Neuroscience: Computational and Mathematical Modeling of Neural Systems*. The MIT Press; Revised ed. edition, 2001.
- [39] DEHAENE, S., SERGENT, C., AND CHANGEUX, J. P. A neuronal network model linking subjective reports and objective physiological data during conscious perception. *Proc Natl Acad Sci U S A* 100, 14 (2003), 8520–8525.
- [40] DOYLE, F. J., AND HENSON, MICHAEL, A. *Nonlinear system theory*. Nonlinear Process Control, 1981.
- [41] EBRAHIM, E. A Self-Contained Introduction to Lie Derivatives. [http://web.math.ucsb.edu/~ebrahim/lieverivs\\_tame.pdf](http://web.math.ucsb.edu/~ebrahim/lieverivs_tame.pdf), 2010.
- [42] EDELMAN, G. M. *Neural Darwinism : the theory of neuronal group selection*. Basic Books, 1987.
- [43] EL KACIMI ALAOUI, A. *Fundamentals of Foliation Theory*. Springer Basel, Basel, 2014.
- [44] ENGELBORGH, K., LUZYANINA, T., AND ROOSE, D. Dde-biftool: a matlab package for bifurcation analysis of delay differential equations. *ACM Trans. Math. Softw.* 28, 1 (2002), 1–21.
- [45] ERDŐS, P., AND RÉNYI, A. On random graphs. I. *Publ. Math. Debrecen* 6 (1959), 290–297.
- [46] FITZHUGH, R. Impulses and Physiological States in Theoretical Models of Nerve Membrane. *Biophysical Journal* 1, 6 (1961), 445–466.
- [47] FORNITO, A., ZALESKY, A., AND BREAKSPEAR, M. The connectomics of brain disorders. *Nature Reviews Neuroscience* 16, 3 (2015), 159–172.
- [48] FOX, M., AND RAICHEL, M. Spontaneous fluctuations in brain activity observed with functional magnetic resonance imaging. *Nature Reviews* 8 (2007), 700–711.
- [49] FOX, M., SNYDER, A., VINCENT, J., CORBETTA, M., VAN ESSEN, D., AND RAICHEL, M. The human brain is intrinsically organized into dynamic, anticorrelated functional networks. *Proc. Natl. Acad. Sci. U.S.A.* 102, 27 (2005), 9673–9678.
- [50] FRIEDMAN, J. L. Lie derivatives , forms , densities , and integration. <http://www.ictp-saifr.org/schoolgr/Lecture0Friedman.pdf>, 2017.

- [51] FUKUOKA, Y., HABU, Y., AND FUKUI, T. A simple rule for quadrupedal gait generation determined by leg loading feedback: a modeling study. *Scientific Reports* 5 (2015), 8169.
- [52] GAITERI, C., AND RUBIN, J. E. The interaction of intrinsic dynamics and network topology in determining network burst synchrony. *Frontiers in Computational Neuroscience* 5 (2011).
- [53] GALLOS, L. K., MAKSE, H. A., AND SIGMAN, M. A small world of weak ties provides optimal global integration of self-similar modules in functional brain networks. *Proceedings of the National Academy of Sciences of the United States of America* 109, 8 (2012), 2825–2830.
- [54] GARCIA, G. C., LESNE, A., HILGETAG, C. C., AND HÜTT, M. T. Role of long cycles in excitable dynamics on graphs. *Physical Review E - Statistical, Nonlinear, and Soft Matter Physics* 90, 5 (2014), 1–11.
- [55] GERSCHGORIN), S. G. S. Über die abgrenzung der eigenwerte einer matrix. *Bulletin de l'Académie des Sciences de l'URSS. Classe des sciences mathématiques et na* (1931), 749–754.
- [56] GIRVAN, M., AND NEWMAN, M. E. J. Community structure in social and biological networks. *Proceedings of the National Academy of Sciences* 99, 12 (2002), 7821–7826.
- [57] GOLUBITSKY, M., STEWART, I., AND TÖRÖK, A. Patterns of Synchrony in Coupled Cell Networks with Multiple Arrows. *SIAM Journal on Applied Dynamical Systems* 4, 1 (2005), 78–100.
- [58] GONG, P., AND VAN LEEUWEN, C. Emergence of scale-free network with chaotic units. *Physica A: Statistical Mechanics and its Applications* 321 (2003), 679–688.
- [59] GONG, P., AND VAN LEEUWEN, C. Evolution to a small-world network with chaotic units. *EPL (Europhysics Letters)* 67, 2 (2004), 328–333.
- [60] GORBAN, A. N. Extremal property of a simple cycle. <http://arxiv.org/abs/1301.2379>, 2013.
- [61] GORBAN, A. N., JARMAN, N., STEUR, E., VAN LEEUWEN, C., AND TYUKIN, I. Y. Leaders do not look back, or do they? *Mathematical Modelling of Natural Phenomena* 10, 3 (2005), 212–231.
- [62] HARMARK, T. Vector fields, flows and Lie derivatives. <http://www.nbi.dk/harmark/Killingvectors.pdf>, 2008.

- [63] HE, Y., CHEN, Z. J., AND EVANS, A. C. Small-World Anatomical Networks in the Human Brain Revealed by Cortical Thickness from MRI. *Cerebral Cortex* 17, 10 (Oct. 2007), 2407–2419.
- [64] HEBB, D. O. *The Organization of Behavior: A Neuropsychological Theory*, new ed ed. Psychology Press, June 2002.
- [65] HODGKIN, A. L., AND HUXLEY, A. F. A quantitative description of membrane current and its application to conduction and excitation in nerve. *The Journal of Physiology* 117, 4 (1952), 500–544.
- [66] HONEY, C. J., SPORNS, O., CAMMOUN, L., GIGANDET, X., THIRAN, J. P., MEULI, R., AND HAGMANN, P. Predicting human resting-state functional connectivity from structural connectivity. *Proceedings of the National Academy of Sciences* 106, 6 (2009), 2035–2040.
- [67] HUMPHRIES, M. D., AND GURNEY, K. Network small-world-ness: A quantitative method for determining canonical network equivalence. *PLoS ONE* 3, 4 (04 2008), 1–10.
- [68] IMS, R. A. The ecology and evolution of reproductive synchrony. *Trends in Ecology and Evolution* 5, 5 (1990), 135–140.
- [69] INNOCENTI, G. M., AND PRICE, D. J. Exuberance in the development of cortical networks. *Nature Reviews Neuroscience* 6, 12 (2005), 955–965.
- [70] IZHIKEVICH, E. M. Class 1 neural excitability, conventional synapses, weakly connected networks, and mathematical foundations of pulse-coupled models. *Trans. Neur. Netw.* 10, 3 (1999), 499–507.
- [71] IZHIKEVICH, E. M. Simple model of spiking neurons. *IEEE transactions on neural networks / a publication of the IEEE Neural Networks Council* 14, 6 (2003), 1569–1572.
- [72] IZHIKEVICH, E. M. Which model to use for cortical spiking neurons? *IEEE transactions on neural networks / a publication of the IEEE Neural Networks Council* 15, 5 (2004), 1063–1070.
- [73] IZHIKEVICH, E. M. Polychronization: Computation with Spikes. *Neural Computation* 18, 2 (2006), 245–282.
- [74] IZHIKEVICH, E. M., GALLY, J. A., AND EDELMAN, G. M. Spike-timing Dynamics of Neuronal Groups. *Cerebral Cortex* 14, 8 (2004), 933–944.

- [75] JARMAN, N. J., TRENGOVE, C., STEUR, E., TYUKIN., I. Y., AND VAN LEEUWEN, C. Spatially constrained adaptive rewiring in cortical networks creates spatially modular small world architectures. *Cognitive Neurodynamics* 8, 6 (Dec. 2014), 479–497.
- [76] JIRSA, V., AND MÜLLER, V. Cross-frequency coupling in real and virtual brain networks. *Frontiers in Computational Neuroscience* 7, 78 (2013), 1–25.
- [77] KALISMAN, N., SILBERBERG, G., AND MARKRAM, H. The neocortical microcircuit as a tabula rasa. *Proceedings of the National Academy of Sciences of the United States of America* 102, 3 (2005), 880–885.
- [78] KANEKO, K. Spatiotemporal chaos in one-and two-dimensional coupled map lattices. *Physica D: Nonlinear Phenomena* 37 (1989), 60–82.
- [79] KANEKO, K., Ed. *Theory and Applications of Coupled Map Lattices*. John Wiley & Sons., Chichester, UK, 1993.
- [80] KELSO, J. A. Multistability and metastability: understanding dynamic coordination in the brain. *Philos. Trans. R. Soc. Lond. B. Biol. Sci.* 367, 1591 (2012), 906,918.
- [81] KELSO, J. A., CASE, P., HOLROYD, T., HORVATH, E., RACZASZEK, J., TULLER, B., AND DING, M. Multistability and metastability in perceptual and brain dynamics. *In Ambiguity in Mind and Nature* (1995), 159–184.
- [82] KELSO, S. *Dynamic patterns: The self-organization of brain and behaviour*. A Bradford Book, The MIT Press, 1995.
- [83] KHALIL, H. K. *Nonlinear Systems*. Prentice-Hall, New Jersey, 1996.
- [84] KIRST, C., AND TIMME, M. How precise is the timing of action potentials? *Frontiers in Neuroscience* 3, 1 (2009), 2–3.
- [85] KNIERIM, J. J. The hippocampus. *Current Biology* 25, 23 (2015), R1116–R1121.
- [86] KOENIG, W., AND LIEBHOLD, A. Avian predation pressure as a potential driver of periodical cicada cycle length. *The American Naturalist* 181 (2013), 145–149.
- [87] KONDOR, R., AND VERT, J.-P. *Kernel Methods in Computational Biology*. The MIT Press, 2004.
- [88] KOON, W. S. Poincare map, floquet theory, and stability of periodic orbits. [http://www.cds.caltech.edu/archive/help/uploads/wiki/files/190/Lecture6\\_6.pdf](http://www.cds.caltech.edu/archive/help/uploads/wiki/files/190/Lecture6_6.pdf), 2006.

- [89] KRUGMAN, P. *The self-organizing economy*. Wiley-Blackwell, 1996.
- [90] KUBICKI, M., AND WESTIN, C. Diffusion tensor imaging and its application to neuropsychiatric disorders. *Harvard Review of Psychiatry* 10, 6 (2002), 324–336.
- [91] KWOK, H. F., JURICA, P., RAFFONE, A., AND VAN LEEUWEN, C. Robust emergence of small-world structure in networks of spiking neurons. *Cognitive Neurodynamics* 1, 1 (2007), 39–51.
- [92] LAFFERTY, J., AND KONDOR, R. I. Diffusion Kernels on Graphs and Other Discrete Input Spaces. *ICML '02 Proceedings of the Nineteenth International Conference on Machine Learning* (2002), 315–322.
- [93] LAMME, V. F., SUPER, H., AND SPECKREIJSE, H. Feedforward, Horizontal and Feedback Processing in the Visual Cortex. *Current Opinion in Neurobiology* 8 (1998), 529–535.
- [94] LASALLE, J. P. Some Extensions of Liapunov’s Second Method. *IRE Transactions on Circuit Theory* 7, 4 (1960), 520–527.
- [95] LATORA, V., AND MARCHIORI, M. Efficient behavior of small-world networks. *Physical Review Letters* 87, 19 (2001), 198701.
- [96] LATORA, V., AND MARCHIORI, M. Is the Boston subway a small-world network? *Physica A: Statistical Mechanics and its Applications* 314, 1-4 (Nov. 2002), 109–113.
- [97] LAUGHLIN, S. B., DE RUYTER VAN STEVENINCK, R. R., AND ANDERSON, J. C. The metabolic cost of neural information. *Nature neuroscience* 1, 1 (1998), 36–41.
- [98] LI, M., AND BELMONTE, J. Ground rules of the pluripotency gene regulatory network. *Nature Reviews Genetics* 18 (2017), 180–191.
- [99] LOW, L., AND CHENG, H.-J. Axon pruning: an essential step underlying the developmental plasticity of neuronal connections. *Philos. Trans. R. Soc. Lond. B. Biol. Sci.* 361, 1473 (2006), 1531–154.
- [100] M. MAMEI, M., MENEZES, R., TOLKSDORF, R., AND ZAMBONELLI, F. Case studies for self-organization in computer science. *J. Syst. Archit.* 52, 8 (2006), 443–460.
- [101] MANTZARIS, A. V., BASSETT, D. S., WYMBS, N. F., ESTRADA, E., PORTER, M. A., MUCHA, P. J., GRAFTON, S. T., AND HIGHAM, D. J. Dynamic network centrality summarizes learning in the human brain. *Journal of Complex Networks* 1, 1 (2013), 83–92.

- [102] MARTIN, P. Morphogenesis: Shroom in to close the neural tube. *Current Biology* 14, 4 (2004), 150–151.
- [103] MEUNIER, D., LAMBIOTTE, R., FORNITO, A., ERSCHKE, K. D., AND BULLMORE, E. T. Hierarchical modularity in human brain functional networks. *Frontiers in Human Neuroscience* 3, October (2009), 1–12.
- [104] MILO, R., SHEN-ORR, S., ITZKOVITZ, S., KASHTAN, N., CHKLOVSKII, D., AND ALON, U. Network motifs: Simple building blocks of complex networks. *Science* 298, 5594 (2002), 824–827.
- [105] MONTOYA, J. M., AND SOLÉ, R. V. Small World Patterns in Food Webs. *Theoretical Biology* 214, 3 (Feb. 2002), 405–412.
- [106] MORMANN, F., LEHNERTZ, K., DAVID, P., AND ELGER, C. Mean phase coherence as a measure for phase synchronization and its application to the eeg of epilepsy patients. *Physica D*. 144 (2000), 358–369.
- [107] MOSSA, F., WARD, L. M., AND SANNITA, W. G. Stochastic resonance and sensory information processing: a tutorial and review of application. *Clinical Neurophysiology* 115 (2004), 267–281.
- [108] NEWMAN, M. E. J. Assortative Mixing in Networks. *Physical Review Letters* 89, 20 (Oct. 2002), 208701+.
- [109] NEWMAN, M. E. J. Fast algorithm for detecting community structure in networks. *Physics Review E* 69, 6 (2004).
- [110] NEWMAN, M. E. J. Modularity and community structure in networks. *PNAS* 103, 23 (2006), 8577–8582.
- [111] NEWMAN, M. E. J., Ed. *Networks: An introduction*. Oxford University Press, Oxford, UK, 2010.
- [112] PALLA, G., DERÉNYI, I., FARKAS, I., AND VICSEK, T. Uncovering the overlapping community structure of complex networks in nature and society. *Nature* 435 (2005), 814–818.
- [113] PANARDO, I. *Stability of periodic systems and Floquet Theory*, 2015.
- [114] PANTELEY, E., AND EL-ATI, A. On practical stability of a network of coupled nonlinear limit-cycle oscillators. *Proceedings - 2013 IEEE International Conference on Systems, Man, and Cybernetics, SMC 2013* (2013), 1548–1553.

- [115] PAPO, D. Time scales in cognitive neuroscience. *Frontiers in Physiology* (2013).
- [116] PAVLOV, A., POGROMSKY, A., VAN DE WOUW, N., AND NIJMEIJER, H. Convergent dynamics, a tribute to Boris Pavlovich Demidovich. *Systems and Control Letters* 52, 3-4 (2004), 257–261.
- [117] PECORA, L. M., AND CARROLL, T. L. Master Stability Functions for Synchronized Coupled Systems. *Physical Review Letters* 80, 10 (1998), 2109–2112.
- [118] PETKOV, G., GOODFELLOW, M., RICHARDSON, M. P., AND TERRY, J. R. A critical role for network structure in seizure onset: A computational modeling approach. *Frontiers in Neurology* 5, DEC (2014), 1–7.
- [119] PIKOVSKY, A., ROSENBLUM, M., AND KURTHS, J. *Synchronization: a universal concept in nonlinear sciences*. The Cambridge nonlinear science series. Cambridge University Press, Cambridge, 2001. Description par l'diteur <http://www.loc.gov/catdir/description/cam021/2001018104.html>.
- [120] POGROMSKY, A., SANTOBONI, G., AND NIJMEIJER, H. Partial synchronization: from symmetry towards stability. *Physica D* 172 (2002), 6587.
- [121] POGROMSKY, A. Y. Passivity Based Design of Synchronizing Systems. *International Journal of Bifurcation and Chaos* 08, 2 (1998), 295–319.
- [122] PURVES, D., AUGUSTINE, G., FITZPATRICK, D., KATZ, L., LAMANTIA, A.-S., MCNAMARA, J., AND WILLIAMS, S. *Neuroscience*. Sunderland (MA): Sinauer Associates, 2001.
- [123] RAMIREZ, J. P., OLVERA, L. A., NIJMEIJER, H., AND ALVARE, J. The sympathy of two pendulum clocks: beyond Huygens observations. *Scientific Reports* 6 (2016), 1–16.
- [124] RAMKISOENSING, A., AND MEIJER, J. Synchronization of biological clock neurons by light and peripheral feedback systems promotes circadian rhythms and health. *Frontiers in Neurology* 6, 128 (2015), 1–16.
- [125] REYNOLDS, C. Flocks, herds, and schools: A distributed behavioral mode. *Computer Graphics* 21, 4 (1987), 25–34.
- [126] RUBINOV, M., KNOCK, S. A., STAM, C. J., MICHELOYANNIS, S., HARRIS, A. W. F., WILLIAMS, L. M., AND BREAKSPEAR, M. Small-world properties of nonlinear brain activity in schizophrenia. *Human Brain Mapping* 30, 2 (2009), 403–416.

- [127] RUBINOV, M., AND SPORNS, O. Complex network measures of brain connectivity: uses and interpretations. *NeuroImage* 52, 3 (2010), 1059–1069.
- [128] RUBINOV, M., SPORNS, O., VAN LEEUWEN, C., AND MICHAEL., B. Symbiotic relationship between brain structure and dynamics. *BMC Neuroscience* 10, 55 (2009).
- [129] RUDIE, J. D., BROWN, J. A., BECK-PANCER, D., HERNANDEZ, L. M., DENNIS, E. L., THOMPSON, P. M., BOOKHEIMER, S. Y., AND DAPRETTO, M. Altered functional and structural brain network organization in autism. *NeuroImage: Clinical* 2, 1 (2013), 79–94.
- [130] RULKOV, N. F. Modeling of spiking-bursting neural behavior using two-dimensional map. *Phys. Rev. E* 65 (2002), 041922.
- [131] SAMELSON, H. On the brouwer fixed point theorem. *Portuguese Mathematical* 22 (1963), 189–191.
- [132] SCARDOVI, L., ARCAK, M., AND SONTAG, E. D. Synchronization of Inerconnected Systems With Applications to Biochemical Networks: An Input-Output Approach. *IEEE transactions on automatic control* 55, 6 (2010), 1367–1379.
- [133] SEARLE, S. R. On inverting circulant matrices. *Linear Algebra and Its Applications* 25, C (1979), 77–89.
- [134] SEJNOWSKI, T. J., AND TESAURO, G. Building network learning algorithms from hebbian synapses. In *Brain Organization and Memory: Cells, Systems, and Circuits.*, J. L. McGaugh, N. M. Weinberger, and G. Lynch, Eds. Oxford University Press, New York, NY, 1989, pp. 338–355.
- [135] SIMIONE, L., RAFFONE, A., WOLTERS, G., SALMAS, P., NAKATANI, C., BELARDINELLI, M. O., AND VAN LEEUWEN, C. ViSA: A Neurodynamic Model for Visuo-Spatial Working Memory, Attentional Blink, and Conscious Access. *Psychological Review* 119, 4 (2012), 745–769.
- [136] SINGER, W. Synchronization of cortical activity and its putative role in information processing and learning. *Annual Review Physiology* 55 (1993), 349–374.
- [137] SONG, S., MILLER, K. D., AND ABBOTT, L. F. Competitive Hebbian learning through spike-timing-dependent synaptic plasticity. *Nat Neurosci* 3, 9 (2000), 919–926.
- [138] SPORNS, O. *Networks of the Brain*, 1st ed. The MIT Press, 2010.

- [139] SPORNS, O. The human connectome: a complex network. *Annals of the New York Academy of Sciences* 1224, 1 (2011), 109–125.
- [140] STEUR, E., OGUCHI, T., VAN LEEUWEN, C., AND NIJMEIJER, H. Partial synchronization in diffusively time-delay coupled oscillator networks. *Chaos* 22, 4 (2012).
- [141] STEUR, E., TYUKIN, I., GORBAN, A., JARMAN, N., NIJMEIJER, H., AND VAN LEEUWEN, C. Coupling-modulated multi-stability and coherent dynamics in directed networks of heterogeneous nonlinear oscillators with modular topology. *IFAC-PapersOnLine* 49, 14 (2016), 62–67.
- [142] STEUR, E., TYUKIN, I., AND NIJMEIJER, H. Semi-passivity and synchronization of neuronal oscillators. *IFAC Proceedings Volumes (IFAC-PapersOnline)* 2, PART 1 (2009), 21–26.
- [143] STEUR, E., VAN LEEUWEN, C., AND MICHIELS, W. Partial synchronization manifolds for linearly time-delay coupled systems. *21st International Symposium on Mathematical Theory of Networks and Systems* (2014).
- [144] STROGATZ, S. *Nonlinear Dynamics and Chaos: With Applications to Physics, Biology, Chemistry and Engineering*. Westview Press, 2001.
- [145] STROGATZ, S. *Sync: The emerging science of spontaneous order*. Penguin UK, 2004.
- [146] SUTTON, R. S., AND BARTO, A. G. *Reinforcement Learning: An Introduction*. MIT Press, Cambridge, MA, USA, 1998.
- [147] TELESFORD, Q. K., JOYCE, K. E., HAYASAKA, S., BURDETTE, J. H., AND LAURENTI, P. J. The Ubiquity of Small-World Networks. *Brain Connectivity* 1, 5 (2011).
- [148] TRAUB, R. D., AND WONG, R. K. Cellular mechanism of neuronal synchronization in epilepsy. *Science* 216, 4547 (1982), 745–747.
- [149] TRAVERS, J., AND MILGRAM, S. An Experimental Study of the Small World Problem. *Sociometry* 32, 4 (Dec. 1969), 425–443.
- [150] VAN DEN BERG, D., GONG, P., BREAKSPEAR, M., AND VAN LEEUWEN, C. Fragmentation: loss of global coherence or breakdown of modularity in functional brain architecture? *Frontiers in Systems Neuroscience* 6, 20 (2012), 1–8.
- [151] VAN SOMMEREN, E. J., VAN DER WERF, Y. D., ROELFSEMA, P. R., MANSVELDER, H. D., AND DA SILVA, F. H. Slow brain oscillations of sleep, resting state, and vigilance. *Prog. Brain Res.* 195 (2011), 3–15.

- [152] VARELA, F., LACHAUX, J.-P., RODRIGUEZ, E., AND MARTINERIE, J. The brainweb: Phase synchronization and large-scale integration. *Nature Reviews Neuroscience* 2 (2001).
- [153] WARD, M. J. Notes on floquet theory i. [www.math.ubc.ca/ward/teaching/m605/every2.floquet1.pdf](http://www.math.ubc.ca/ward/teaching/m605/every2.floquet1.pdf), 2007.
- [154] WATTS, D. J., AND STROGATZ, S. H. Collective dynamics of 'small-world' networks. *Nature* 393, 6684 (1998), 440–442.
- [155] WAXMAN, S. G., KOCSIS, J. D., AND STYS, P. K. *The Axon: Structure, Function and Pathophysiology*. New York: Oxford University Press, 1995.
- [156] WITT, U. Self-organization and economics - what is new? *Structural Change and Economic Dynamics* 8 (1997), 489 – 507.
- [157] WITTMELER, S., SONG, G., DUFFIN, J., AND POON, C. S. Pacemakers handshake synchronization mechanism of mammalian respiratory rhythmogenesis. *Proceedings of the National Academy of Sciences of the United States of America* 105, 46 (2008), 18000–18005.
- [158] WOLF, R. C., SAMBATARO, F., LOHR, C., STEINBRINK, C., MARTIN, C., AND VASIC, N. Functional brain network abnormalities during verbal working memory performance in adolescents and young adults with dyslexia. *Neuropsychologia* 48, 1 (2010), 309–318.
- [159] WU, C. W. On a conjecture regarding the synchronization in an array of linearly coupled dynamical systems. *IEEE Transactions on Circuits and Systems I: Fundamental Theory and Applications* 43, 2 (1996), 161–165.
- [160] YOLDEMIR, B., BAJAMMAL, M., AND ABUGHARBIEH, R. Dictionary based super-resolution for diffusion mri. In *Computational Diffusion MRI* (2014), pp. 203–213.
- [161] ZHANG, L. I., AND POO, M.-M. Electrical activity and development of neural circuits. *Nature Neuroscience* 4 Suppl (2001), 1207–1214.